GEOPHYSICAL AND HYDROGEOLOGICAL INVESTIGATIONS FOR GROUNDWATER IN THE LAKE KENYATTA SETTLEMENT SCHEME, LAMU DISTRICT, COAST PROVINCE, KENYA.

BY

CHRYSANTHUS M. N. GICHERUH

A thesis submitted in partial fulfilment for the degree of Master of Science (Geology) in the University of Nairobi

NAIROBI 1993

GEOPHYSICAL AND HYDROGEOLOGICAL INVESTIGATIONS FOR GROUNDWATER IN THE LAKE KENYATTA SETTLEMENT SCHEME, LAMU DISTRICT, COAST PROVINCE, KENYA. ''

BY

CHRYSANTHUS M. N. GICHERUH

A thesis submitted in partial fulfilment for the degree of Master of
Science (Geology) in the University of Nairobi

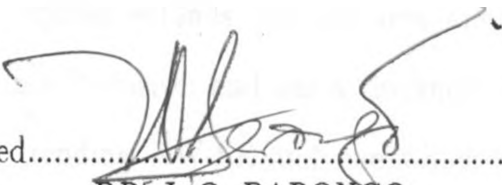**NAIROBI 1993**

DECLARATION

This is my original work and has not been submitted for a degree in any other University .

Signed...

CHRYSANTHUS M. N. GICHERUH

The thesis has been submitted for examination with our knowledge as University supervisors

Signed...

DR. J. O. BARONGO

Signed...

PROF. S. J. GACIRI

ABSTRACT

This thesis presents results of geophysical and hydrogeological investigations for groundwater in the Lake Kenyatta settlement scheme, Lamu District, Coast Province, Kenya. During the Pleistocene, the area was a beach and had sand dunes which have since been eroded and filled up with sand giving the present undulating relief. Inversion of ground resistivity sounding data yields resistivities and thicknesses that are consistent with geology. The area consists mostly of highly fissured coral limestone 5-30 m thick underlying a low resistivity substratum comprising sands, clays, sandy clays and clayey sands. The deeper coral limestone layers show consistent low resistivities, perhaps due to hard water in the solution caverns. The geoelectric sections reveal a pinch and swell structure of the coral limestone underlain by marine sediments. The freshwater/saltwater interface consistently displays an undulating wavy structure at a depth of 20 to 40 m below the ground surface and extends over the entire area.

The freshwater aquifer is mainly found in the highly cavernous fossil coral reef present under most of the area underlain by freshwater-bearing marine sands and silty clays. The aquifer extends over an area approximately 10 km^2, the freshwater below the lake inclusive; and has a thickness approximately 20 m. A hydrogeological basin trending NW-SE and one which coincides with the area of highest groundwater potential has been delineated in terms of geometry and extent. This trend coincides with the structural trend, thus suggesting that the groundwater flow is structurally controlled.

From the piezometric maps and hydrographs, it is concluded that the lake level approximately corresponds with the groundwater table through seeps in the lake bed. Groundwater generally replenishes the lake from the north and discharges

i

towards the south. During storm rainfall and high lake levels, groundwater storage is partly recharged by inflow from the lake and deep percolation. Discharge from the lake follows the shallow channel running from the lake to the southern shore stops and only recharge of groundwater into the lake occurs mainly on the northern shore of the lake.

The groundwater at the northern and north-eastern shore of the lake has low and stable salinity of electrical conductivity of 400 to 500 S/cm, increasing only relatively slowly during prolonged dry spells. Due to recharge by the lake water, groundwater on the south-eastern shore of the lake has a highly fluctuating salinity depending on the seasonal climatic conditions. Water from the existing boreholes smells of hydrogen sulphide. For further groundwater development in the Lake Kenyatta settlement scheme, it is recommended that boreholes for groundwater abstraction be sited within the Lake Kenyatta aquifer preferably along the structual lines. A well field designed above the flood level of the area on the north coast would serve as a constant source of groundwater supply where the water quality is stable and the possibility of communication remote, besides a greater coral limestone thickness. However, any abstraction should be subject to a meticulous safe yield calculation from a long duration testpumping.

ACKNOWLEDGEMENTS

The idea of doing an MSc. research at Lake Kenyatta Settlement Scheme first occurred to me during a vacational field study with "Groundwater Survey (K) Ltd" in September 1989 where I came across a report on a short geophysical fieldwork previously carried out in the area. I therefore take this opportunity to thank the University of Nairobi for awarding me a scholarship to take up an MSc. course through which I was able to carry out this research.

During the preparation of successive drafts of my MSc. thesis, the most generous helper was my supervisor, Dr. J. O. Barongo. The treatment of the inversion technique is taken from his PhD thesis, by some stimulating graduate supervision. It is he who introduced me to the inversion theory, the singular value decomposition (SVD) algorithm and tensorial representation of resistivity and conductivity as applied to ground resistivity modelling. He also introduced me to computer modelling in the interpretation phase. I would like to thank him for his individual kindness he showed me and, with the exception of one or two convivial cases, for concealing any dismay at my dilating progress. He provided me with a great deal of patient encouragement while suggesting valuable alterations to certain sections of the text. He read all parts of my original manuscript at different stages and, from very fruitful discussions, made a number of very helpful criticisms. He made many other valuable contributions in the absorbing hours of discussion.

I gratefully acknowledge the formal and informal assistance accorded to me in writing this thesis by my other supervisor, Prof. S. J. Gaciri. Besides the legacy from past work and lectures and experience in groundwater hydraulics, I had the good fortune to receive a constant flow of ideas and encouragement from him. Specific thanks are due to him for numerous improvements in the final manuscript.

As my University supervisors, I find joy and significance in giving both Dr. J. O. Barongo and Prof. S. J. Gaciri compliments from the bottom of my heart for such a segaceous supervision.

Some very special thanks go to Mr. Pieter G. Van Dougen, Managing Director of "Groundwater Survey (K) Ltd" for his broad interest and encouragement throughout my undergraduate studies and research period. His learned comments and positive criticisms of my manuscript helped improve its content and quality. I am sure his immense eminence derives from his vast cascade of scientific studies coupled with a long productive professional experience. To me, he is singled out as the man who introduced me to the geophysical methods applied to groundwater exploration and offered me numerous opportunities to work in his company "Groundwater Survey (K) Ltd" during vacations during my undergraduate studies. He provided me with all the geophysical equipment I needed during my fieldwork together with an appreciable financial assistance, and offered me computer facilities for the forward modelling. Moreover, he allowed me access to his rich library facilities. For all these, I express a heartfelt gratitude and wish him many more fruitful and satisfying years of professional practice. Further acknowledgements go to the GTZ-GASP Team Leader, Dr. Michael Van Boguslawski for allowing me access to the monitoring data for the well and lake.

Countless colleagues, friends and relatives have contributed positively to the accomplishing of my research study. It is impossible to mention all who directly or indirectly helped and encouraged me in this work. But I could mention George Nyangweso, Wilson Ngecu, Phillip Visser, Edwin Mukira, Kamau Gachie, Kagwe Githu, Mrs. Mary Gichinga, George Masila, John Gichinga, Peter Mbono and Joseph Mucheri, to all of whom I say a hearty thank you. In the course of my

Contents

List of Figures

List of Tables

Chapter 1

INTRODUCTION

1.1 Statement of the problem

The presence of saltwater in wells in the Lake Kenyatta settlement scheme is such a predominant problem in groundwater exploration that it calls for some detailed investigation. The severity of the problem of saltwater intrusion in the study area was first identified during groundwater investigation by "Groundwater Survey (K) Ltd" (G.S.K.) in 1987 in which it was concluded that: "The major problem encountered in the location of fresh groundwater for the development of the Lake Kenyatta settlement scheme is the pervasive presence of saltwater at shallow depths with generally only a very thin lens of freshwater perched on the denser saltwater" (G.S.K.,1987).

The presence of saltwater in the wells is mainly attributted to the encroachment of seawater into wells located near the sea shore (Fig. 1.1) leading to contamination of the boreholes with the excessive mineral content. As soon as the salt content exceeds a certain limit, the water ceases to be fit for human consumption. This problem, further complicated by variation in local hydrological and hydrogeological condition is a complex one. It must be realized that once the

1
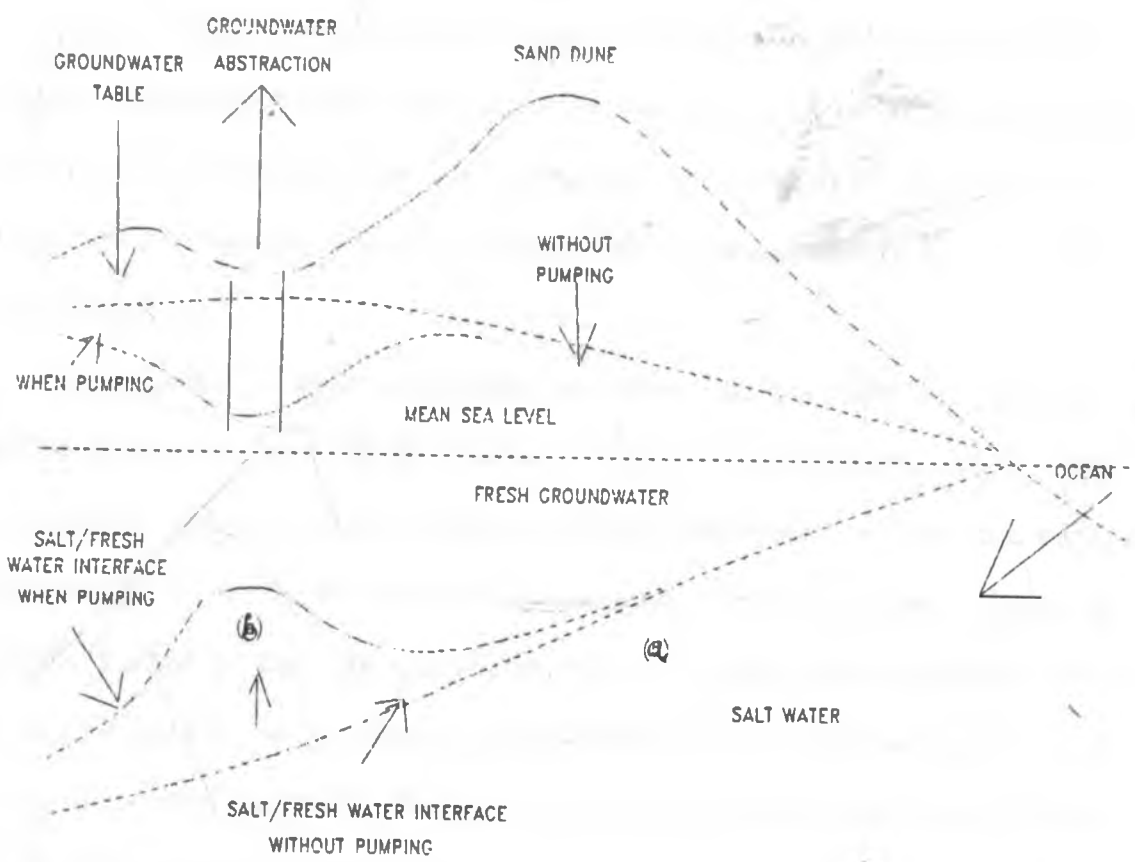
Fig. 1.1 Schematic diagram showing the ocurrence of saltwater intrusion due to (a) enchroachment from the sea, (b) overpumping

aquifer is contaminated with saltwater, it may take years to remove the salt even with adequate fresh groundwater available to flush out the saltwater. Therefore, greatest care must be exercised to prevent wells from being driven into the saltwater layer and, in the case of correctly driven wells, to prevent the possibility of overpumping.

Legget (1939) observed that overpumping is often responsible for the contamination by saltwater of wells adjacent to the sea coast, noting that wells along the shores of the oceans have been made brackish by this means where saltwater became mixed to varying degrees with the freshwater because of excessive drawdown of the latter.

The existence of wells is indicative of the existence of water-bearing strata, and if these are adjacent to the sea, then it follows that at some point the fresh groundwater will be in contact with the infiltrated saltwater intruding in a wedge shape (Fig.1.1). It has been found that the zone of diffusion between the two is relatively small so that any appreciable change from the normal position of the groundwater (e.g. due to overpumping) will result in a corresponding change in the position of the saltwater. Because two fluids of different densities are involved, a boundary surface (interface) is formed wherever the fluids are in contact. The shape and nature of the interface is governed by the equilibrium of the freshwater and the saltwater.

The problem of saltwater intrusion has increased as population centres and concomitant water demands in the coastal areas have developed. The coastal areas underlain by aquifers containing saltwater present special problems in developing freshwater supplies notwithstanding the water needs accompanying a large influx of population into the coastal areas. The importance of protecting the coastal

aquifers against this continual threat has led to this investigation in the Lake Kenyatta Settlement Scheme.

The investigation involved mapping geophyscally the saltwater/freshwater interface in the area and presenting a regional contour map indicating the depth to the same. With the level of saltwater/freshwater interface as the lower confining surface of the freshwater aquifer in the area, the approximate depth of the interface from the topographic surface can give an indication of the possible depletion and quality deterioration of the freshwater layer. It will also act as a guide to any drilling for groundwater in the area. Further, due to the increasing water demand, it would be of paramount importance to delineate particular areas of high groundwater potential free from saltwater for future drilling in the settlement scheme. This is important since the close proximity of seawater can introduce saltwater into the fresh groundwater even without overdraft unless care is exercised in developing underground water supplies. A centralized freshwater supply for large scale domestic, livestock and agricultural use therefore necessitates careful siting of boreholes in sufficiently large freshwater aquifers.

Evaluation of the interplay between the Lake Kenyatta surface water, the fresh groundwater and the saltwater from the Indian Ocean also points to the future and feasibility of groundwater abstraction over various periods in the area.

1.2 Purpose and scope of the study

1.2.1 Introduction

Water resources are increasingly becoming important in Coastal Kenya, Lamu District in particular. In the Lake Kenyatta Settlement Scheme, this has been due to the fact that urban centres are expanding rapidly. Moreover, increasing popula-

tion, industries and tourist activities demand a proportionate increase in available freshwater for domestic and industrial purposes. Due to this increasing demand, it has been necessary to explore and exploit the groundwater with the intention of supplementing the scarce surface drainage. However, saltwater intrusion presents an irrefutable problem in the development of groundwater supplies in the area.

1.2.2   Aims and objectives

The aims and objectives of the study are as follows:

1. To identify potential areas for future groundwater development in the area.

2. To assess the current status of groundwater development potential in the Lake Kenyatta Settlement Scheme.

3. To infer, establish and delineate the freshwater/saltwater interface in the study area.

4. To estimate geophysically the depth to the coral limestone in the study area.

5. To construct an iso-resistivity contour map for the area.

These objectives will include recommendations of borehole sites in the most suitable place(s) for better yields, and avoiding saltwater intrusion.

1.3   Area of study

The area of study is located in the Lake Kenyatta Settlement Scheme region (Figs. 1.2 and 1.3) around Lake Kenyatta (formerly Lake Mukunguya) in Lamu District in the northern coast of Kenya. It covers an area of 240 square kilometers, lying between the Tana river delta in the south and Ishakani town in the north-east near the Kenya-Somali border. Besides, the eastern boundary with the Indian Ocean,
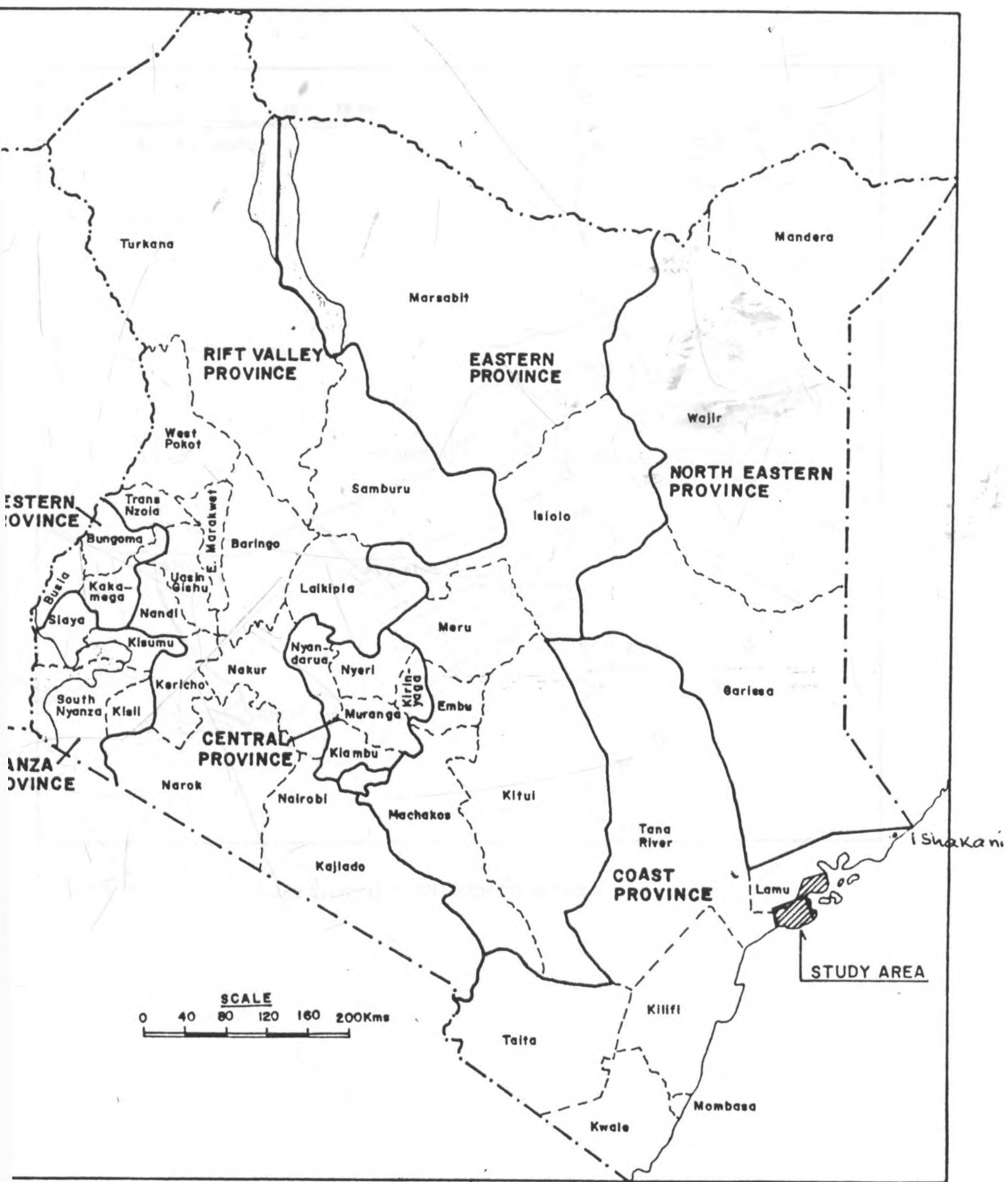
Fig. 1.2   Map of Kenya showing the location of the study area
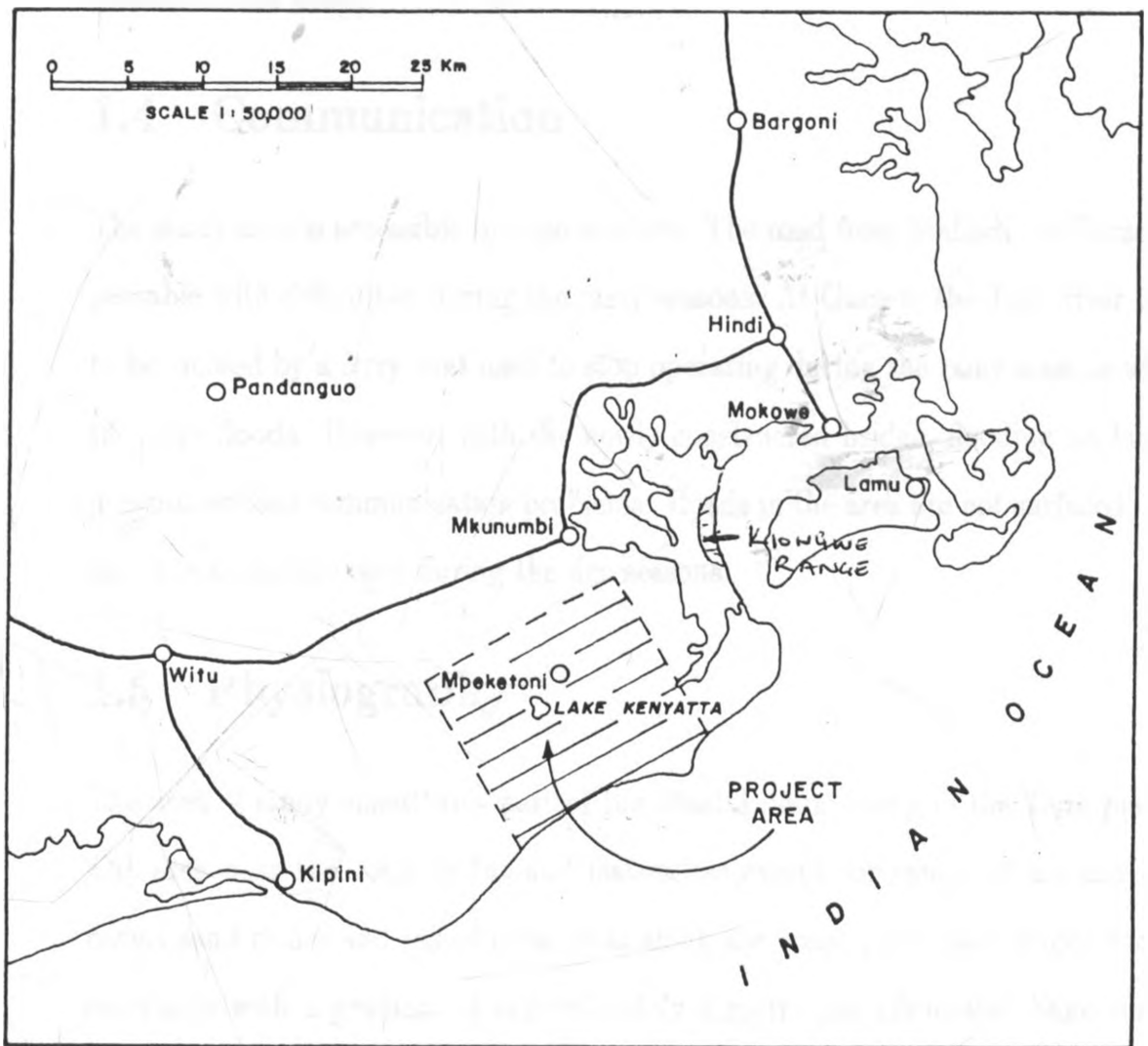
Fig. 1.3   The Lake Kenyatta settlememt scheme

the district area borders Tana River district to the west and south and Garissa district to the north.

1.4 Communication

The study area is accessible by road and sea. The road from Malindi via Garsen is passable with difficulties during the rainy seasons. At Garsen, the Tana river used to be crossed by a ferry that used to stop operating during the rainy seasons when the river floods. However, with the newly constructed bridge, flooding no longer presents serious communication problems. Roads in the area are not surfaced, and are thus accessible only during the dry seasons.

1.5 Physiography

The area of study constitutes part of the coastal plain, being in the Tana plains. The area near the coast is flat and featureless except for ranges of ancient and recent sand dunes and raised coral reefs along the coast. The plain slopes south-eastwards with a gradient of approximately 1 metre per kilometre. Sand dunes in the Kiongwe range and at Lamu island attain heights of up to 60 m above sea level.

1.6 Climate

The climate of the study area is equatorial coastal with characteristics such as slight temperature variation, high humidity, pronounced rainy season, high evapotranspiration and monsoon winds. The average rainfall per year recorded at Mpeketoni for 31 months is 1147 mm. Long rains occur between April and June

with light showers through July. Short rains occur between October and December and are fairly reliable. The long-term 10-year moving average for the Lamu meteorological station is presented in Figure 1.4. This average fluctuates between 100 and 1000 mm, while the actual yearly totals fluctuate between 500 and 1200 mm. From rainfall records, it is evident that rainfall during 1987 is concentrated in May while in 1988, it is evenly spread over the three months of April, May and June. From the daily records, it is observed that high rainfall intensity occurred during the first week of May 1987 and, to a lesser extent, during the second week of April, 1988. During 1989 up to July 1990, rainfall has been below average.

The mean maximum and minimum temperatures are 36.5^0 C and 19.5^0 C, respectively. The mean humidity is 75%. The hottest months are December to April while May to July are the coldest. The prevailing winds are the north-east Monsoon (Kaskasi) from November to March and the south-east Monsoon (Kusi) between April and October. Evaporation is high and amounts to 2327 mm per year for Lamu meteological station with maximum and minimum at only 5% from the average.

1.7   Literature review

The pioneer work on groundwater investigation in Lamu district was undertaken by Grundy (1953), whose recommendation led to the establishment of Lamu Water Supply Scheme in 1957. His report mainly dealt with Shella sand dunes of which he points out as having high porosity and permeability characteristics. However, he discounts the possibility of large scale water supply from the dunes due to cementation and composition of the sands and also the inherent evaporation rates. Patterson (1957) carried out a groundwater investigation in the Lamu coastline

9
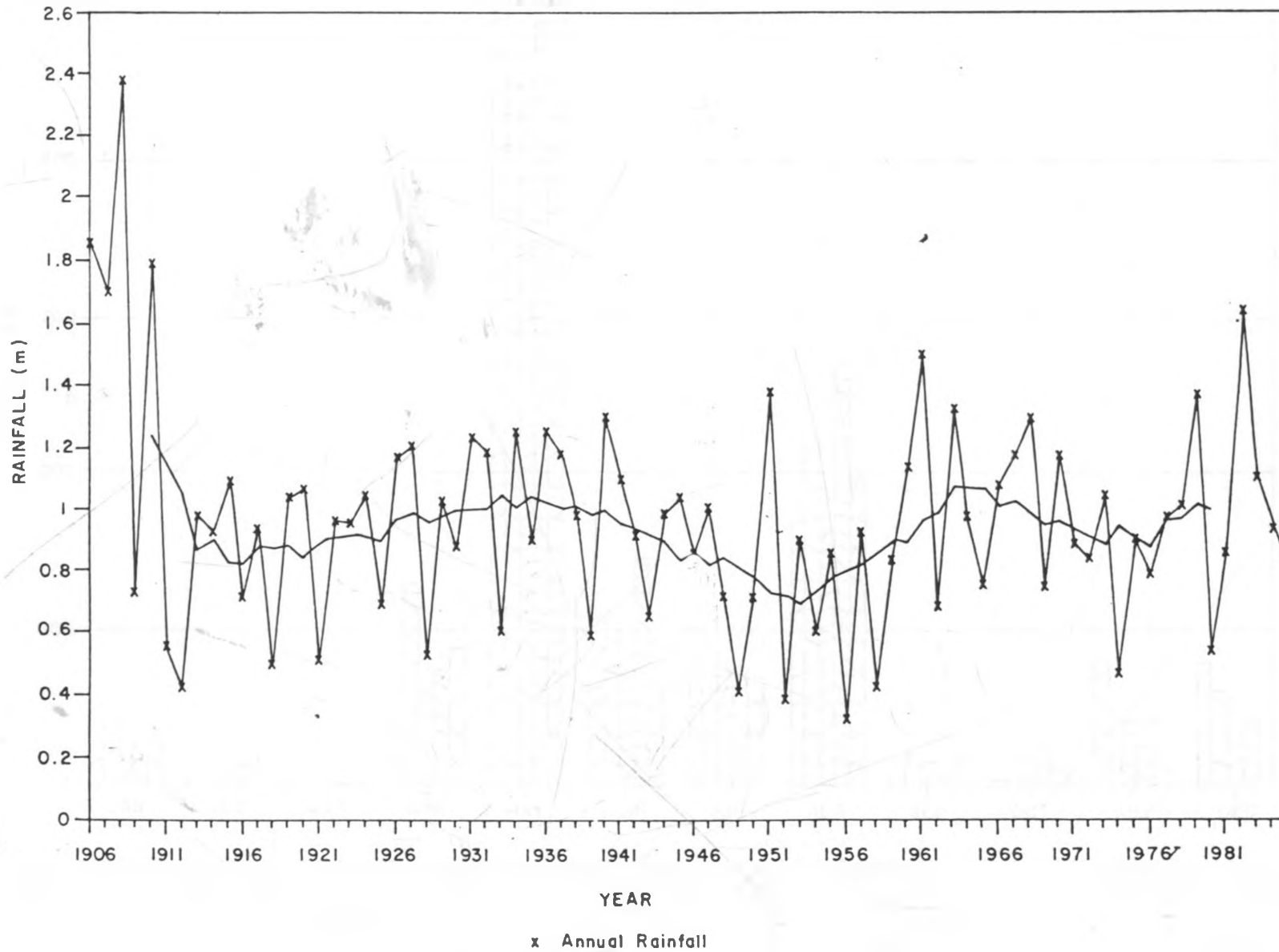
x   Annual Rainfall

Fig. 1.4   Annual rainfall and 10-year moving average for Lamu meteorological station
Source: Meteorological Department, Lamu
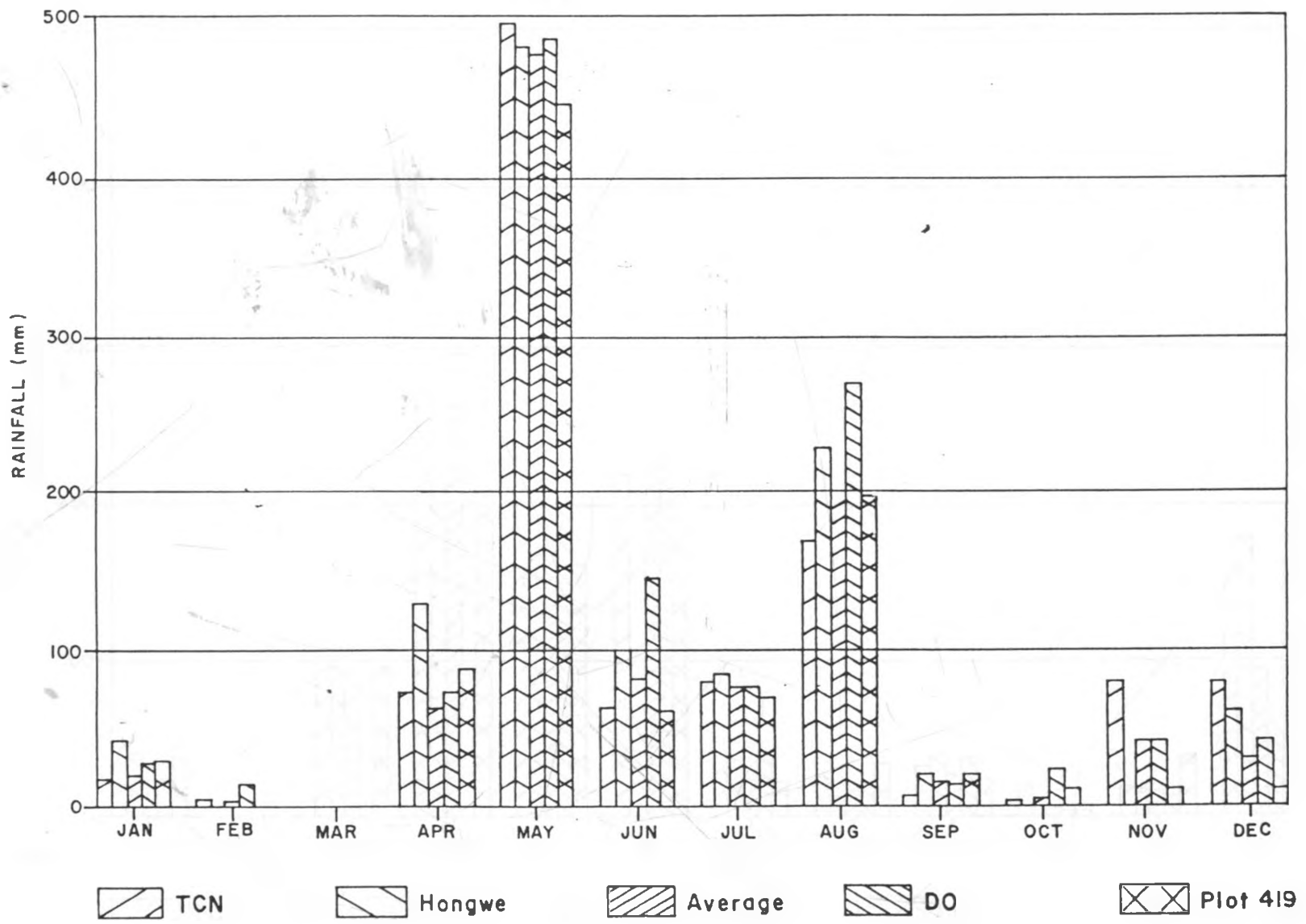
Fig. 1.5 (a)   Rainfall LKSS
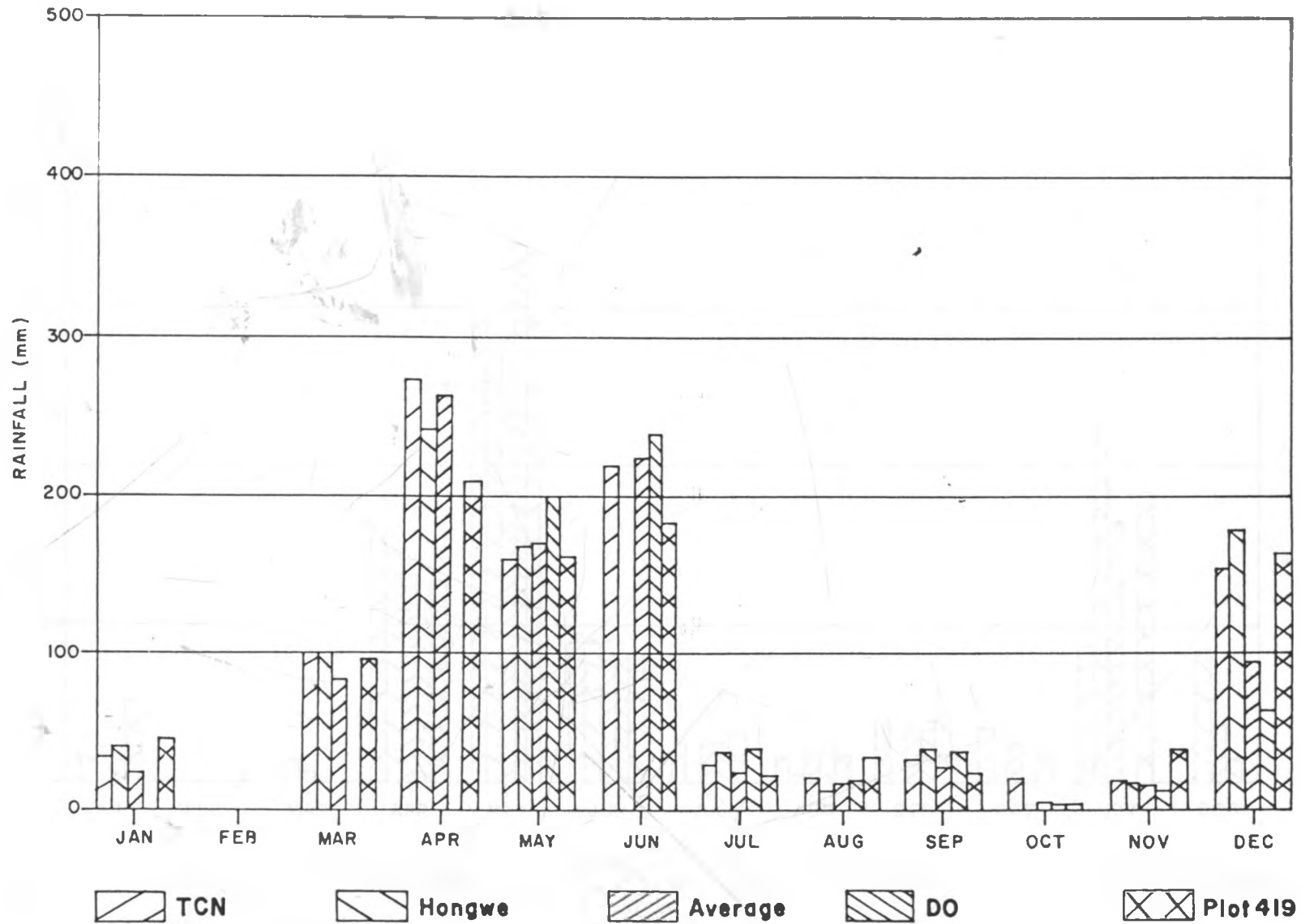
Fig 1.5 (b)   Rainfall LKSS 1988
Source: GTZ-GASP rainfall data - 11 records
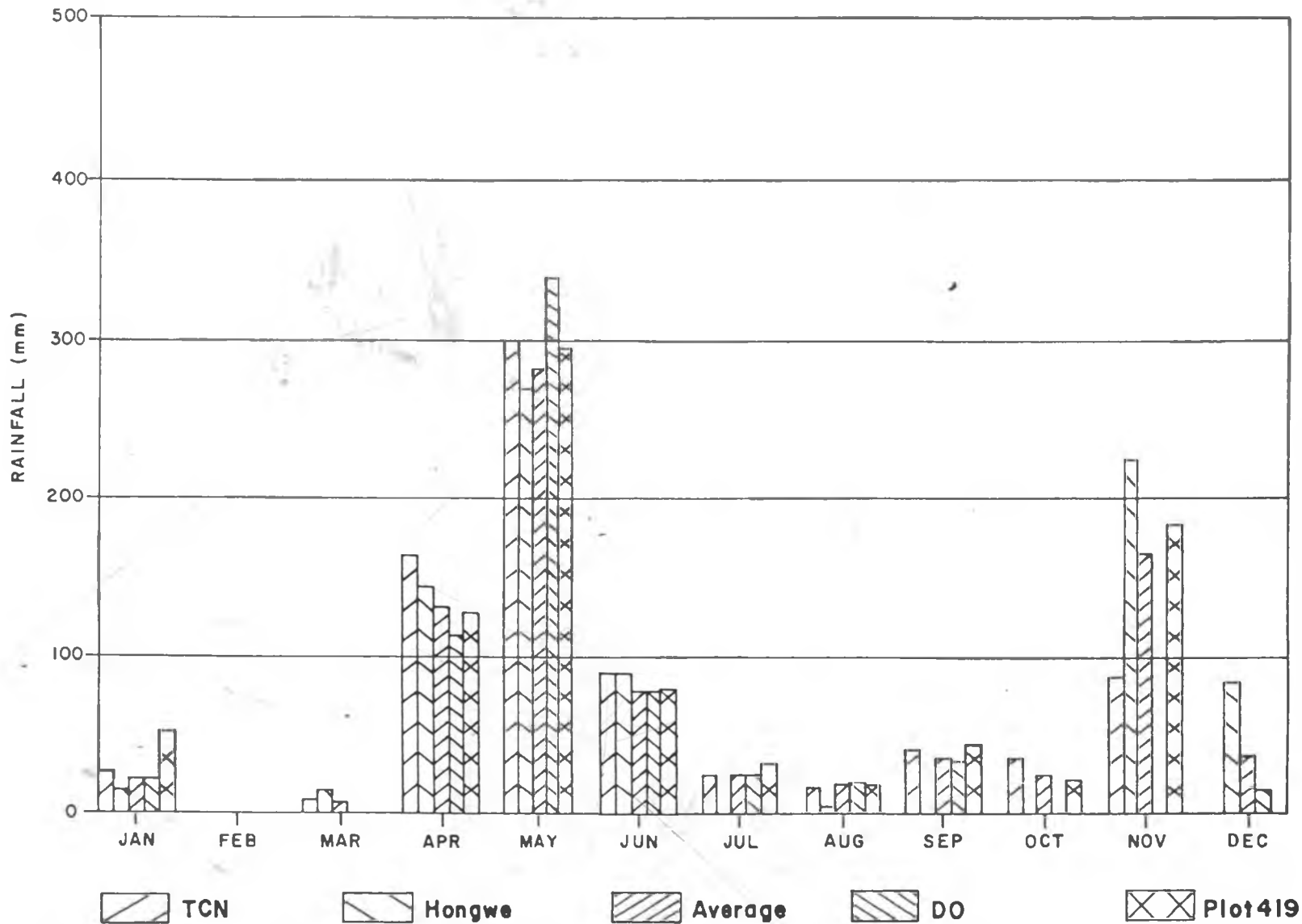
Fig. 1.5 (c)   Rainfall LKSS 1989

Source: GTZ-GASP rainfall data - 11 records
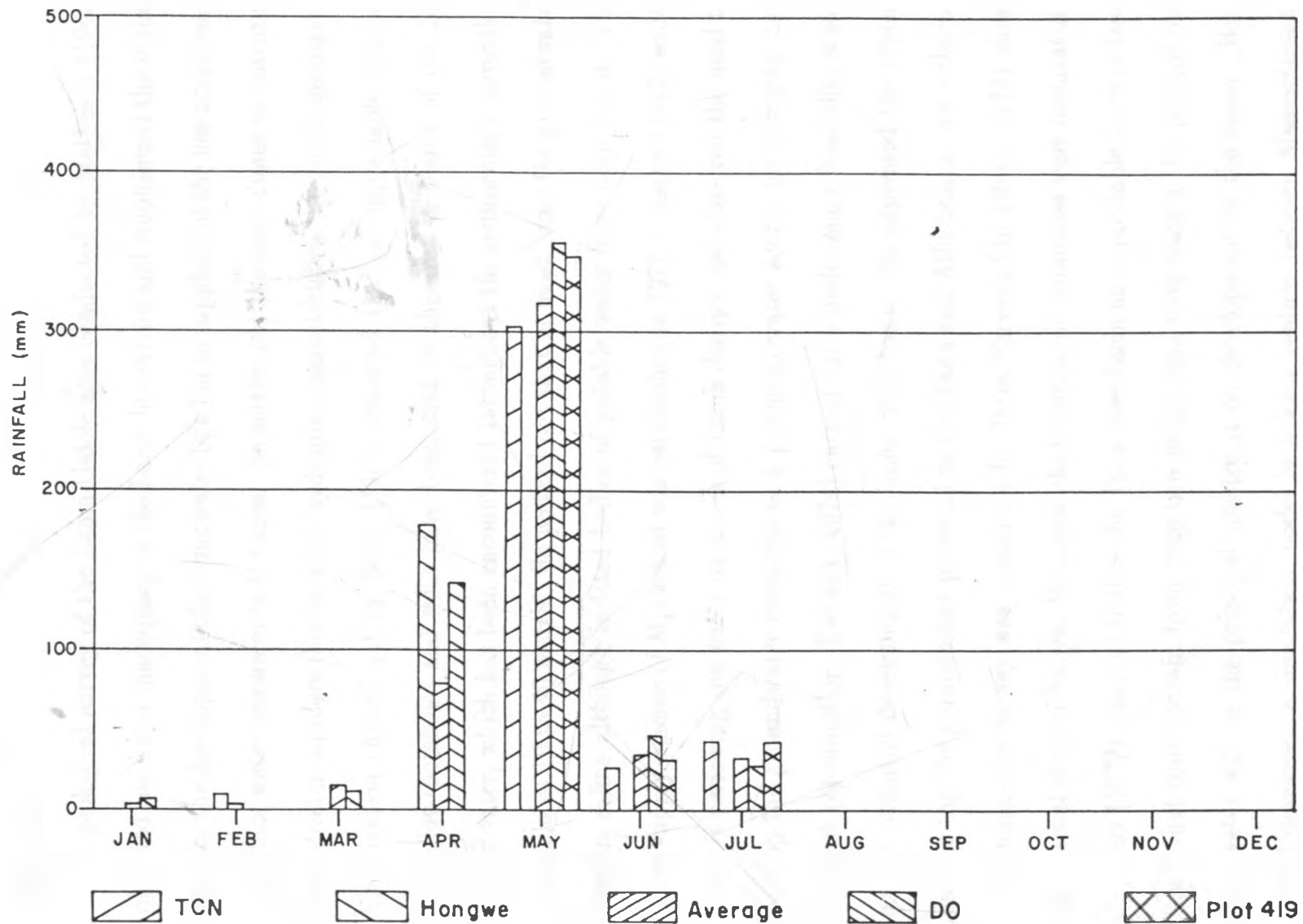
Fig. 1.5 (d)   Rainfall LKSS 1990

Source: GTZ-GASP rainfall data - 11 records

and emphasized the need and possibility for groundwater development in the Lamu hinterland.

A geological survey of the Lamu-Galole area conducted by Matheson (1963) observed the water inadequacy in the Lamu hinterland and emphasized the urgent need for the development of groundwater in a bid to supplement the low occurrence of surface water resources in the area. He singles out the sand dunes as potential groundwater aquifers due to their hydraulic characteristics. A hydrogeological investigation carried out by Selby (1969) observed that an appreciable number of shallow boreholes and wells have been sunk in the area in search of potable groundwater, which has been encountered throughout the sedimentary formation at depths of 10 to 20 metres. He pointed out that in most cases the groundwater appears saline although isolated bodies of potable water have been found. The water supply scheme of Mpeketoni was established in 1971. Classen (1973) wrote a report reviewing the water resources of Lamu district and observed the need to develop the groundwater resources as a potential water source for domestic and livestock consumption. Ewbank (1974) carried out a preliminary feasibility study on the potential development of the Tana river basin. He expressed the urgent need to tap the groundwater potential in the Tana and Athi basins. An airborne electromagnetic survey was conducted by Terra Surveys Ltd (Hetu, 1978) along the coastal strip of Kenya. No major electromagnetic anomalies were delineated.

Barr (1979) observed that in the Tana river basin an appreciable track of land exists that could benefit from irrigation using Tana river waters. He pointed out that water will be the principal constraint on development in the basin. Barr (1979) developed a simulation model in a joint venture between Massachussets Institute of Technology (MIT) and Tippets-Abbets-McCarthy-Stratton (TAMS)

15

(1980) Engineers and Architects for the river Tana basin. The model was designed as a monthly increment, general purpose simulation model for evaluating the hydrological and economic consequences of various plans for surface water development of the river basin. TARDA (1982) explains the need for groundwater investigation as a consequece of the source surface water drainage in the coastal Kenya. Bouguer gravity measurements were taken by Terra Surveys Ltd (1982), but again, no significant Bouger anomaly was detected in the area of study. It was therefore concluded that the sediments continue to a considerable depth. Cowiconsult (1983) was commissioned by the government for the Lake Kenyatta Water Supply Project. A surface water scheme was recommended in view of the fact that groundwater in the wells is mostly saline, and only low borehole yields of 1-5 m^3 per hour are prevalent in the area. It was also observed that fresh water occurs consistently in two types of deposits, that is, the sand dunes and the raised coral reefs. It was concluded that due to their large areal extent, the dune formation may constitute an appreciable reservoir of fresh groundwater. Recommendations were made that geophysical and hydrogeological surveys be carried out in the Lake Kenyatta Settlement Scheme to establish potential groundwater reservoirs to further supplement the low occurrence of surface water.

Van Dougen and Kruseman (1984), in a safari report submitted to the Water Resources Assessment Programme (WRAP), identified the major problems associated with water supply in the Lamu area also covering the Lake Kenyatta Settlement Scheme and the steps to be taken to alleviate the acute water shortage for the area in order to satisfy the immediate additional requirements related to the construction activities on the island (hospital, jetty, etc.) and the ice factory. The need to establish a water supply system that can satisfy the present and fu-

16

ture demands of the mainland as well as those of Lamu and Manda island was highlighted. A programme was also proposed to investigate on how to establish guidelines for the protection of the aquifer systems and for the establishment of additional public or private water supply systems on Lamu island. This proposal includes: inventory, water well inventory, reconnaissance drilling, surface geophysical investigations, electrical conductivity (EC) and water level monitoring network, water balance study and groundwater modelling. A review of the hydrogeology of Lamu and Mokowe areas was also presented.

Three small scale geophysical surveys were carried out by the Water Resources Assessment Division of the Ministry of Water Development (WRAP, 1985, 1986, 1988). 26 resistivity soundings (VES) were carried out by WRAP to provide a reference for the surveys carried out in Hindi and Mapogoni areas and for future investigations. Lamu district was part of an extensive seismic survey carried out in the fifties. This survey was carried out by oil companies in search of oil and gas reservoirs. Since they were not interested in the first few hundred metres, the results do not have any value for the purpose of groundwater investigations. At the end of the resistivity fieldwork, a horizontal loop EM profile was run with a coil seperation of 50 m and a station inteval of 10 m. Measurement was done at every station with 6 frequencies (222, 444, 888, 1777, 3555 Hz), the out-of-phase and in-phase responses, it was concluded that the resistivity is decreasing with increasing depth. The low response of the out-of-phase component at the high frequency range indicates a good conductor at relatively shallow depth which was thought to be clay. The detection of the clay layers was only qualitative.

A water resources study was conducted by Diettrich (1985) for the rural water supply of the Lake Kenyatta and Hindi Settlement Schemes in which he recom-

mended the establishment of a more detailed groundwater investigation in the Lake Kenyatta Settlement Scheme. Diettrich (1985) observed that in this area, groundwater deposits are superficial and occur in sheets of geologically recent sediments. He subdivided the sediments into three classes: (1) Mobile dunes along the shore line, (2) Unconsolidated fossil dunes inland and (3) Fossil coral reefs inland. He made the first approximation of the permeability of the various formations in the area, based on grain size analysis; and pioneered in the evaluation of the water budget in the area surrounding Lake Kenyatta. It is his recommendations that have been adopted by the German Assited Settlement Project (GASP) in their activities regarding water supply in the Lamu area. In 1987, a detailed groundwater investigation was carried out by Groundwater Survey (K) Ltd (GSK), for GASP in the Lake Kenyatta Settlement Scheme, Witu Hindi, Hongwe, the Tewe sand dunes and Mkunumbi. Their recommendations and that of Diettrich have led to construction of numerous boreholes and wells in the area. The results of the GSK survey are quite positive as a considerable underground storage reservoir was detected near Lake Kenyatta. It was suggested that the Lake water was reclaiming highly permeable fossil coral limestone which was encountered at depth. At the request of the Lamu District Developement Committee (D.D.C.), a water resources reconnaissance study was conducted by WRAP. This reconnaissance study involved geophysical work employing the resistivity method. The conclusions of the study were that near Lake Kenyatta, an underground coral reef exists with high permeability which stores freshwater originating from the lake. Also, low-lying areas along the coast are unreliable as a source of large scale supplies, and that there is little capacity for fresh water storage. From GSK (1987) and WRAP (1988) reports, it is recommended that further follow-up investigations be

18

carried out to assess the extent and nature of occurrence of fresh groundwater in the Lake Kenyatta Settlement Scheme in order to provide design, construction and abstraction parameters for a centralized water supply system.

The Lamu District Development Plan (DDP) (1989-1993) report puts the expansion of the existing water supply on top of the priority list. It notes that existing wells and djabias should be renovated and new ones established (DDP, Lamu pg. 16). In the plan, it is lamented over the scarcity of surface freshwater resources and permanent rivers in the district, there being only drainage-ways forming seasonal rivers. The Shella dunes are also mentioned as a resource for freshwater. The report emphasizes the fact that much of the water for human and livestock consumption is obtained from subsurface source and that most of the groundwater sources are saline. It is recommended that the Lake Kenyatta Water Supply be expanded to cater for a greater area. GSK (1990) conducted some further hydrogeological investigations in the area to design a well field for a centralized water supply. During those investigations which formed part of the present study, two existing boreholes in the area were test pumped and the yield calculated to be over 25 m³/hour. This is quite a high yeild. Borehole 2 was found to be directly related to the Lake, thus there is a steady flow between the two. A survey conducted to study the Lake Kenyatta crossection by Howard Humphreys (K) Ltd and presented by Groundwater Survey (K) Ltd (1990) to GASP provides some very important information on the relationship between the lake level, the lake surface area and the volume of the lake (Fig. 1.6). It is observed that the volume of the lake and its surface area vary with depth.
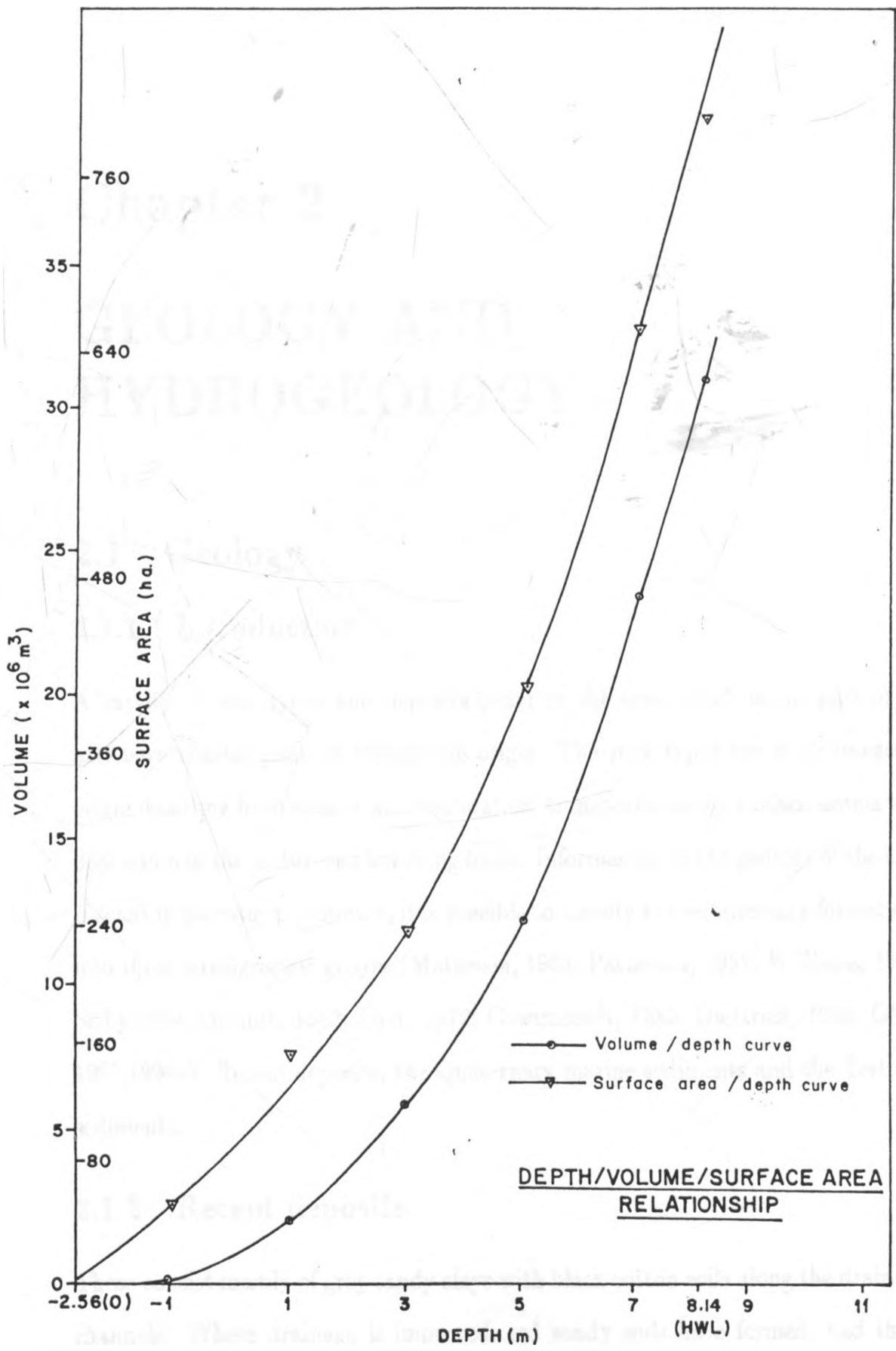
Fig. 1.6   Lake Kenyatta cross-section survey
         Source: Groundwater Survey (K) Ltd, 1990

Chapter 2

GEOLOGY AND HYDROGEOLOGY

2.1 Geology

2.1.1 Introduction

A variety of rock types and deposits occur in the area which forms part of an extensive coastal plain of Pleistocene origin. The rock types are of sedimentary origin resulting from erosion and denudation, transportation by surface agents and deposition in the featureless low-lying basin. Information on the geology of the area is scant in literature. However, it is possible to classify the sedimentary formations into three stratigraphic groups (Matheson, 1963; Patterson, 1957; Williams, 1962; Selby,1969; Grundy, 1953; Barr, 1979; Cowiconsult, 1983; Diettrich, 1985; GSK, 1987,1990a): Recent deposits, the Quaternary marine sediments and the Tertiary sediments.

2.1.2 Recent deposits

These consist mainly of grey sandy clays with black cotton soils along the drainage channels. Where drainage is improved, red sandy soils have formed, and these

also represent the detrital and alluvial deposits that resulted from the erosion and deposition of the Tertiary dunes. Most prominent of the recent deposits are the first row of high coastal dunes, composed of predominantly white, unconsolidated sands, distinguishable from the fossil dunes by less cementation and colouring.

Other recent fluvial, lacustrine and marine deposits consisting of sands, mud and silt have accumulated in and around the ephemeral streams, Lake Kenyatta and the mangrove swamps of the Mto wa Mkunumbi estuary. Since flooding occurs due to both occasional high tides and heavy rainfall, it becomes difficult to distinguish between deposits of marine and continental origin in the lowlands surrounding the estuary.

2.1.3 Quaternary marine deposits

2.1.3.1 Introduction

The quaternary marine sediments form the bulk of Quaternary deposits. They extend beyond 30 metres depth below the present ground surface. The sediments consist of grey or yellow-grey sands and clayey sands. Matheson (1963) explains their formation during the Pleistocene as a result of complex sea level fluctuations (regressions and transgressions) during which time coral reefs were formed and later decomposed. During the low sea levels, the coastal rivers cut channels in the lagoons behind the coral reefs. These channels were later drowned when the sea levels rose again. The present creeks (Dodori creek, Mto Wange) in the area are an example of these channels. The raised Pleistocene coral reef which developed along the length of the coast forms the base of the islands in the area and remnants are also found inland at shallow depths (WRAP, 1988). Coral reefs are found embedded in these deposits at various depths.

22

2.1.3.2 Lagoonal deposits

The lagoonal sands and clays deposited on the edge of a Pleistocene sea appear to be sparsely fossiliferous consisting of poorly consolidated grey, pale grey-brown and rusty-brown clayey sands, sandy clays and marls with intercalations of reddish to pale, brown sands. Mineralogical analysis (Caswell , 1953) reveals that the sands are poorly cemented by gypsum and limonite, and mainly comprise quartz with scattered grains of magnetite, ilmenite and pale pink garnets.

2.1.3.3 The fossil dunes

These are located behind the first row of the recent dunes along the coastal area. These are probably of upper Pleistocene (Williams, 1962), at that time situated along a coastline which has since regressed to the present position. The wind-blown reddish-brown sands of these fossil dunes cover extensive areas of the coastal plains inland, sometimes having formed dune features further inland (e.g., Hongwe hill north-west of Lake Kenyatta). The sands have been consolidated to some degree by ferricrete cementation, thus displaying a distinct reddish colour. Cementation of the sand particles of the fossil dunes reduces their storage capacity.

2.1.3.4 Limestone

Although poorly exposed in the area, the limestones, which are mouthed by the reddish-brown wind-blown sands, are in some parts easily identified due to extensive karstification, visible in the form of numerous sinkholes filled with aeolian and alluvial deposits. These features are easily recognised on aerial photographs and topographic maps as pans. The sinkholes signify the presence of freshwater (high content of carbon dioxide and oxygen) since limestone is more soluble in freshwater

than in brackish or saline water, as can be observed in the Lake Kenyatta area where a chain of interconnected sinkholes has formed in the overflow channel of the lake (Fig. 2.1). Since part of these fossil reefs now occurs above the present sea level, it may be deduced that they must have formed during periods of higher sea level, though not all the limestone encountered in the area is necessarily part of a fossil coral reef.

2.1.4   Tertiary sediments

Tertiary sediments in the area consist of alternating series of sands, sandy clays and clayey sands ranging from Miocene to Pliocene. They underlie Quaternary deposits and continue to greater depths. Mundane range in the eastern part of the coastal area forms a long dune ridge at some distance from the coast and rises conspicuously. This is probably a fossil dune ridge composed of terra rosa decomposition products of the Miocene limestones (Matheson, 1962). A small fossil dune is also found south-east of Mpeketoni. Occasionally and especially within the Miocene series, limestone occurs.

2.1.5   Stratigraphy

A summary of the stratigraphy of the Kenyan coast has been presented by Williams (1963) who identified the variety of deposits along the coastline as lagoonal clayey sands and marls, fossil dune sands, raised coral reefs and associated coquinoid limestones. Table 2.1 shows a summary of the stratigraphy of the area. Approximate ages of various deposits have been deduced from their position with respect to the major fluctuations in sea level during the Pleistocene period (Table 2.1). Studies along the coast (Caswell, 1953; Thompson, 1956; Williams, 1962) indicate
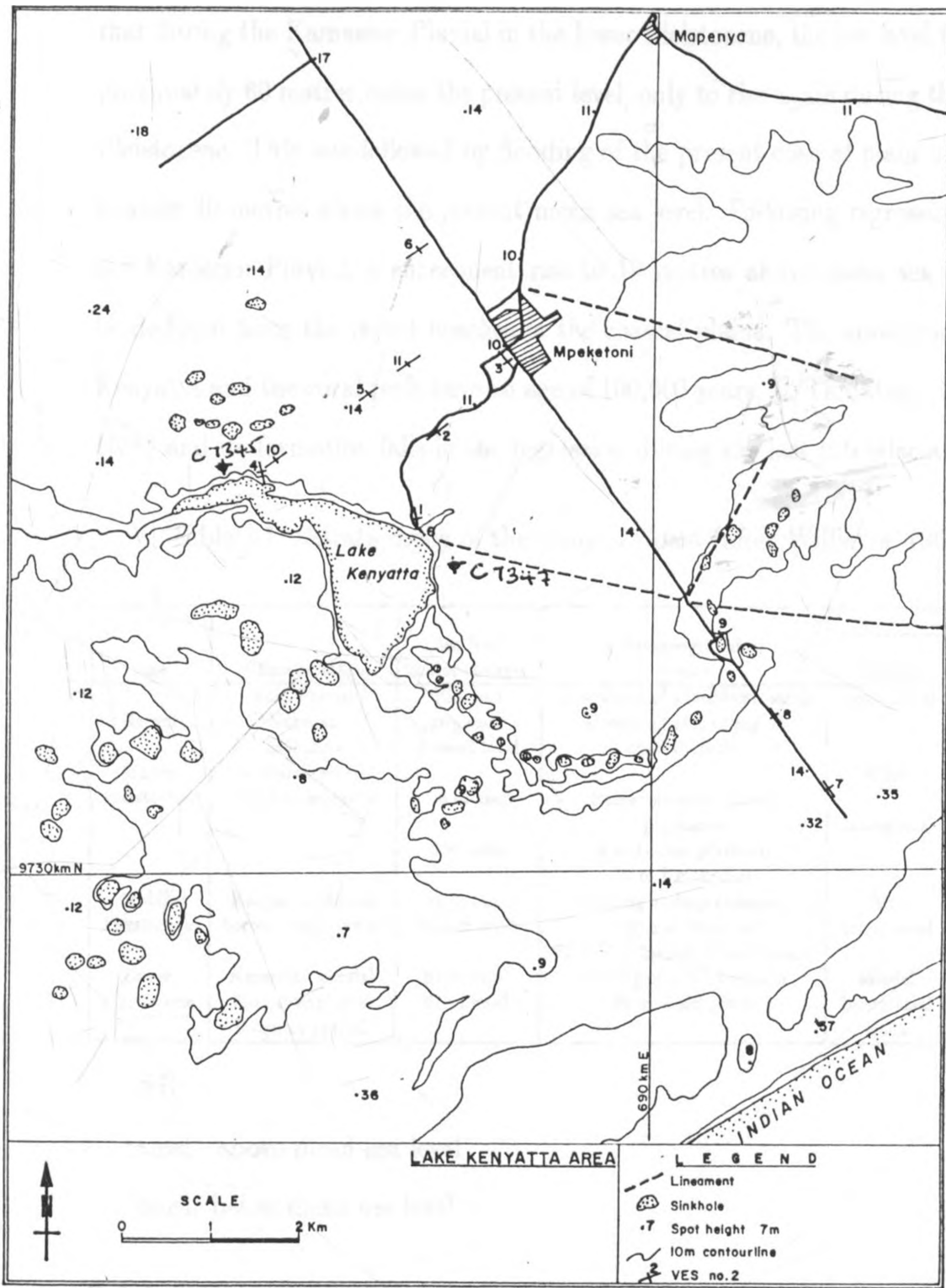
Fig. 2.1   Sinkholes and linearments in the Lake Kenyatta settlememt scheme area
Source: Aerial photograph inerpretation

that during the Kamasian Pluvial in the lower Pleistocene, the sea level fell to approximately 60 metres below the present level, only to rise again during the middle Pleistocene. This was followed by flooding of the present coastal plain to approximately 40 metres above the present mean sea level. Following regression during the Kanjeran Pluvial, a subsequent rise to 10 metres above mean sea level can be deduced from the raised beaches in the coastal plains. The area around Lake Kenyatta and the coral reefs have an age of 100,000 years, U/Th dating (Oostrom, 1988) and its formation falls in the regression during the last Interglacial.

Table 2.1   Stratigraphy of the Kenyan Coast (after Williams, 1962)

Age	Climatic stage	Sea level major changes	Palaeogeographical events	Europe	
				Climate	Sea level
Recent	Post Pluvial Nakuran Makalian	Rise and aggregation to present level	Deposition of windblown sands Drowning and silting of coastal creeks	Post-glacial	Flaudrain transgression
Upper Pleistocene	Gamblian pluvial Third interpluvial	4.5 m amsl	Raised beaches, caves, platforms	Würm Interglacial	Low 7.5 m amsl
		9 m amsl	9 m marine platform 30 m Knickpoint		18 m amsl
Middle Pleistocene	Kanyeran pluvial Second interpluvial	45 m bmsl 30.5 m bmsl	Cutting of deep channels Growth of coral reefs 61 m Knickpoint, 37 m terrace	Riss Interglacial	Very low 52 m bmsl
Lower Pleistocene	Kamasian pluvial First interpluvial Kageran pluvial	61 m bmsl 61 m bmsl	Cutting of coral platform 76 m Knickpoint	Mindel Interglacial Gunz	Very low 61 m bmsl Lower

NB:

amsl - above mean sea level

bmsl: below mean sea level

2.1.6   Structure

The lineaments in the area that are most conspicuous are the fractures and faults, and are only observable from aerial photographs. This is because of thick sediments, thus the buried linearments cannot be observed from the surface. They are

either parallel or perpendicular to the present coastline (Fig. 2.1). The seasonal rivers in the north-east seem to be controlled by the fracture system. Many of the linearments are accompanied by sinkholes.

2.2   Hydrogeology

2.2.1   Introduction

Thorough and accurate information on the hydrogeology and hydrology of the study area and Lamu district in general is virtually non-existent in the literature. This has been probably due to the fact that no hydrogeological/hydrological research has been undertaken in the area and partly due to the fact that the major previous work undertaken in the area had been commisioned to either engineers or hydrologists and hydrogeologists with biased interest in the outcome of their work. As of today, after numerous feasibility studies supported by the Kenyan government, others by the German Technical Cooperation (GTZ) through GASP, the only mode of water supply found feasible is groundwater. Proposals have been made and recommendations presented on the possibility of exploiting either of the four major water sources, and within close proximity of the area:-

1) Surface water from River Tana - The feasibility study was performed by Cowiconsult (1983).

2) Surface water from Lake Kenyatta.

3) Groundwater - Feasibility study was undertaken by Diettrich (1985), Groundwater Survey (K) Ltd (1987, 1990).

4) Roof catchment.

The major controversy over the most feasible and cost-effective water supply source has mainly emanated from the complexity of the water situation in the area.

27

This has been caused partly by the complex interactions between the groundwater aquifer (fresh groundwater), the intrusion of saltwater from the sea, pockets of fossil water, the Lake Kenyatta surface water, evapotranspiration and other climatic forces, not to mention the economic factors governed by the proximity of adequate surface water and the use of the water.

Studies have not succeeded in furnishing measurements of important hydrogeological parameters of the deeper lying formations. Much effort has been devoted to investigating the reservoir's response to natural variations in precipitation, evaporation and tidewater as well as to its response to abstraction of water. Besides, no abstraction parameters have been determined for the existing wells.

2.2.2 Availability of groundwater

2.2.2.1 Introduction

An appreciable number of shallow hand dug wells and boreholes have been sunk in the area in search of potable groundwater. Groundwater is encountered throughout the sedimentary formations at depths of 10 to 20 metres. In most cases, the groundwater appears to be saline although isolated potable groundwater lenses have been found. Cowiconsult (1983) observed that the yields are low and approximate 1-5 m^3/hr. However, recent studies on the test pumping results of two boreholes near Lake Kenyatta have revealed a very high yield of approximately 20-30 m^3/hr. The high recharge rate of borehole c-7347 is verified from testing and recovery (Fig. 2.2 a,b). Locations of the boreholes arepresented in Appendix IV.

Diettrich (1985) characterized the groundwater aquifers as superficial, occurring in sheets of geologically recent sediments:(i) mobile dunes along the shoreline,

28

Second Test — 28 August 1990
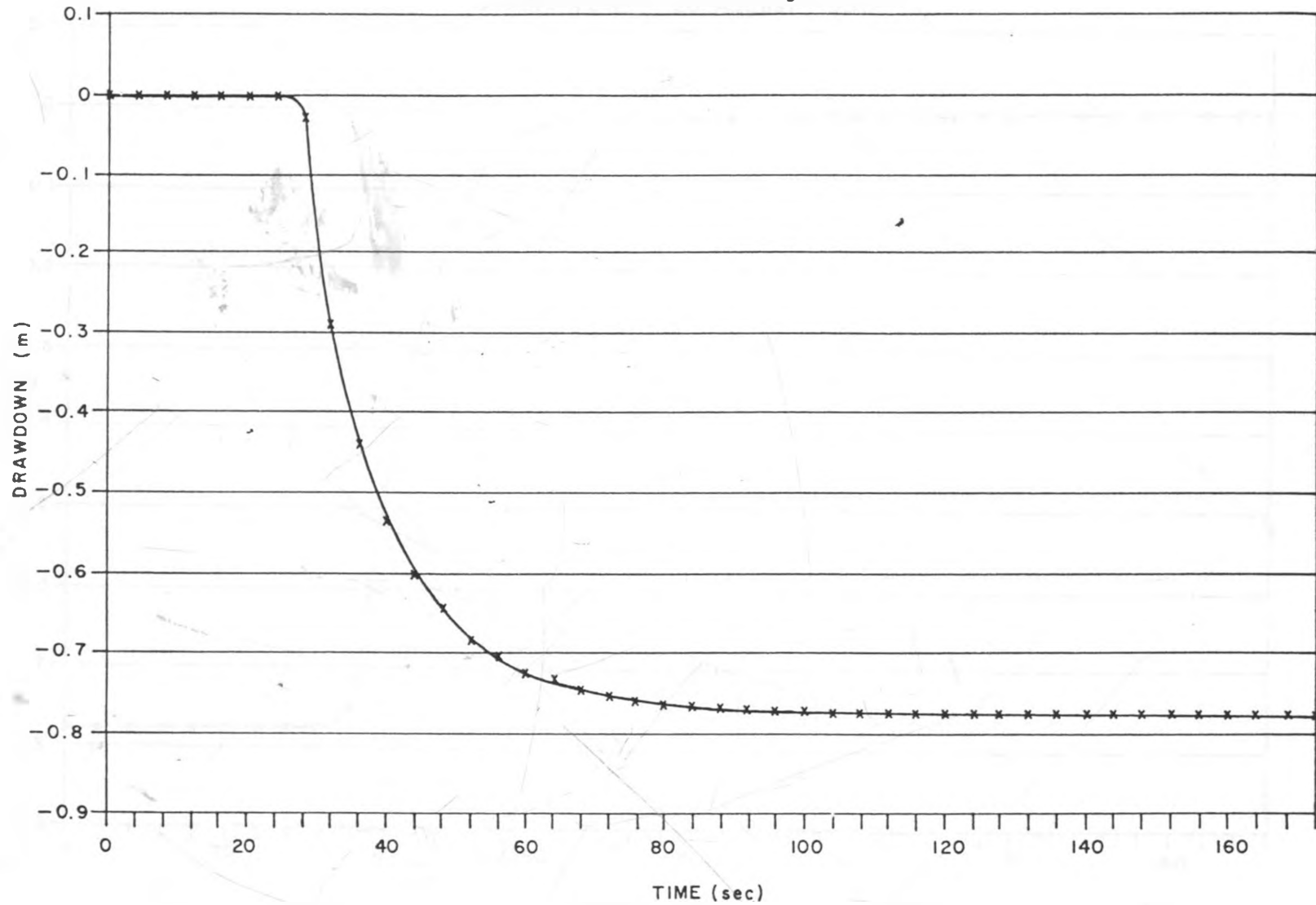
Fig. 2.2 (a)   Pump test and recovery test for borehole C-7347
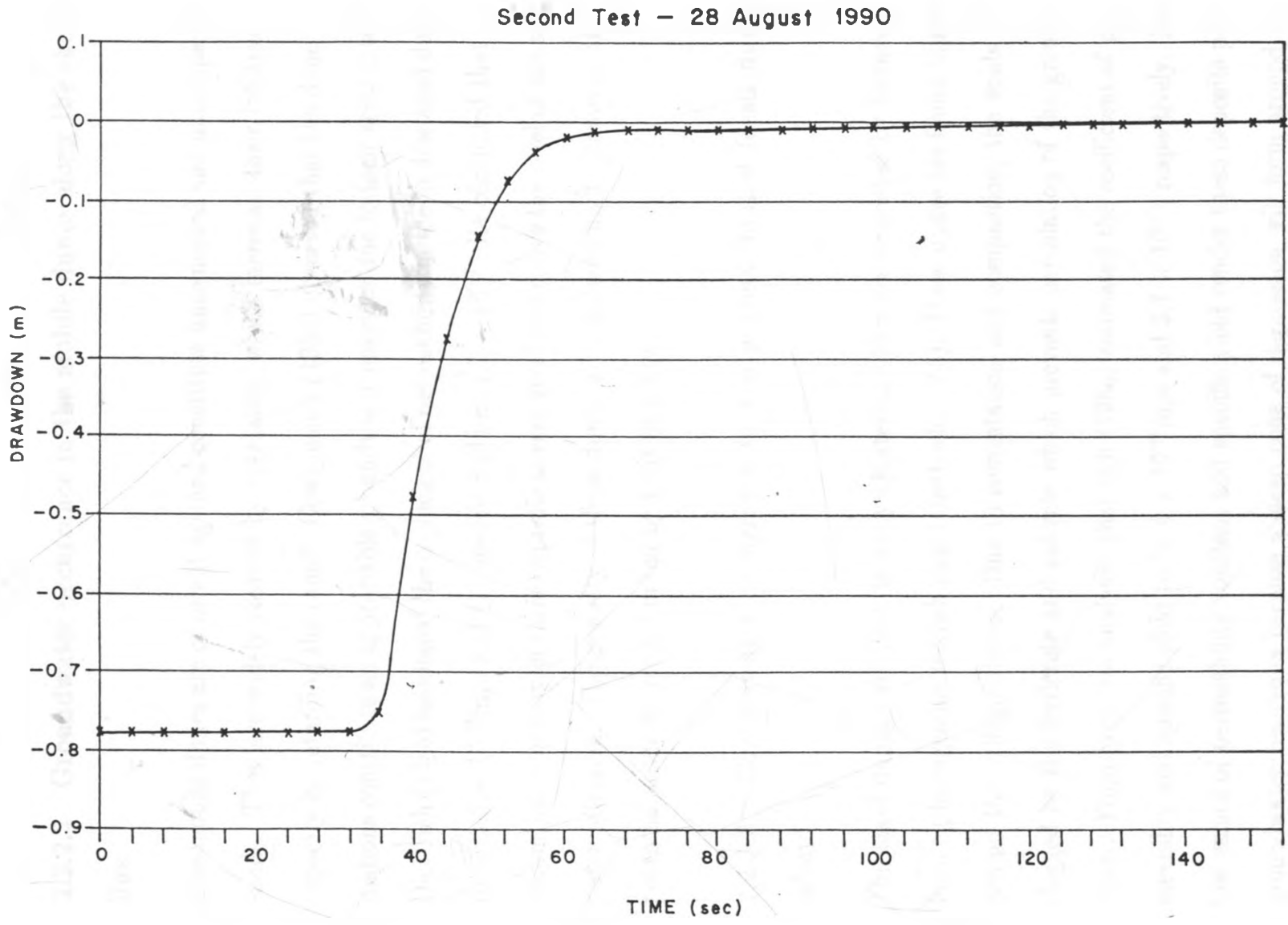
Fig. 2.2 (b)   Pump test and recovery test for borehole C-7347

(ii) unconsolidated fossil dunes inland, and (iii) isotropic fossil coral reefs inland.

2.2.2.2 Groundwater occurrence in the mobile dunes along the shoreline

The mobile dunes are of recent age and constitute uncemented and uncompacted sands. They are widely covered by vegetation which increases their infiltration capacity by retarding the runoff. Cowiconsult (1983) observed that the dune formations constitute an appreciable groundwater reservior due to their areal extent. Diettrich (1985) estimated the coefficient of permeability in the mobile sand dunes to be 3.6×10^{-4} m/s and the specific yield as 1.7×10^{-7}. He concluded that the groundwater quality in these deposits is very good and above the level of the salt-water intrusion. The porosity of these dunes is considered high. However, their potential water source is limited by their mobility.

2.2.2.3 Groundwater occurrence in the unconsolidated fossil dunes inland

The fossil dunes date back to early Quaternary and are cemented by ferricrete, forming ferrugenous reddish soils (Diettrich, 1985). These dunes are found inland behind the drifting dunes. Due to cementation and compaction, the voids are clogged by the ferricrete and calcrete which prevents percolation of the groundwater. From grainsize analysis, Diettrich (1985) estimated the coefficient of permeability and specific yield to be 4×10^{-5} m/s and 3.7×10^{-3}, respectively. The low values of permeability constant and specific yield render these deposits poor groundwater reservoirs because a steep cone of depression will form around the well and may reach the interface. Besides, the low permeability and porosity re-

31

duces the infiltration rate and storage capacity necessary for the formation of an adequate freshwater layer.

2.2.2.4   Groundwater occurrence in the isotropic coral reef inland

It was observed (Cowiconsult, 1983) that, where present and extensive, the reef formation offers good reservoir conditions. The fossil coral reefs are observed in aerial photographs as a line of pans. These pans are karstic sinkholes filled with silty debris and are found in an irregular pattern inland. The fossil coral reefs have been sedimented by clays or fine sand. Some of the reefs form channels draining water from the adjoining formations. Their areal extent range from approximately 100 to 25,000 m^2, hence the specific yield is limited. Diettrich (1985) estimated the coefficient of permeability and specific yield to be 7.9×10^{-3}m/s and 5.5×10^{-6}, respectively. This high coefficient of permeability gives the coral reefs a high drainage capacity. Where reefs have contact to the interface, the salinity of the water is high. This is the most common phenomenon in the Lake Kenyatta Settlement area, thus, about 80% of the area is unsuitable for well sites due to interaction of the groundwater aquifer and the saltwater at the interface. Some of the water from wells dug into coral reefs with clay have a soda taste and a milky colour due to high pH values accelerating inorganic contamination.

The groundwater potential of the reservoirs in the sand dunes and coral reefs may therefore be seen as dependent on: (1) volume of the reservoir, (ii) freshwater table elevation, (iii) replenishment of the reservoir, (iv) porosity of the reservoir formation, (v) natural discharge, and (vi) evapotranspiration rates. Bodies of impermeable material (clays, clayey sands and silts) and layers within the formation will affect the reservoir capacity as well as influence the flow pattern. Besides,

presence of buried coral reefs influences the volume and reservoir hydrogeologic conditions considerably.

Due to karstification, the secondary porosity and permeability of the fossil reefs are very high. In places where freshwater recharge by rainwater percolation and channel infiltration is greater than evaporative losses, such cavitied limestone functions as an excellent aquifer, thus depressing the saltwater/freshwater interface. It is therefore evident that the fossil coral reefs are the most significant fresh groundwater aquifers, as their cavitied structure facilitates decomposition and karstification.

2.2.2.5 Groundwater occurrence in the recent deposits

Due to their unconsolidated nature, porosity and permeability are high, providing a favourable environment for perched fresh groundwater aquifer system above the saltwater/freshwater interface, perhaps at sufficient depth to limit evapotranspiration losses through vegetation and capillary action. In the estuarine areas with frequent saline inundations, no freshwater is to be expected, while freshwater alluvium is unlikely to yield adequate quantities due to the shallow saltwater/freshwater interface.

2.2.3 Water table elevation

The importance of the movement and configuration of the water table in assessing the total and exploitable water reserves in the settlement area cannot be overemphasized. The shape of the water table allows information about the transmissivity and the natural discharge to be discerned. Cowiconsult (1983) noted that freshwater forms a line-shaped body floating on the saline seawater in the sand dunes

which rest on permeable formations. The size of such a freshwater body will depend on the geographical extent of the permeable formations and the elevations of the freshwater table above the mean sea level. Replenishment of the reservoir occurs through infiltration of precipitation, thus it is a crucial factor for the long-term exploitation of the groundwater resources. Observation of the water table fluctuations, rainfall, evapotranspiration, runoff and infiltration rates can be correlated in order to arrive at realistic values of the parameters necessary for the prediction of future natural recharge of the reservoirs. The natural discharge from the reservoirs is governed by the water table elevation and formation hydrogeological parameters.

2.2.4   The saltwater/freshwater interface

Marine saltwater intrusion presents a predominant problem in the exploitation of groundwater resources in the area. The phenomenon derives from the marine saltwater intruding with a gentle dip landwards depending on the type of formation and the hydrogeological conditions. The depth of the saltwater/freshwater interface varies considerably. Saltwater intrusion in the Lake Kenyatta Settlement Scheme wells is mainly caused by: (i) sinking the wells too dip, (ii) high rates of abstraction, (iii) frequent intervals of discharging the wells, (iv) small well diameters, (v) high evapotranspiration rates, and (vi) narrow aquifer boundaries. The latter cause is considered the most common in the area. The problem of saltwater intrusion is further complicated by the presence of fossil saltwater buried during sporadic periods of sea regressions and transgressions in the past. Cowiconsult (1983) concluded that the high content of chloride in the inland wells is caused by salts that have remained in the soil since it was deposited in the sea water. While

it is suggested that there is fossil groundwater in existence, its monopoly as the sole cause of salinity in the groundwater is obviously nullified by the observed increases in electrical conductivity in wells during dry seasons and decreases during wet seasons, which suggests a hydrodynamic saltwater/freshwater interface.

2.2.5 Water Balance

2.2.5.1 Introduction

The qualitative water balance presented below (Fig 2.3) aims at showing the factors that interplay in the Lake Kenyatta area hydrologic system. The water flows are indicated by letter Q. Although some of the factors can be derived from the available data, e.g., rainfall, thickness of aquifer, surface area of the lake, etc., no attempt whatsoever has been made to estimate the magnitude of the various hydrologic components. The various water flows are as follows (GSK, 1990):-

Q_1 - Rainfall on area comprised by aquifer system excluding lake surface.

Q_2 - Rainfall on lake surface.

Q_3 - Infiltration into the soil.

Q_4 - Evapotranspiration by soil and vegetation.

$Q_5(a)$ - Runoff into the lake.

$Q_5(b)$ - Runoff not into the lake.

Q_6 - Deep percolation into aquifer.

Q_7 - Evaporation from lake surface.

Q_8 - Groundwater discharge from aquifer into the lake.

Q_9 - Lake water discharge into aquifer.

Q_{10} - Surface water discharge from lake.

Other parameters of use in the water balance considerations:

35
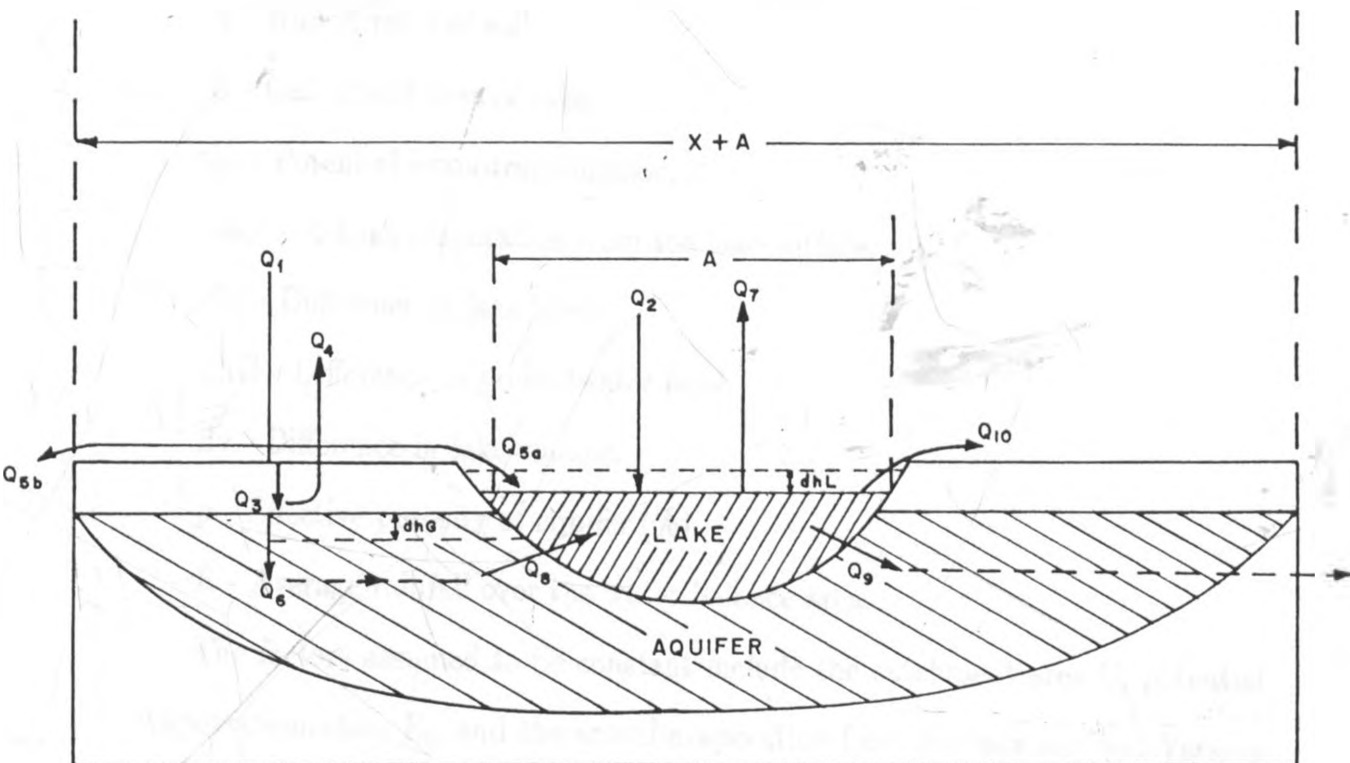
Fig. 2.3   Water balance

A - Surface area of lake.

V - Volume of lake.

X - Surface area of aquifer system outside lake surface.

V - Runoff ratio of soil.

C - Catchment area of lake.

E_0 - Potential evapotranspiration.

Eact - Actual evaporation from the lake surface.

dhl - Difference in lake level.

dhG - Difference in groundwater level.

dv - Difference in lake volume.

p - Effective porosity of aquifer (%)

R - Average rainfall over the water balance area.

The factors assumed to be constant include the catchment area C, potential evapotranspiration E_0, and the actual evaporation from the lake surface. Various situations will be discussed.

2.2.5.2 Water balance during dry period

In this case,

$$0 = Q_5(a) = Q_{10} = Q_1 = Q_3 = Q_4 = Q_5(b) = Q_6.$$

The water balance for the lake is

$$dhl \times A = Q_5(a) + Q_2 + Q_8 - Q_{10} - Q_7 - Q_9 = Q_8 - Q_7 - Q_9.$$

In this situation there is no recharge of aquifer by the lake water. Thus,

$$Q_9 = 0.$$

Thus,

$$Q_8 = Q_7 + A \times dhl.$$

2.2.5.3 Water balance during wet periods with lake water level higher than the ground water levels

In this case there is no groundwater flow into the lake since the lake levels are higher than the groundwater levels around the lake. Thus, the lake water is recharging the aquifer. The water balance for the lake is:

$$Q_8 + Q_5(a) + Q_2 - Q_7 - Q_{10} - Q_9 = dV.$$

Now

$$Q_8 = Q_{10} = 0,$$

therefore

$$Q_5(a) + Q_2 - Q_7 - Q_9 = dV.$$

Note that in this case there is no overflooding. If overflooding occurs, then Q_8 is present and thus

$$Q_8 + A_5(a) + Q_2 - Q_7 - Q_9 = dV.$$

2.2.5.4 Soil infiltration

The infiltration into the soil (Q_3) is equal to the rainfall minus the surface runoff, i.e.,

$$Q_3 = Q_1 - (Q_5(a) + Q_5(b)).$$

The infiltration into the soil is high as evidenced by the generally flat topography, lack of drainage channels and the high porosity and permeability of the sandy soil.

2.2.5.5 Deep percolation

The determination of the amount of deep percolation, it involves the monitoring of the changes in groundwater levels and rainfall distribution and the estimation

of the amount of surface runoff and evapotranspiration. It is a complex task which might give some very erroneous outcome. However, it can be stated that

$$Q_3 = Q_4 + Q_6.$$

Thus

$$Q_6 = Q_3 - Q_4.$$

2.2.5.6 Evapotranspiration by soil and vegetation

Though hard to quantify, it is obvious that lateral flow of the infiltrated ground-water in the sandy clays overlying the coral aquifer is negligible. Therefore

$$Q_3 = Q_4 = Q_6,$$

from which

$$Q_4 = Q_3 - Q_6.$$

2.2.5.7 Overflow of the lake

Surface water discharge from the lake is quite rare. At 8.14 metres above mean sea level, the lake discharges water by overflow. It is noted that in 1986 and 1987, the lake reached a level of about 6 metres above mean sea level and 4.6 metres above mean sea level, respectively. Long-term records of the lake level are not available, thus posing a definite problem in any attempt to quantify the possibility of the lake surface overflow. From the foregoing, it may be observed that the hydrological cycle of the Lake Kenyatta area is a normal one for tropical terrains with a thick soil cover, dense vegetation cover and limited runoff. Most of the water percolates into the soil while only a small percentage runs off. Most of the infiltrared water percolates only a few metres into the soil. The top part of infiltrated water stored as soil moisture is absorbed by roots of vegetation and

39

evapotranspired by the plant leaves. The deeper part of soil moisture rises through capillarity and reach the plant roots. Only a small portion of the water infiltrated into the soil percolates below the vadose zone, below the reach of the plant roots and capillarity to replenish the groundwater storage. It is noteworthy that the amounts of Q_8 and Q_9 vary significantly with variation in the lake levels. At high lake levels the infiltration of lake water into the aquifer exceeds the discharge from the aquifer into the lake, while with lower lake levels more groundwater will flow into the lake than out of the lake. It is obvious that no permanent lake can exist without a substantial groundwater storage beneath it. The long term average annual evaporation of approximately 3 mm^3/year (GSK, 1990) from the lake is approximately equal to the average annual rainfall on the lake surface plus the average annual runoff which recharges the lake. It can be concluded that the fluctuations from year to year are compensated by increase or decrease in water stored underground.

Chapter 3

BASIC THEORY

3.1   Choice of survey method

Various geophysical methods have in the past been applied in groundwater investigations. Zohdy et al. (1974) identify the standard methods as telluric, seismic, magnetotelluric, induced polarization, electromagnetic, magnetic, spontoneous polarization, gravity and resistivity. The magnetotelluric and telluric methods have not been extensively used in groundwater investigations, but they can be of importance in reconnaissance studies of large basins. The magnetic method has been used and found good in the exploration of basaltic aquifers. The spontaneous polarization (SP) method has been used in detecting leaks in surface water reservoirs and canals, while the induced polarization (IP) method is very useful especially as ι complementary method to the resistivity method.

The gravity method is useful in locating buried river channels where density ιntrasts are remarkable. It is a cheap, rapid and inexpensive method of deter- ιning the location of the buried channel in terrains where there is a density ιtrast between the aquifer and the underlying bedrock. The seismic method is ful in groundwater exploration especially in the determination of the overbur-

den overlying consolidated material. It has also been used to delineate the depth to the aquifer, and location of fractures and fault zones. Of necessity, the overburden must be of low seismic velocity as compared to the bedrock for the seismic method to be applicable. It may therefore be used to complement the resistivity method whose resolution deteriorates when the resistivity of the overburden and bedrock are nearly equal. The major disadvantages of the seismic method are its low sensitivity to grading of formations and alteration and its high cost. However, the method is widely used because it yields unique and unambiguous results.

Though originally developed primarily for mineral exploration, the electromagnetic (EM) methods have been widely adopted for groundwater exploration. It is advantageous to the resistivity method especially in areas with a highly resistive surface layer (e.g. sand) since, in the EM method, no contact resistivity is experienced due to its inductive principle. In this particular study, detection of the saltwater and clay layers would be easily undertaken using the EM method. The disadvantage of the method is that it experiences the problem of skin depth. Of the various geophyphical methods, the direct current (D.C.) electrical method (or resistivity method) has been the most commonly used technique in groundwater investigations. It is known that the resistivities of rock formations depend largely upon the amount of water, the salinity of water (i.e., the total dissolved solids in water) and the distribution of water in the rock, i.e., porosity and permeability. Saturated rocks have lower resistivities than unsaturated and dry rocks. The higher the porosity of the saturated rocks the lower its resistivity; and the higher the salinity of the saturating fluids, the lower the resistivity. The presence of clay and conductive minerals also reduces the resistivity of the rock. Therefore, the resistivity method can be used to provide information on the occurrence of

aquifers. It has been used extensively in parts of the world (Morris, 1964; Zohdy, 1974; Parasnis, 1979; Carruthers, 1985; Fetter, 1980) and proved successful.

The D.C. resistivity method which provides information concerning the electrical properties of the subsurface is particularly well suited for this investigation. The significant difference in the conductivity of fresh and saltwater results in good sounding resolution, making recognition of geological formations and estimating their water quality relatively unambiguous. Surface measurements of resistivity can be used to estimate the porosity and permeability of aquifers (Griffiths, 1976).

Barker (1981) observed that passage of electric current through rocks takes place by ionic conduction in the groundwater contained in pores and fissures. An increase in salinity of the groundwater leads to a corresponding decrease in rock resistivity and this effect is most noticeable in relatively clay-free rocks. For this reason, the electrical sounding method is the most suitable for investigating salinity (Barker, 1981). Cnudde (1976) noted that resistivity sounding is an important tool for detection of saline layers in aquifers. He concluded that resistivity soundings and traverses are important aids for the mapping of depth, thickness and degree of salinization of groundwater. The resistivity method has been successfully applied in delineating saltwater/freshwater aquifers in the West African Coast and to determine the volume of freshwater sand (Mathiez and Huot, 1984). The method has been recommended for groundwater exploration (Mwangi, 1981; Barongo 1989; Mathenge, 1989).

The resistivity method is a unique method in mapping the freshwater/saltwater interface whereas neither the gravity, the magnetic nor the seismic method can supply such information (Breusse, 1963; Zohdy, 1980; Van Dam, 1976). They concur that clay layers which sometimes confine fine sandy aquifers can easily be detected

by the resistivity method. Breusse (1963) expressed its credibility and advantage over other methods: "The resistivity method is characterized by its easy operation, flexibility, fast adaptation to varied problems and is economical". The method is also based on sound mathematical and scientific theory so that data can be collected and interpreted with a fair degree of accuracy. Alternating current (A.C.) is not usually used due to the skin effect, such that the current mainly tends to confine at the surface of the earth, thence, obliterating the current flow pattern in the subsurface, whereby the alternating current decreases exponentially with depth. This causes a rapid decrease in current density with depth, and consequently a shallower depth of penetration. The skin effect is more pronounced at higher frequences and larger resistivity contrasts. Thus, for optimum penetration, low frequencies should be used whenever the A.C. resistivity method is applied.

Barker et al. (1988) noted that the EM profiling and resistivity sounding techniques give reliable and consistent information on changes in the subsurface layering and lithology; the two methods are faster and cheaper than any other techniques. The observations were made during a geophysical borehole siting in the Victoria province, Zimbambwe, in 1983. Barker (1981) concluded that sounding techniques are ideally suited to the investigation of subhorizontal features in the subsurface using ABEM SAS 300 digital terrameter. He observed that this method greatly reduces the effects on the sounding curve of near-surface lateral resistivity variations and allows checks to be made in the field on the reliability of the data obtained.

Zohdy et al. (1974) noted that in H, A, KH, HA and similar type sections, the terminal branch on the sounding curve often rises at an angle of 45, indicating igneous or metamorphic rocks of very high resistivity (>1000 Ωm). In the presence

of conductive sedimentary rocks saturated with saltwater (ρ<5 m), the so-called "electric basement" of high resistivity rocks may correspond to sandstones or limestones having resistivity of only 200-500 Ωm. He noted that increases in the value of longitudinal conductance S from one sounding station to the next indicates an increase in the total thickness of the sedimentary section, a decrease in average longitudinal resistivity ρ_L or both. Zohdy (1980) mapped successfully the freshwater/saltwater interface in south-west United States with Schlumberger and equatorial electrical soundings. The apparent resistivity contour of 10 ohm-m delineates qualitatively the area where mineralized groundwater is to be expected at shallow depth. It was observed that resistivity less than 10 Ωm belong to the saline groundwater while clay layers have resistivity 0.5 - 5 Ωm. In view of the advantages of the method and its applicability to the objectives set for the study, it was chosen to be used.

3.2 The direct current electrical method

3.2.1 Introduction

The direct current electrical method was first applied in 1912 by Conrad Schlumberger whose pioneer work has been described by Kunetz (1966). It is based on the effect of subsurface variation in conductivity on the current flow within the earth and hence the electric potential distribution. The effect on the potential at the surface is dependent on the size, shape, location and electrical resistivity of the subsurface formation. Information on the subsurface distribution of these formations can therefore be derived from potential measurements at the surface. The theory of vertical electrical soundings (VES) is sufficiently documented in numerous geophysics texts such as Telford et al. (1990),Keller and Frischknecht (1966),

Parasnis (1979), Grant and West (1965), Zohdy (1980) among many others.

In performing a vertical electrical sounding, a commutated direct or very low frequency (<1 Hz) alternating current is passed into the ground by means of two electrodes and the potential difference between a second pair between these is measured. From the potential difference, the current and the electrode seperation, the apparent resistivity can be calculated. To investigate the subsurface variation in formation resistivities and thicknesses, the distance between the current electrode is expanded so as to increase the depth of penentration of the current. The potential electrodes are also changed at desirable intervals to stabilize the current and ensure high sensitivity and resolution.

In a homogeneuos and isotropic formation, the calculated apparent resistivity corresponds to the true resistivity of the formation. The apparent resistivity values are plotted for various electrode spacings as curves. These curves are matched with pre-determined standard master curves and to computer generated curves for a model consisting of a number of layers. Determination of subsurface resistivity variations from the VES measurements can furnish information on the structure, composition and vertical distribution of lithologic formations.

3.2.2   Basic assumptions

The theory of the vertical electrical sounding is based on the following basic assumptions (Koefoed, 1979):

(1) The subsurface comprises a sequence of horizontally stratified layers.

(2) Each of the layers is homogeneous and isotropic.

(3) Vertical interfaces and lateral resistivity inhomogeneties are non-existent.

(4) The current is passed into the ground by a point source located at the

surface of the earth and generates the field.

These assumptions form the basis for the formulation of the theory and interpretation of resistivity sounding data assuming ideal models.

3.2.3 True and apparent resistivity

If measurements were to be made over an infinite or semi-infinite space of homogeneous and electrically isotropic medium fulfilling the assumptions discussed in section (3.2.2), the resisitivity value computed from field measurements would be the true resistivity of that medium. However, in real practice, measurements are made over inhomogeneous and anisotropic medium in which case the measured potential difference will be different from the one measured over a homogeneous material, hence, the calculated ρ from the field measurements is called apparent resisitivity ρ_a. It is equal to the true resisitivity only when the latter is uniform throughout the subsurface. The apparent resisitivity ρ_a is only a crude average of the true resisitivity, which is a function of several variables.

3.2.4 Apparent resistivity and potential distribution in the earth

Zohdy et al. (1974) and Kunetz (1966) defined the resistivity of an earth material as the resistance of a sample of the material of unit cross-sectional area and unit length. The unit commonly used is ohm-metre (Ωm). The potential at a point refers to the potential difference between the given point and some relatively distant point. This is the parameter which is measured in electrical surveys.

Suppose a point current source at the surface of an isotropic homogeneous half space conducts an electric current which flows radically outwards perpendicular to a hemispherical surface. For a current I passed into such a homogenous and

isotropic earth of infinite extent and resistivity ρ, the potential V due to this current at a distance R is

$$V = \frac{I\rho}{2\pi r} \qquad (3.1)$$

If we consider a pair of current electrodes in which A puts a current into the ground and B removes it, the potential difference ΔV measured between two potential electrodes M and N is

$$\Delta V = \frac{\rho I G}{2\pi} \qquad (3.2)$$

where

$$G = \frac{1}{AM} - \frac{1}{BM} - \frac{1}{AN} + \frac{1}{BN} \qquad (3.3)$$

and

ρ = apparent resistivity

Therefore

$$\rho = K\frac{\Delta V}{I} \qquad (3.4)$$

where $K = 2\pi/G$ is the geometric factor.

In the case of soil and rock, one almost invariably measures the apparent resistivity, since one usually deals with superimposed layers of different lithological composition and a liquid and gaseous phase in addition to the solid phase each of which affects the electrical conductivity.

Electrodes A, M, N and B are placed in the ground in a straight line (Fig. 3.1). A and B are the current electrodes. Thus, the current flows between the points
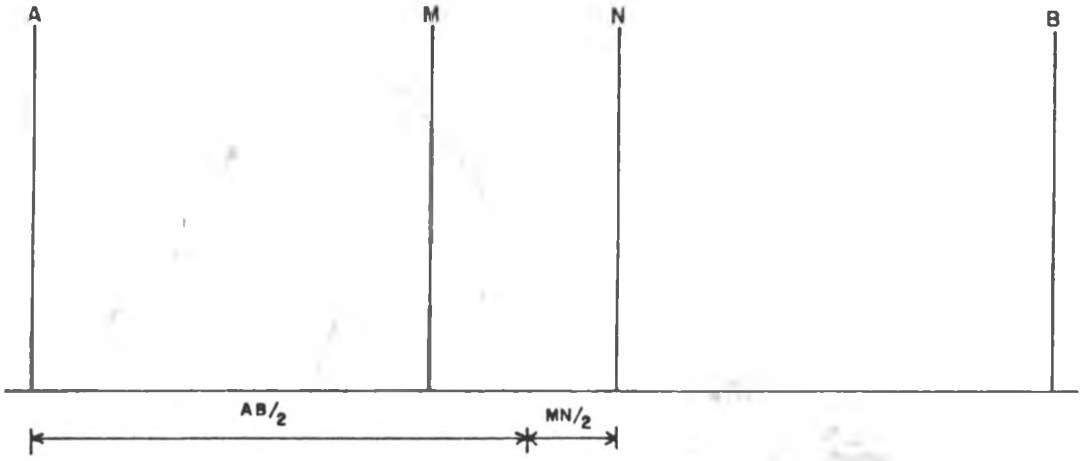
Fig. 3.1   Electrode arrangements in a straight line on the ground surface
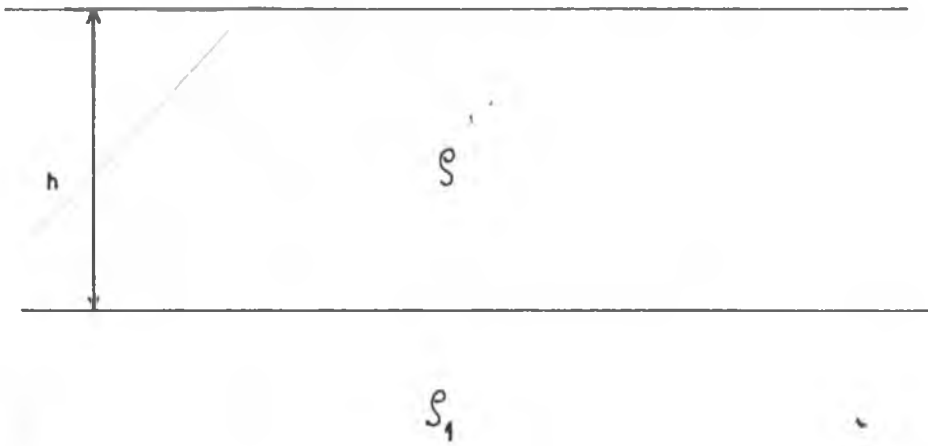
Fig. 3.2   Different layer thicknesses and resistivities vertically downwards

(a)

(b)
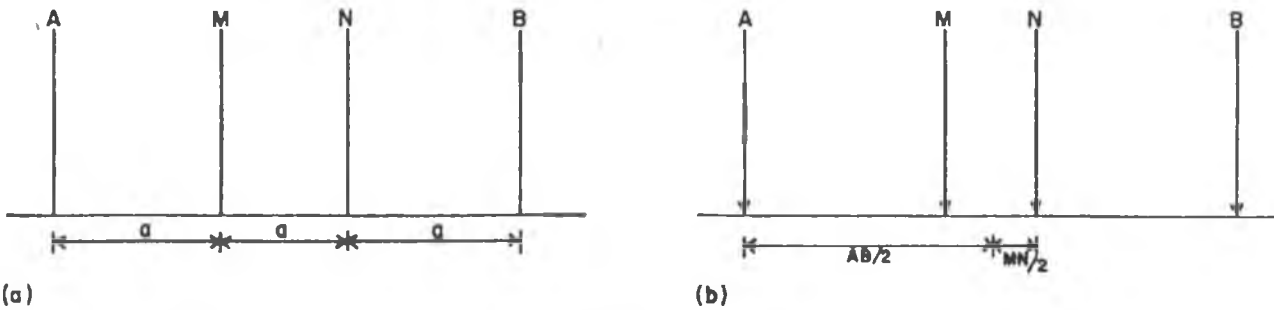
Fig. 3.3 (a)   Electrode arrangement in the Wenner configuration

Fig. 3.3 (b)   Electrode arrangement in the Schlumberger configuration
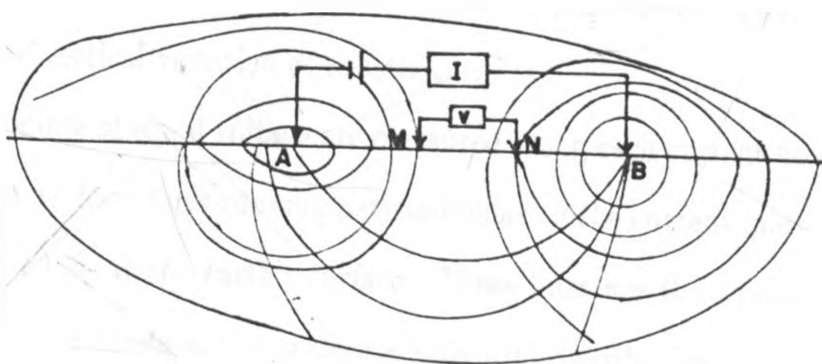
Potential lines and current flow lines below the earth's surface (After Flathe and Leibold, 1976)

as shown in Figure 3.4. The intensity of the current is measured between the two points using an Ampere-meter. When AB is much smaller than the thickness of the first layer h (Fig. 3.2), most of the current is distributed in the layer and ρ_a is equal to ρ_1. However, as AB is increased, some of the current penetrates into the second layer so that the potential difference is due to both layers. As AB is further increased, the current penetrates deeper into the second layer and the potential difference would approach that measured without the top layers. Hence ρ_a tends to ρ_2. This process of expanding the current electrodes while keeping the midpoint of the configuration fixed is called the vertical electrical sounding (VES). It reveals the vertical variation of resistivity.

Now if points of equal voltage are measured along each current flow line in the ground, then we have lines running perpendicular to the current lines, and ending with a right angle at the earth's surface. These lines are the equipotential lines (Fig. 3.4). There exists at the surface a potential distribution depending on the subsurface resistivity which is measured between M and N using a voltmeter. It is a measure of the current density below the earth's surface whose change will proportionally cause changes in the distribution. The algebraic addition of the potential set up by each electrode A and B yields the equation

$$V = \frac{\rho I}{2\pi}(\frac{1}{AM} - \frac{1}{BM} - \frac{1}{AN} + \frac{1}{BN}) \tag{3.5}$$

Thus,

$$\rho = \frac{\Delta V}{I}(\frac{2\pi}{\frac{1}{AM} - \frac{1}{BM} - \frac{1}{AN} + \frac{1}{BN}}) \tag{3.6}$$

51

3.3 Electrode configurations

The electrode configurations used in electrical methods are well documented in the geophysical literature (e.g. Keller and Frischknecht, 1966; Kunetz, 1966; Parasnis, 1979; Telford et al., 1990; Koefoed, 1979) but the most popular for vertical electrical sounding are Wenner and Schlumberger arrays.

In the Wenner configuration, four electrodes A, M, N, and B are placed in the ground along a straight line (Fig. 3.3 (a)) so that AM = MN =NB=a. For this array, (3.11) reduces to

$$\rho_a = 2\pi a \frac{\Delta V}{I} \tag{3.7}$$

In the Schlumberger array (Fig. 3.3 (b)), the four electrodes are placed such that AM = NB and MN is small compared to AB. The apparent resistivity in this array is given by

$$\rho_a = \pi \left(\frac{(AB/2)^2 - (MN/2)^2}{MN} \right) \frac{\Delta V}{I} \tag{3.8}$$

If MN $\ll$ AB, (equation 3.13) is approximately

$$\rho_a \approx \pi \frac{(AB/2)^2}{MN} \frac{\Delta V}{I} \tag{3.9}$$

3.4 Layered earth

If we assume the subsurface consists of horizontal layers, the layers are described by their geo-electric layer parameters, resistivities and thicknesses. Consider a two-layer earth in which a homogeneous and isotropic layer of resistivity ρ_1 and thickness h overlies a second layer of resitivity ρ_2 of infinite thickness. The potential

V at a point P a distance r from a point current source C on the surface is obtained by the electric images method and is given by

$$V(r) = \frac{I\rho_1}{2\pi r}(1 + \sum_{n=1}^{\infty} \frac{2K^2r}{(r^2 + 4n^2h_1^2)^{1/2}})$$
(3.10)

where

$$K = \frac{\rho_2 - \rho_1}{\rho_2 + \rho_1}$$
(3.11)

Equation 3.15 can be expressed in an integral form

$$V(r) = \frac{I\rho_1}{2\pi r}(1 + 2r \int_0^{\infty} Q(\lambda, K, h)J_0(\lambda r)d\lambda)$$
(3.12)

where

$$Q(\lambda) = \frac{K exp(-2h_1\lambda)}{[1 - K exp(-2\lambda h_1)]}$$
(3.13)

where Jo is the Bessel function of order zero and λ is a factor of integration.

Equation 3.17 is obtained by considering three boundary conditions (Sandberg,1979).

1) The potential in the second layer due to the point electrode goes to zero as h_1 tends to infinity.

2) There is potential continuity across the interface

3) The normal current density across the interface is continuous.

53

3.5 Interpretation theory

3.5.1 Introduction

Apparent resistivity curves can be interpreted both quantitatively and qualitatively. In the quantitative interpretation of the observed ρ_a sounding curves, the number of layers and their respective resistivities and thicknesses are determined. These layer parameters may be determined using indirect methods of interpretation by matching the observed apparent resistivity curves with master curves, or by using approximate methods to improve the fit iteratively or by computing model curves which fit the data curve.

3.5.2 Types of curves

The sounding curve obtained in the case shown in Figure 3.2 is a two-layer curve with ρ_a equal to ρ_1, for small AB/2 and a ending or descending to assymptotic value ρ_2. For the Schlumberger array, values of ρ_a/ρ_1 plotted against AB/2 for values of ρ_2/ρ_1 from 0 to ∞ form a set of two-layer master curves (Appendix 1). Inclusion of a second layer of resitivity ρ_2 and thickness h_2 enclosed by the top layer (ρ_1, h_1) and the bottom layer of resistivity ρ_3 of infinite thickness would form types of apparent resistivity curves:

$\rho_1 < \rho_2 > \rho_3$ K-type, Maximum

$\rho_1 < \rho_2 < \rho_3$ A-type, Double ascending

$\rho_1 > \rho_2 < \rho_3$ H-type, Minimum

$\rho_1 > \rho_2 > \rho_3$ Q-type, Double descending

These curve types can be constructed for various values of ρ_2/ρ_1, ρ_3/ρ_1 and h_2/h_1 forming the three-layer master curves. When the number of layers exceeds three they form an extension of three-layer type. For example, a four-layer curve

with the combination $\rho_1 > \rho_2 < \rho_3 > \rho_4$ is a HK-type. Similarly, a four-layer curve with a combination $\rho_1 > \rho_2 < \rho_3 < \rho_4$ is a HA-type. If $\rho_1 > \rho_2 > \rho_3 < \rho_4$ then it is a QH-type.

3.5.3 Curve matching (Approximate method)

The curve matching procedure employed in this study is the auxiliary point method. This is the most commonly used preliminary multi-layer interpretation approximate method (Zohdy, 1965; Orellana and Mooney, 1966; Keller and Frischknecht, 1966; Koefoed, 1979). It was initially published by Ebert (1943) and has been subsequently modified by several authors (Cagniard, 1952; Orellana and Mooney, 1966; Koefoed, 1968; Bhattacharya and Patra, 1968). The method entails matching the branches of the field curve to two- or three-layer master curves successively. The position on the sounding curve at which the abscissa and ordinate of the master curve are unity is marked. The abcissa value of the data curve at the marking is equal to thickness h_1 of the first layer and the ordinate corresponds to ρ_1. The resistivity of the second layer is the product of ρ_1 and the ratio ρ_2/ρ_1 which identifies the master curve. As each segment of the curve is interpreted, the layers comprising the fitted segment(s) of the sounding curve are lumped together to form a fictitious layer with a lumped resistivity ρ' and thickness h'. Consider a three-layer case (ρ_1, ρ_2, ρ_3) with $h_2 \gg h_1$. For small current electrode separations, the sounding curve will be nearly the same as a two-layer case with the same ρ_2/ρ_1. For large separations, the current penetration is deeper and the sounding curve obtained is virtually the same as for a two-layer case with an overlying layer of thickness $h' = h_1 + h_2$ and resistivity ρ' given by $h'/\rho' = h_1/\rho_1 + h_2/\rho_2$. The fictitious layer helps to fit the other segments to a two-layer master curve. Solutions of

55

ρ' and h' for possible values of h_2 for the fictitious layers are presented as auxiliary point graphs that are empirically determined from three-layer curves and plotted on logarithmic scale of the same modulus as the master curve. The application of the auxiliary point method to obtain initial parameters is illustrated in section (5.3) by examples.

3.5.4 Kernel function and resistivity transform

The potential at a point on a two-layer model is given by equation 3.17. The potential over an n-layered earth was derived by Stefanescu (1930) as

$$V_n = \frac{I\rho_1}{2\pi} \int_0^\infty (1 + 2Q(\lambda)) J_0(\lambda r) d\lambda \qquad (3.14)$$

which is of the same form as equation 3.17 because

$$\int_0^\infty J_0(\lambda r) d\lambda = \frac{1}{r} \qquad (3.15)$$

$Q(\lambda)$ in equation 3.18 is called the Kernel function of resistivity and contains information on the layer parameters, resistivities and thicknesses, of all the layers.

Equation 3.14 can also be expressed in the form

$$\rho_a = -\frac{2\pi r^2}{I} \left(\frac{\partial V}{\partial r}\right) \qquad (3.16)$$

where r = AB/2. The term $\partial V/\partial r$ in equation 3.21 can be obtained by partial differentiation of equation 3.19 taking into account

$$\frac{\partial}{\partial r} \{J_0(\lambda r)\} = -\lambda J_1 \lambda r \qquad (3.17)$$

where J_1 is the Bessel function of order one. For Schlumberger configuration, the equation of the apparent resistivity is therefore

56

$$\rho_a = \rho_1 r^2 \int_0^\infty (1 + 2Q(\lambda))J_1\lambda d\lambda \tag{3.18}$$

Equation 3.23 can be rewritten as

$$\rho_a = r^2 \int_0^\infty T(\lambda)J_1(\lambda r)\lambda d\lambda \tag{3.19}$$

where

$$T(\lambda) = \rho_1(1 + 2Q(\lambda)) \tag{3.20}$$

$T(\lambda)$ is called resistivity transform and is found from the layer parameters by Pekeri's recurrence method. By Hankel transform of equation 3.24 (Bracewell, 1965),

$$T(\lambda) = \int_0^\infty \frac{\rho_a}{r} J_1(\lambda r) dr \tag{3.21}$$

Kunetz (1966) was the first one to note that equation 3.26, or its equivalent, could be transformed to one having the form of a linear convolution integral. This transformation was first utilized by Ghosh (1971a, b)

3.5.5   Computation of ρ model curves

Owing to limited combinations of resistivities and thicknesses and because master curves are available for up to three layers only, some of the sounding curves may not be matched with any of the available master curves. However, theoretical model curves can be computed for these unavailable curves. Vast collections of model curves are available in the published literature. Model curves for three-layer model includes those by Compagnie Generale de Geophysique (1963), The

57

Netherlands Rijkswaterstaat (1975), Homilius and Mundry (1979), Bhattacharya and Patra (1968). For three-layer and four-layer earth models, model curves by Orellana and Mooney (1966), Mooney and Wetzel (1956) and Koefoed (1979). In the present study, two-layer model curves and auxiliary point charts extracted from Bhattacharya and Patra (1968) were used.

Computation of models curves can be done by a number of methods including numerical integration, the point image method, decomposition into partial fractions and the linear filter method (Koefoed, 1979). The computation of ρ_a model curves is almost exclusively performed by linear filter method (Ghosh, 1971a, b). Ghosh(1971a, b) showed that, based on a horizontally layered earth model, a ρ_a model curve can be computed simply by convolution of digital coefficients with the resistivity transform values.

The transform values are calculated from the model layer parameters by the recurrence method. The convolution method, therefore, involves solving equation 3.24. To interpret with computer generated curves, the thicknesses and resistivities which could have produced the field sounding curve are estimated using an approximate method (partial curve matching by the auxiliary point method) and the computer generates the model curve. Since the master curves are available for the two-layer models, an extension is made to interpret multi-layer field curves. Further computational details are presented in Barongo (1989).

3.5.6 The iterative interpretation methods

Iterative methods are based on comparison of the sounding curve with the computed model curve of an assumed layered model. To generate a model curve, initial guess parameters of a sounding curve are obtained by an approximate method as

described in section 3.5.3. If the model curve does not fit the sounding curve, the layer parameters are adjusted and the process repeated until a satisfactory fit is achieved. Adjustment of the layer parameters can be done by human judgement and it improves with experience. This process ia called non-automatic iterative method and constitutes the forward resistivity modelling. Automatic iterative method is one in which the computer adjusts the input layer parameters automatically and the curve fitting procedure is such that the input parameters are recursively convolved and adjusted till the best fit is achieved. This constitutes the inverse method. Koefoed (1979) has discussed the non-automatic iterative method involving judgement on which layer and parameter to be adjusted to improve the fit and the corresponding amount by which the parameters should be changed. He observes that the relative change in the value of the layer parameter must be twice as large as the relative difference between the model curve and the sounding curve. The forward method employed in the study entailed both non-automatic and semi-automatic methods. The semi-automatic method is one in which some of the parameters are fixed while others are automatically adjusted to obtain the best fit. Illustrations of the application of the iterative methods have been presented in sections 5.4 and 5.5.

3.5.7 Inversion theory

Consider a system of linear equations

$$
\begin{aligned}
a_1 x_1 + a_2 x_2 + a_3 x_3 &= d_1 \\
b_1 x_1 + b_2 x_2 + b_3 x_3 &= d_2 \\
c_1 x_1 + c_2 x_2 + c_3 x_3 &= d_3
\end{aligned}
\tag{3.22}
$$

where a,b and c are known coefficients and d is a known quantity while x is an unknown variable (e.g., resistivity or thickness).

To solve for X numerically, we resort to matrix methods. From equation 3.33

$$\begin{pmatrix} a_1 & a_2 & a_3 \\ b_1 & b_2 & b_3 \\ c_1 & c_2 & c_3 \end{pmatrix} \begin{pmatrix} x_1 \\ x_2 \\ x_3 \end{pmatrix} = \begin{pmatrix} d_1 \\ d_2 \\ d_3 \end{pmatrix} \tag{3.23}$$

from which

$$\begin{pmatrix} x_1 \\ x_2 \\ x_3 \end{pmatrix} = \begin{pmatrix} a_1 & a_2 & a_3 \\ b_1 & b_2 & b_3 \\ c_1 & c_2 & c_3 \end{pmatrix}^{-1} \begin{pmatrix} d_1 \\ d_2 \\ d_3 \end{pmatrix} \tag{3.24}$$

Equation 3.34 is of the form $Ax = d$ while equation 3.35 is of the form $X = A^{-1}d$.

From equation 3.24, ρ_a is calculated and this corresponds to d_1, d_2, d_3 ...., responsively, in equation 3.35. We also have the raw field data for each AB/2 station.

According to Barongo (1989), let a set of n observed data be represented by a non-linear functional $F_i(P_j)$, where P_j are the parameters to be solved for. Since inversion theory uses the concept of linear analysis, we must linearize the functional $F_i(P_j)$. This is done using Taylor's series expansion

$$F_i(P_j) = F_i(P_j) + \frac{\partial F_i(P_j)}{\partial P_j} \Delta P_j + \frac{\partial^2 F_i(P_j)}{\partial^2 P_j} \Delta P_j^2 + ... \tag{3.25}$$

Ignoring the second and higher order terms, we arrive at

$$F_i(P_j) = F_i(P_j) + \frac{\partial F_i(P_j)}{\partial (P_j)} \tag{3.26}$$

The relationship between the observed and calculated data can therefore be written as

$$d_i = F_i(P_j) + \frac{\partial F_i(P_j)}{\partial P_j} \Delta P_j \tag{3.27}$$

from which the residual between the observed and calculated data, Δd_i, is obtained as

$$\Delta d_i = d_i - F_i(P_j) = \frac{\partial F_i)}{\partial P_j} \mid_{P_j^0} \Delta P_j \tag{3.28}$$

Letting $(\partial F_i(P_j)/\partial P_j) \mid_{P_j^0} = A_{ij}$, we have

$$\Delta d_i = A_{ij} \Delta P_j \tag{3.29}$$

from which the parameter perturbations, ΔP_j, are given by

$$\Delta P_j = A_{ij}^{-1} \Delta d_i \tag{3.30}$$

For the calculated data to approximate the observed data, we need to make the data residual Δd as small as possible (i.e., $\Delta d \longrightarrow 0$) This is accomplished through the least square inversion method. Since the problem involved in this case is generally non-linear, several iterations are needed in order to arrive at the optimum solution. At each iteration, the calculated parameter perturbation is added to the previous parameter value to obtain a new one. Thus

$$P_j(old) + \Delta P_j = P_j(new) \tag{3.31}$$

The iterative process stops after some condition (such as assigned maximum number of iterations has been reached or convergence has occurred to below a certain given threshold) has been achieved.

The derivative of the matrix A_{ij} can be calculated using any of the well known numerical techniques such as backward, central or forward difference methods. Thus, in the backward method

$$\frac{\partial(A_{ij})}{\partial P_j} = \frac{F_i(P_j) - F_i(P_j + \Delta P_j)}{\Delta P_j} \qquad (3.32)$$

Lack of stability of the inverse matrix is one major problem that tends to cripple inversion of non-linear problems. A thorough treatment of the stability problem is presented by Barongo (1989) who states that the inverse method involves the evaluation of physical parameters (resistivities and thicknesses) of the layered earth model which yield good approximations to the observed results, but these solutions are not unique. Barongo (1989) cites such factors as noisy data and the non-linear nature of the problem as the main causes of instabiltity. Besides, spurious convergence or divergence may occur due to erratic iterative process caused by 'ill-posed' problem as a result of the eigenvalues of matrix A_{ij} being zero or close to zero. Further instability can also be brought about at the linearization stage of the non-linear function of the problem.

3.6   Physical basis of the interpretation of salt-water and freshwater layers

If we assume that the air which occupies the pores is an absolute insulator, while the solid phase a very limited electrical conductor as compared to any soil moisture present in the pores or secondary cavities, the specific layer resistivity R_s may therefore be defined as a function of : the specific resisitivity R_w of the water present in the porespace, the formation factor F, and the level of saturation of the pores with water S_w where $0 < S_w < 1$. The relationship is expressed by Archie's formula

$$R_s = \frac{R_w F}{S_w^2}(ohm - m) \qquad (3.33)$$

with the formation factor F as a function of the angularity of the grains a, where 0.6<a<1.5; the porosity P, where 0<P<1; and the cementation factor m, where 1.5<m<3. We therefore have

$$F = a \times P^{-m}(dimensionless) \qquad (3.34)$$

In the case of clay layers, the conductivity of the clay particles must be taken into account as well, with R_c as the so-called clay factor:

$$\frac{1}{R_s} = \frac{S_w^2}{F \times R_w} + \frac{1}{R_c}(S/m) \qquad (3.35)$$

With complete saturation, that is, below the water table, $S_w = 1$. Similarly, below the saltwater/freshwater interface, $S_w = 1$.

From the electrical conductivity (400-500μS/cm) of fresh dune-water, a resistivity of 20-25 ohm-m can be calculated as follows:

$$R_w = \frac{10000}{Ec}ohm - m \qquad (3.36)$$

where R_w is the absolute resistivity of water and Ec is the electrical conductivity of the water. Therefore $R_w = 10000/400 = 25$ ohm-m or $R_w = 10000/500 = 20$ ohm-m. Thus, assuming a formation factor of approximately 2-3 for fine dune sands, the resistivity of freshwater-bearing layers in the dunes will be approximated to 40-60 ohm-m by using equation 3.24. Similarly, the resistivity of seawater bearing layers can be calculated at around unity as follows: $R\omega = \frac{10000}{EC}$ Ohm-m. The EC of saline water = 10000 μS/cm. Therefore, $R_s = \frac{10000}{10000} \times F = 1 \times 2 = 2$ ohm-m,

where $F = 1$, $R_s = 1$. For this reason, the values observed with low resistivity (0-5 ohm-m) are taken to represent the saltwater bearing formations

Table 3.1. The classification of saline groundwater (after Carroll, 1962)

	T.D.S. mg/l	Ec μS/cm (approx.)
Freshwater	0 - 1000	0 - 670
Brackishwater	1000 - 10000	670 - 6700
Salinewater	10000 - 100000	6700 - 67000
Brine	> 100000	> 67000

T.D.S = Total dissolved solids

Note that

$$\rho_w = 10^2/Ec \qquad (3.37)$$

1mg/l T.D.S. = 1.56 μS/cm Ec for water in the range of 100 - 5000 μS/cm

3.7 Limitations of the resistivity method

3.7.1 Non-uniqueness

The interpretation of a multi-layer sounding curve generally is not unique. This means that a given electrical sounding curve can correspond to a variety of sub-surface distributions of layer thicknesses and resistivities. Other limitations are inherent in the conventional methods of electrical soundings.

3.7.2 Principles of equivalence and suppression

The transverse resistance $T = \rho_i h_i$ and longtitudinal conductance $S = h_i/\rho_i$ are two fundamental properties of a resistivity sounding. Consider the geoelectric section shown in Figure 3.5. If $\rho_1 < \rho_2 > \rho_3$ (K-type) and the resistivity and thickness

where F = 1, R$_s$ = 1. For this reason, the values observed with low resistivity (0-5 ohm-m) are taken to represent the saltwater bearing formations

Table 3.1. The classification of saline groundwater (after Carroll, 1962)

	T.D.S. mg/l	Ec μS/cm (approx.)
Freshwater	0 - 1000	0 - 670
Brackishwater	1000 - 10000	670 - 6700
Salinewater	10000 - 100000	6700 - 67000
Brine	> 100000	> 67000

T.D.S = Total dissolved solids

Note that

$$\rho_w = 10^2/Ec \qquad (3.37)$$

1mg/l T.D.S. = 1.56 μS/cm Ec for water in the range of 100 - 5000 μS/cm

3.7 Limitations of the resistivity method

3.7.1 Non-uniqueness

The interpretation of a multi-layer sounding curve generally is not unique. This means that a given electrical sounding curve can correspond to a variety of sub-surface distributions of layer thicknesses and resistivities. Other limitations are inherent in the conventional methods of electrical soundings.

3.7.2 Principles of equivalence and suppression

The transverse resistance T = $\rho_i h_i$ and longtitudinal conductance S = h_i/ρ_i are two fundamental properties of a resistivity sounding. Consider the geoelectric section shown in Figure 3.5. If $\rho_1 < \rho_2 > \rho_3$ (K-type) and the resistivity and thickness

Fig. 3.5   Geoelectric section of a three-layer earth

of the second layer are such that T remains constant, the apparent resistivity curves in both cases will be equivalent. Similarly, if $\rho_1 > \rho_2 < \rho3$ (H-type), changing the resistivity and thickness of the second layer so that S is constant results in equivalent apparent resistivity curves. In both cases, neither ρ_2 nor h_2 can be determined separately unless h_2 is larger compared to h_1. Theoretically, these curves can be shown to be unique, but due to the measuring errors in practice, they appear to be equivalent (Parasnis, 1979). However, ρ_2 and h_2 can only be changed within certain limits for equivalence to occur. Koefoed (1976) showed that the condition of equivalence as given by T and S are only approximate; in reality equivalence is much more complicated.

If the second layer (Fig. 3.5) has a resistivity intermediate between ρ_1 and ρ_3 its effects on the ρ_a curve is suppressed unless it is thick enough relative to its depth. This is the principle of suppression. A sounding curve obtained over a four- or five-layer section may be nearly equivalent to one obtained over a three-layer section. Generally, this is attributted to the principle of suppression (Maillet, 1947). The error caused by the effect, in interpreting the depth of contacts, is sometimes referred to as pseudoanisoticpy (Gensley and Rouget, 1937; Flathe 1955, 1961).

The principles of equivalence and suppression often lead to ambiguity in the interpretation of ρ_a curves unless either the resistivity or thickness is known, for example, from borehole logs.

3.7.3 Surface and buried inhomogeneities

When conducting a Schlumberger vertical electrical sounding, the potential electrodes MN are fixed for several AB spacings. The potential difference decreases

66

with the increase of AB so that if MN is not increased, the potential would be too small to be measured accurately. In practice then, MN is increased for a set of AB spacings with a two-point overlap. This change in MN causes the Schlumberger sounding curves to be segmented. However, if AB$\gg$MN and the curve slopes steeply, the segments may be seperated by up to 6% of ρ_a. A correction can be applied by shifting the segment (Kunetz, 1966; Zohdy et al. 1974) or by linear digital filtering method (Koefoed, 1979).

Another cause of disjointed segments in Schlumberger ρ_a curves is caused by the presence of near-surface lateral variation (electrode effect) when MN is varied, for fixed AB. The curve can be corrected by shifting, up or down, the segments of the curve. This is an advantage of the Schlumberger configuration over the Wenner configuration. By making crossed soundings (soundings having the same centre but expanded at right angles to one another), it is easy to recognize the presence of lateral inhomogeneties in the su⌐surface. ρ_a curves can be distorted by the presence of buried inhomogeneities, for example, layers of limited extent. The intensity of distortion depends on the size of the inhomogeneity with respect to its depth of burial and the electrode spacing; the resistivity contrast between the inhomogeneity and the surrounding rock, the geometry of the inhomogeneity and the orientation of the array used. Hence, the effects are complicated and sometimes impossible to detect and correct for.

3.7.4 Relative thickness of a layer

The detectability of a layer of given resistivity depends on its relative thickness which is defined as the ratio of the bed thickness to its depth of burial (Zohdy, 1974). The smaller the relative thickness of a given layer, the smaller the chance

of its detectability on a sounding curve.

3.7.5   The skin effect and electrode polarization

The theory demands the use of D.C. current in resistivity measurements. A.C. currents do not penetrate into the deeper layers. This effect, called the skin effect, is greater in the presence of good conductors like clays and can be reduced by use of very low frequency a.c. currents. However, the use of alternating (or commutated) current largely removes the effects of variable self potential (SP) caused by natural (telluric) currents in the ground and also polarization at the potential electrodes. In practice, when d.c. currents are used, the SP must be "backed" off and non-polarizable potential electrodes employed. In this study very low frequency a.c. current was employed, while non-polarizable ceramic pots with copper sulphate solution were used as potential electrodes. In effect, this removed polarization at the potential electrodes, suppressed the skin effect and the effects of the telluric currents.

3.7.6   The resistivity of the rocks

The resisitivity of the rock formation depends largely on the amount of water present, conductivity of the water and the porosity of the rock. Most dry rocks have higher resistivities than water bearing rocks. The higher the salinity of the saturating water, the lower the resistivity. The presence of clays and other conduc
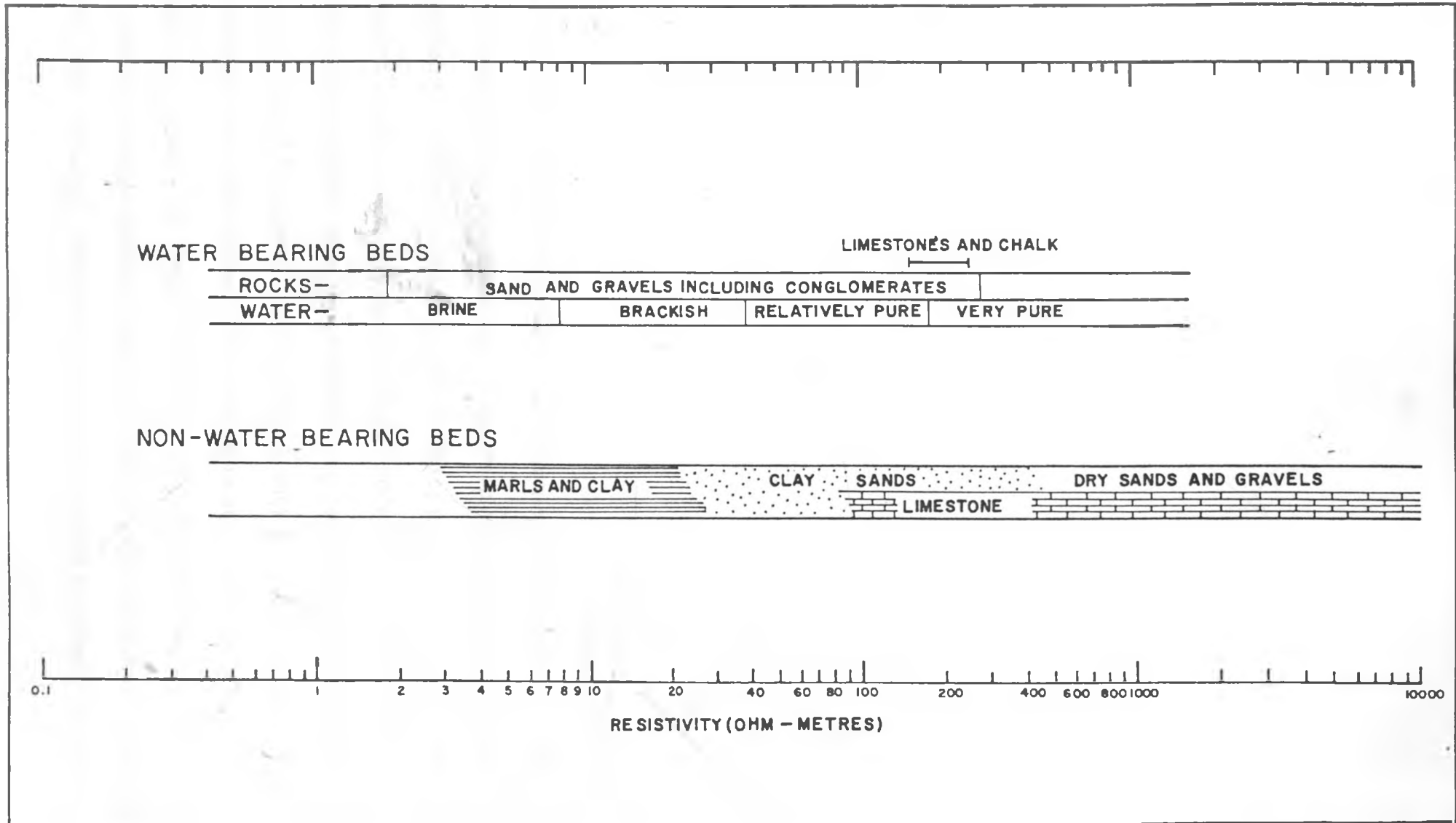
Fig. 3.6 Rock and aquifer resistivities (After Flathe, 1955 and Hunting data files)

tive minerals lowers the resistivity of the rock formations. Therefore, rocks have wide and overlapping ranges of resistivity values. Generalized ranges of some of the rocks have been published in the literature (Keller and Frischknecht, 1966; Parasnis, 1979) (Fig. 3.6). The wide range of rock values enables the distinction between different rock types, thus making resistivity prospecting possible. Thus, sandstones can be distinguished from limestones and sandy aquifers from shales. One setback of the wide, overlapping ranges of resistivity values is that rocks with the same resistivity are difficult to distinguish. Thus, it is impossible to distinguish between saltwater saturated sands and clays. This can only be resolved by utilizing additional complementary information (e.g., from borehole logs and geology) to dispel the ambiguity.

Chapter 4

INSTRUMENTATION AND FIELD PROCEDURES

4.1 Introduction

The Schlumberger sounding configuration was employed throughout the fieldwork. The topography of the area is generally even and gentle, thus the terrain effects are negligible. A team of five people was involved in carrying out the soundings. One person was positioned at the sounding station and two people at the location of each of the electrodes on either side of the sounding station. A sounding with a spread of 260 m took approximately one and a half hours. However, where poor contact due to dry loose sands was experienced, or where thick bushes exist, the time spent on each sounding was more.

4.2 Instrumentation

The instrument used is a Swedish Atlas Copco ABEM Terrameter Model SAS 300B that combines both the transmitter and receiver as one unit. The transmitter is powered by a rechargeable NiCd battery. The transmitter delivers a very low

frequency current into the ground and the receiver digitally displays the apparent resistance that is internally calculated after averaging the signal voltage electronically over a finite number of cycles per second. With good contact and stable readings, one cycle sufficed for each AB measurement position (each cycle consisting of a normal and a reverse current sounding). At greater electrode spacings (and subsequent low potential readings), four cycles per second were usually selected and the average value displayed by the terrameter. The apparent resistance reading displayed by the terrameter is subsequently multiplied by the geometrical constant for that electrode configuration to give the apparent resistivity.

Other equipment used included assorted cables, steel and non-polarizable ceramic electrodes (porous pots). Despite relative dry soil and sand in most places, surface resistivities (except for some isolated soundings in dry loose sands) were low enough to enable good soundings to be made. The copper sulphate solution was used in the porous pots electrodes in order to improve contact, stability of readings and, besides, to inhibit the formation of electric fields around the electrodes. The current electrodes were driven into the ground by hammering, while the sounding traverse was prepared by clearing the bush by use of "pangas". Two hammers, potential reels, marking tape, clips and measuring tape were also used. An auger was used to bore holes for the porous pots.

4.3 Reconnaissance studies

Inventory on the available geological and hydrological information was undertaken on a desk study in the Department of Geology, University of Nairobi. This involved studying the past reports on work done and a literature review on the area. Aerial photography and topographic maps were studied and as much information as

possible extracted. This was followed by reconnaissance hydrogeological survey of the area that was undertaken between 13th and 22nd April, 1990. This formed part of a preliminary field study of the area prior to the geophysical survey that followed later in August and September of the same year. It entailed a general overview of the water situation in the area, the geology, physiography, water resources assessment and identification of potential sites for geophysical investigation of groundwater and generally, an inventory of the logistics involved in the fieldwork. From the reconnaissance study, and based on inventory data of the entire study area, it was felt that the most viable area for geophysical investigation is the area within the proximity of Lake Kenyatta, where the groundwater in the wells displays low conductivity values, thus potential areas for groundwater abstraction.

4.4 Field procedures

4.4.1 Introduction

Before the start of resistivity investigation for potential groundwater development sites, a number of locations were identified on the basis of general geological information, topography and hydrological information. The area surrounding Lake Kenyatta, the fossil and recent dunes were taken as the high groundwater potential areas. Initial soundings were located close to or in these areas, followed by a more general VES inventory of the study area. To avoid losing bearings in the thick bushes, the proper positions were checked by features recognized on both the topographic maps and on the ground such as motorable tracks, houses or trees and sink holes.

4.4.2 Resistivity measurements

It was paramount to collect adequate information as quickly as possible owing to the limited time and funds available for the study. Besides, the equipment had been provided by private sources and as such, could not be retained in the field for long. Considerable time was saved by the use of the Schlumberger configuration as the potential electrodes M and N were moved only a few times in a single sounding. Deep soundings were achieved by using the Schlumberger array since only two current electrodes were spread far to achieve maximum AB/2. The surface lateral inhomogeneities were easily detected as 'jumps' on the Schlumberger apparent resistivity sounding curves which are easily corrected.

4.4.3 Schlumberger array sounding

The basic arrangement of the Schlumberger array is as shown earlier in Figure 3.3 (b). The ABEM terrameter was placed at the centre of a sounding spread, where a wooden peg was driven into the ground and to which two current and two potential cables were tied. Potential electrode positions for MN/2 = 0.5, 5 and 10 metres were measured using a tape measure and small holes augered into which porous pot potential electrodes were placed, filled with saturated copper sulphate solution and corked; the holes were then filled with soil. The copper sulphate solution prevents polarization at the electrodes and stabilizes the readings. Steel current electrodes were used, and driven into the ground using hammers. The current electrode spacings AB/2 (see Table 4.1) were carefully marked with coloured adhesive tape to the current cables. For each sounding, current cables were reeled out as measurements were taken and wound back to the centre after maximum AB/2 spacings were reached. The current electrode spacings AB/2 were increased

74

Table 4.1   Current electrode spacings and corresponding geometric constants

AB/2 (m)	MN/2 (m)		
	0.5	5.0	10.0
1.5	6.3		
2.0	11.8		
2.5	18.8		
3.0	27.5		
4.0	49.5		
5.0	77.8		
6.0	112		
8.0	200		
10.0	313		
12.0	452		
15.0	706	62.8	
20.0	1260	118	
25.0	1960	188	
30.0	2830	275	126
40.0	5030	495	236
50.0		778	377
60.0		1120	550
70.0		1530	754
80.0		2260	1120
100.0		3130	1560
130.0			2640
160.0			4010
200.0			6270

at approximately equal logarithmic distances.

For a majority of soundings, one cycle per second sufficed, but where poor contacts on unstable readings were experienced, four cycles per second were used and the average apparent resistance displayed by the terrameter. The geometrical factor K had been pre-calculated for various MN/2 and AB/2 spacings using the relation shown in equation 3.9. Most of the sounding stations were separated by 300 to 400 m intervals. Alternative soundings were made where the ρ_a curves exhibited abrupt change. A total of 117 soundings have been interpreted, which include sixty soundings made during the fieldwork and fifty seven done in preceeding years, mostly in 1987 by GSK Ltd.

4.4.4 Data presentation and initial interpretation in the field

For each electrode position, the apparent resistance $\Delta V/I$ was computed automatically by the terrameter and digitally displayed. The ρ_a was calculated using a pocket calculator utilizing equation 3.9. The consecutive values of ρ_a were plotted on a bilogarithmic paper against AB/2 values to obtain a sounding curve in the usual way (e.g., Fig 4.1 for sounding curves MPK 44). This allowed a general visual check on the sounding as they proceeded, and any ambiguities, in which case the measurements were repeated before the data were centrally processed and interpreted. Plotting of the data was done on a bilogarithmic graph paper of the same modulus as the master curves used in the interprtation (Bhattacharya and Patra (1968) 2-layer master curves with modulus 62.5 mm per cycle).

STATION NO.

AB/2 (m)
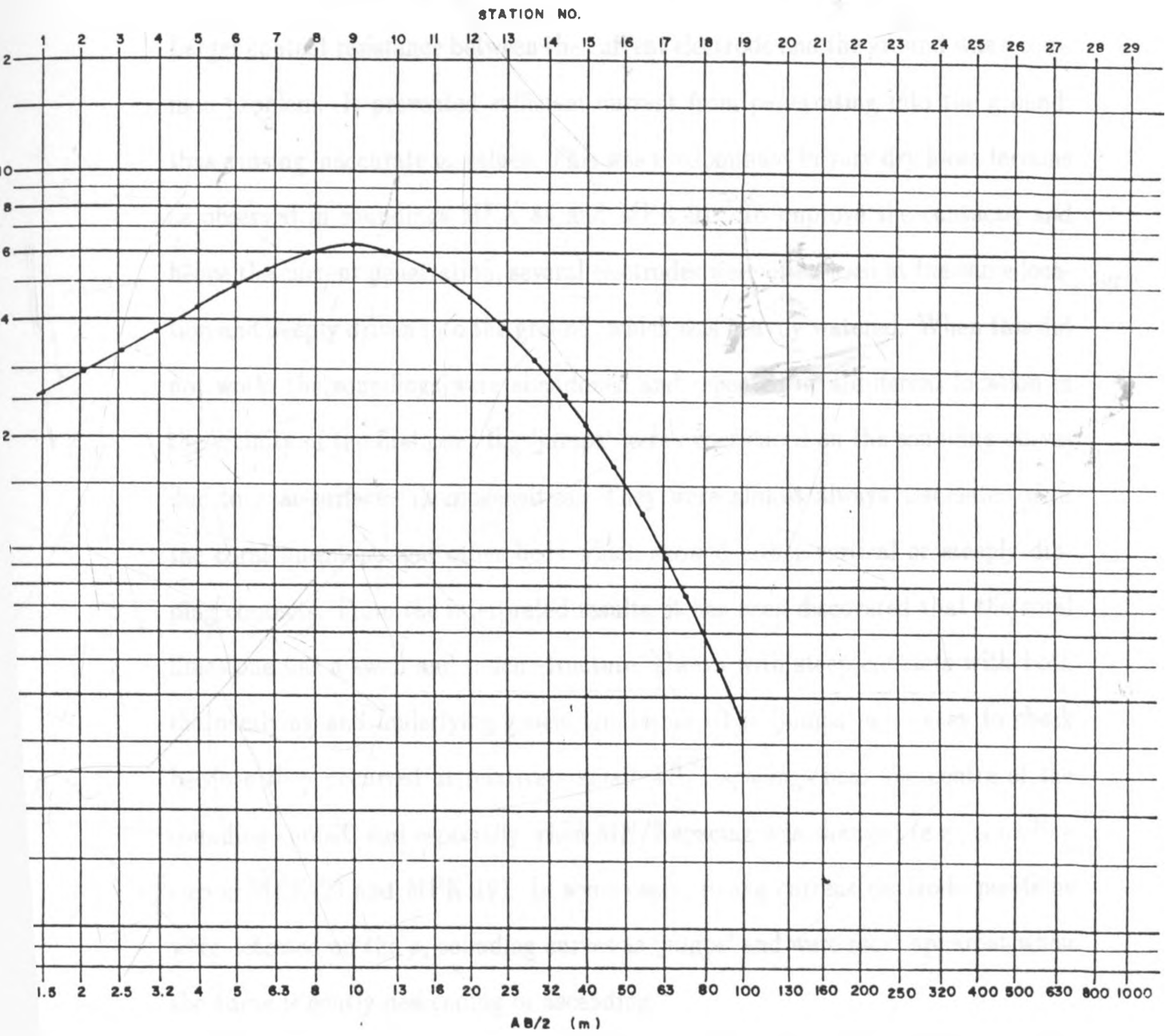
Fig. 4.1 Sounding curve over station MPK 44

4.5 Problems in sounding measurements

Larger contact resistance between the current electrode and the ground was a common problem. It prevented sufficient current from penetrating into the ground, thus causing inaccurate ρ_a values. This was predominant in very dry loose terrains as observed in soundings MPK 84 and MPK 91. To improve the contacts, and hence the current penetration, several electrodes were often used at the same location and deeply driven into the ground, which was heavily watered. When this did not work, the soundings were abandoned and repeated at a different location in the vicinity of the first one. Big 'jumps' were experienced on the sounding curves due to near-surface inhomogeneities. They were almost always associated with the coral limestone and other beds which showed either vertical or steeply dipping contacts. From the interpreted results, it has been discovered that the coral limestone has a swell and pinch structure, always with steep contacts with both the overlying and underlying geoelectric layers. The 'jumps' were easy to check because they occurred at relatively small AB/2 spacings near the centre of the sounding spread, and especially when MN/2 spacing was changed (e.g., sounding curves MPK 23 and MPK 19). In some cases, wrong current electrode positions were detected on the ρ_a sounding curves as 'jumps' and were most apparent when the curve is gently descending or ascending.

The wrong current electrode position problem was mainly caused by poor communication between the field operators and the observer at the centre of the spread. For communication purposes, use of radios can save a lot of time especiallly for large AB/2 spacings. Since such radios were not available, instructions were made by the observer at the centre by shouting loudly. Erratic, errononeous readings made several soundings to be prematurely abandoned. These could have

78

been mainly caused by stray currents in the ground during rainy spells and mainly experienced in the coral formations.

Chapter 5

ANALYSIS OF FIELD DATA

5.1 Introduction

Over a very long period, vertical electrical sounding (VES) data have been ana-
lyzed using manual curve matching procedures (e.g., Zohdy, 1965; Orellana and
Mooney, 1966; Koefoed, 1979). However, alternative developments (e.g., Inman,
1975) have introduced faster inversion techniques using computers, thus rendering
the manual techniques almost obsolete and only as methods of generating initial
guess parameters to be used in the inversion procedures. In the present study, the
analysis of geophysical data has been carried out both qualitatively and quantita-
tively.

Qualitatively, the sounding curves were only identified according to class types
A, Q, H, K or a combination of these, all of which have been exhaustively dis-
cussed in chapter 3. Combinations of these type curves were common in the study
area. Quantitative interpretation entailed the partial curve matching technique
involving the auxiliary point method to obtain approximate layer parameters (i.e.,
resistivities and thicknesses) for a one-dimensional earth model. These parame-
ters were then used as initial input parameters in the computer programs, one for

obtaining the forward solution and the other for solving the inverse problem.

5.2 Types of apparent resistivity (ρ_a) curves observed in the study area

In the entire study area, the sounding curves are generally uniform, except a few which show localized variability. Individual VES locations are shown on the VES location map in Appendix VI. This can be attributted to the relatively uniform geology and structural set up of the area. It is therefore often easy to assign them to a particular region. However, different shapes of the curves were obtained at stations located very close to each other when the surficial material varied, for example, top dry loose sands and wet sandy loam soils adjoining each other. In the study area, five groups of sounding curves were distinguished. Typical curves for each group are shown in Figure 5.1, numbered 1 to 5, on the same axes.

Group 1 which comprises KQ-type curves mainly occurs in the south-western section of the area near the shore of the lake and in the interior where there are topographic lows. This group (e.g., sounding at station MPK 44) depicts a 4-layer earth medium of clays, sands, coral and saltwater. It mainly occurs where sedimentation and deposition of surface clayey deposits have taken place. The depth to the coral and its thickness are large, while the saltwater/freshwater interface is relatively deep below the ground surface. This group comprises 15% of all the soundings carried out in the area.

Group 2, AKQ-type curves, occurs in the second row from the lake after Group 1. The curves represent more than five layers which, from top, consist of a layer of clayey soils, a layer of clays, calcareous layers, a layer of corals, a calcareous layer and a saltwater layer (e.g., sounding at station MPK 30). They comprise 10% of
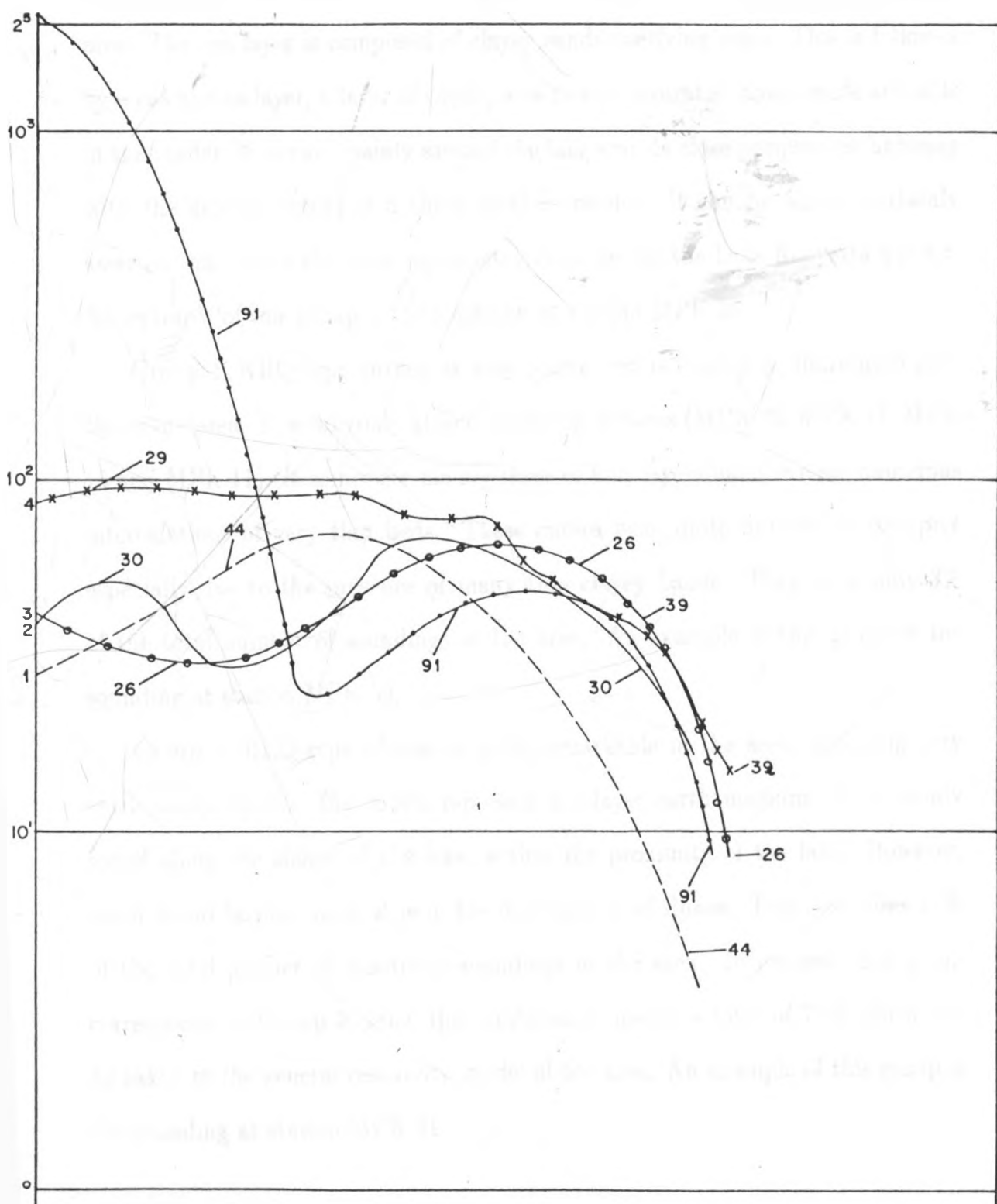
Fig. 5.1   Types of sounding curves observed in the area, 44, 91 are VES numbers

the total number of resistivity soundings carried out in the area.

Group 3, HKQ-type curves, represents a 5-layer earth medium. This is most common and forms more than 55% of the total number of soundings made in the area. The top layer is composed of clayey sands overlying clays. This is followed by a calcareous layer, a layer of corals, a saltwater-saturated layer, sands and silts in that order. It occurs mainly around the lake and its close peripheries, agreeing with the general extent of a thick coral limestone. It can be almost certainly asserted that this is the most representative model for the Lake Kenyatta aquifer. An example of this group is the sounding at station MPK 26.

Group 4, KHQ-type curves, is very scarce and is randomly distributed over the entire area. It occurs only at four sounding stations (MPK 39, MPK 17, MPK 15 and MPK 11). It comprises mainly three or four layers but there are numerous intercalations of very thin beds. These curves were quite difficult to interpret especially due to the presence of many thin clayey bands. They form only 3% of the total number of soundings in the area. An example of this group is the sounding at station MPK 39.

Group 5, HKQ-type curves, is quite remarkable in the area, depicting very thick sandy layers. The curves represent a 5-layer earth medium. It is mainly found along the shores of the lake, within the proximity of the lake. However, when found farther away, it is in the dry loose sand dunes. This comprises 17% of the total]umber of resistivity soundings in the area. In general, this group corresponds to Group 3; thus, the combination makes a total of 72% which can be taken as the general resistivity model of the area. An example of this group is the sounding at station MPK 91.

5.3 Interpretation by the curve matching technique

The interpretation procedures involved in the auxiliary point curve matching technique have been discussed in chapter 3. This technique was used to obtain initial input parameters, that is resistivities and thicknesses of respective layers, which are later used in the computer inversion programs. The application of the auxiliary point curve matching procedure is illustrated in the following practical examples:

Example 1: KHK-type curve - MPK 39

This example (Fig. 5.2) illustrates the practical procedure for the interpretation of a 6-layer KHK-type curve using 2-layer master curves and auxiliary point charts. The field curve was first classified as a KHK-type on the double logarithmic graph paper (modulus 62.5mm). Using an inked pen, the sounding curve and a few horizontal and vertical lines from the graph paper were traced on a transparent paper. An attempt was then made to fit a 2-layer master curve to the first ascending branch. In this case, the resistivity ratio $\rho_2/\rho_1 = 4$ was found to be the most fitting. The origin of the master curves was marked by the first point A. The coordinates of point A on the field curves gave $\rho_1 = 62$ Ωm and $h_1 = 0.8$ m ; and the ratio $\rho_2/\rho_1 = 4$ gave the resistivity of the second layer $\rho_2 = 248$ Ωm. Since this branch formed the first branch of the K-type curve, the auxiliary curve for ratio 4 (on K-type auxiliary chart) was traced from point A.

Next, the descending branch of the field curve was fitted to a 2-layer master curve of resistivity contrast 2.5 Ωm ensuring that the origin moved along the auxiliary dashed line and maintaining the axes of the trace and those of the master curves parallel. The position of the origin on the dashed line was marked as the
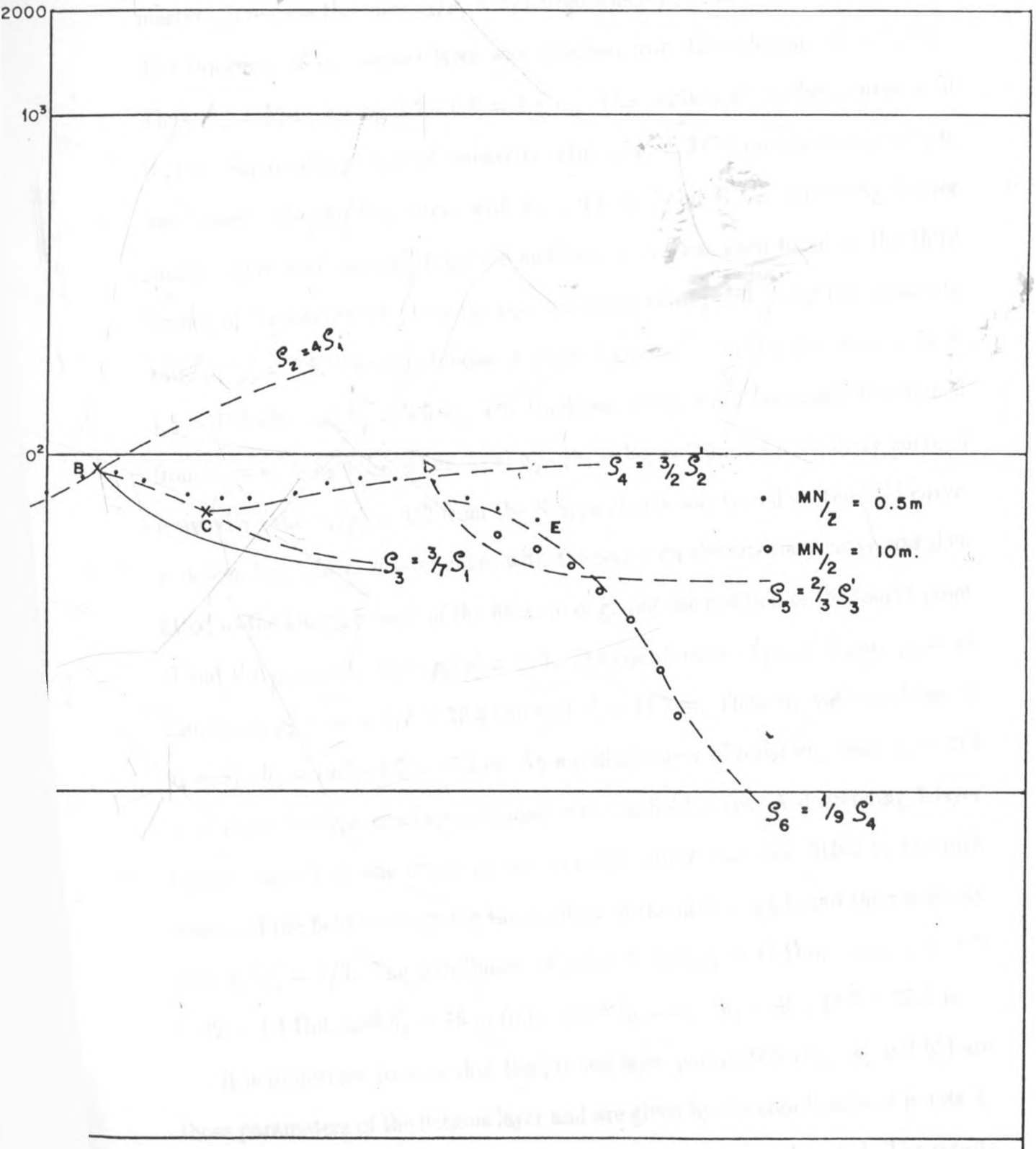
Fig. 5.2   Interpretation of sounding MPK 39 using the auxiliary point method

second point B whose coordinates gave $\rho_1' = 9.5 \ \Omega m$ and $h_1' = 2.2$ m; the fitted master curve gave the ratio $\rho_3/\rho_1' = 3/7$ from which $\rho_3 = 40.7 \ \Omega m$ was calculated. The thickness of the second layer was obtained from the relation: $h_1' = h_1 + h_2$. Thus, $h_2 = h_1' - h_1$ giving 2.2 - 0.8 = 1.4 m. This section of the field curve is of H-type. An auxiliary curve of resistivity ratio $\rho_3/\rho_1' = 3/7$ from the H-type charts was traced onto the field curve with its origin at point B. An ascending 2-layer master curve with the origin on the auxiliary curve was then fitted to the third branch of the field curve giving the position of the third point C and the resistivity ratio $\rho_4/\rho_2' = 1.5$. The coordinates of point C gave $\rho_2' = 70 \ \Omega m$ and so $\rho_4 = 70 \times 1.5 = 105 \ \Omega m$ and $h_2' = 4.5$ m. The thickness of the third layer was determined from $h_2' = h_1 + h_2 + h_3$. Thus, $h_3 = h_2' - (h_1 + h_2) = 2.3$ m. An auxiliary curve of resistivity ratio $\rho_4/\rho_2' = 3/2$ from the K-type charts was traced on the field curve. A descending 2-layer master curve with the origin on the auxiliary curve was then fitted to the fourth branch of the field curve giving the position of the fourth point D and the resistivity ratio $\rho_5/\rho_3' = 2/3$. The coordinates of point D gave $\rho_3' = 44 \ \Omega m$, hence $\rho_5 = 44 \times 2/3 = 29.3 \ \Omega m$ and $h_3' = 14.7$ m. Thus, h_4 was calculated as $h_4 = h_3' - h_2' = 14.7 - 4.5 = 10.2$ m. An auxiliary curve of resistivity ratio $\rho_5 = 2/3 \times \rho_4'$ from the type charts was traced onto the field curve. A descending 2-layer master curve with the origin on the auxiliary curve was then fitted to the fifth branch of the field curve giving the position of the fifth point E and the resistivity ratio $\rho_6/\rho_4' = 1/9$. The coordinates of point E gave $\rho_4' = 42 \ \Omega m$, hence $\rho_6 = 1/9 \times 42 = 4.4 \ \Omega m$, and $h_4' = 45$ m from which $h_5 = h_4' - h_3' = 45 - 14.7 = 30.3$ m.

It is important to note that the primed layer parameters (e.g., ρ_2' and h_2') are those parameters of the fictious layer and are given by the coordinates of points A, B, C, D, ..., depending on the number of geo-electric layers depicted. The results

of the interpretation of field curves from sounding station MPK 39 are given in Table 5.1 below.

Table 5.1. Interpretation results from sounding station MPK 39 by the auxiliary point method.

ρ_1	h_1	ρ_2	h_2	ρ_3	h_3	ρ_4	h_4	ρ_5	h_5	ρ_6
62.0Ωm	0.8m	248.0Ωm	1.4m	40.7Ωm	2.3m	105.0Ωm	10.2m	29.3Ωm	30.3m	4.4Ωm

Example 2: HK-type curve - MPK 72

This example (Fig 5.3) illustrates the practical procedure for the interpretation of a 4-layer HK-type field curve by 2-layer master curves and auxiliary point charts. The field curve was first identified as an HK - type. A 2-layer master curve with resistivity ratio $\rho_2/\rho_1 = 1/9$ was fitted to the first descending branch. The origin of the master curve was marked on the transparent field curve as point A. The coordinates of point A on the field curve gave $\rho_1 = 99$ Ωm and $h_1 = 0.5$ m; and the ratio $\rho_2/\rho_1 = 1/9$ gave the resistivity of the second layer $\rho_2 = 11.0$ Ωm. Since this forms the first branch of the H-type curve, the auxiliary point curve with the ratio 1/9 was traced from the position of point A. Subsequently, the ascending branch of the field curve was fitted to a 2-layer master curve with ratio $\rho_3/\rho'_1 = 3$. The fitting was done while keeping the origin point on the master curves on the trace. When a perfect fit was found, the position of the origin point on the trace was marked as point B whose coordinates gave $\rho'_1 = 15.0$ Ωm and $h'_1 = 5.3$ m. Therefore, from the ratio $\rho_3/\rho'_1 = 3$, $\rho_3 = 3 \times 15 = 45$ Ωm. Since $h'_1 = h_1 + h_2 = 5.3$ m, the thickness of the second layer, $h_2 = 5.3 - 0.5 = 4. 8$ m. The auxiliary curve with resistivity ratio $\rho_3/\rho'_1 = 3$ from the K-type charts was traced onto the field curve with its origin at point B. A descending 2-layer master curve with the origin on the auxiliary curve was then fitted to the last portion of the
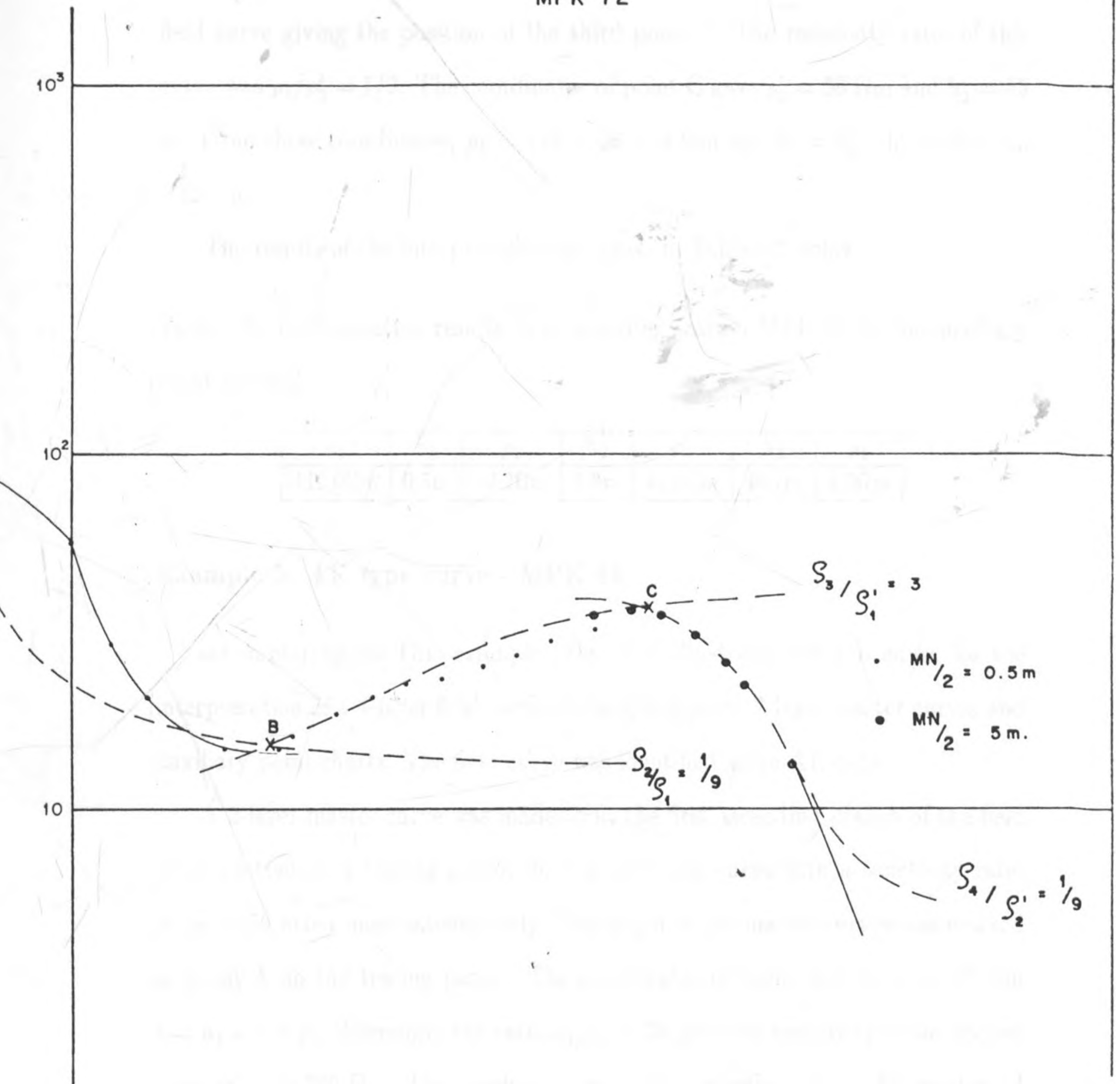
Fig. 5.3   Interpretation of sounding MPK 72 using the auxiliary point method

field curve giving the position of the third point C. The resistivity ratio of this curve was $\rho_4/\rho_2' = 1/9$. The coordinates of point C gave $\rho_2' = 36$ Ωm and $h_2' = 55$ m. From these coordinates, $\rho_4 = 1/9 \times 36 = 4$ Ωm and $h_3 = h_2' - h_1' = 55 - 5.3$ =49.7 m.

The results of the interpretation are given in Table 5.2 below.

Table 5.2. Interpretation results from sounding station MPK 72 by the auxiliary point method.

ρ_1	h_1	ρ_2	h_2	ρ_3	h_3	ρ_4
110.0Ωm	0.5m	12.2Ωm	4.8m	45.0Ωm	49.7m	4.0Ωm

Example 3: AK-type curve - MPK 81

setcounterpage89 This example (Fig. 5.4) illustrates the procedure for the interpretation of a 4-layer field curve of the AK-type by 2-layer master curves and auxiliary point charts. The field curve was identified as an AK-type.

A 2-layer master curve was made to fit the first ascending branch of the field curve plotted on a tracing paper. In this case, one curve with a resistivity ratio $\rho_2/\rho_1 = 39$ fitted most satisfactorily. The origin of the master curves was marked as point A on the tracing paper. The coordinates of point A gave $\rho_1 = 10$ Ωm and $h_1 = 0.8$ m. Therefore, the ratio $\rho_2/\rho_1 = 39$ gave the resistivity of the second layer as $\rho_2 = 390$ Ωm. The auxiliary curve with the ratio $\rho_2/\rho_1 = 39$ was traced from the position of point A. Next, the ascending branch of the field curve was fitted to a 2-layer master curve with resistivity ratio $\rho_2/\rho_1 = 39$ while maitaining the origin on the auxiliary dashed line. The position of the origin on the dashed line was marked as the second point B whose coordinates gave $\rho_1' = 22$ m and h_1' = 2.8 m. The fitted master curve gave the ratio $\rho_3/\rho_1' = 4$ from which $\rho_3 = 88$ Ωm
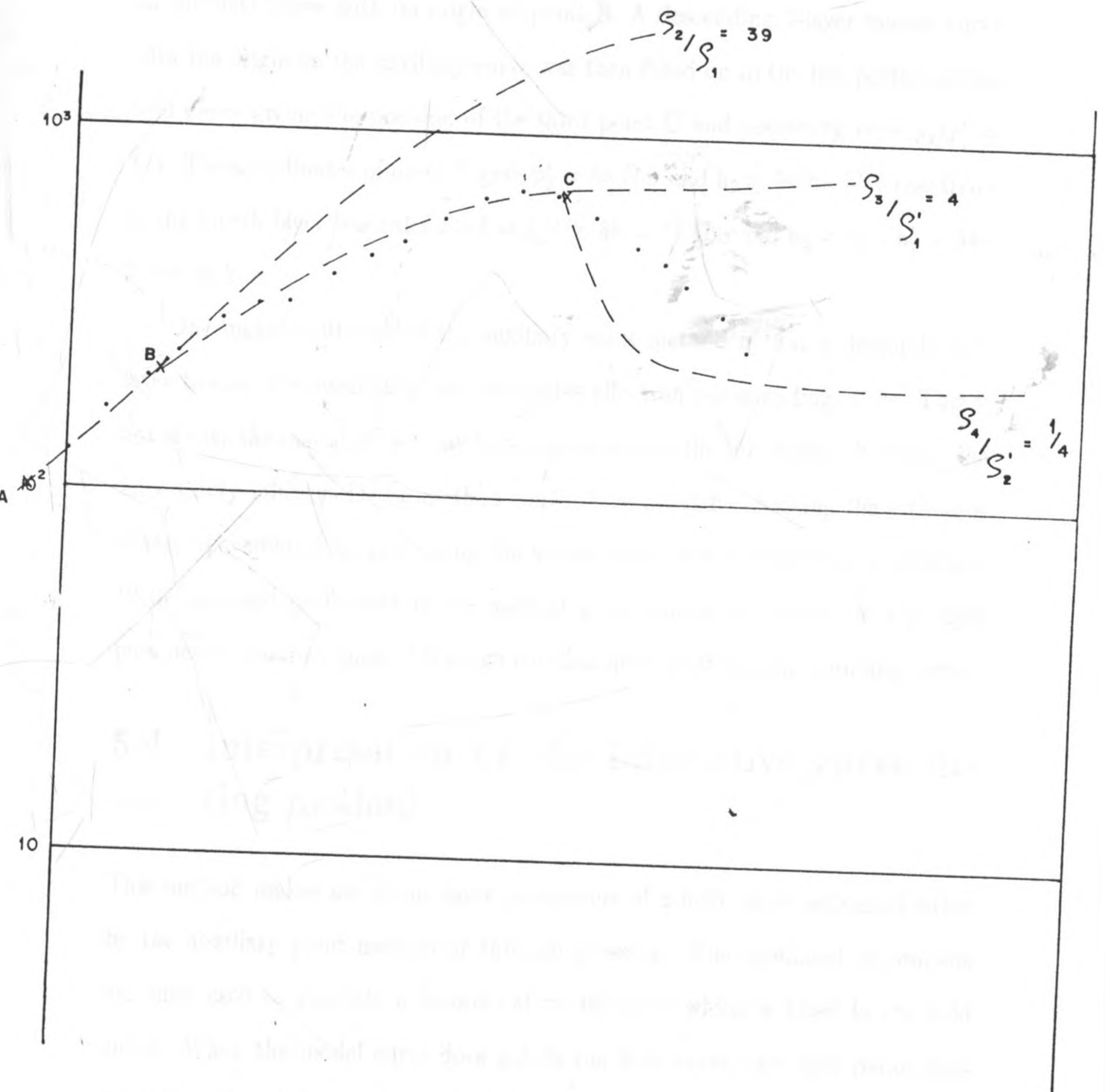
Fig. 5.4 Interpretation of sounding MPK 81 using the auxiliary point method

was determined. The thickness of the second layer was calculated from $h_1' = h_2 + h_1$, thus $h_2 = 2.8 - 0.8 = 2.0$ m. An auxiliary curve of ratio $\rho_3/\rho_1 = 4$ was traced on the field curve with its origin at point B. A descending 2-layer master curve with the origin on the auxiliary curve was then fitted on to the last portion of the field curve giving the position of the third point C and resistivity ratio $\rho_4/\rho_2' = 1/4$. The coordinates of point C gave $\rho_2' = 68$ Ωm and $h_2 = 34$ m. The resistivity of the fourth layer was calculated as $1/4 \times 68 = 17$ Ωm and $h_3 = h_2' - h_1' = 34 - 2.8 = 31.2$ m.

One major limitation of the auxiliary point method is that it demands each layer to have a considerable and noticeable effect on the sounding curve. This is not always the case since we may have suppression of the thin layers. However, the uncertainty inherent in the method could be resolved by checking the estimates of layer parameters by generating the actual curve such a model would produce. With increased proficiency in the method accompained by experience, the layer parameters could be guessed through correlation of neighbouring sounding curves.

5.4   Interpretation by the interactive curve fitting method

This method makes use of the layer parameters of a field curve estimated either by the auxiliary point method or through guessing. The estimated parameters are then used to generate a theoretical model curve which is fitted to the field curve. When the model curve does not fit the field curve, the layer parameters are adjusted and the process repeated until a satisfactory fit is obtained. The final interpretation results are based on resistivity ranges which do not necessarily conform with the geological succession.

Mainly used in this study was the non-automatic forward modelling method in which layer parameters were adjusted by personal judgement. Thus, a decision was made on which layer and what parameters to be adjusted to improve the fit and the amount by which the parameters were to be changed. The software used was an interpretation package 'Schlumbg' developed by Hemker (1985) and written in Pascal to run on an IBM compatible PC. The program provides a database for resistivity sounding data and calculates the resistivity model parameters that give the best fit to the apparent resistivity field data.

Various ambiguities, some arising during the fieldwork and others apparent during the interpretation session, were observed. While the majority of them can be adequately explained, it is not always possible to correct a sounding curve for the effects observed.

Example 1: Sounding at station MPK 58

The following example illustrates the application of the interactive curve fitting method in the interpretation of a five layer sounding curve. The initial input parameters obtained from the curve matching auxiliary point method are shown in Table 5.3 below.

Table 5.3. Interpretation results from sounding station MPK 58 by the auxiliary point method.

Layer	1	2	3	4	5
$\rho(\Omega m)$	56.3	22.3	102.5	18.3	4.8
h(m)	0.9	6.7	13.2	10.3	

On using the above layer parameters in the program 'Schlumbg', the generated curve did not fit the observed curve. Consequently, the parameter values were changed manually and run again and the process repeated several times until the

theoretical curve fitted smoothly through the field curve (Fig.5.5). This method relied on personal judgement and improved with experience.

Example 2: Sounding at station MPK 20

The following example illustrates the application of the same method but in which some of the layer parameters of the geoelectric section are kept constant while others are varied to achieve the best fit. Interpreted curves along a given profile were compared with corresponding field curves and a correlation between them found which could lead to the correct determination of the parameters, especially where correlation holds good in terms of shape and magnitude of corresponding layer parameters in a given decade. Thus, a general model could fit a number of sounding curves along a profile with few or no ambiguities.

The initial input parameters obtained by the auxiliary point method are shown in Table 5.4 below.
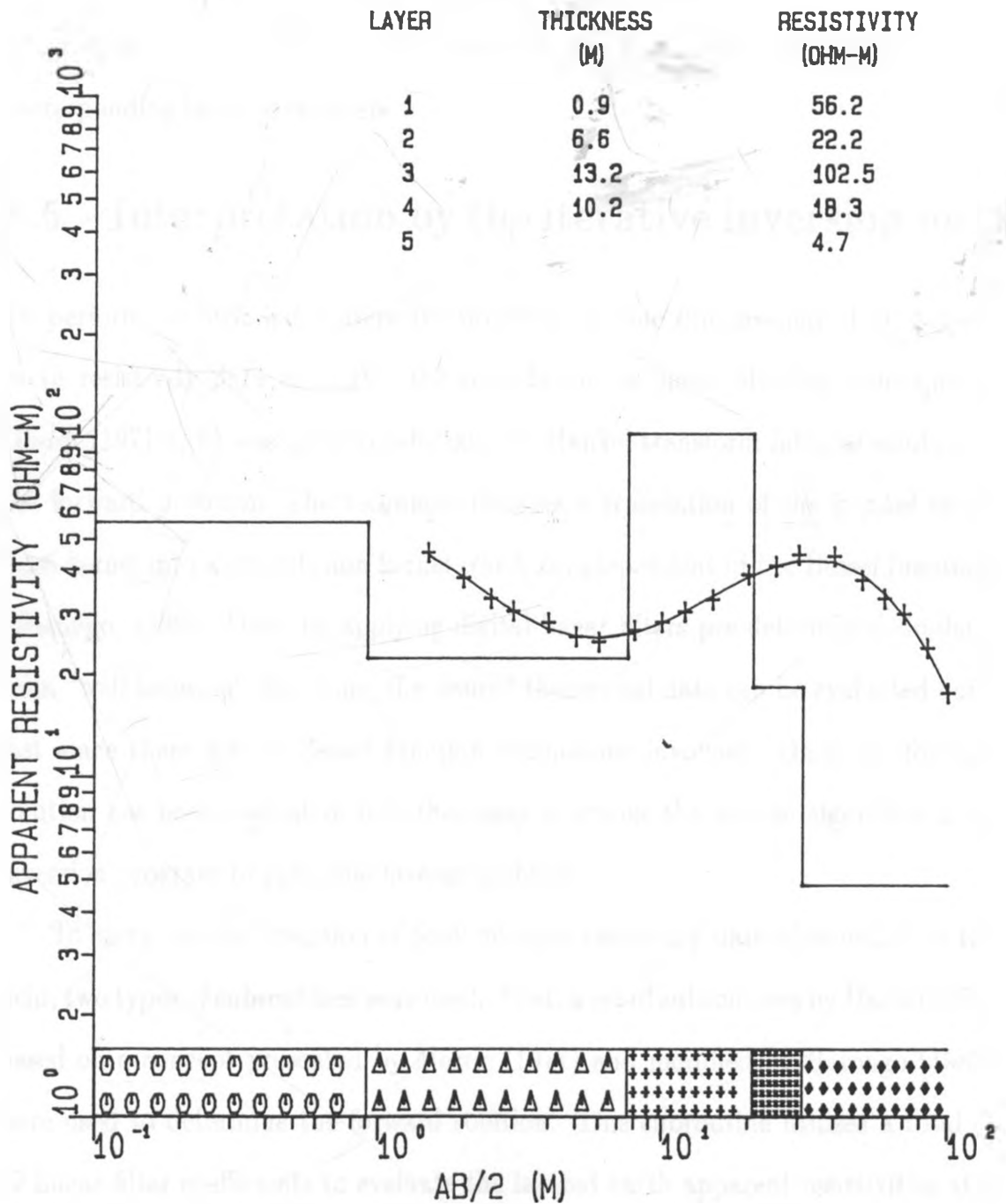
Fig. 5.5 Interpretation results of sounding MPK 58 using non-automatic forward method

Table 5.4. Interpretation results from sounding station MPK 20 by the auxiliary point method.

Layer	1	2	3	4
$\rho(\Omega m)$	71.0	17.1	102.4	1.5
h (m)	0.7	7.3	30.1	

Figure 5.6 shows the sounding curve and the fitted theoretical curve and the corresponding layer parameters.

5.5   Interpretation by the iterative inversion method

To perform an automated iterative inversion on one dimensional (1-D) layered earth resistivity data on a PC, the convolution or linear filtering technique by Ghosh (1971 a, b) was used to calculate the Hankel transform integral solution of the forward problem. The technique involves a translation of the Hankel transform kernel into a convolution kernel which is independent of the Bessel functions (Barongo, 1989). Then, by applying digital linear filters pre-determined similarly from "well behaved" functions, the desired theoretical data can be evaluated quite fast since there are no Bessel function evaluations involved. Once the forward solution has been evaluated, it is then easy to invoke the inverse algorithm in an inversion program to solve the inverse problem.

To carry out the inversion of Schlumberger resistivity data obtained from the field, two types of subroutines were used: First, a set of subroutines by Davis (1979) based on a concept presented by Merric (1977) and modified by Barongo (1989) were used to determine the forward solution. This subroutine utilizes a total of 29 linear filter coefficients to evaluate the layered earth apparent resistivities at a logarithmic sampling of six samples per decade starting from a minimum current electrode spacing, AB/2, of 1 metre (Barongo, 1989). Second, another set of
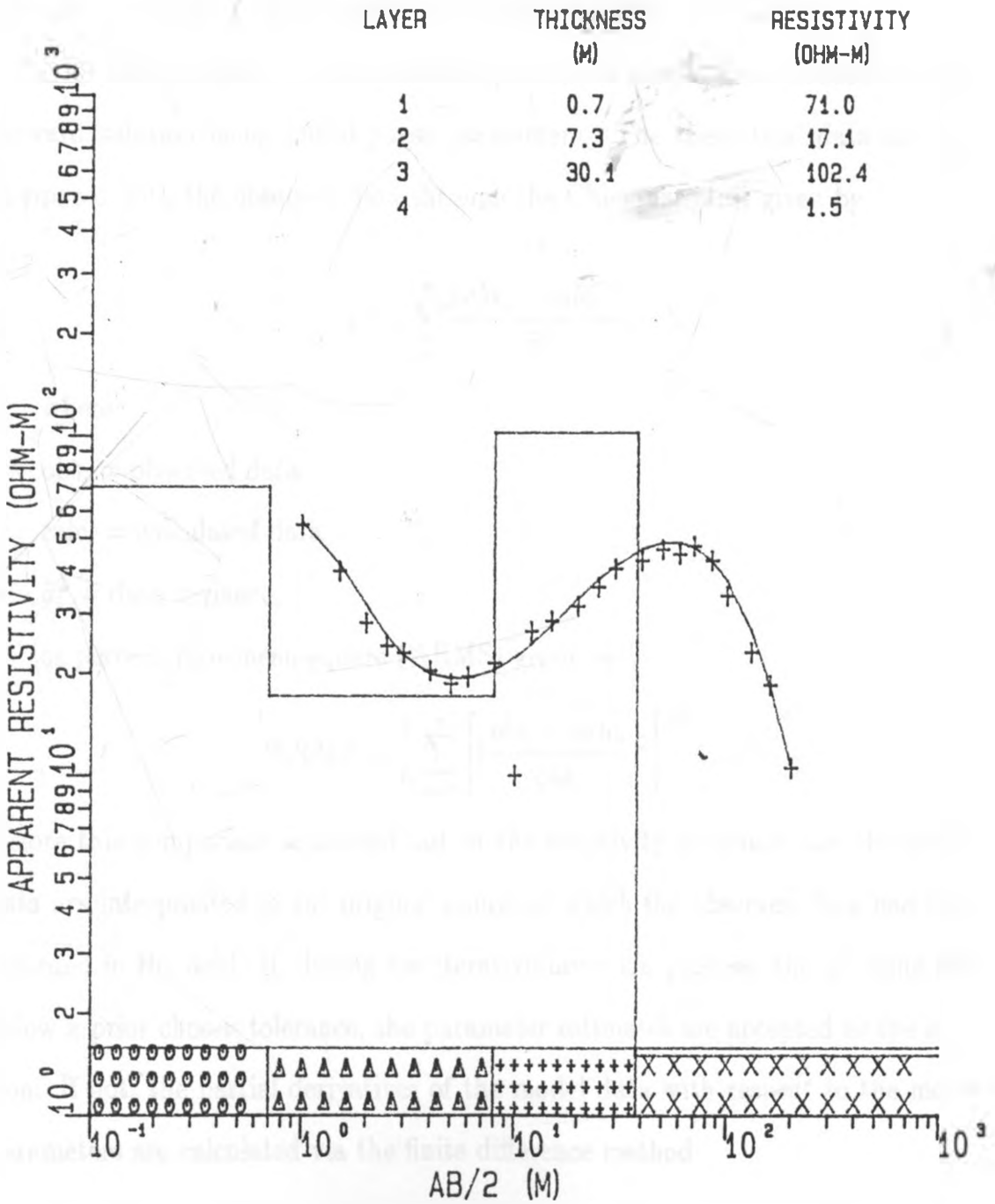
Fig. 5.6   Fitted curve by semi-automatic forward method and interpreted layer parameters for sounding MPK 20

subroutines developed by Barongo (1989) based on singular value decomposition (SVD) with rigde regression were used to determine the inverse solution. Both subroutines written in FORTRAN 77 were called in a main program (Barongo, personal communication) to carry out the least squares inversion in an iterative manner since the vertical electrical sounding problem is non-linear.

The first iteration of the inversion procedure entails the calculation of the forward solution using initial guess parameters. The theoretical data are then compared with the observed data through the Chi-square test given by

$$\chi^2 = \sum_{i=1}^{n} \frac{(obs_i - calc_i)^2}{\hat{\sigma}_i^2},$$

where

obs_i = observed data,

$calc_i$ = calculated data,

$\hat{\sigma}_i^2$ = data variance,

or percent root-mean-square (%RMS) given by

$$\%RMS = \frac{1}{n} \sum_{i=1}^{n} \left[\left(\frac{obs_i - calc_i}{obs_i} \right)^2 \right]^{1/2};$$

Before this comparison is carried out in the resistivity inversion, the theoretical data are interpolated to the original points at which the observed data had been recorded in the field. If, during the iterative inversion process, the χ^2 value falls below a prior chosen tolerance, the parameter estimates are accepted as the solution. If not, the partial derivatives of the model data with respect to the model parameters are calculated via the finite difference method

$$Aij = \frac{F_i(p_j + \Delta p_j) - F_i(p_j)}{\Delta p_j},$$

$$i, j = 1, 2, 3, \ldots\ldots$$

where

A_{ij} = elements of Jacobian matrix A,

p_j = parameter perturbations,

$F_i(p_j)$ = model data before perturbation,

$F_i(p_j + \Delta p_j)$ = model data after perturbation.

In order to stabilize the whole inversion process, it is necessary to scale the Jacobian matrix A, the data residuals and parameter perturbations, respectively, as follows:

$$A_{scaled} = W^{-1/2} A D^{1/2},$$

$$c_{scaled} = W^{-1/2} c,$$

and

$$\Delta p_{scaled} = D^{-1/2} \Delta p,$$

where W is a matrix that represents the covariance of the ith datum with the jth datum. But, if we assume the observational data errors to be uncorrelated, W is simply a diagonal matrix whose elements are represented by σ^2. It is used as a "weighting matrix" when the data are noisy. D is a matrix whose elements are given by (Barongo, 1989)

$$D_{ii} = D_{kj} = (\delta_{kj}(\sum_{i=1}^{n} A_{ik}^2))^{-1},$$

$$k = 1, 2, 3, \ldots, m$$

$$j = 1, 2, 3, ..., m$$

where δ is Kronecker delta or identity matrix.

Using an SVD subroutine, the scaled (and possibly "weighted") matrix is decomposed into its orthogonal eigenvalues and eigenvectors. An inverse matrix of eigenvalues and eigenvectors in which a Marquardt parameter is added is calculated. The new parameters are calculated according to

$$(p_j)' = p_j + \left(\frac{V\Lambda U^T}{\Lambda^2 + \phi I}\right)\Delta d_i$$

where

V represents eigenvector matrix for parameters,

U represents eigenvector matrix for data,

T means 'transpose' of matrix U,

Λ represents eigenvalue matrix,

ϕ represents Marquardt parameter,

I represents identity matrix.

The Marquardt parameter is a damping constant introduced by Levenberg (1944) and later refined by Marquardt (1963). It is used to increase the magnitude of the small or zero eigenvalues without affecting the large ones.

The new parameters, as calculated above, are used as the model parameters in the second iteration during which a second χ^2 value is calculated. But, before the process continues to the next step, the new χ^2 value is compared with the preceding one. If it is found to be smaller, the Marquardt parameter is reduced by a factor of 10, and if it is larger, it is raised by the same factor and the process proceeds through the subsequent iterations. If at some stage during the iterations the χ^2

value remains constant, an instruction in the program stops the iteration process after six consecutive χ^2 constant values and the results proceed on to the part of the program which deals with solution appraisal. The optimum solutions are then printed out. However, if the problem continually converges, instructions in the program stop the process after the χ^2 value falls below a prior chosen tolerance or after some pre-determined maximum number of iterations has been reached.

Figure 5.7 shows the standard plot of the root-mean-square (RMS) error versus the Marquardt parameter. The plot, known as the "ridge trace" (Hoerl and Kennard, 1970), gives an optimum value that corresponds to the minimum RMS error. It is the value used to estimate the best model solution. Thus, the Marquardt parameter is used to find the optimum value that would bring convergence. This operation satisfies the condition that, for a non-linear inverse problem, several iterations are necessary to reach a solution and each iteration may require a different value of ϕ. If ϕ approaches zero, the estimator converges rapidly to a solution if it is near the minimum on the ridge regression curve, but it may diverge if it is too far from it.

After completing the above operation, the solution parameters are appraised. This entails calculation of the parameter correlation matrix, parameter standard deviations, data errors, resolution, information, weights, final solution eigenvectors and final solution eigenvalues. The flowchart of the program used in the inversion (Barongo, 1989) is shown in Figure 5.8.

5.6 Inversion of Schlumberger resistivity data

The inversion procedure described in section 5.5 was employed for the interpretation of Schlumberger resistivity data. Most of the inversion results are illustrated
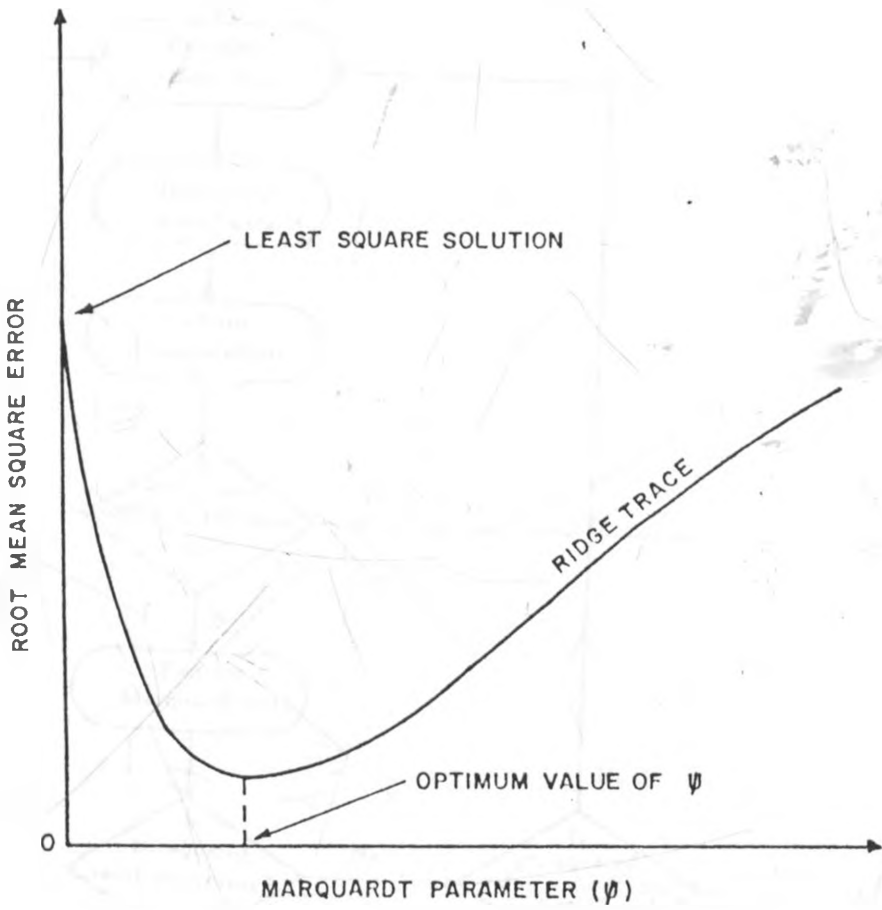
Fig. 5.7 Plot of root-mean-square (RMS) error versus Marquardt parameter (After Barongo, 1989)
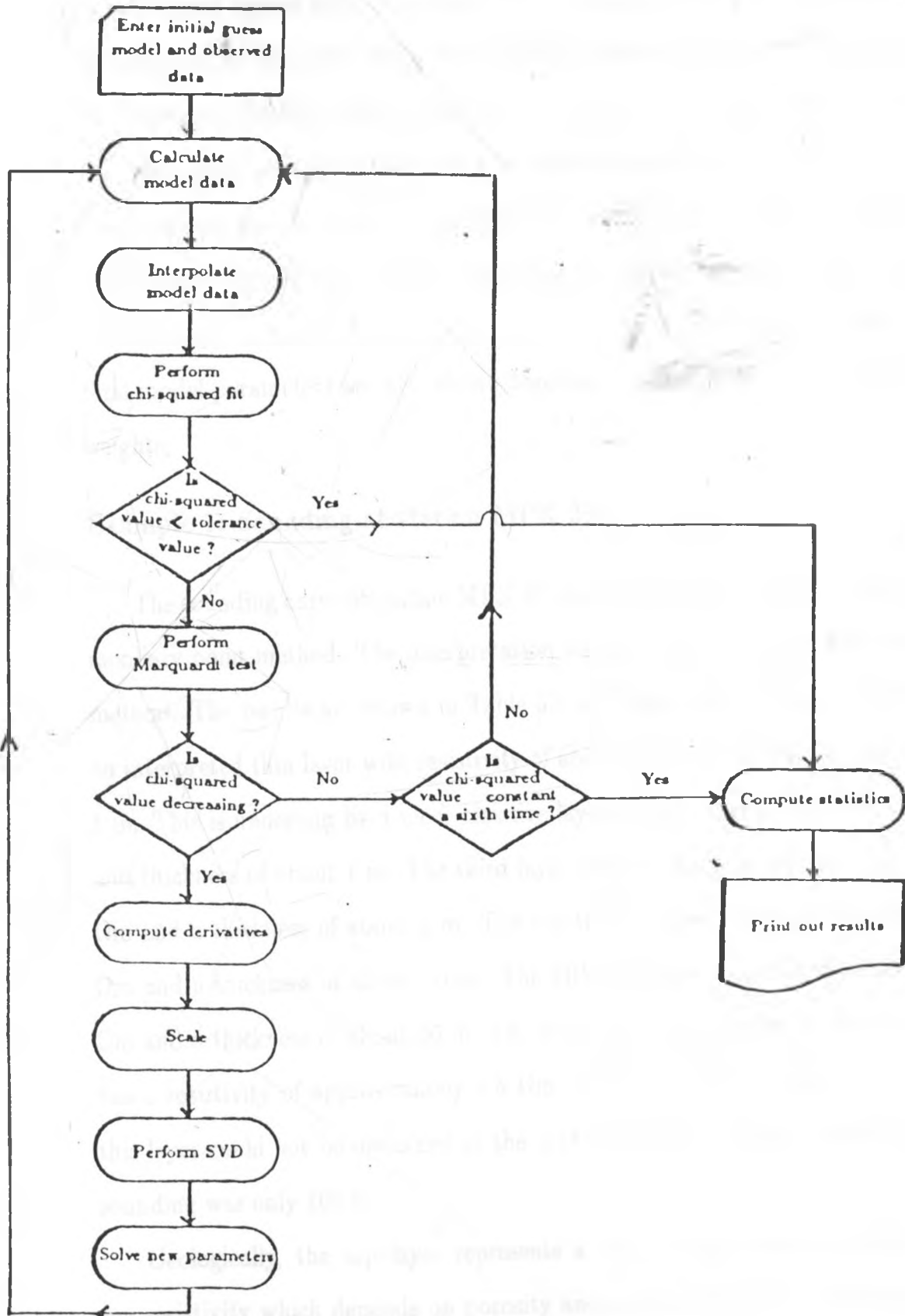
Fig. 5.8   Flow chart of program for ground resistivity inverse problem (After Barongo, 1989)

102

in tables and figures (Fig. 5.9, 5.10, 5.11). In each table are columns showing the iteration number, the Marquardt constant applied at each iteration and the corresponding %RMS values. Besides, the initial or starting guess parameters, the final model parameters and the true model parameters used to generate the observed data are also shown. In addition, two columns to the right show the longitudinal conductance (thickness/resistivity) and transverse resistance (thickness × resistivity) calculated for each case. The data and the appraisal statistics of the final model parameters are also shown together with resolution, information and weights.

Example 1: Sounding at station MPK 39

The sounding curve at station MPK 39 was interpreted in section 5.3 using the auxiliary point method. The interpretation was repeated here using the inversion method. The results are shown in Table 5.5 and Figure 5.9. The figure indicates an interpreted thin layer with resistivity of about 72 Ωm and a thickness of about 1 m. This is underlain by a more resistive layer with resistivity of about 189 Ωm and thickness of about 1 m. The third layer beneath has a resistivity of about 55 Ωm and a thickness of about 2 m. The fourth layer has a resistivity of about 83 Ωm and a thickness of about 10 m. The fifth layer has a resistivity of about 41 Ωm and a thickness of about 36 m. The sixth layer which is the most conductive has a resistivity of approximately 1.5 Ωm. Unfortunately, the bottom extent of this layer could not be discerned as the maximum AB/2 spacing reached for this sounding was only 100 m.

Geologically, the top layer represents a zone of moist sandy soils of varying resistivity which depends on porosity and moisture content. The third layer

Table 5.5   Inversion results of sounding MPK 39

ITERATION	MARQT CONST.	CHI-SQUARE VALUE	%RMS
1	.10E-01	.62E+02	.13E+02
2	.10E-01	.02E+02	.73E+01

CONVERGED WITHIN CHI-SQUARE TEST, END ITERATIONS

INITIAL GUESS MODEL PARAMETERS

LAYER	THICKNESS (m)	RESISTIVITY (Ωm)	THICK/RES (S)	THICK × RES (Ωm^2)
1	.8	62.0	.01	49.6
2	1.4	248.0	.01	347.2
3	2.3	40.7	.06	93.6
4	10.2	105.0	.10	1071.0
5	30.3	29.3	1.03	887.8
6		4.4		

FINAL MODEL PARAMETERS

LAYER	THICKNESS (m)	RESISTIVITY (Ωm)	THICK/RES (S)	THICK × RES (Ωm^2)
1	1.0	72.4	.01	69.6
2	1.1	167.3	.01	189.2
3	1.5	54.7	.03	83.2
4	10.3	83.1	.12	856.3
5	35.8	41.1	.87	1473.6
6		1.5		

FINAL MODEL PARAMETERS AND STATISTICS

PARAMETER	FINAL SOLUTION	STANDARD DEVIATION	RESOLUTION
1	1.0	165.0	.62
2	1.1	658.4	.54
3	1.5	933.4	.54
4	10.3	641.2	.37
5	35.5	139.5	.46
6	72.4	77.8	.63
7	167.3	481.5	.47
8	54.7	901.4	.44
9	83.1	277.3	.67
10	41.1	220.7	.49
11	1.5	76.14	.75

PARAMETER CORRELATION MATRIX, LOWER LEFT HALF

	1	2	3	4	5	6	7	8	9	10	11
1	1.00										
2	-.96	1.00									
3	.83	-.95	1.00								
4	-.69	.83	-.95	1.00							
5	-.36	.47	-.62	.79	1.00						
6	.99	-.91	.76	-.61	.79	1.00					
7	.99	-.99	.89	-.76	-.41	.95	1.00				
8	.84	-.96	1.00	-.94	-.59	.77	.91	1.00			
9	.64	-.79	.93	-1.00	-.80	.57	.71	.91	1.00		
10	.46	-.59	.75	-.90	-.97	.40	.52	.72	.91	1.00	
11	.39	-.51	.65	-.82	-1.00	.34	.44	.63	.83	97	1.00

FINAL MODEL DATA AND STATISTICS

SPACING (m)	OBSERVED DATA (Ωm)	CALCULATED DATA (Ωm)	ERROR (Ωm)	WEIGHTS	INFORMATION
1.5	85.2	84.0	1.2	38.7	.97
2.0	93.5	90.0	3.4	46.6	.69
2.5	95.3	94.5	0.8	48.4	.71
3.0	95.2	96.9	-1.7	48.3	.69
4.0	91.9	97.5	-5.6	45.0	.79
5.0	90.8	95.1	-4.3	43.9	.71
6.0	90.0	91.9	-1.9	43.2	.70
8.0	90.2	86.1	4.1	43.4	.75
10.0	91.7	82.3	9.4	44.8	.62
12.0	83.2	79.6	3.7	36.9	.65
15.0	77.9	76.5	1.5	32.3	.74
20.0	76.6	71.3	5.3	31.3	.69
25.0	77.4	66.0	11.4	31.9	.66
30.0	56.6	60.6	-4.0	17.1	.71
40.0	47.4	51.1	-3.7	12.0	.81
50.0	42.2	43.1	-0.9	9.5	.72
60.0	37.4	36.3	1.1	7.5	.66
70.0	30.4	30.6	-0.2	4.9	.58
80.0	21.8	25.8	-4.0	2.5	.84
100.0	15.9	17.6	-1.7	1.4	1.00

FINAL SOLUTION EIGENVALUES

2.15 1.90 1.37 .80 .49 .13 .07 .03 .009 004 .0009

105
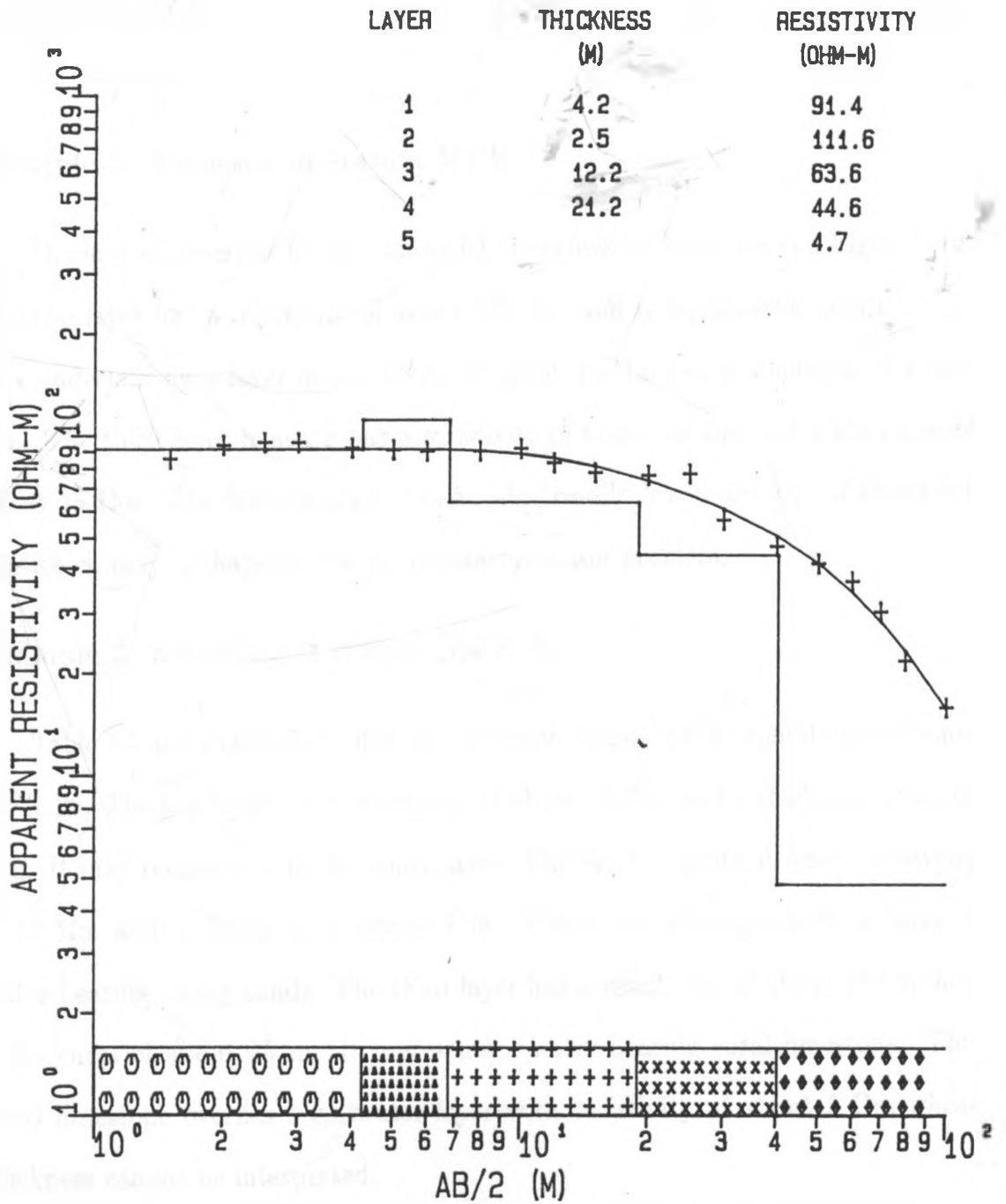
Fig. 5.9   Inversion results of sounding MPK 39

may represent calcareous, wet sands overlying a thick coral limestone. The coral limestone overlies low resistivity saltwater bearing sediment. The layers with resistivities of 83 Ωm and 41 Ωm may be the same geologic layer but with different characteristics such as saltwater content and amount of coral limestone in it. The total thickness of the coral limestone is about 40 m and lies about 4 m below the ground surface.

Example 2: Sounding at station MPK 72

The inversion results for this sounding are shown in Table 5.6 and Figure 5.10. The top layer has a resistivity of about 177 Ωm and a thickness of about 0.5 m. It is underlain by a layer of resistivity of about 14 Ωm and a thickness of about 7 m. The third layer beneath has a resistivity of about 55 Ωm and a thickness of about 35 Ωm. The layer beneath has an abnormally low resistivity of about 0.1 Ωm which may perhaps be due to an interpretation problem.

Example 3: Sounding at station MPK 20

Table 5.7 and Figure 5.11 show the inversion results for the sounding at station MPK 20. The top layer has a resistivity of about 75 Ωm and a thickness of about 1 m. It may represent a moist sandy layer. The layer beneath it has a resistivity of 18 Ωm and a thickness of about 7 m. This layer corresponds to a layer of water-bearing clayey sands. The third layer has a resistivity of about 78 Ωm and a thickness of about 35 m. It represents a water-bearing coral limestone. This coral limestone overlies a saltwater layer with resistivity of about 3 Ωm whose thickness cannot be interpreted.

The drilling results shown in Figure 5.12 indicate that the top layer consists

Table 5.6   Inversion results of sounding MPK 72

ITERATION	MARQT CONST.	CHI-SQUARE VALUE	%RMS
1	.10E-01	.13E+03	.17E+02
2	.10E-01	.23E+02	.70E+01
3	.10E-02	.46E+02	.99E+01
3	.10E-01	.23E+02	.70E+01
4	.10E-01	.25E+02	.73E+01
4	.10E+00	.23E+02	.70E+01
5	.10E+00	.21E+02	.67E+01

CONVERGED WITHIN CHI-SQUARE TEST, END ITERATIONS

INITIAL GUESS MODEL PARAMETERS

LAYER	THICKNESS (m)	RESISTIVITY (Ωm)	THICK/RES (S)	THICK × RES (Ωm^2)
1	.5	250.0	.00	125.0
2	6.5	16.4	.40	106.6
3	28.1	65.2	.43	1832.1
4		4.7		

FINAL MODEL PARAMETERS

LAYER	THICKNESS (m)	RESISTIVITY (Ωm)	THICK/RES (S)	THICK × RES (Ωm^2)
1	.5	176.6	.00	93.5
2	6.5	14.0	.47	91.6
3	35.0	55.1	.64	1931.9
4		.1		

FINAL MODEL PARAMETERS AND STATISTICS

PARAMETER	FINAL SOLUTION	STANDARD DEVIATION	RESOLUTION
1	.5	4.5	.62
2	6.5	5.5	.74
3	35.0	20.2	.36
4	176.6	3.9	.67
5	14.0	3.0	.77
6	55.1	13.7	.51
7	.1	8.4	.54

PARAMETER CORRELATION MATRIX, LOWER LEFT HALF

	1	2	3	4	5	6	7
1	1.00						
2	-.49	1.00					
3	.25	-.82	1.00				
4	-.94	.39	-.19	1.00			
5	-.71	.74	-.41	.57	1.00		
6	-.28	.89	-.96	.21	.46	1.00	
7	-.14	.55	-.89	.11	.24	.74	1.00
	1	2	3	4	5	6	7

FINAL MODEL DATA AND STATISTICS

SPACING (m)	OBSERVED DATA (Ωm)	CALCULATED DATA (Ωm)	ERROR (Ωm)	WEIGHTS	INFORMATION
1.5	53.6	49.7	3.9	12.9	.85
2.0	27.4	30.1	-2.7	3.4	.66
2.5	20.4	18.9	1.5	1.9	.76
3.0	16.5	16.3	0.1	1.2	.57
4.0	14.4	16.0	-1.6	0.9	.66
5.0	14.9	15.2	-0.3	1.0	.51
6 0	15.6	15.4	0.2	1.1	.43
8.0	18.1	16.9	1.2	1.5	.40
10 0	20.4	18.3	2.1	1.9	.44
12.0	21.9	19.9	2.0	2.2	.49
15.0	22.8	22.4	0.4	2.3	.50
20.0	24.1	26.1	-2.0	2.6	.46
25.0	26.3	29.0	-2.7	3.1	.46
30.0	29.4	31.1	-1.7	3.9	.48
40.0	32.7	33.4	-0.7	4.8	.51
50.0	35.5	33.7	1.8	5.7	.44
60.0	35.6	32.5	3.1	5.7	.40
70.0	30.9	30.5	0.4	4.3	.47
80.0	25.3	26.4	-1.1	2.9	.61
100.0	23.0	22.0	1.0	2.4	.61
130.0	13.8	14.4	-0.6	0.9	.98

FINAL SOLUTION EIGENVALUES

1.69   1.50   1.25   .51   .24   .18   .05

109
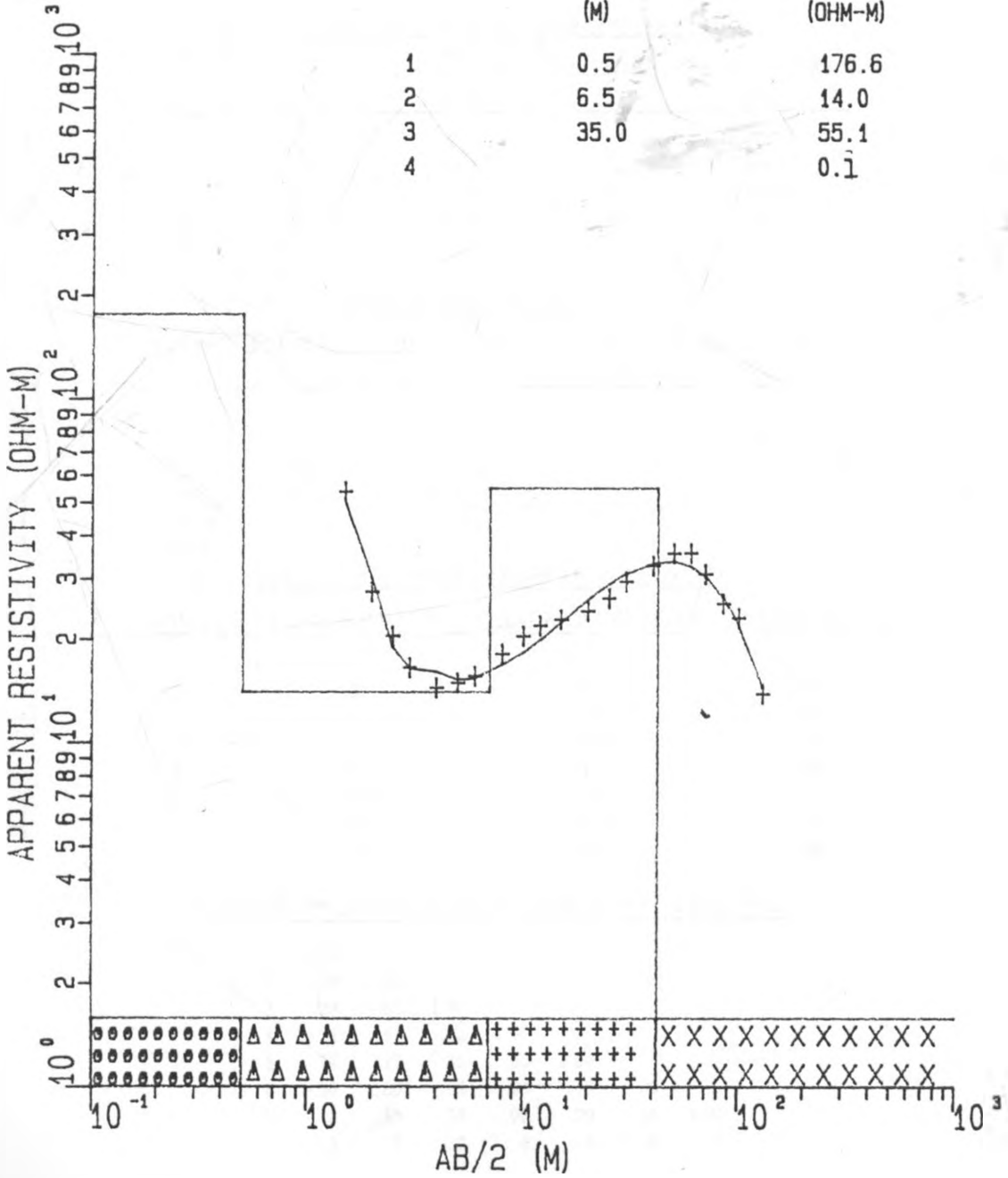
Fig. 5.10   Inversion results of sounding MPK 72

110

Table 5.7   Inversion results of sounding MPK 20

ITERATION	MARQT CONST.	CHI-SQUARE VALUE	%RMS
1	.10E-01	.59E+02	.74E+01
2	.10E-01	.24E+02	.47E+01
3	.10E-02	.24E+02	.47E+01
4	.10E-02	.23E+02	.46E+01

CONVERGED WITHIN CHI-SQUARE TEST, END ITERATIONS

INITIAL GUESS MODEL PARAMETERS

LAYER	THICKNESS (m)	RESISTIVITY (Ωm)	THICK/RES (S)	THICK $\times$ RES (Ωm^2)
1	.7	71.0	.01	49.7
2	7.3	17.1	.43	124.8
3	30.1	102.4	.29	3082.2
4		1.5		

FINAL MODEL PARAMETERS

LAYER	THICKNESS (m)	RESISTIVITY (Ωm)	THICK/RES (S)	THICK $\times$ RES (Ωm^2)
1	.6	75.3	.01	45.9
2	6.8	17.9	.38	122.3
3	34.8	78.0	.45	2712.5
4		3.4		

FINAL MODEL PARAMETERS AND STATISTICS

PARAMETER	FINAL SOLUTION	STANDARD DEVIATION	RESOLUTION
1	.6	5.0	.98
2	6.8	5.8	.98
3	34.8	16.8	.85
4	75.3	4.1	.99
5	17.9	3.5	.99
6	78.0	13.2	.91
7	3.3	4.3	.99

PARAMETER CORRELATION MATRIX, LOWER LEFT HALF

	1	2	3	4	5	6	7
1	1.00						
2	-.59	1.00					
3	.29	-.83	1.00				
4	-.94	.47	-.22	1.00			
5	-.77	.79	-.45	.62	1.00		
6	-.30	.86	-.98	.23	.46	1.00	
7	-.13	.45	-.77	.09	.20	.66	1.00
	1	2	3	4	5	6	7

FINAL MODEL DATA AND STATISTICS

SPACING (m)	OBSERVED DATA (Ωm)	CALCULATED DATA (Ωm)	ERROR (Ωm)	WEIGHTS	INFORMATION
1.5	39.9	38.7	1.2	3.4	.91
2.0	28.1	29.7	-1.6	1.7	.61
2.5	24.0	23.9	0.1	1.2	.73
3.0	22.9	21.6	1.3	1.1	.53
4.0	20.3	20.1	0.2	0.9	.52
5.0	18.6	19.7	-1.1	0.7	.55
6.0	19.5	19.9	-0.4	0.8	.49
8.0	21.4	21.3	0.1	1.0	.42
10.0	24.4	23.1	1.3	1.3	.41
12.0	26.6	25.1	1.5	1.5	.46
15.0	28.5	28.4	0.1	1.7	.51
20.0	30.5	33.4	-2.9	2.0	.48
25.0	35.9	37.4	-1.5	2.7	.41
30.0	43.7	40.6	3.1	4.0	.37
40.0	45.3	44.4	0.9	4.3	.45
50.0	45.6	45.7	-0.1	4.4	.47
60.0	44.3	45.2	-0.9	4.2	.44
70.0	45.3	43.2	2.0	4.3	.39
80.0	40.1	39.0	1.1	3.4	.40
100.0	32.8	34.0	-1.2	2.3	.50
130.0	23.0	24.3	-1.3	1.1	.63
160.0	18.4	16.9	1.5	0.7	.55
200.0	10.5	10.7	-0.2	0.3	.96

FINAL SOLUTION EIGENVALUES

1.72   1.51   1.18   .48   .33   .17   .05
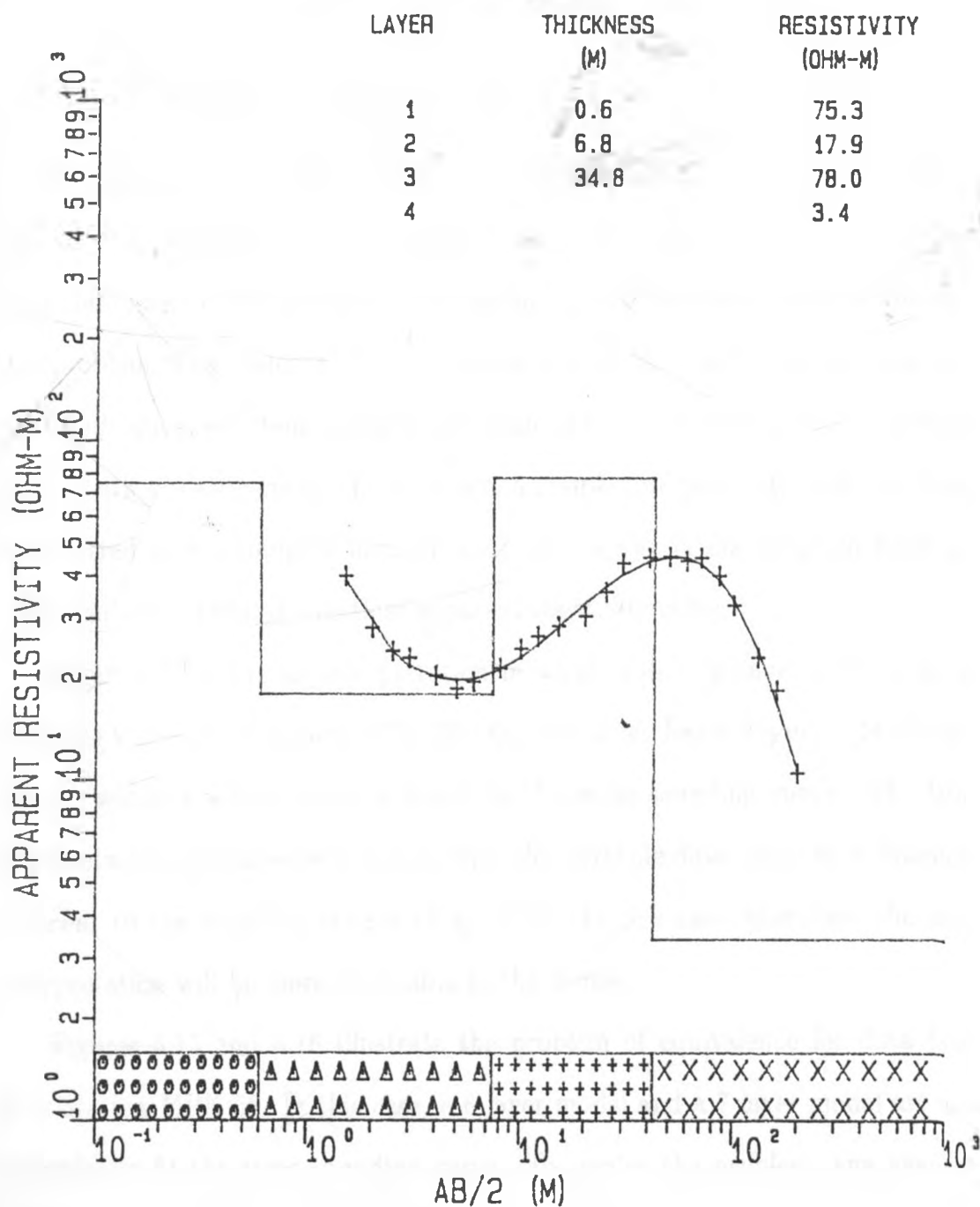
Fig. 5.11   Inversion results of sounding MPK 20

of clayey sandy top soil which is underlain by sandy clay with decomposed coral. The third layer represents a water-bearing coral limestone.

5.7 Problems associated with the interpretation of vertical electrical resistivity data

5.7.1 Problem of equivalence

As discussed earlier (see section 3.7.2), geoelectric models may have similar apparent resistivity curves although the parameters used to generate these curves have completely different values. This similarity may be due to what is known as the 'problem of equivalence'. Where several equally likely solutions are possible in such a situation, selection is practically made of the solution that most reasonably agrees with known geology. In principle, a simple interpretation with few layers is preferred over a complex interpretation with many layers although both may mathematically yield an identical apparent resistivity curve.

Figure 5.13 shows an interpretation in which a 4-layer curve is fitted to the sounding curve from station MPK 20. On the other hand, Figure 5.14 shows a case in which a 6-layer curve is fitted to the same sounding curve. The latter interpretation correlates very closely with the borehole data taken from boreholes adjacent to the sounding station (Fig. 5.12). In this case, therefore, the latter interpretation will be more preferable to the former.

Figures 5.15 and 5.16 illustrate the problem of equivalence for data taken from station MPK 38. In this case, a 6-layer model and a 7-layer model are used to perfectly fit the same sounding curve. To resolve the problem, any available geologic and/or other information should be used.
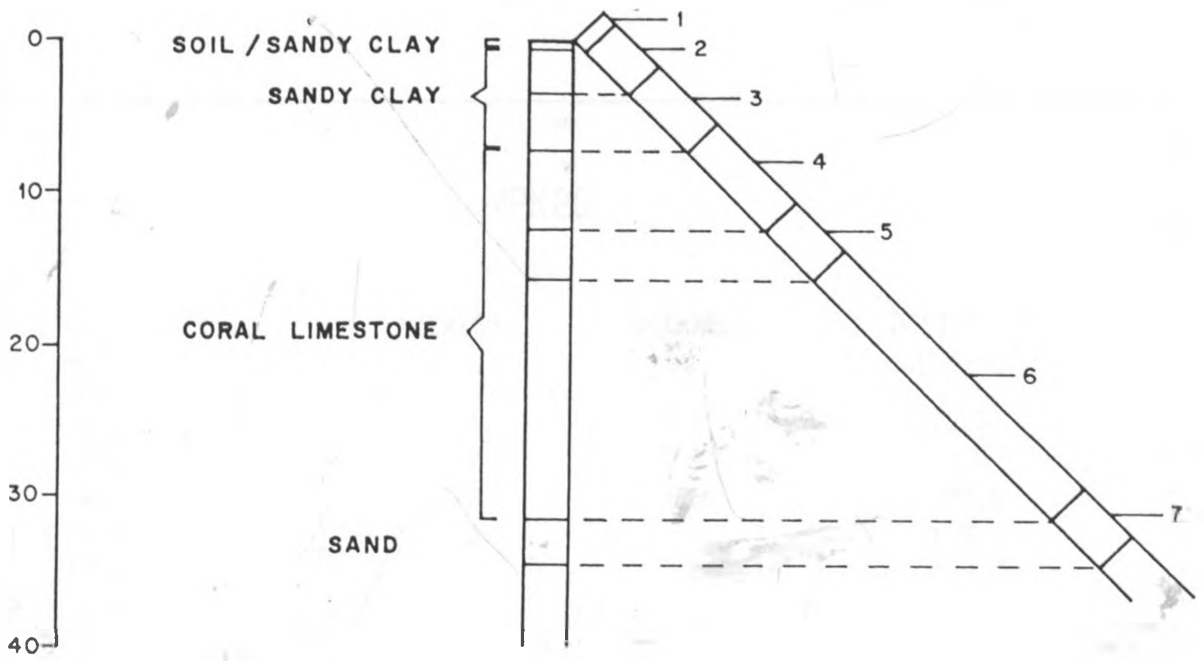
1. Clay top sandy soil (brown)
2. Sandy clay
3. Sandy clay with decomposed coral limestone
4. Unconsolidated coral with frequent cavities
5. Unconsolidated decomposed coral with cavities
6. Unconsolidated decomposed coral with clay lenses
7. Medium grained sand

Fig. 5.12   Drill hole results for borehole C-7345 next to sounding MPK 20

115

Fig. 5.13   4-layer model curve fitted to sounding MPK 20

116

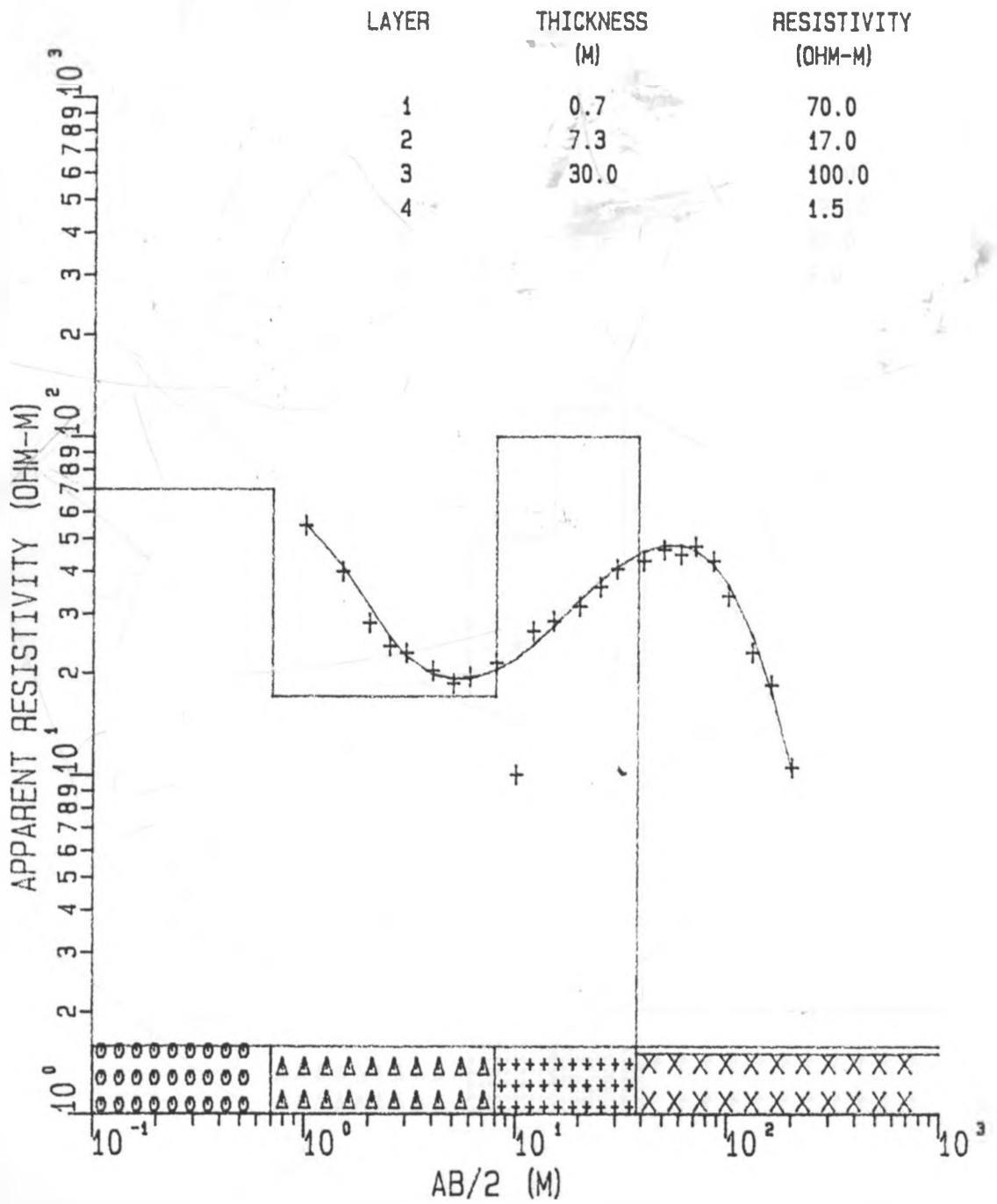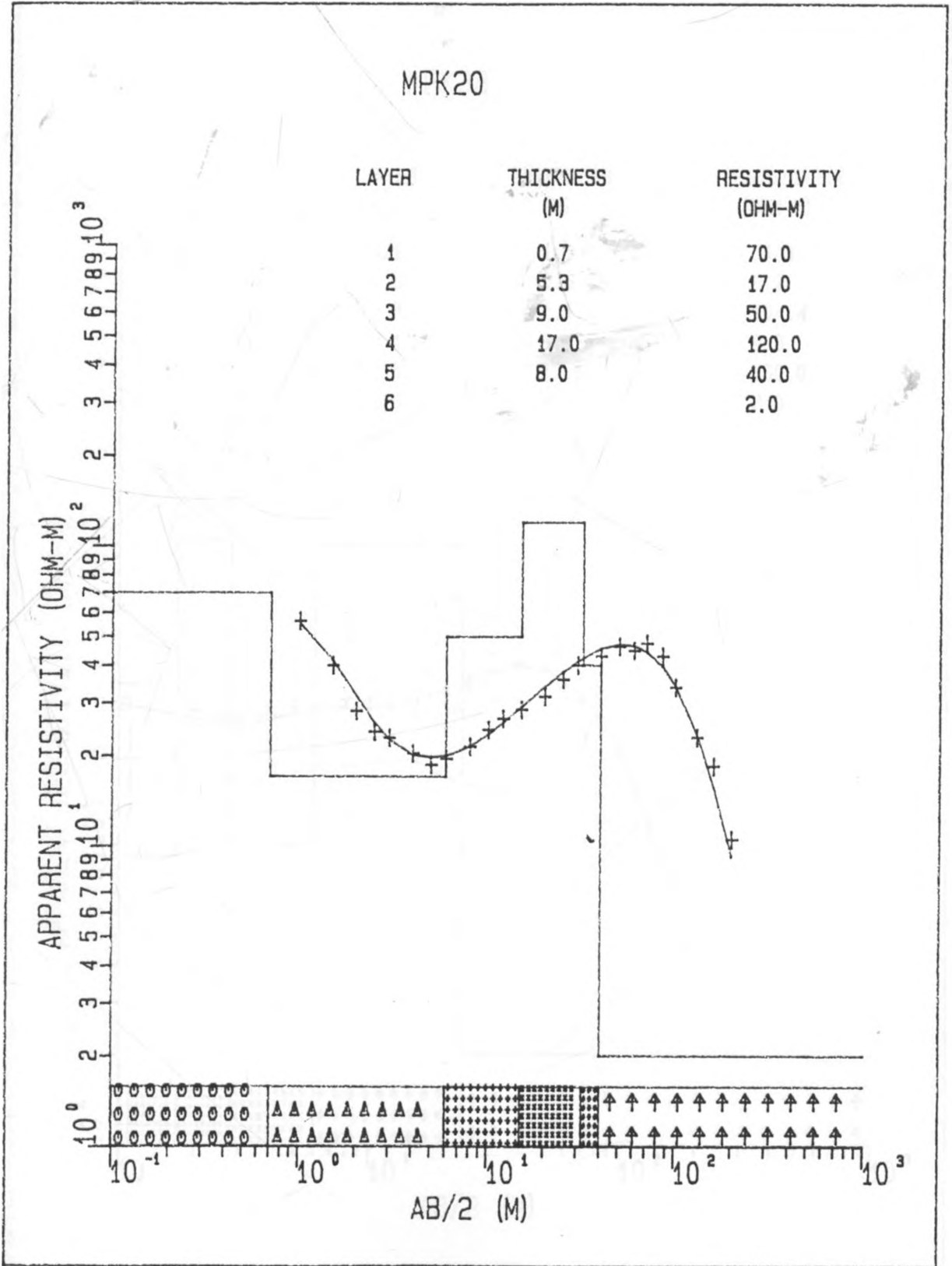Fig. 5.14   6-layer model curve fitted to sounding MPK 20 to show principle of equivalence

117
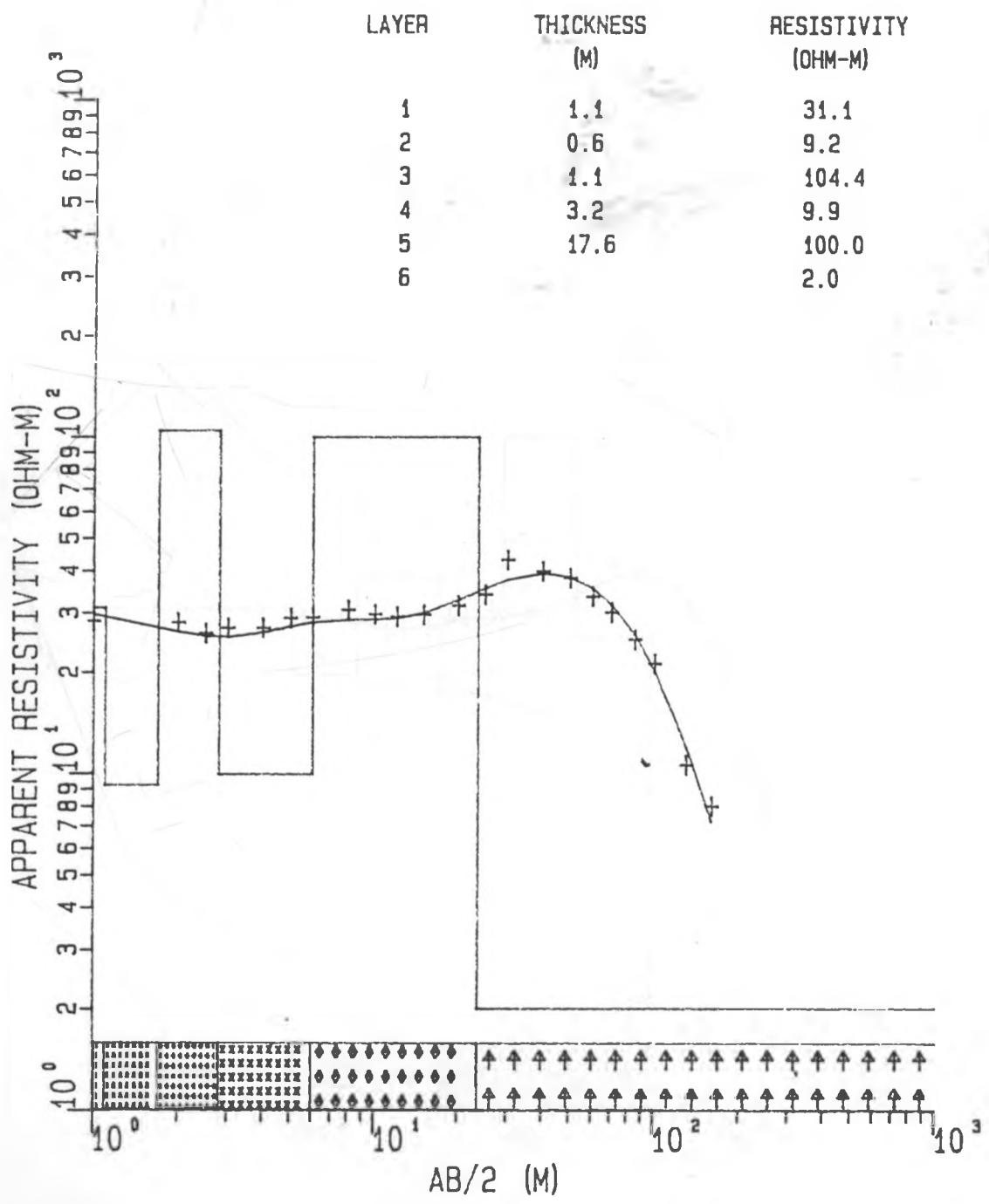
Fig. 5.15   6-layer model curve fitted to sounding MPK 38

118
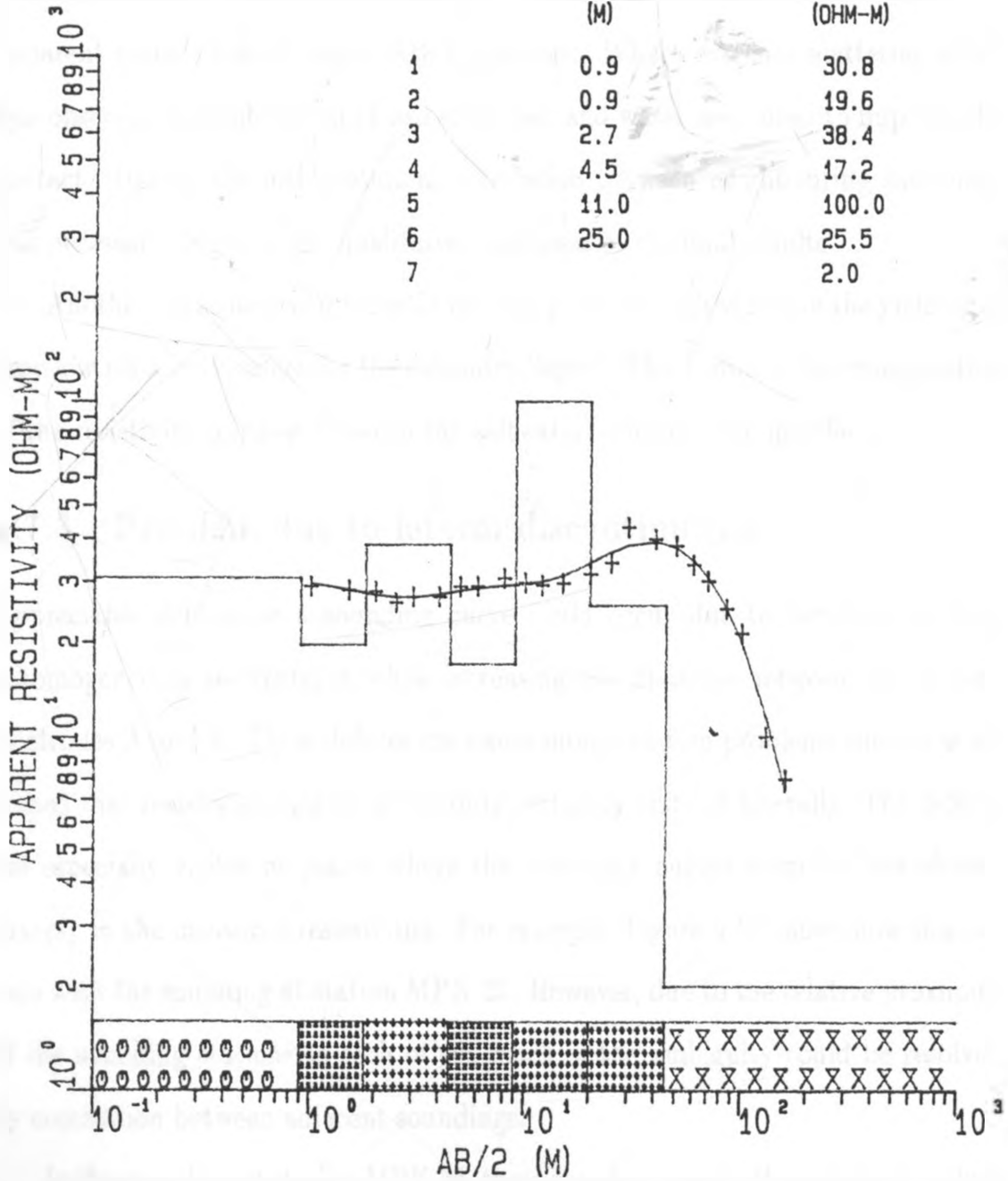
Fig. 5.16   7-layer model curve fitted to sounding MPK 38 to show principle of equivalence

5.7.2 Problem of high resistivities on the ground surface

The problem of this nature is inherent in places where dry loose sands are encountered. In the study area, difficulties were encountered when introducing the electric current into the dry sands. Because of the high contact resistance between the current electrodes and the dry sands, there resulted a wide scatter of apparent resistivities at larger AB/2 spacings. Where extreme scattering effect was observed, a combination of two steel rods and water were used to improve the contact. During the interpretation, correlation between neighbouring soundings was necessary to give some qualitative appraisal of the final results.

Another consequence of the poor contact problem was evident in the yielding of very low resistivity values for the saltwater 'layer'. This is due to the exaggeration of the resistivity contrast between the saltwater/country rock interface.

5.7.3 Problem due to lateral discontinuities

Appreciable defects on a sounding curve could occur due to localized surficial inhomogeneities encountered while increasing the distance between the current electrodes A and B. These defects can cause interpretation problems since it is assumed that resistivity changes occur only vertically and not laterally. The defects are especially visible at places where the resistivity curves seem to "overshoot" sharply in the measured resistivities. For example, Figure 5.17 shows how this occurs with the sounding at station MPK 23. However, due to the relative proximity of the sounding stations to each other, much of the ambiguity could be resolved by correlation between adjacent soundings.

In the sounding at station MPK 23, there is a sharp rise in the resistivity values between spacings AB/2 = 30 m and AB/2 = 70 m forming an overshoot. Between
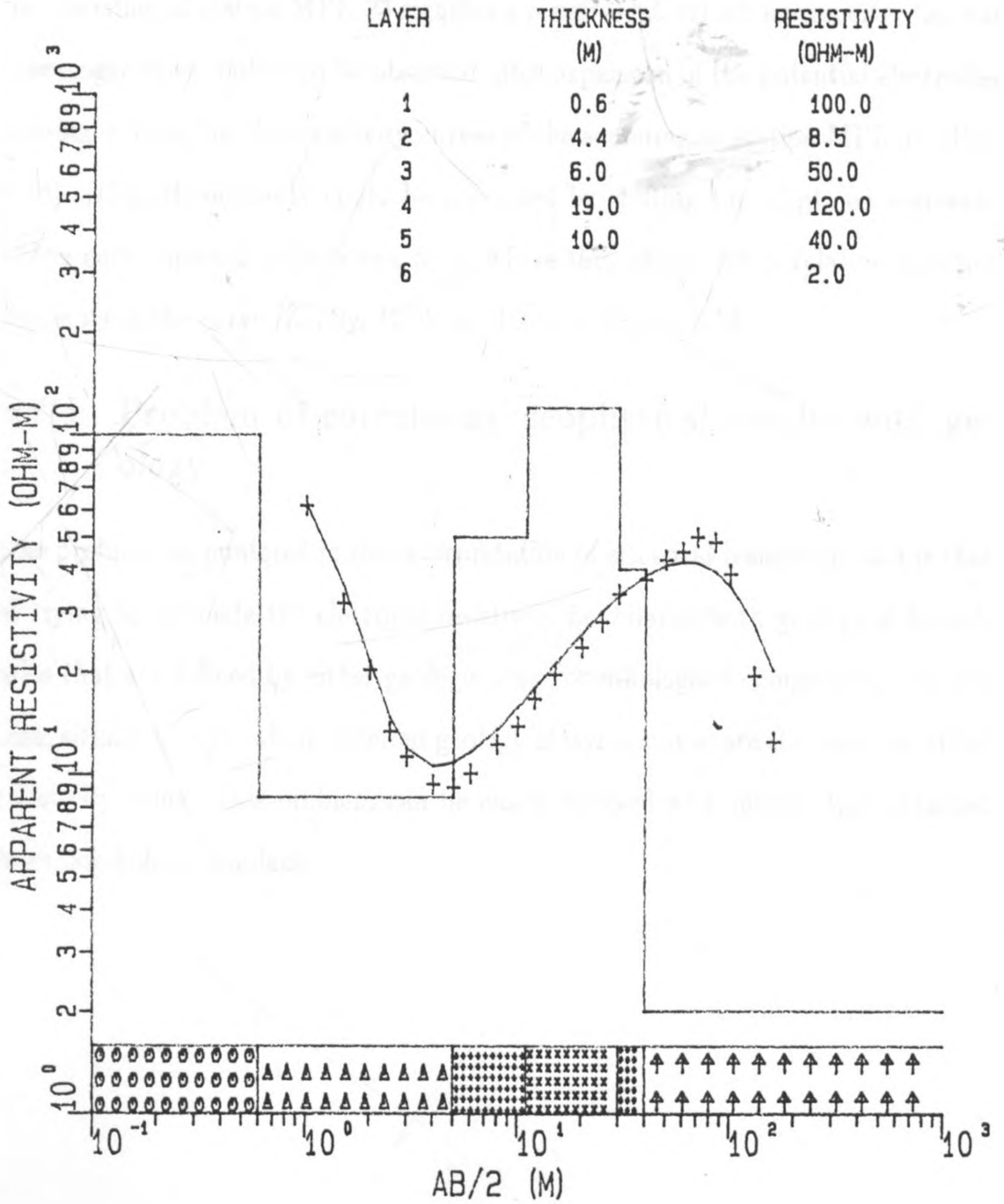
Fig. 5.17   Overshoot in measured resistivity data in sounding MPK 23

spacings $AB/2 = 70$ m and $AB/2 = 160$ m, there is a sudden drop in resistivities. The two branches of the sounding curve form a sharp cusp that could not be fitted with the computer generated curves, and if so done, produced unfairly high or low resistivity and thickness values for the corresponding layers. The type of cusp in the sounding at station MPK 23 signifies a resistive lateral inhomogeneity. Lateral inhomogeneities could also be observed after expansion of the potential electrodes causing a 'jump' in the resistivity curves of the sounding at station MPK 19 (Fig. 5.18). This discontinuity could be corrected by shifting the displaced segments of the curve upward (or downward) to where they should be in relation to other segments of the curve (Zohdy, 1974) as shown in Figure 5.18.

5.7.4 Problem of correlating geophysical results with geology

One problem encountered in the interpretation of electrical resistivity data is that of trying to correlate the electrical resistivity boundaries with geological boundaries that are defined by either geological age or lithological composition. In this case, situations arise where different geological layers may share the same electrical resistivity value. This problem can be easily resolved with information obtained from boreholes if available.
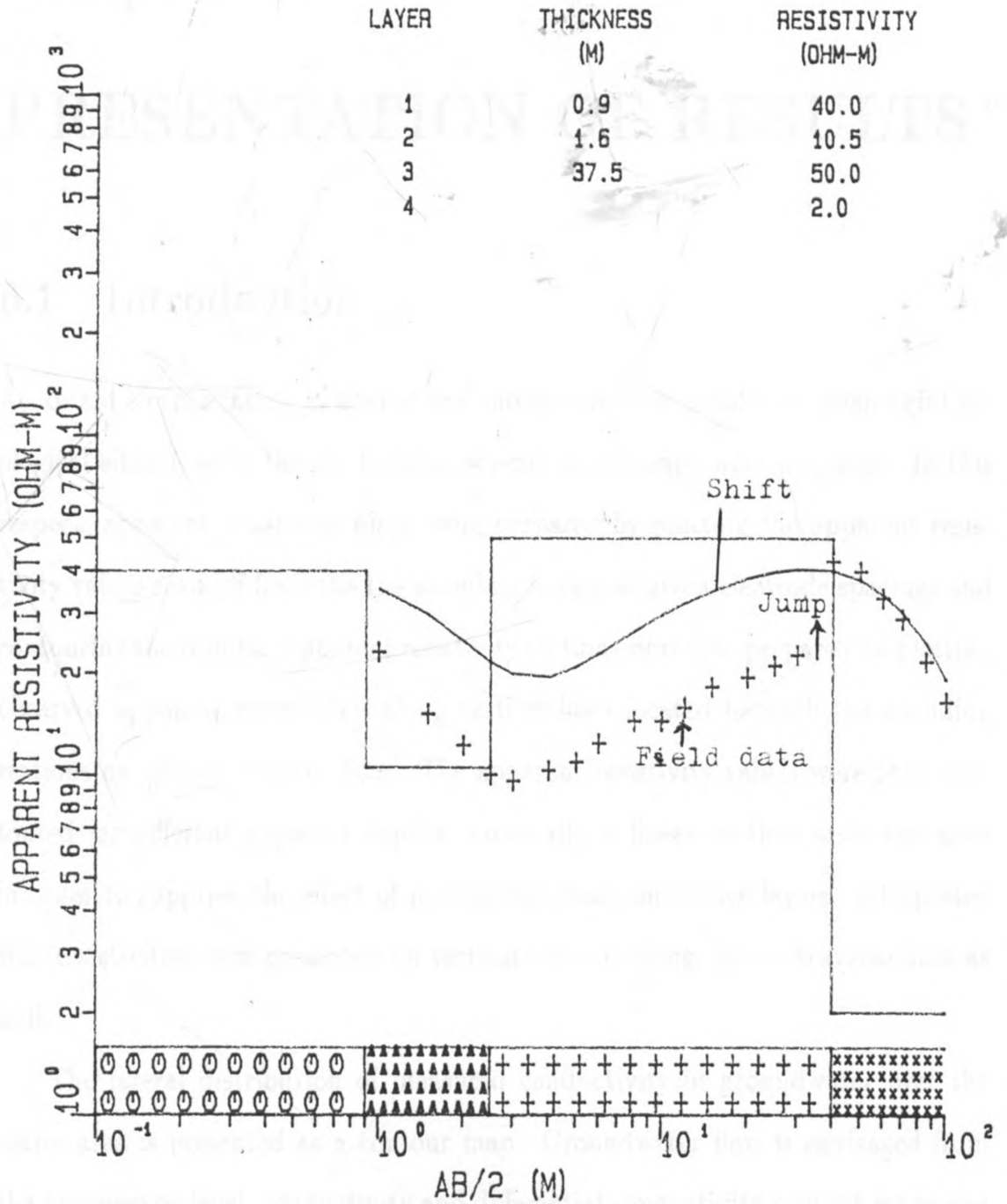
Fig. 5.18   Jump in measured resistivity data in sounding MPK 19

Chapter 6

PRESENTATION OF RESULTS

6.1 Introduction

As an aid to correlating measured and interpreted field results to meaningful geological situations in the study area, several result maps were prepared. In this respect, apparent resistivity maps were prepared by plotting the apparent resistivity values read off from the the sounding curves at given electrode spacings and contouring the results. Apparent resistivity sections were also prepared by plotting observed apparent resistivities along vertical lines located beneath the sounding stations on chosen traverse lines. The apparent resistivity values were then contoured for different apparent depths. Generally, a linear vertical scale was used in order to suppress the effect of near-surface non-conductive layers. Interpreted true resistivities were presented on vertical sections along chosen traverse lines as well.

The lateral distribution of measured conductivity of groundwater over the entire area is presented as a contour map. Groundwater flow is envisaged from the piezometric level, conductivity and differential conductivity contour maps and hydrographs. Depth to the freshwater/saltwater interface and to the coral as well

as the coral thickness and extent of the aquifer are also discussed.

6.2 Distribution of apparent and true resistivities

6.2.1 Lateral distribution of apparent resistivities

6.2.1.1 Introduction

Apparent resistivity maps have been presented. It should be emphasized, however, that an apparent resistivity map for a given current electrode spacing does not represent the aereal variation of the true resistivity at the depth corresponding to that particular electrode spacing but, instead, it only indicates the general lateral variation in apparent resistivity in the area at nearly half the current electrodes separation.

6.2.1.2 Apparent resistivities for $AB/2 = 25$ m

The resistivity pattern displayed for this depth is one of variance (Fig.6.1). Clusters of high resistivities ranging between 20 and 70 Ωm are observed on the northern part of the study area. A similar high resistivity density with a range of 40-60 Ωm is observed at the southern part. The general trend shows an increase in resistivity towards the central part. Farther away from Lake Kenyatta, the resistivity values display a distinctive decrease. The eastern section shows relatively high resistivity values of up to 90 Ωm. The high resistivity values for the area near the lake depict a fresh water-bearing formation whose salinity depends on the composition and increases radially outward from the lake. The iso-resitivity contour maps were plotted with an interval of 10 Ωm.

Fig. 6.1 Lateral distribution of apparent resistivity for AB/2 = 25 m

126

6.2.1.3 Apparent resistivities for AB/2 = 40 m

Like in the case of AB/2 = 25 m, apparent resistivities for AB/2 = 40 m (Fig. 6.2) show unique trends with peak values of up to 60 Ωm at the northern part of the study area and another peak at the southern part. Generally, the resistivity increases eastwards to a maximum of 80 Ωm. Farther away from the lake, resistivity values go below 15 Ωm depicting a trend towards high salinity. Localised pockets of high resistivity are observed. This could be interpreted as a coincidence with local aquifer systems. On the northern part, resitivity values drop to less than 15 Ωm.

6.2.1.4 Apparent resistivities for AB/2 = 50 m

The apparent resistivity distribution for this depth (Fig. 6.3) displays similar trends as observed for AB/2 = 25 m and AB/2 = 40 m. However, it is noteworthy that the apparent resistivity values are generally decreasing with increasing probing depth. The resistivity reaches peak values at three distinct positions - 55 Ωm, 50 Ωm and 75 Ωm in the northern, southern and eastern peaks, respectively. These peaks denote local low conductivity bodies. Elsewhere from south-west to north-east, the apparent resistivity increases away from the lake to a maximum depicting the extensive fresh groundwater body. Beyond the peaks in a direction away from the lake, the resistivity decreases very rapidly to less than 15 Ωm, thus indicating the horizontal extent of the fresh groundwater body. Locally, highly conductive zones are observed. These could be representative of clay lenses consisting of marine sediments saturated with fossil saltwater. These saltwater bodies are of limited extent and have been confirmed from groundwater conductivity measurements in the project area.

Fig. 6.2 Lateral distribution of apparent resistivity for AB/2 = 40 m

128
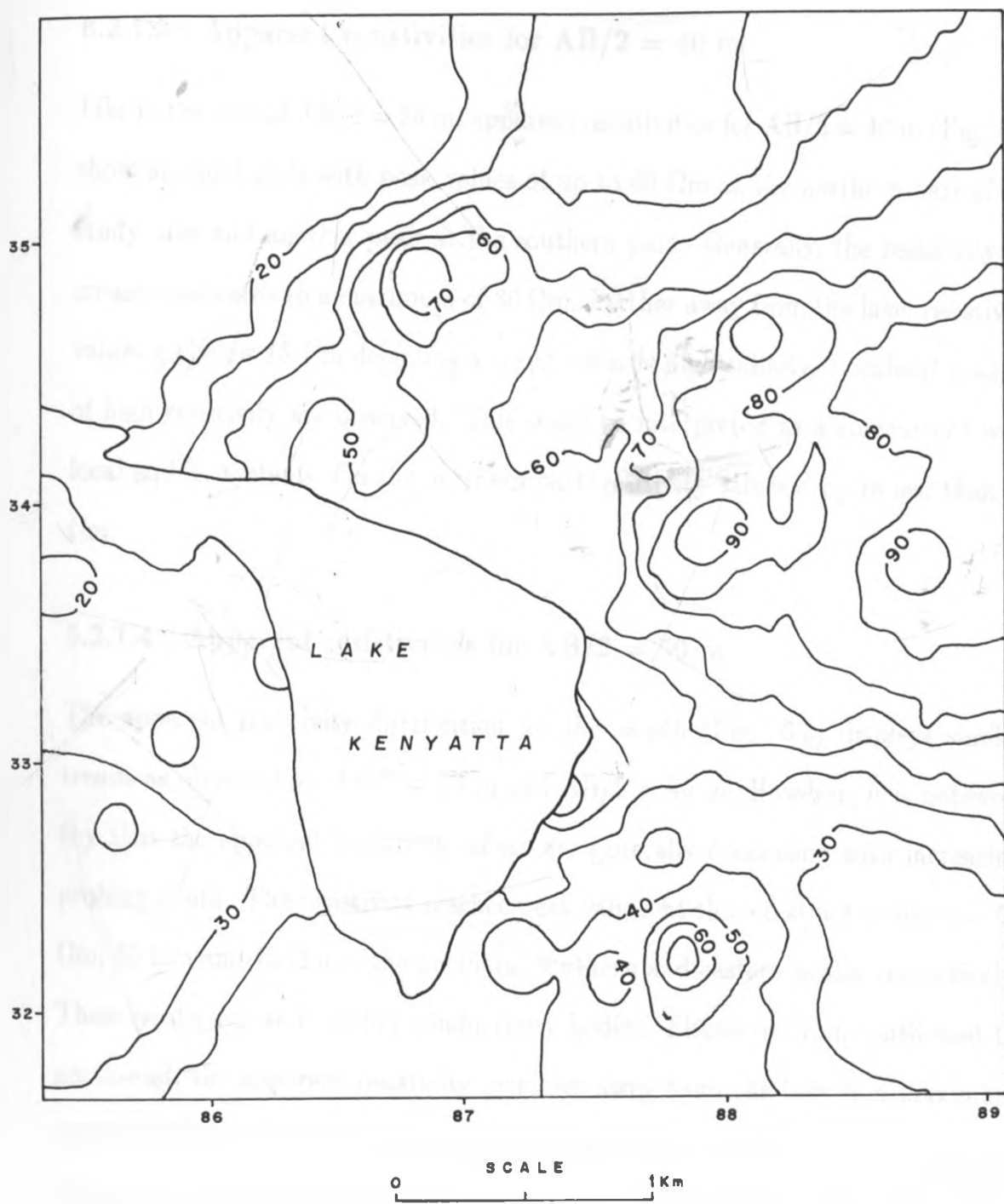
Fig. 6.3 Lateral distribution of apparent resistivity for AB/2 = 50 m

6.2.1.5   Apparent resistivities for AB/2 = 63 m

The apparent resistivities for this depth (Fig. 6.4) display similar patterns to those observed for AB/2 = 25 m, 40 m and 50 m. However, the apparent resistivity values for AB/2 = 63 m are lower than for any other current electrode spacing. The resistivity peaks are observed at the northern, southern and eastern parts of the area with values of 50 Ωm, 50 Ωm and 55 Ωm, respectively. As observed in the previous cases, resistivity generally increases from south-west to north-east to a maximum (peak) after which it decreases. It is viewed that the 20 Ωm contour roughly delineates the boundary between the freshwater-bearing formation and the predominantly saline formation. Local highly conductive bodies are also observed indicating local salinization. Overall, resistivity distribution is simple and gradual.

6.2.1.6   Apparent resistivities for AB/2 = 80 m

Patterns simi;ar to those observed for preceding electrode spacings AB/2 = 25 m, 40 m, 50 m and 63 m are observed (Fig. 6.5). However, the peaks at the northern, eastern and southern parts of the area are of about 45 Ωm. The resistivity gradients are very low for this depth, thus suggesting a high homogeneity of the medium matrix composition. Apparent resistivity values generally increase from south-west towards south-south-east. However, inhomogeneities occur in the form of localized low resistivity bodies with less than 15 Ωm.

6.2.1.7   Apparent resistivities for AB/2 = 100 m

Though patterns of resistivity distribution for AB/2 = 100 m (Fig. 6.6) resemble those of all the other electrode spacings previously considered, several variations can be observed very clearly. The values of the resistivity are quite low compared
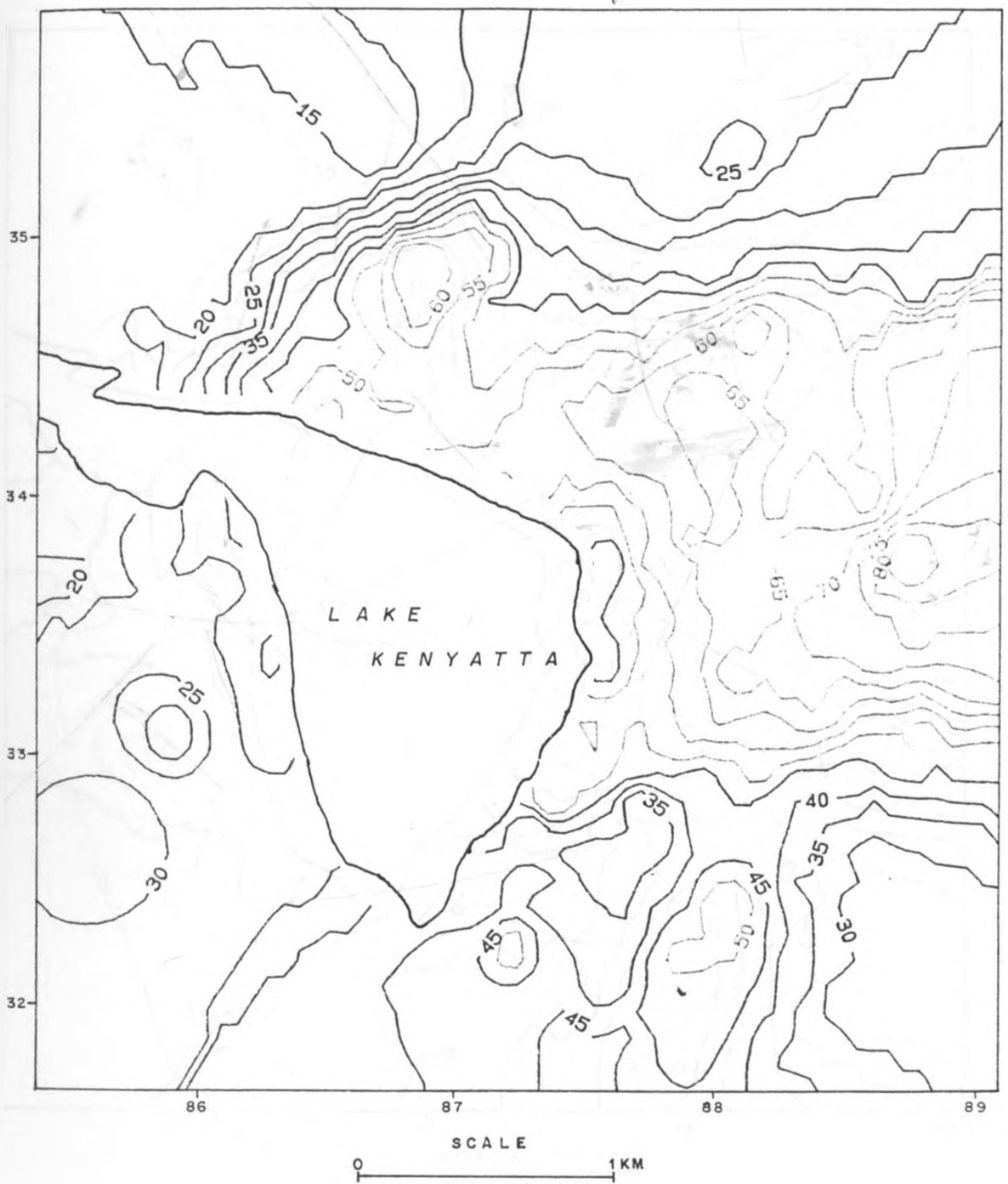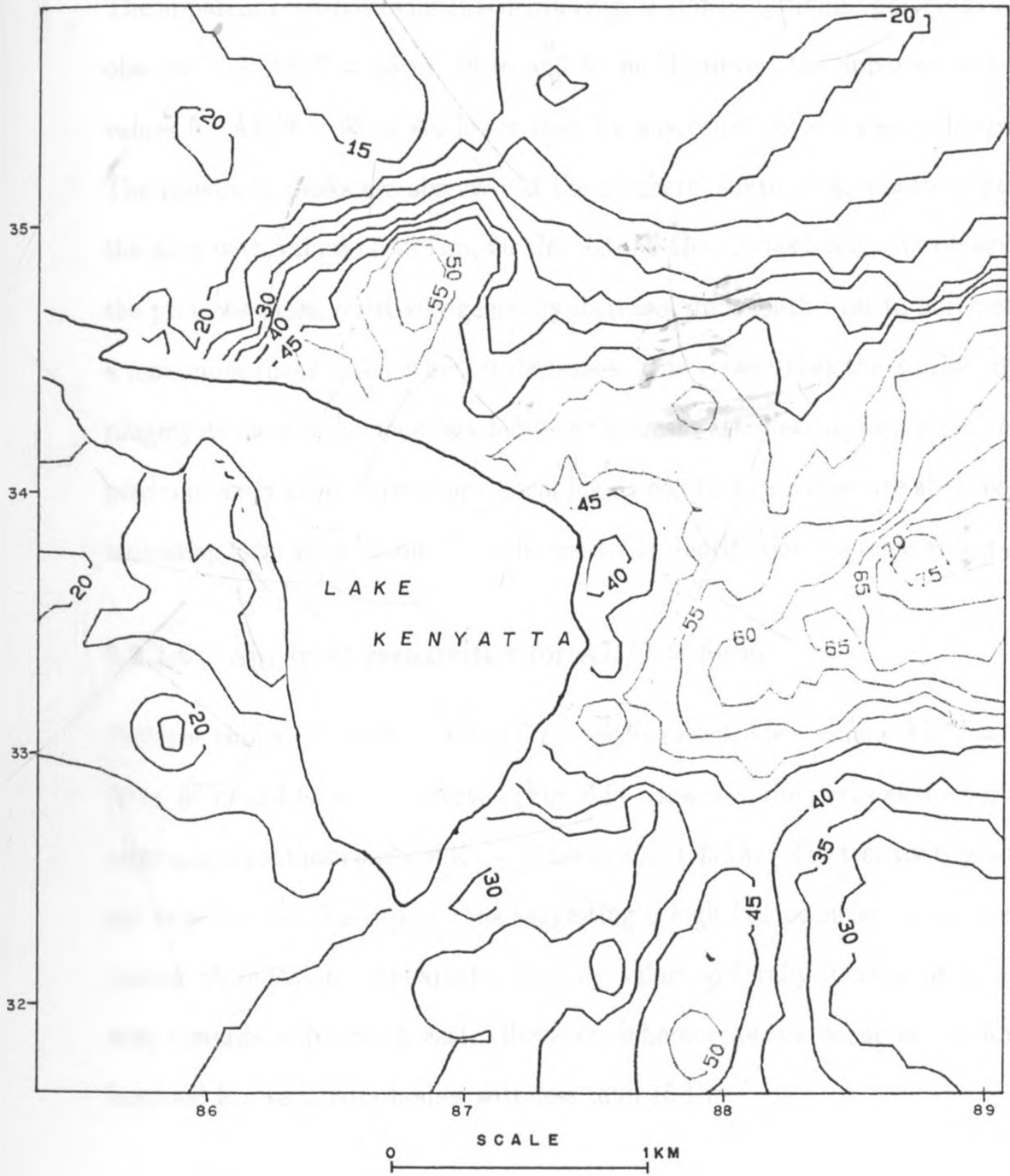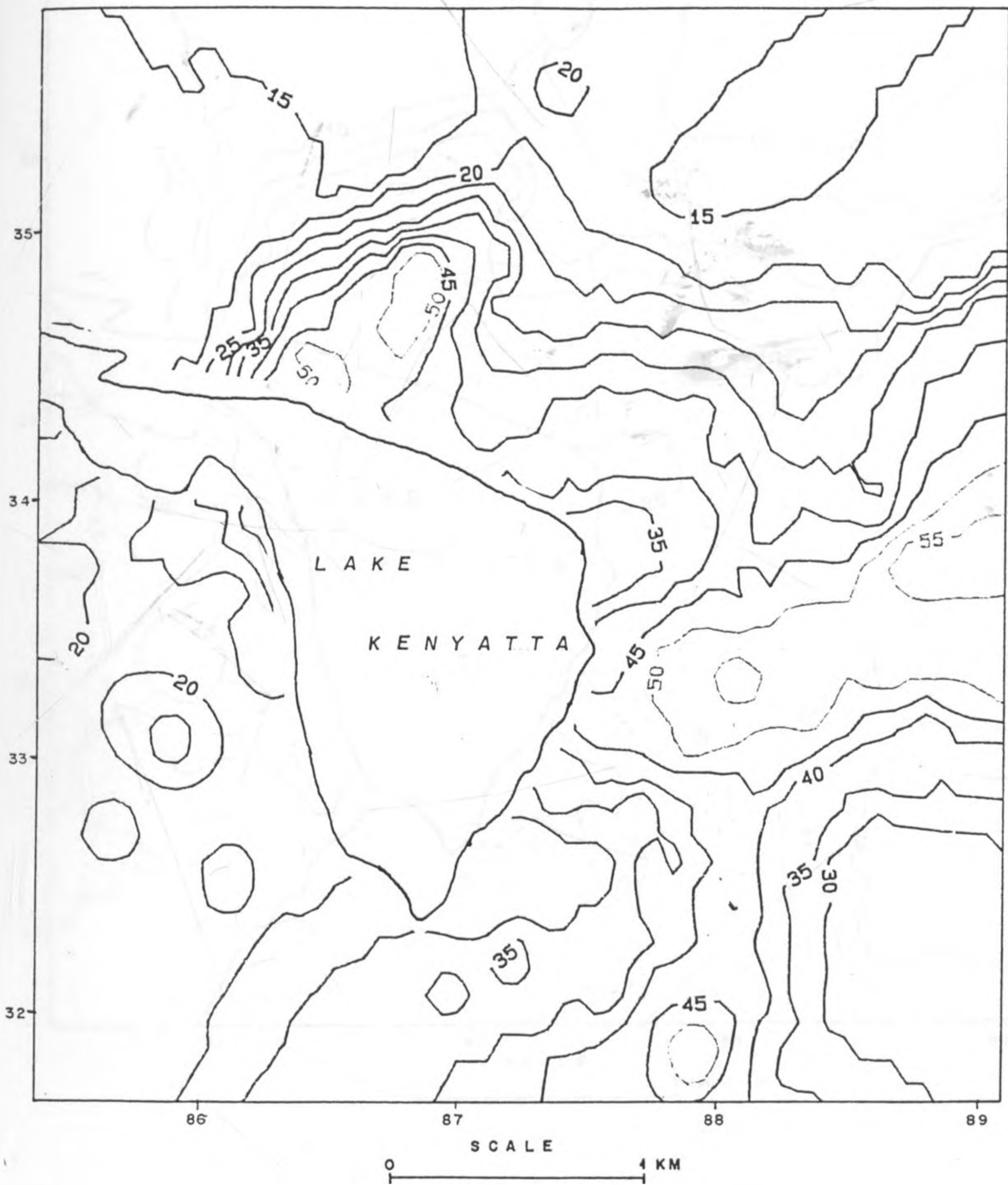
Fig. 6.4   Lateral distribution of apparent resistivity for $AB/2 = 63$ m

131
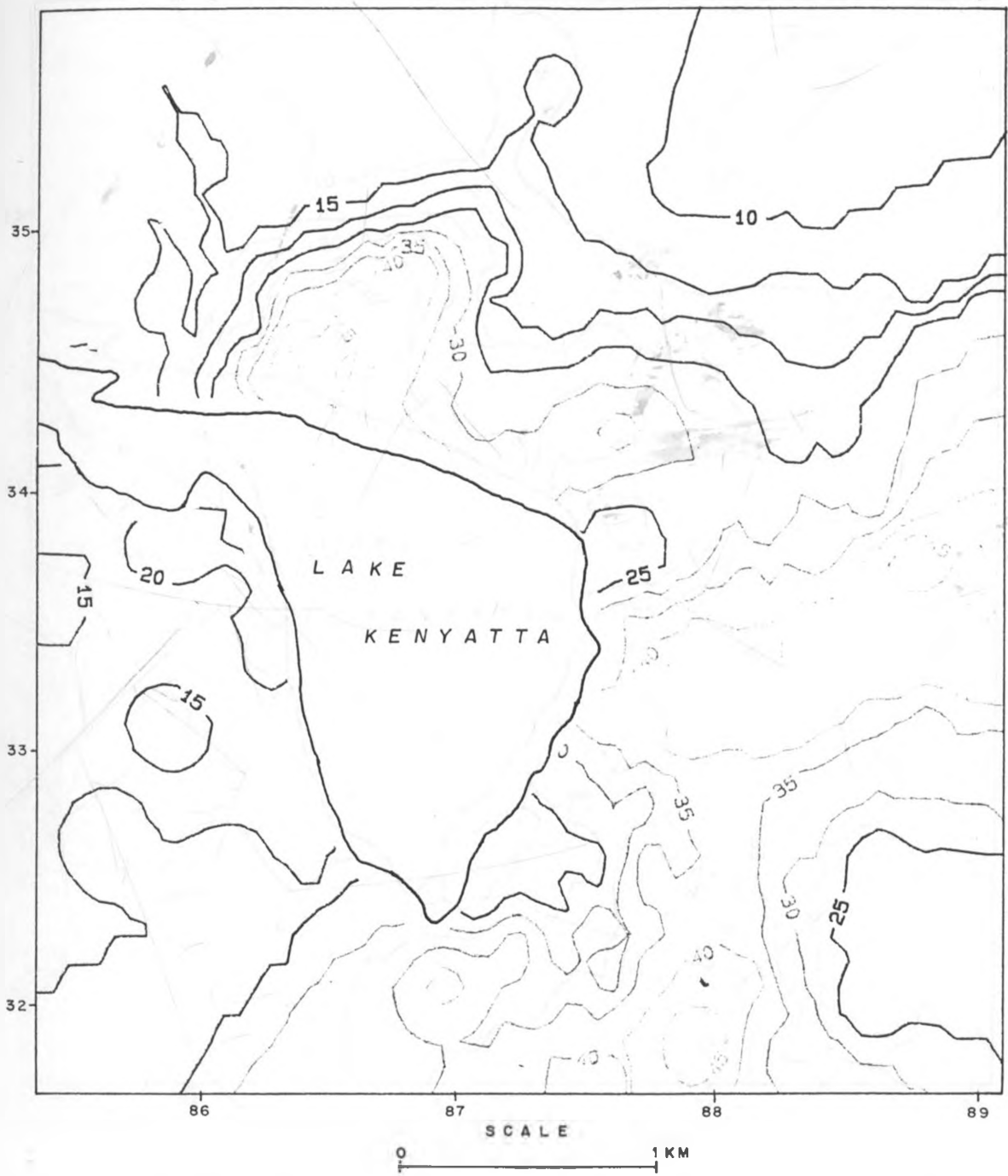
Fig. 6.5 Lateral distribution of apparent resistivity for $AB/2 = 80$ m
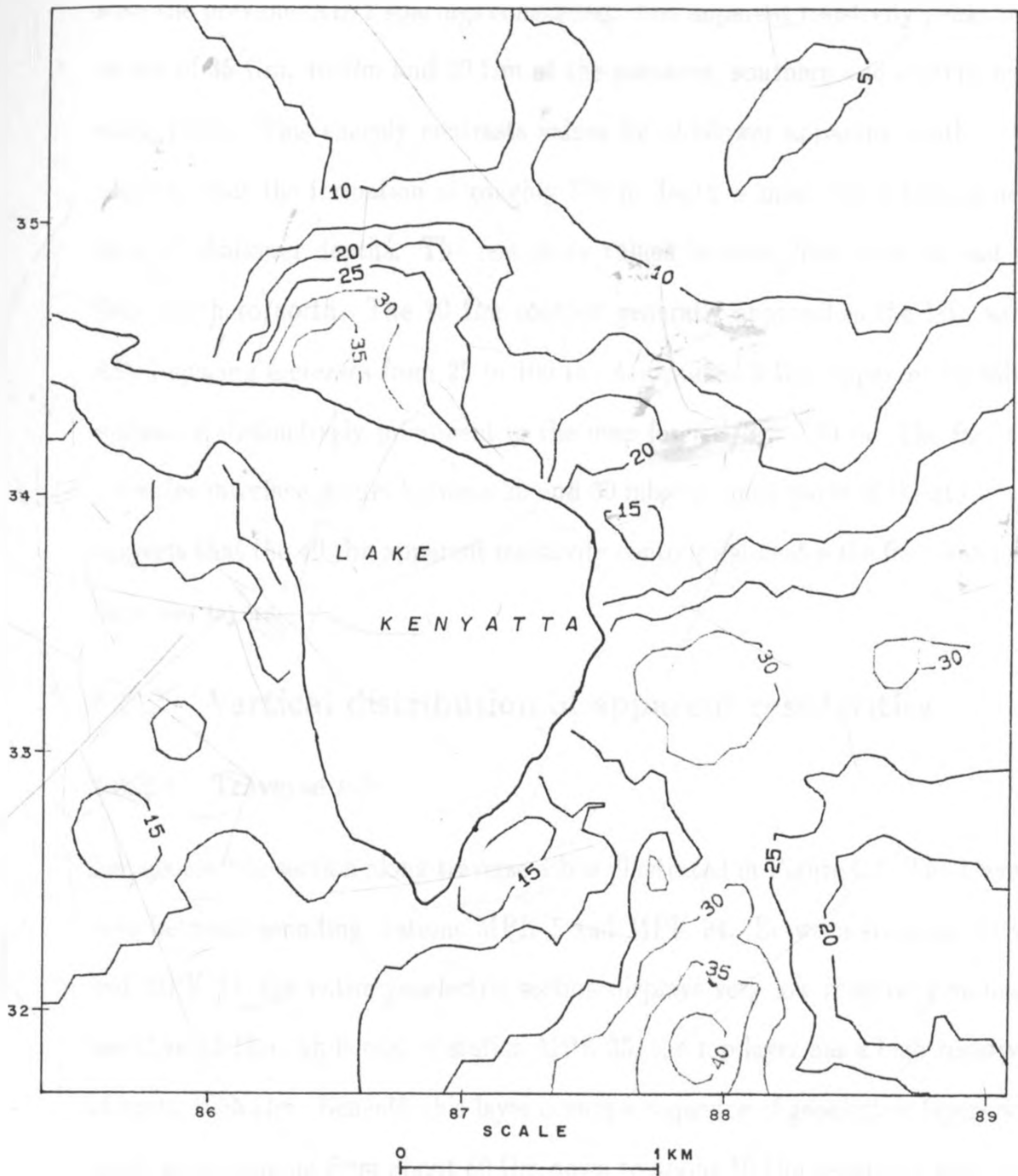
Fig. 6.6   Lateral distribution of apparent resistivity for AB/2 = 100 m

with the previous AB/2 spacings considered. The apparent resistivity peaks reach values of 35 Ωm, 40 Ωm and 30 Ωm at the northern, southern and eastern parts, respectively. This sharply contrasts values for shallower apparent depths. This suggests that the formation at roughly 100 m depth is much more homogeneous than at shallower depths. The resistivity values increase from west to east and from south to north. The 10 Ωm contour generally approaches the lake as the AB/2 spacing increases from 25 to 100 m. A localized 5 Ωm apparent resistivity contour is distinctively prominent in the map for AB/2 = 100 m. The fact that saltwater interface occurs between 20 and 60 mbgl in most parts of the study area suggests that the 40 Ωm apparent resistivity contour delineates the freshwater and saltwater layers.

6.2.2 Vertical distribution of apparent resistivities

6.2.2.1 Traverse a-b

The geoelectric section along traverse a-b is illustrated in Figure 6.7. The traverse runs between sounding stations MPK 1 and MPK 94. Between stations MPK 1 and MPK 17, the entire geoelectric section displays very low resistivity values of less than 15 Ωm, while east of station MPK 33, the top layer has a high resistivity of up to 1055 Ωm. Beneath this layer occurs a sequence of geoelectric layers with resistivities ranging from about 60 Ωm down to about 10 Ωm separated from each other by a magnitude of about 10 Ωm. Distinctive lenses with resistivities of about 50 - 60 Ωm and 60 Ωm are observed at apparent depths of about 25 and 70 metres below ground level (mbgl). The various resistivity zones in this geoelectric section generally display unique horizontal sequencing and layering.
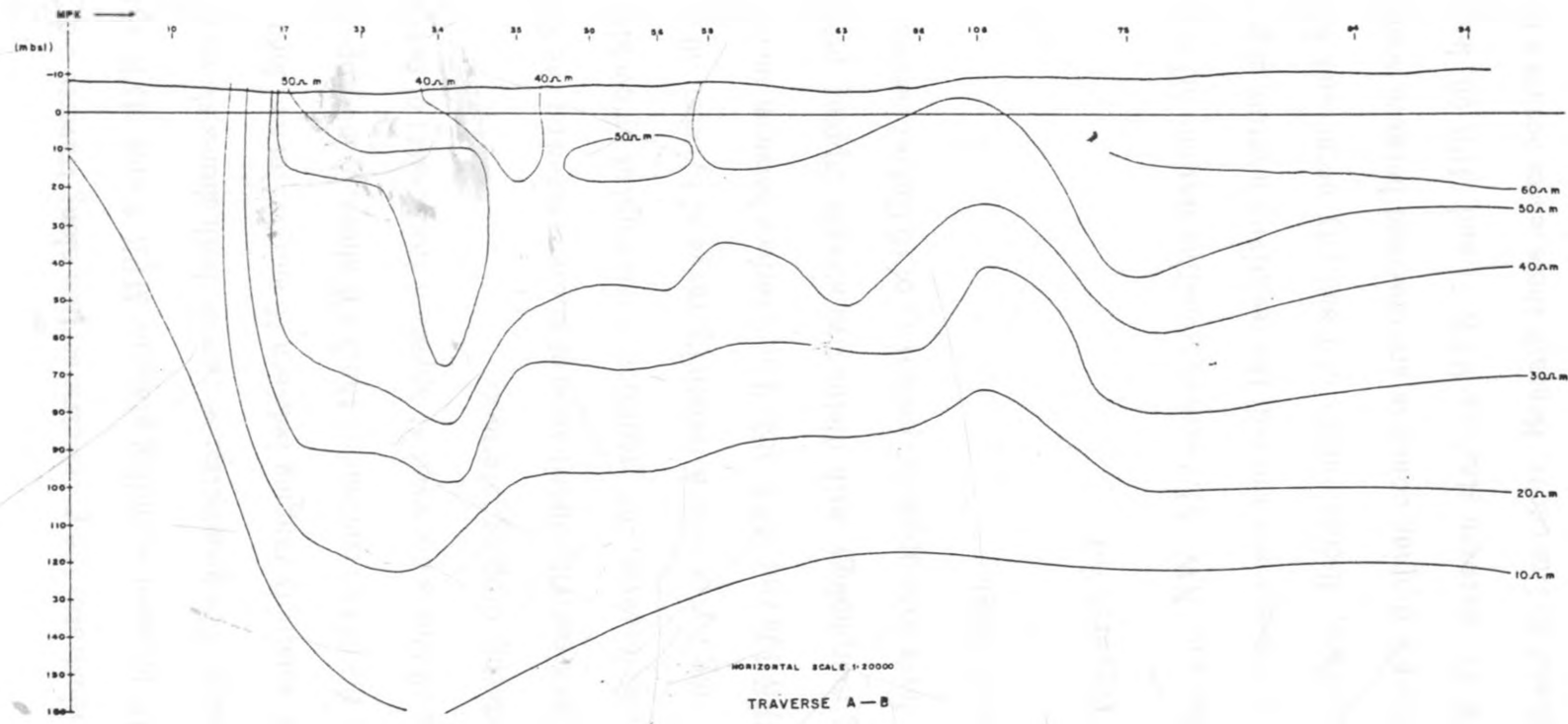
Fig. 6.7   Vertical distribution of apparent resistivity along traverse A-B

135

6.2.2.2 Traverse c-d

Figure 6.8 illustrates the geoelectric section along traverse c-d. The traverse runs NNW - SSE between sounding stations MPK 6 and MPK 103 on the shores of Lake Kenyatta. The geoelectric section on both shores shows gradational layering of apparent resistivity ranging between 10 and 60 Ωm and forming semi-concentric rings round the 60 Ωm contour on the NNW shore. A low apparent resistivity value of less than 10 Ωm is observed at apparent thicknesses of between 100 and 160 m forming a steeply dipping interface.

A similar resistivity distribution as above is noted on the SSE shore of the lake. In this region, however, the gradation is interrupted by ovoidal shaped concentric geoelectric ring layers with a resistivity range of between 30 and 50 Ωm between stations MPK 105 and MPK 103. The interface between successive layers displays undulating morphology with distinctive steeply dipping peaks and troughs. A geoelectric layer with apparent resistivity of 10 Ωm is observed at apparent depths of 100 and 170 mbgl.

6.2.2.3 Traverse e-f

This traverse runs NW - SE between sounding stations MPK 5 and MPK 10 (Fig. 6.9). Like in traverse a-b and c-d, the resistivity layering is generally gradational. Near the surface, discontinuities of resistivity occur and indistinctive patterns emerge. Steeply dipping contacts are observed between sounding stations MPK 3 and MPK 31. Between stations MPK 71 and MPK 96, lenses with resistivities between 50 and 60 Ωm occur. Beneath these lenses occurs a layer with resisitivity that runs down to less than 10 Ωm. It occurs at an apparent depth of between 100 and 150 mbgl. It is discontinuous on the northwest of sounding station MPK

Fig. 6.8   Vertical distribution of apparent resistivity along traverse C-D
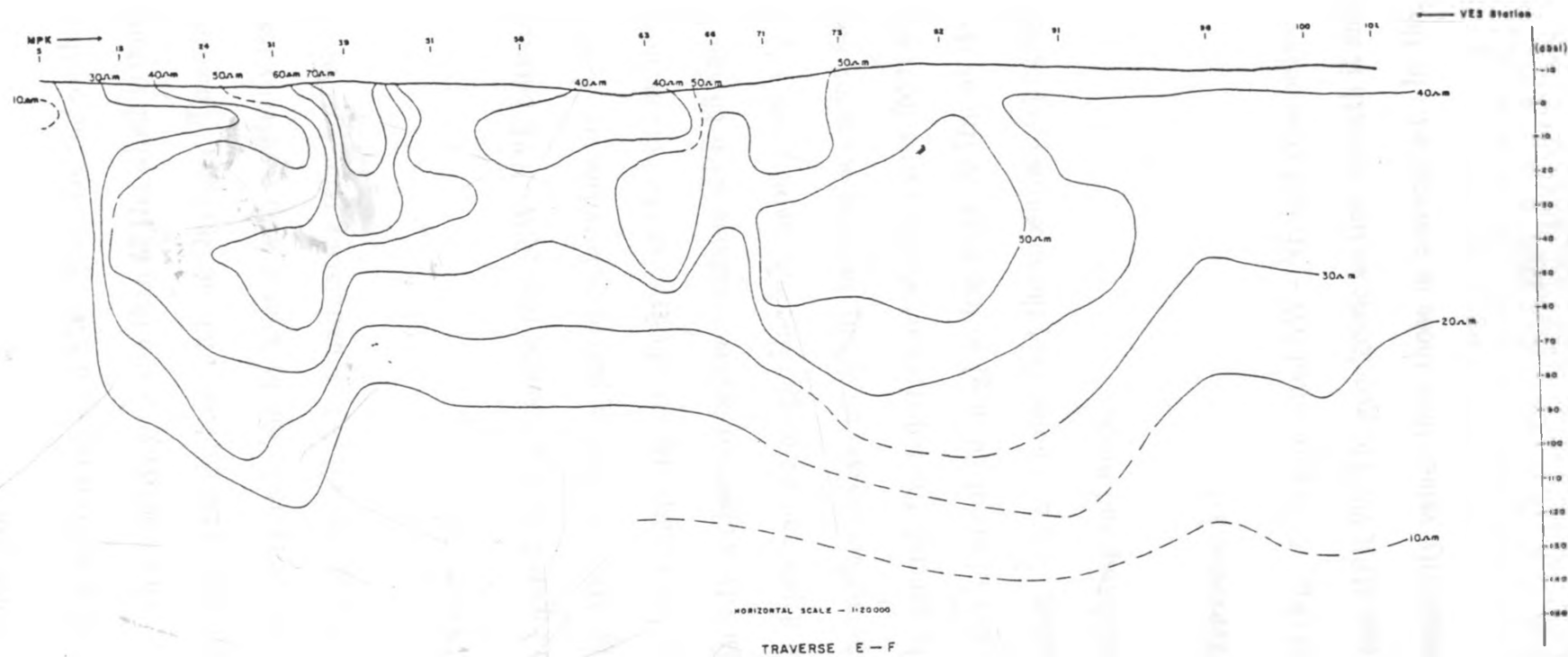
Fig. 6.9 Vertical distribution of apparent resistivity along traverse E-F

63.

6.2.2.4 Traverse g-h

This traverse (Fig. 6.10) is oriented SW - ENE. On the south-western side, there occurs a layer with a resistivity greater than 60 Ωm which is immediately underlain by a 20 - 30 Ωm layer that encloses a 30 - 40 Ωm layer. These are followed beneath by a 10 - 20 Ωm layer underlain by a layer with resistivity less than 10 Ωm. All the layers in this section exhibit an undulating relief with an inclined axis.

6.2.2.5 Traverse i-j

As shown in Figure 6.11, this traverse runs SSW -NNE between sounding stations MPK 109 and MPK 55. High apparent resistivities are observed near the surface whereas very low resistivities are observed at the bottom layers. Concentric layering of resistivity is observed between stations MPK 86 and MPK 72 at between near surface depth and 80 mbgl. Unconformable resistivity layering appears to dominate the surface layers, especially between sounding stations MPK 72 and MPK 61. In general, the apparent resistivity varies from about 184 Ωm at the apparent depth of about 60 mbgl to less than 10 Ωm at the apparent depth of about 120 mbgl. It is also noted that the subsurface topography of the resistivity layers is undulating and wavy.

6.2.2.6 Traverse k-l

Traverse k-l (Fig. 6.12) is oriented SW - NE and runs between sounding stations MPK 116 and MPK 29. The geoelectric section beneath it shows relatively higher apparent resistivity values than those in traverse s-t. In the north-eastern side,

Fig. 6.10 Vertical distribution of apparent resistivity along traverse G-H

HORIZONTAL SCALE — 1:12500

TRAVERSE I— J

Fig. 6.11   Vertical distribution of apparent resistivity along traverse I-J

Fig. 6.12 Vertical distribution of apparent resistivity along traverse K-L

there occurs a geoelectric layer with a resistivity greater than 60 Ωm which is enclosed within a 50 - 60 Ωm layer. The latter is in turn enclosed within a 40 - 50 Ωm layer. These are followed beneath by geoelectric layers with resistivities 30 - 40 Ωm, 20 - 30 Ωm, 10 - 20 Ωm and another with less than 10 Ωm. This therefore shows that the geoelectric section consists of layers with progressively decreasing resistivities from top to bottom.

6.2.2.7   Traverse m-n

This traverse (Fig. 6.13) runs SW - NE between sounding stations MPK 116 and MPK 46. On the south-western shore of Lake Kenyatta, very low apparent resistivity values are observed. The 10 Ωm resistivity layer cannot be precisely traced due to the low apparent resistivity values in the subsurface. On the north-eastern side of the traverse, resistivity layering is basically gradational and unconformable with discontinuities being traced on the topmost layers at apparent depths of approximately 40 Ωm. The 40 Ωm resistivity layer shows extensive wavy and undulating appearance between sounding stations MPK 35 and MPK 40. Clusters of resistivity values are observed between the same stations. The 10 Ωm layer occurs at apparent depths of approximately 60 and 160 mbgl. The top layer has the highest resistivities of up to 156 Ωm while the lowest one has less than 10 Ωm.

6.2.2.8   Traverse o-p

Shown in Figure 6.14, this traverse is oriented SW - NE and runs between sounding stations MPK 112 and MPK 62. On the south-eastern side of the lake, a high resistivity layer encloses a 30 - 40 Ωm resistivity layer. The latter is underlain by a layer with progressively decreasing resistivities down to 10 Ωm and less. On the
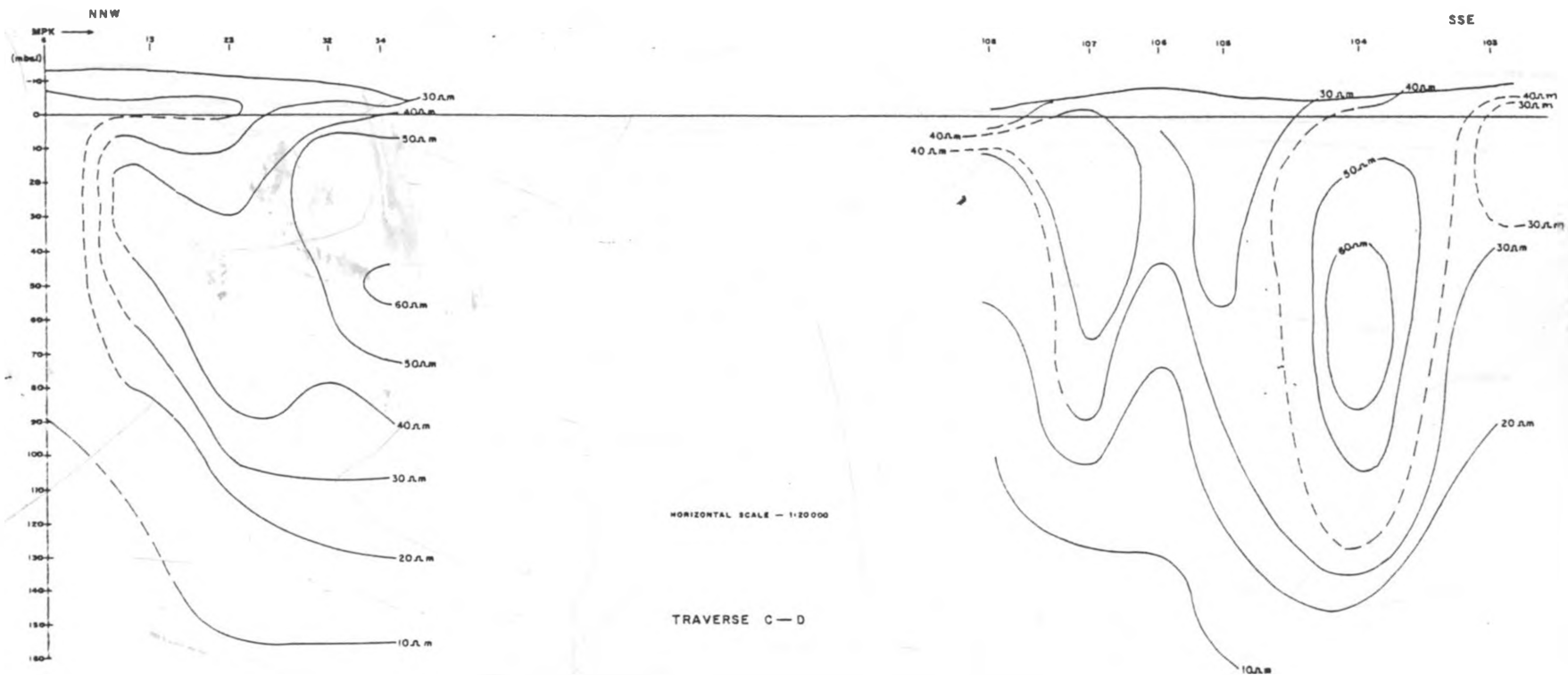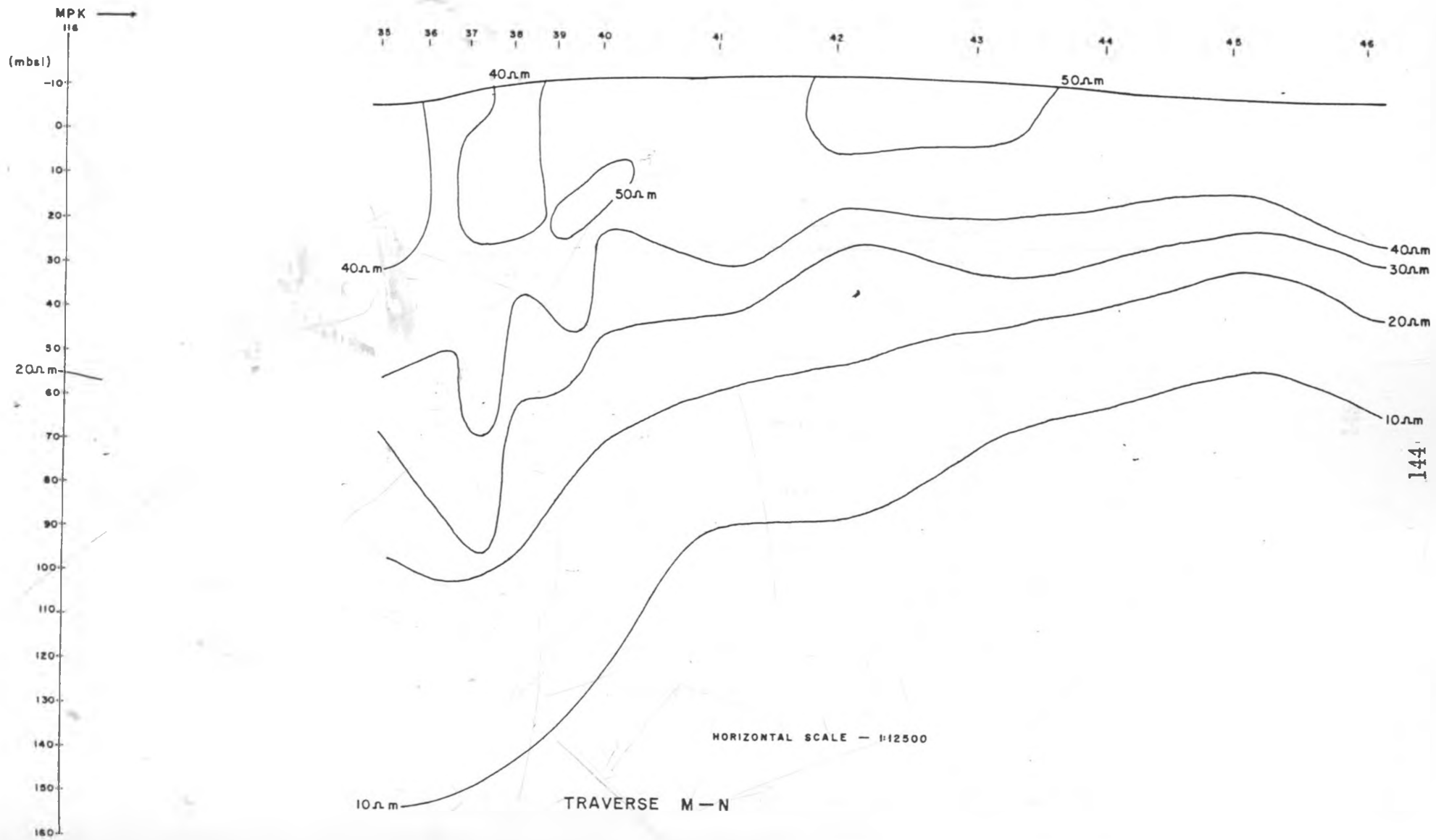
Fig. 6.13   Vertical distribution of apparent resistivity along traverse M-N
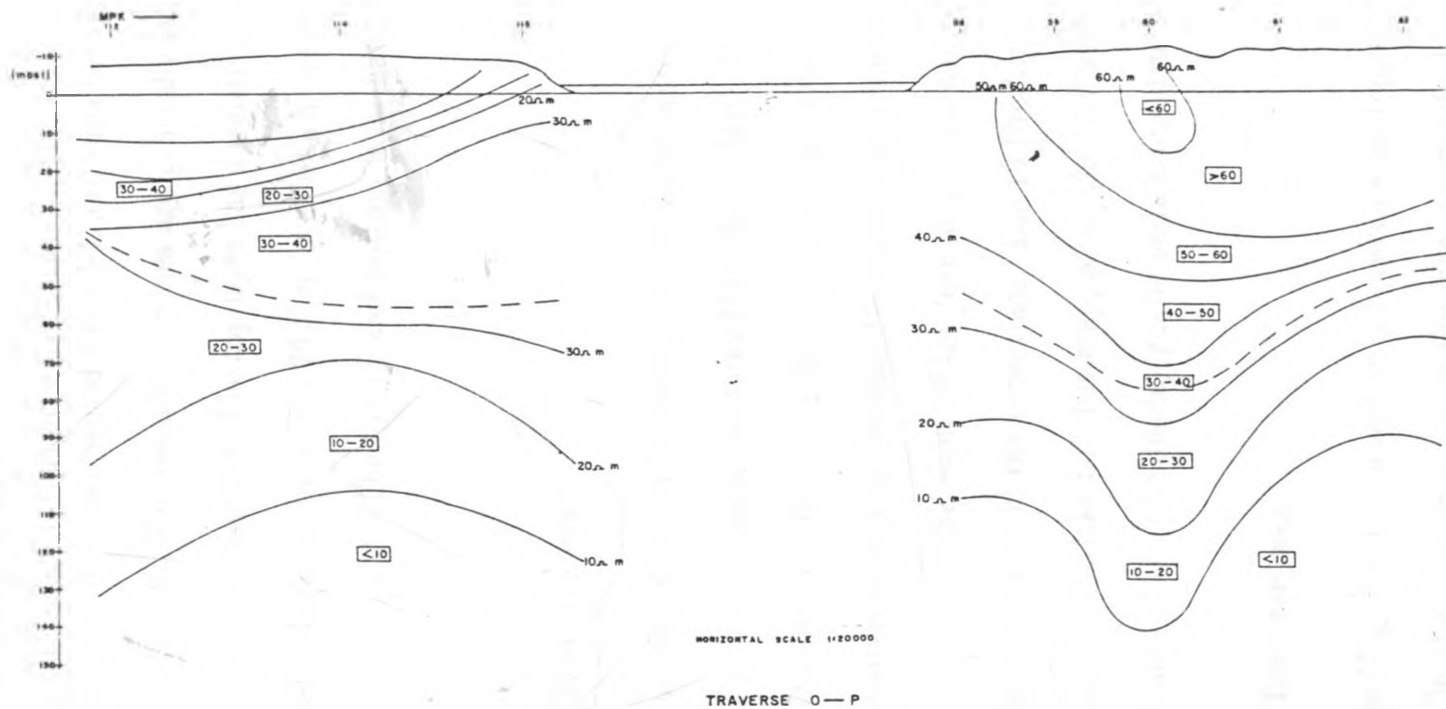
Fig. 6.14 Vertical distribution of apparent resistivity along traverse O-P

north-eastern side of the lake occurs similar gradation.

6.2.2.9   Traverse s-t

This traverse (Fig. 6.15) is oriented SW - NE and runs between sounding stations MPK 1 and MPK 9. The resistivity values are generally low and three distinct geoelectric layers are observed. The top layer has a resistivity greater than 20 Ωm. This is followed beneath by a 15 - 20 Ωm layer which overlies a third layer with resistivities 10 - 15 Ωm. The fourth and bottom layer has a resistivity less than 10 Ωm.

6.2.2.10   Traverse u-v

This traverse (Fig. 6.16) which occurs on the north-western tip of the lake, runs NNW - S.E between sounding stations MPK 3 and MPK 110. On the NNW shore of the lake, the apparent resistivity layer interfaces are steeply dipping towards the lake with resistivities varying between 10 and 50 Ωm. Concentric resistivity layering is observed on the SSE shore of the lake at shallow depths while conformable cross-layering is inherent in the subsurface. The 10 Ωm layer is not delineated on the NNW shore of the lake but it is mapped on the SSE side. The bottom layers on the SSE shore of the lake display gentle undulating structures.

6.2.2.11   Traverse w-x

This traverse (Fig. 6.17) runs east-west between sounding stations MPK 112 and MPK 96. On the western shore of the lake, resistivity layering appears to be dipping towards the lake. The apparent resistivity varies between 20 and 30 Ωm. On the eastern shore of the lake, distinctive undulating and concentric resistivity
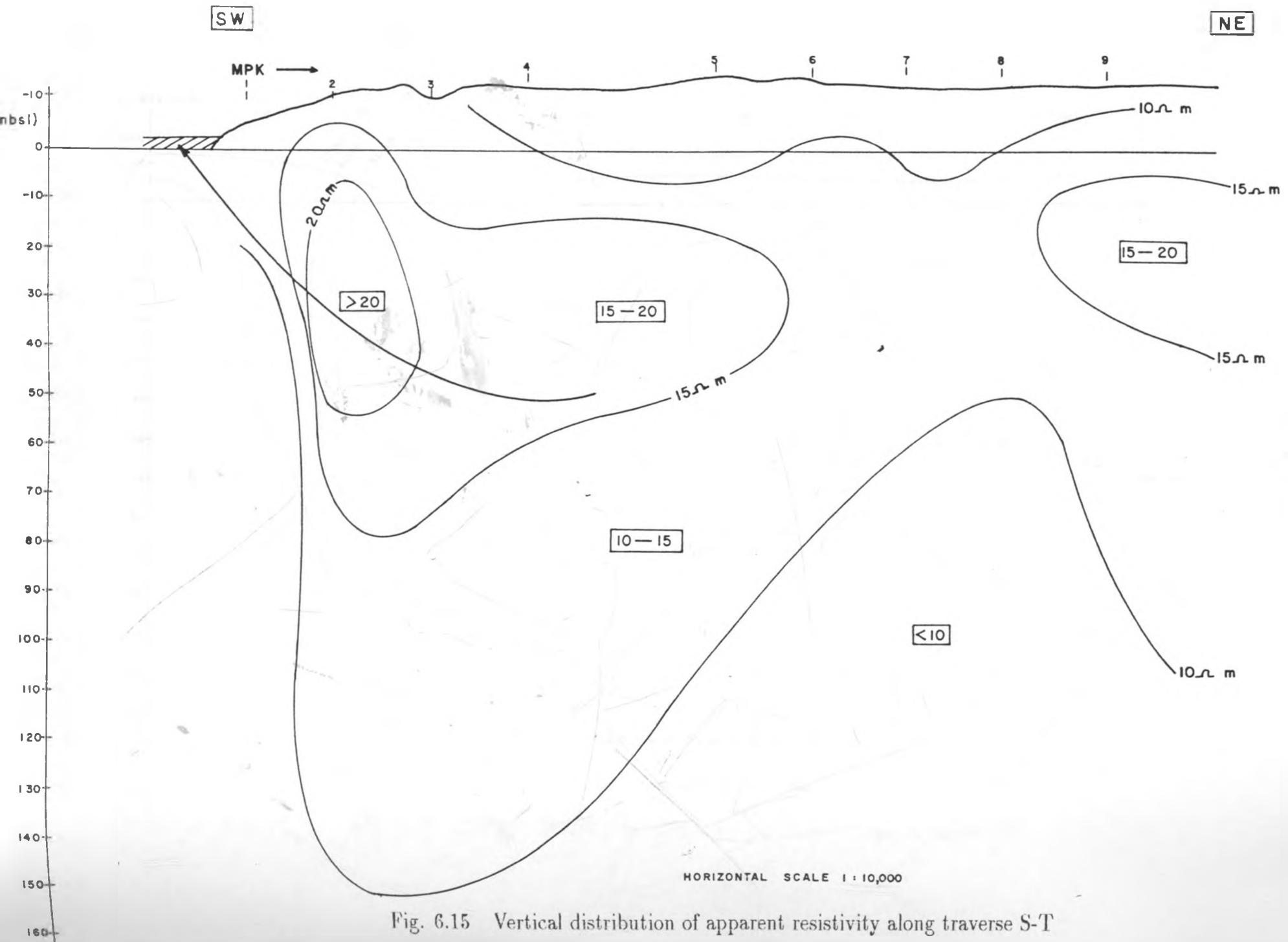
Fig. 6.15 Vertical distribution of apparent resistivity along traverse S-T
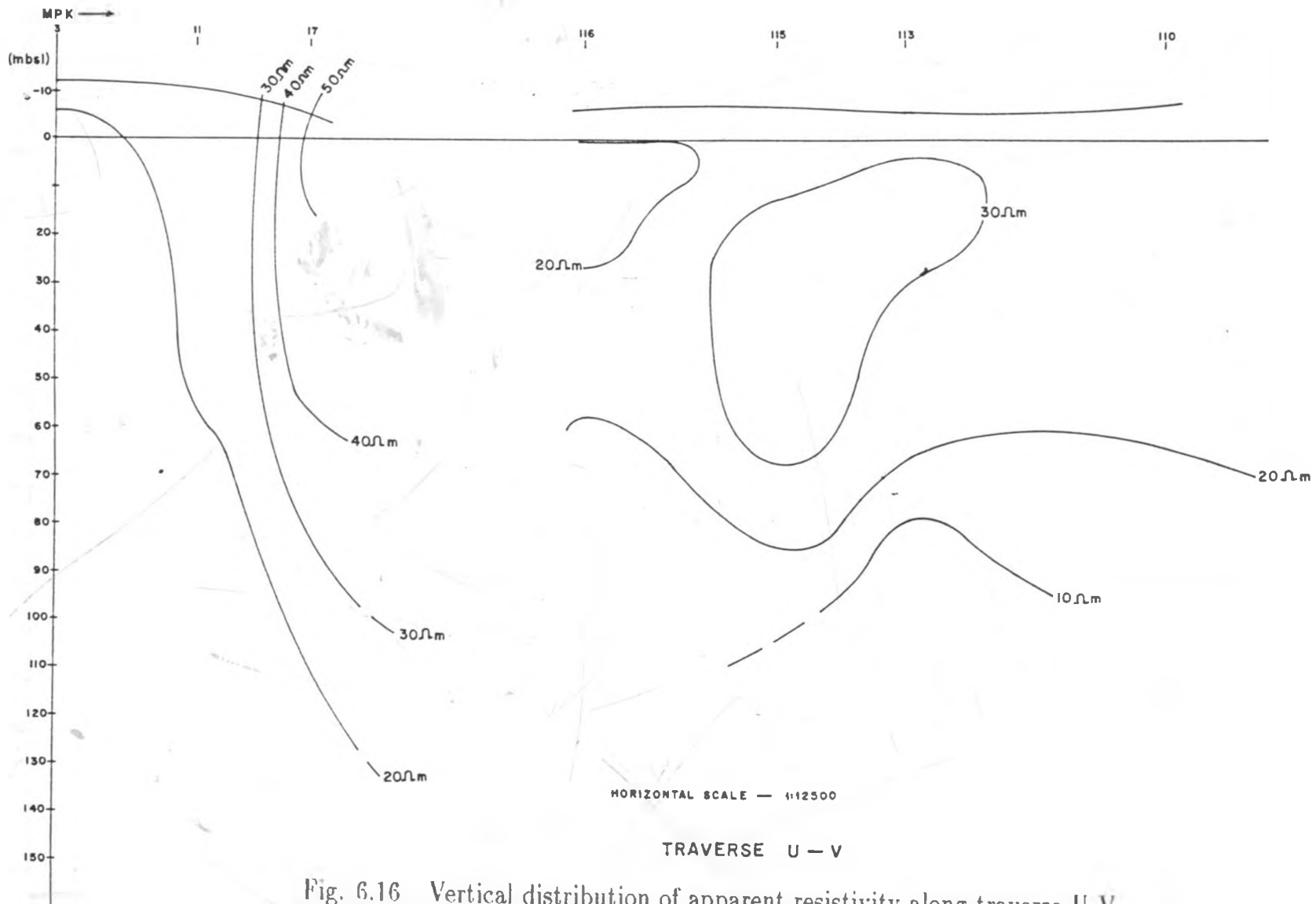
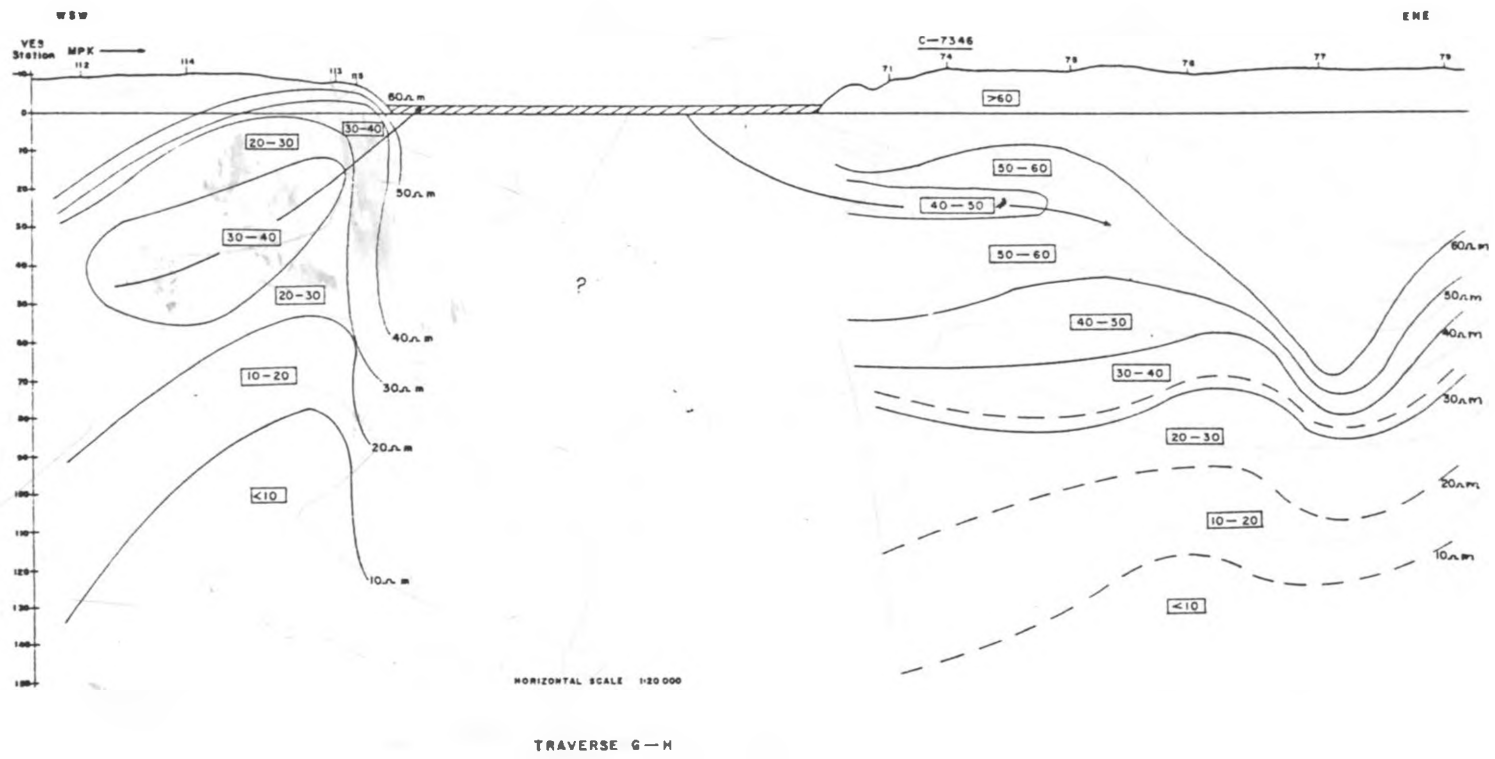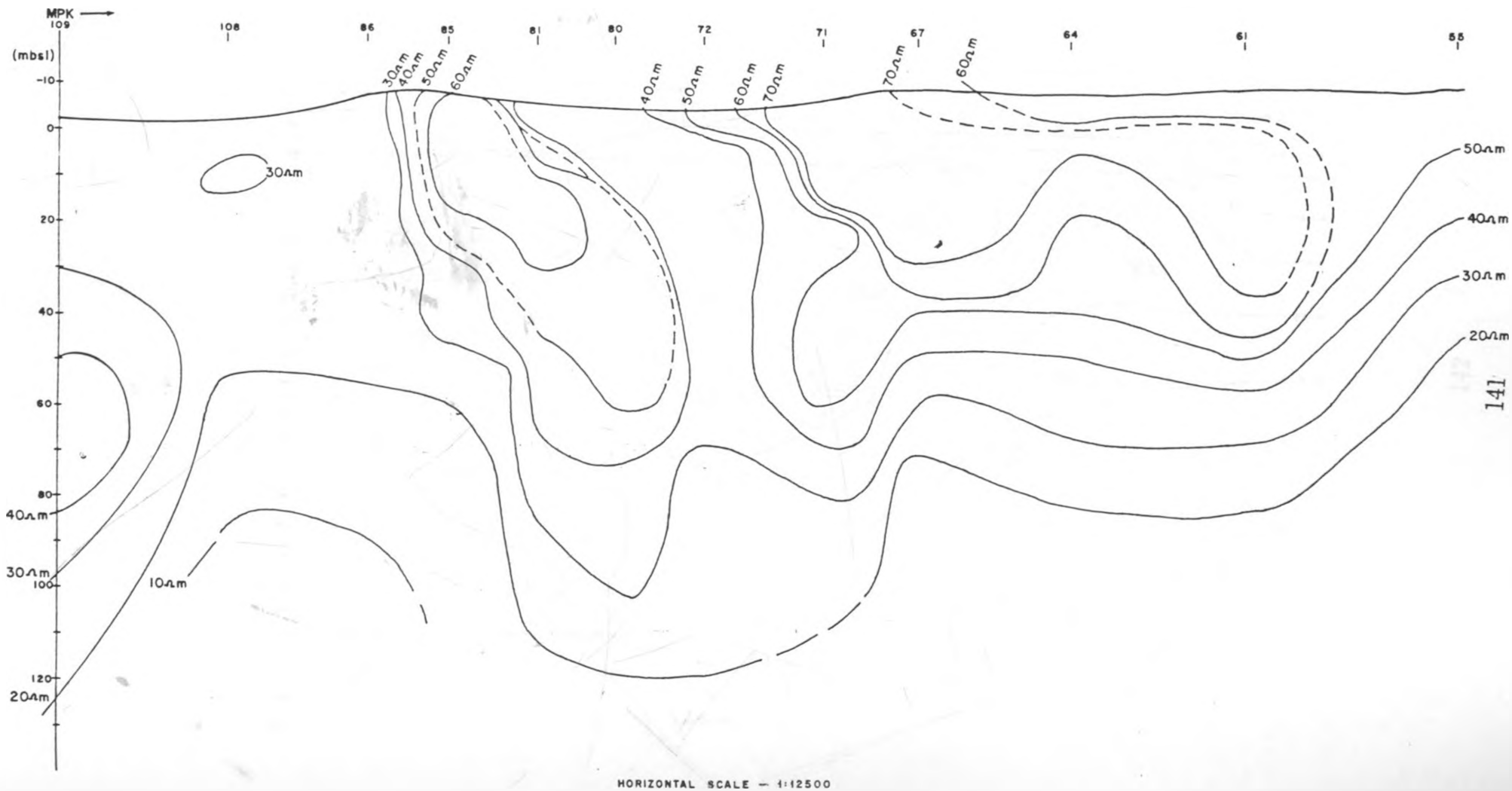Fig. 6.16 Vertical distribution of apparent resistivity along traverse U-V

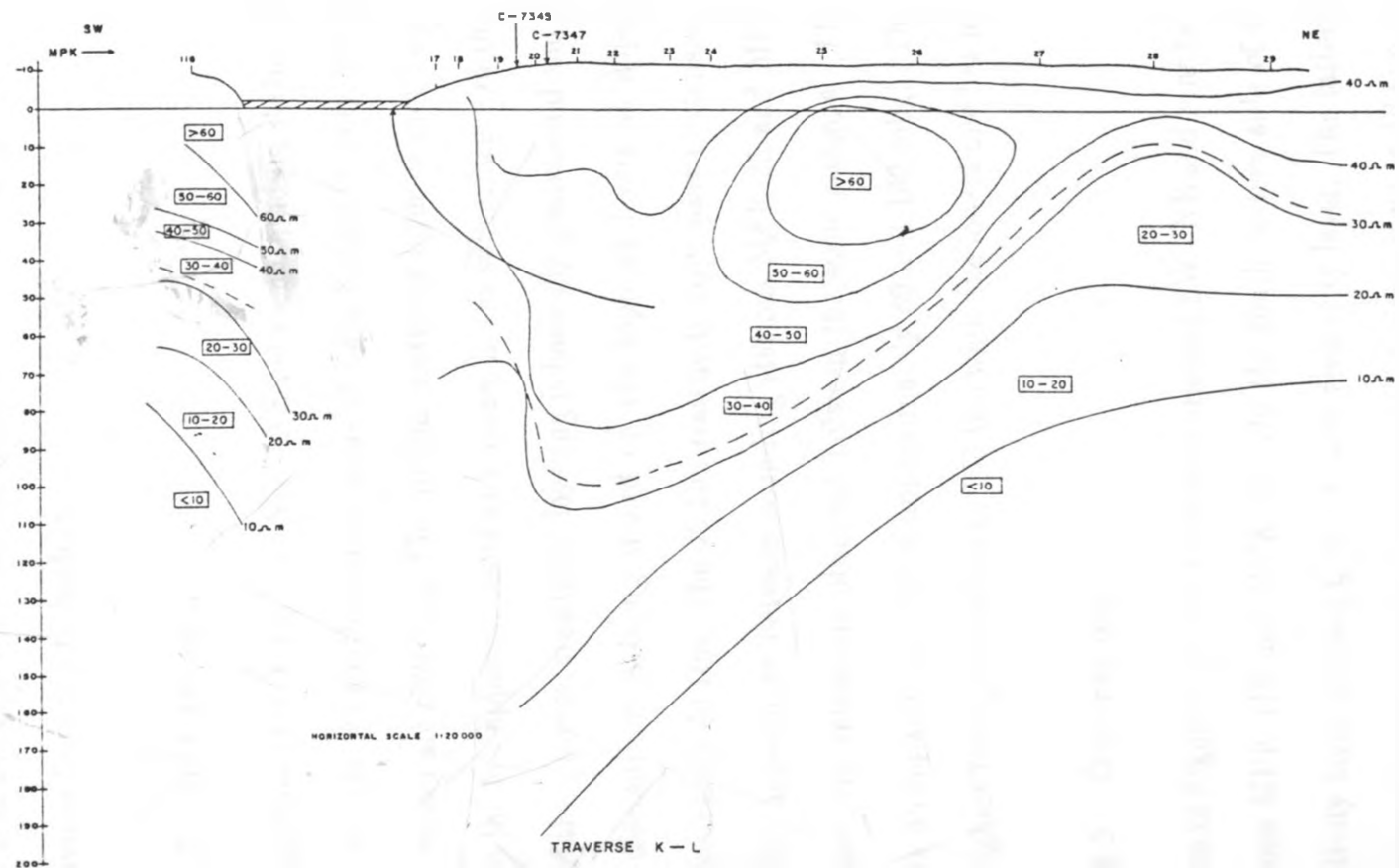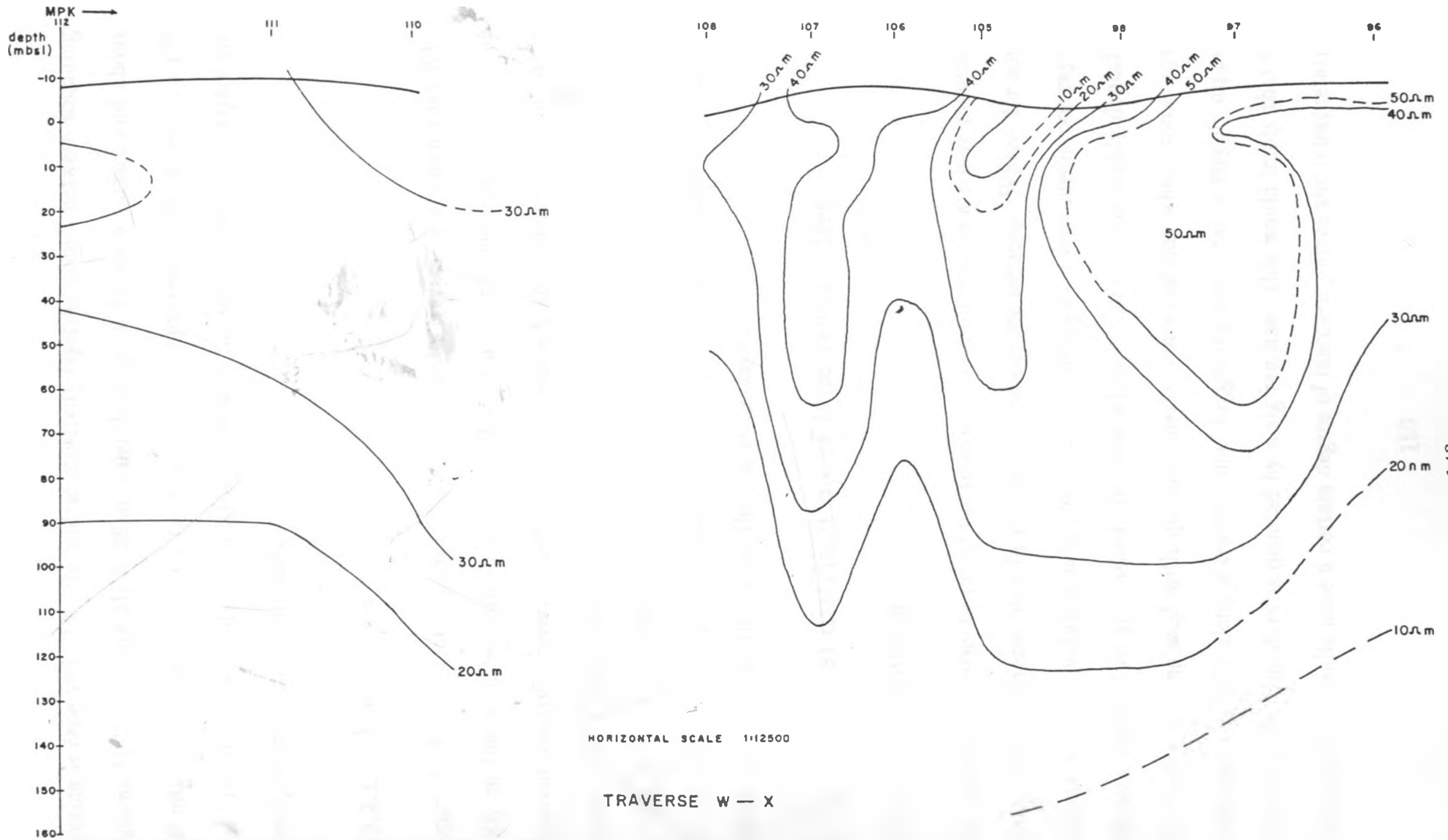Fig. 6.17   Vertical distribution of apparent resistivity along traverse W-X

layering is observed. The concentric resistivity layering occurs between sounding stations MPK 107 and MPK 96 at a depth range of between surface and about 100 mbgl. A 10 Ωm resistivity layer occurs at an apparent depth of between 120 and 170 mbgl. Generally, the interfaces between the various resistivity layers are steeply dipping and undulating.

6.2.2.12 Traverse y-z

Figure 6.18 shows the geoelectric section beneath traverse y-z which runs NW - SE on the south-eastern shore of the lake. Unconformable and discontinuous apparent resistivity layering is observed on the surface layers where some concentric layering also occurs. The concentric rings form between sounding stations MPK 90 and MPK 102 at the apparent depth between surface and 90 mbgl. Beneath the concentric layering are conformable layers with a gradual drop of apparent resistivities down to 10 Ωm for the lowermost layer.

6.2.3 Vertical distribution of true resistivities

6.2.3.1 Introduction

The results of interpretation of the resistivity sounding curves are here presented along various traverse lines in the form of geoelectric sections. Where, for some reasons, the interpretation is doubtful, the boundaries between media portraying different resistivities are dashed. In cases where boundaries are highly doubtful, the dashes are replaced with question marks. In situations where some layers disappear abruptly along a traverse line, suggesting a vertical or steeply dipping boundary, the boundary is denoted by a zig zag line. This would imply that the interpretation results have a certain degree of inaccuracy since the interpretation
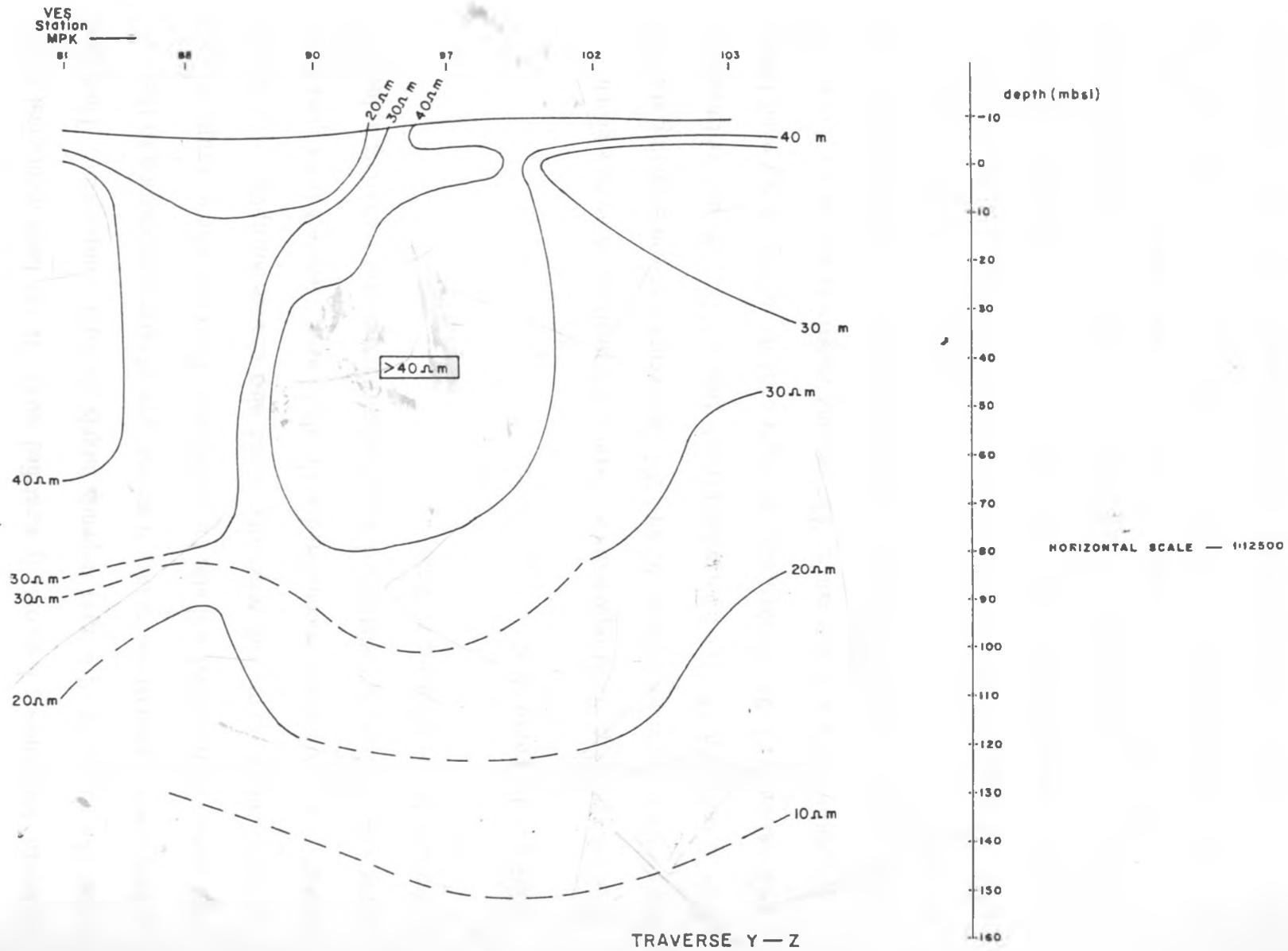
Fig. 6.18   Vertical distribution of apparent resistivity along traverse Y-Z

procedure assumes a horizontally stratified earth. It has been mentioned earlier that the resistivity of a layer depends largely on layer composition. Therefore, where there is gradational change from one type of layer composition to the next, the resistivity measured will also be gradational. However, where abrupt changes in composition occur, the resistivity would also change abruptly. The former situation was commonly encountered in the study area. Geoelectric sections along some traverse lines as constructed using measured apparent resistivity values are described in the following sections.

6.2.3.2 Traverse A-B

This traverse (Fig. 6.19) represents a 5-layer earth medium. A surface geoelectric layer with resistivities between 90 and 256 Ωm occurs between sounding stations MPK 1 and MPK 58. The layer reappears at station MPK 106 and continues beyond station MPK 94. Geologically, the layer consists mainly of dry wind blown sands, dune sands and wet sands. The varying resistivity values are due to the relative degree of water saturation. Underlying this layer is a very thin layer with resistivity 6 Ωm observed at station MPK 33. This layer corresponds to a narrow, shallow, thin clay band embedded between loose sand on the surface and underlying calcarious sandy clays. These clays could be composed of mainly decomposed weathered corals and sands. Beneath this layer is a layer with resistivities 11-42 Ωm which is further underlain by a very thick layer with resistivities 50-188 Ωm. The higher resistivity limit for this layer may reflect presence of dry compact coral while the medium values may be due to water saturated coral. The coral displays a pinch and swell structure. Underlying this layer is a layer with resistivities 17-33 Ωm. It corresponds to a transition zone between the coral limestone and the

152
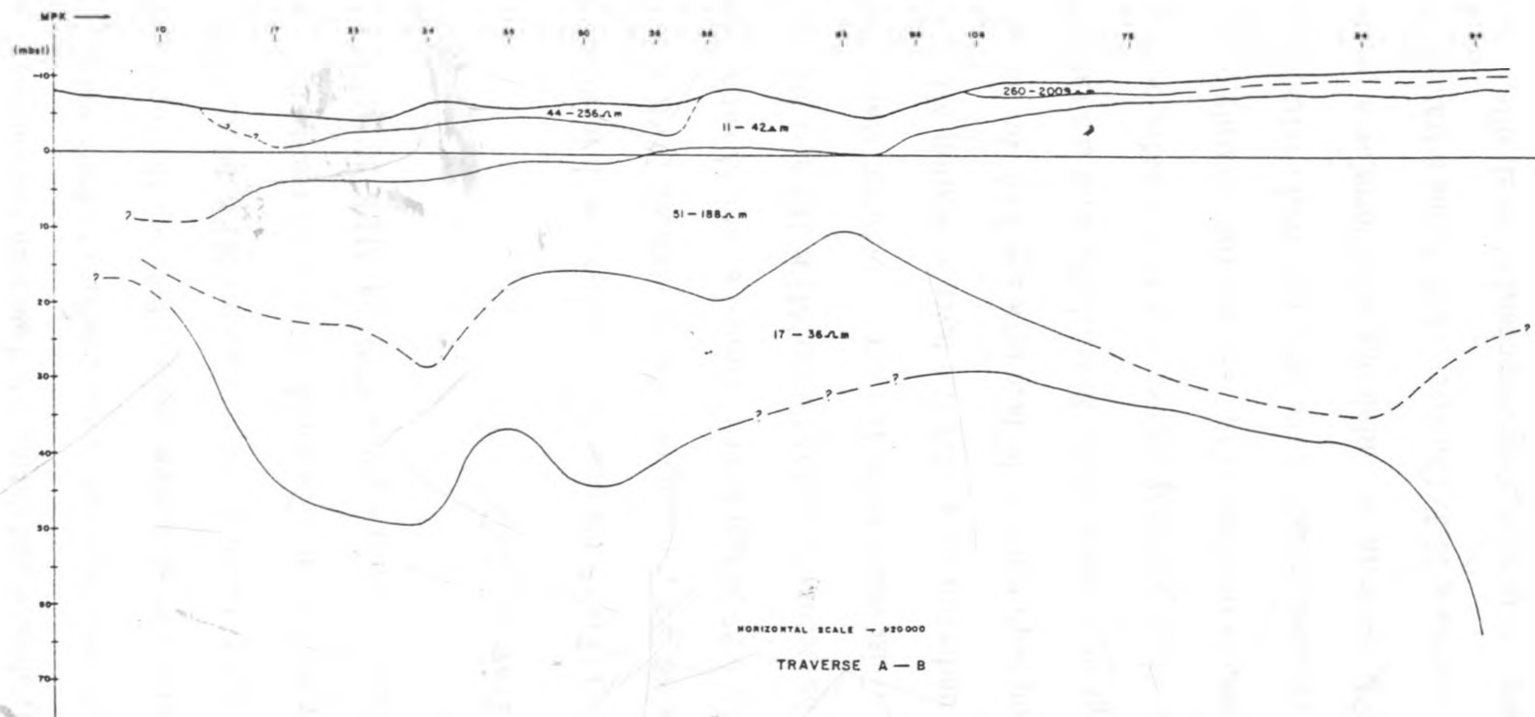
Fig. 6.19　Vertical distribution of true resistivity along traverse A-B

153

underlying saline waters. It forms an undulating interface with the overlying layer and a gently sloping undulating interface with the underlying layer. It is probably composed of coral clays, sands and brackish to fresh water.

A dipping, almost vertical contact between the top layer and the one underlying it occurs between sounding stations MPK 56 and MPK 58. Other steeply dipping contacts occur between the layer with resistivity less than 5Ωm and the 17-33 Ωm layer beneath stations MPK 34, MPK 35, MPK 84 and MPK 94.

6.2.3.3   Traverse C-D

Traverse C-D (Fig. 6.20) runs over a 5-layer earth medium. A surface layer with resistivities 86-353 Ωm occurs between stations MPK 6 and MPK 34. This is underlain by a 23-38 Ωm layer of limited extent. A surface layer with resistivities 186-2327 Ωm occurs between stations MPK 108 and MPK 103. Another surface layer with resistivities 46-60 Ωm occurs between stations MPK 105 and MPK 103. It is underlain by a 1326 Ωm layer at station MPK 104. These layers are underlain on both sides of the lake by a low 3-16 Ωm resistivity layer. This layer may correspond to sandy clays. Beneath the layer is a thick layer with resistivities 52-147 Ωm which probably corresponds to the water-bearing coral limestone. It thickens towards the shore of the lake and rises sharply on the north-western side. On the south-eastern side of the lake, the coral continues and thins out towards station MPK 103 with an undulating relief forming a pinch and swell structure. The coral overlies a 15-39 Ωm layer which forms a transition zone between it and the saltwater.. It is most likely composed of coral, silts, clays and sands. Beneath the coral is a low resistivity 1-7 Ωm layer.

Fig. 6.20   Vertical distribution of true resistivity along traverse C-D

TRAVERSE   C — D

HORIZONTAL SCALE — 1:20 000
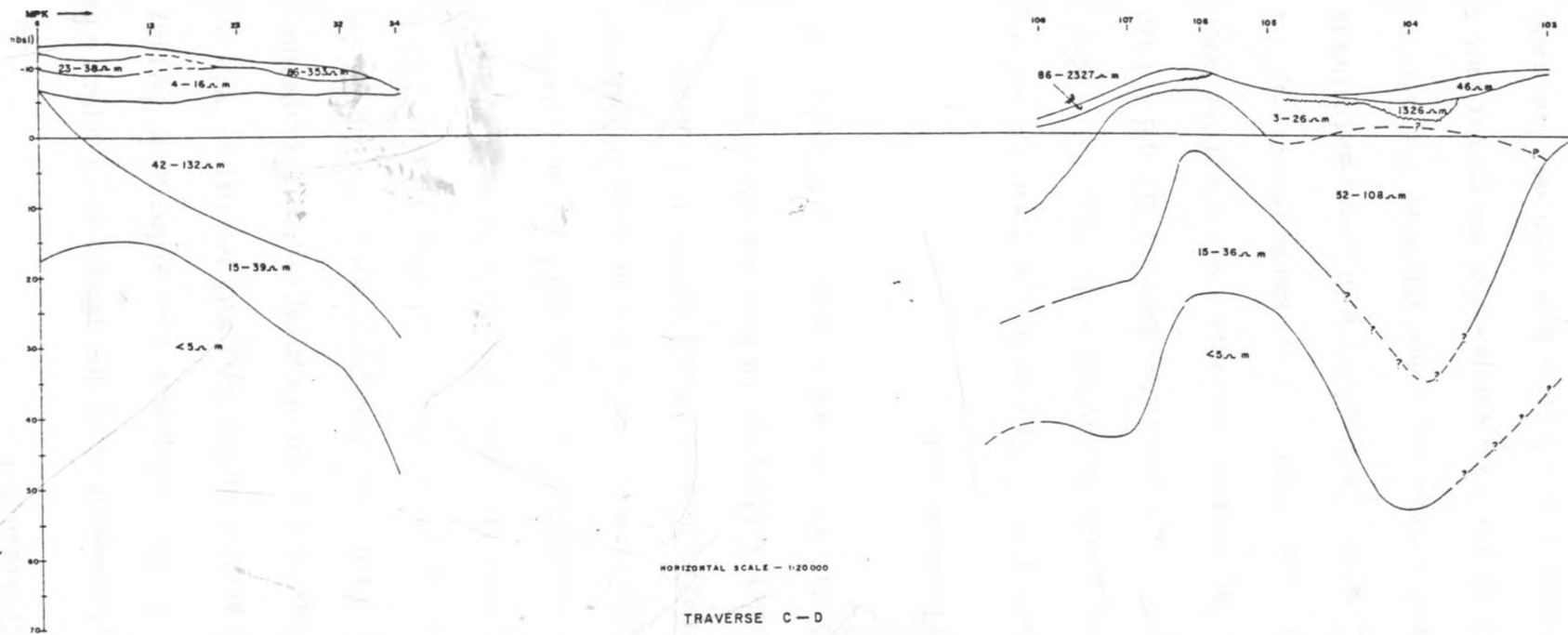
6.2.3.4 Traverse E-F

The geoelectric section along this traverse which depicts a five-layer earth is shown in Figure 6.21. The surface layer has resistivities in the range 54 to 2445 Ωm and is adjacent to another surface layer with resistivities between 28 and 38 Ωm. These layers correspond to sands of varying degree of compaction, porosity and pore water content. Underlying these layers is a 12 - 44 Ωm resistivity layer corresponding to a layer composed of sands, coral, clay and silt. This layer transcends into an underlying thick layer with resistivities between 50 and 188 Ωm. This layer appears to be a continuation of a similar layer encountered beneath traverse A-B. It is composed of cavernous water-bearing coral. Beneath this layer is a thinner layer with resistivities between 18 and 45 Ωm. It is made up of coral, clay, sands and brackish water. Underlying this layer is a bottom layer of saltwater with resistivity less than 5 Ωm. The geoelectric layers in general have an undulating structure.

6.2.3.5 Traverse G-H

This traverse (Fig. 6.22) runs over a geoelectric section of five layers. The top layer has very high resistivities in the range 2187 - 6349 Ωm on the western side of the lake. It has resistivities between 132 and 451 Ωm on the eastern side of the lake. The western and eastern sections of the layer correspond to very dry loose wind blown sands and wet sands, respectively. This layer is underlain on both sides of the lake by a layer with lower resistivities in the range 13-36 Ωm. It is composed of coral, clay, sands and silts. The layer overlies a thicker east-west dipping 43-96 Ωm layer composed of the greater part of coral limestone in the area. Beneath it is a bottom layer with very low resistivities in the range 2-12 Ωm which corresponds to saltwater. This layer occurs at relatively shallow depths
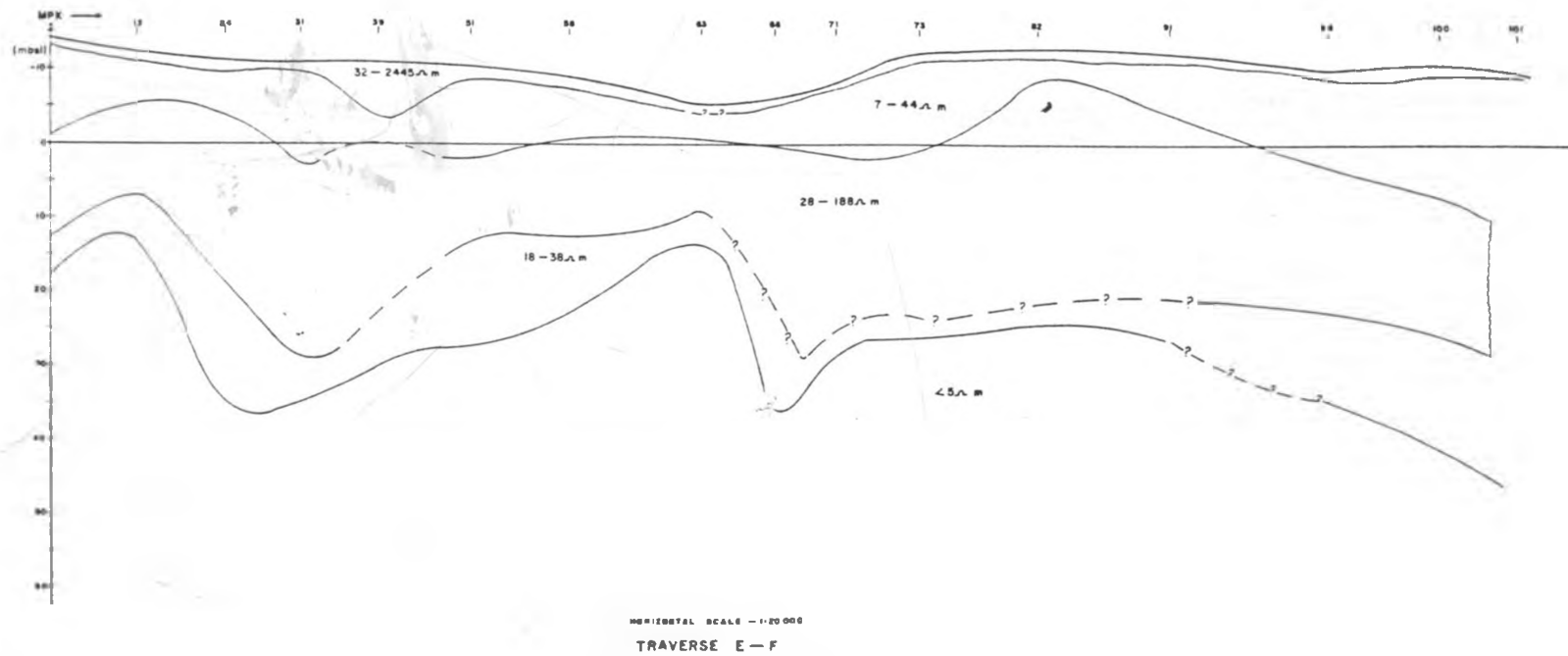
Fig. 6.21   Vertical distribution of true resistivity along traverse E-F

157
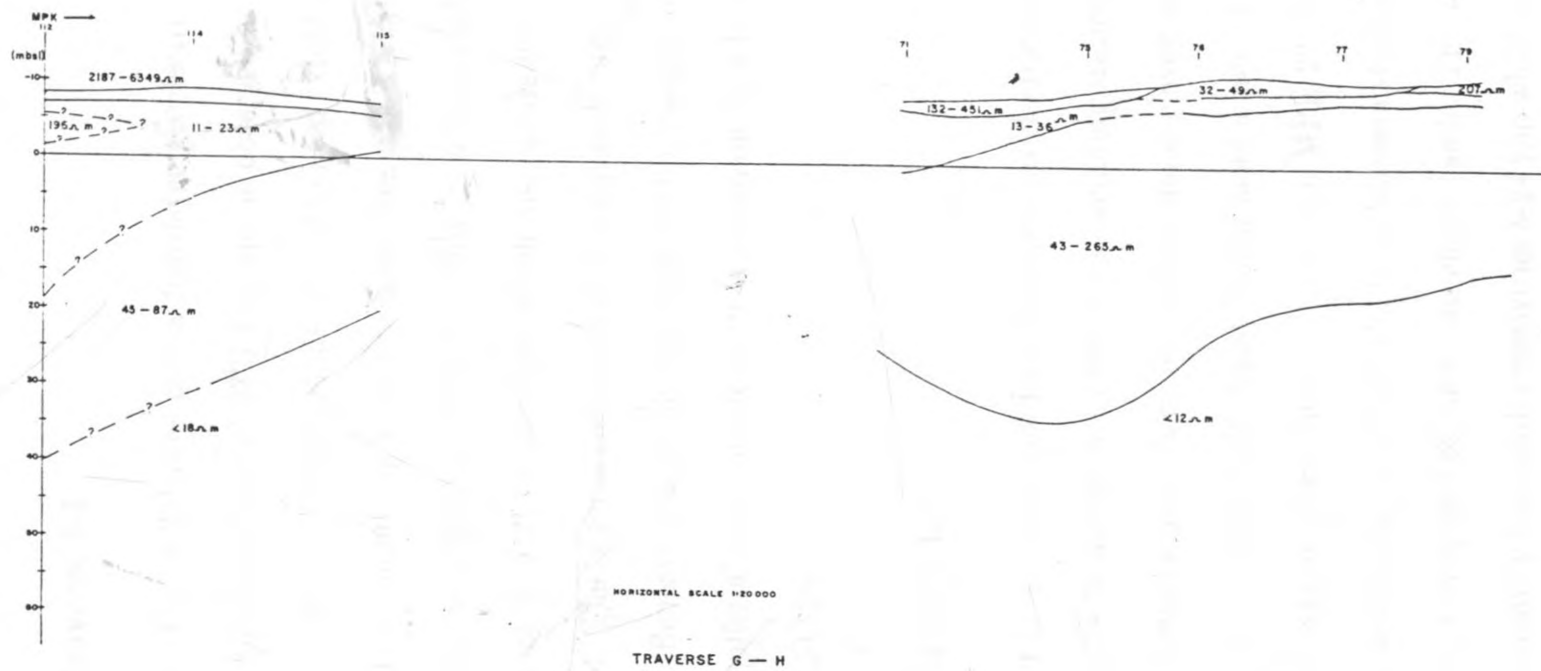
Fig. 6.22   Vertical distribution of true resistivity along traverse G-H

with a more or less evenly dipping interface which is only interrupted with a minor trough between sounding stations MPK 71 and MPK 76.

6.2.3.6   Traverse I-J

Traverse I-J (Fig. 6.23) runs over a four-layer geoelectric section. The surface layer has a high resistivity of 2327 Ωm and is observed at station MPK 108. It corresponds to dry wind-blown sands. It is of limited extent and forms a very steep contact with the underlying 10-36 Ωm layer. Beneath is a thicker 110-388 Ωm layer which disappears at station MPK 67. This layer is unconformably underlain at a steep contact by a 21-34 Ωm layer which disappears between stations MPK 61 and MPK 64. The latter is composed of decomposed coral, clayey sands, silts and sandy clays. Beneath is a 37-130 Ωm layer with a rugged undulating shape. This forms the aquiferial coral limestone. It is underlain by a layer with low resistivity of less than 10 Ωm.

6.2.3.7   Traverse K-L

This traverse (Fig. 6.24) overlies a five-layer geoelectric section. The top layer with resistivities 28-49 Ωm was observed at sounding stations MPK 24 and MPK 29 and is of limited extent. It corresponds to moist clayey sandy soils. Beneath it is a 331 Ωm layer which could depict buried loose sands. This layer is underlain by a 51-113 Ωm layer which thins out at station MPK 22. It reappears at station MPK 20 and terminates to a 25-47 Ωm layer between stations MPK 17 and MPK 22. It is perhaps composed of calcareous clayey sands. This layer is underlain by a thicker low resistivity layer with resistivities 8-24 Ωm which discontinues at station MPK 21. It possibly consists of sandy and silty clays. Beneath is a thick 42-138
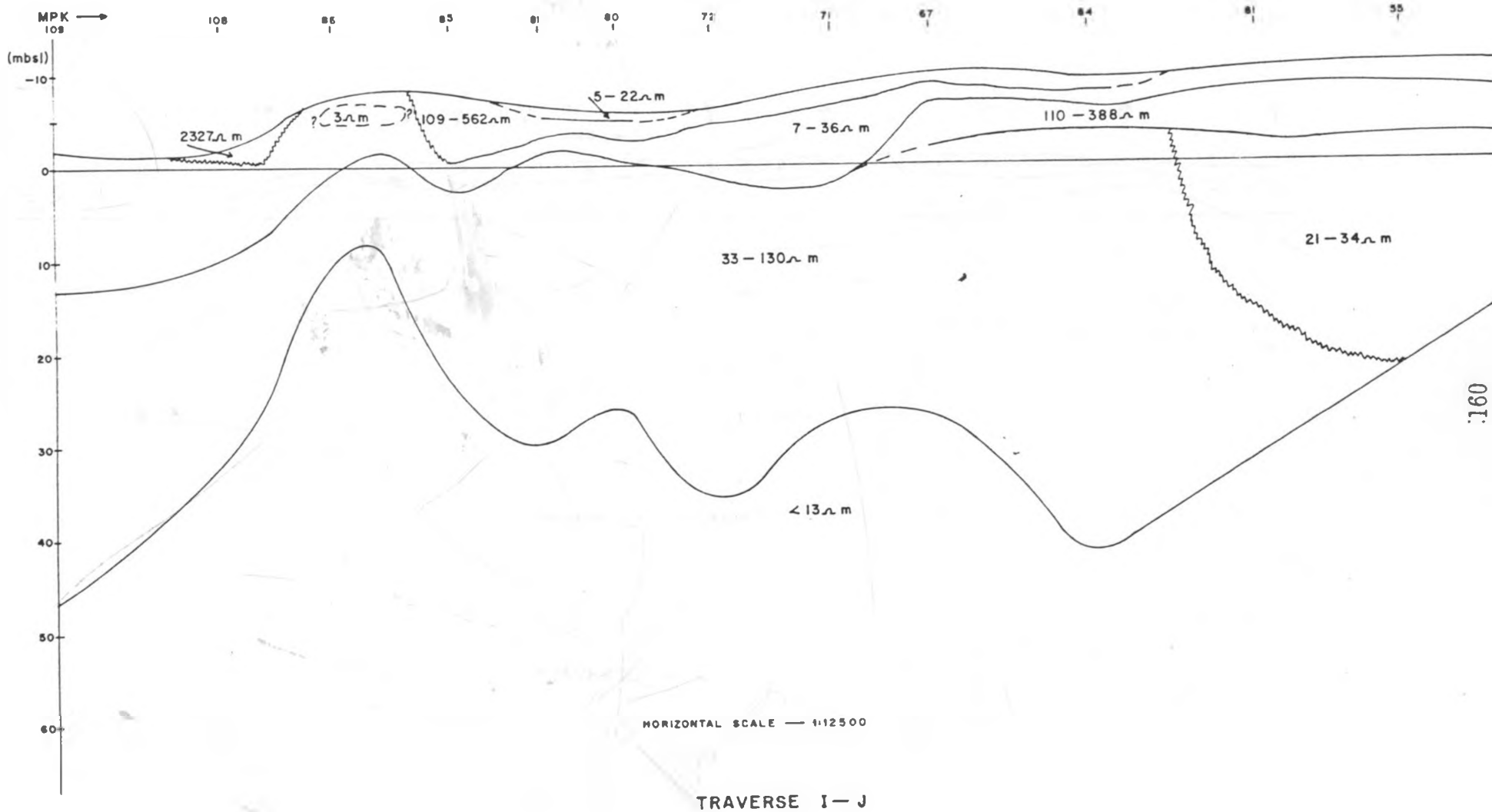
Fig. 6.23 Vertical distribution of true resistivity along traverse I-J
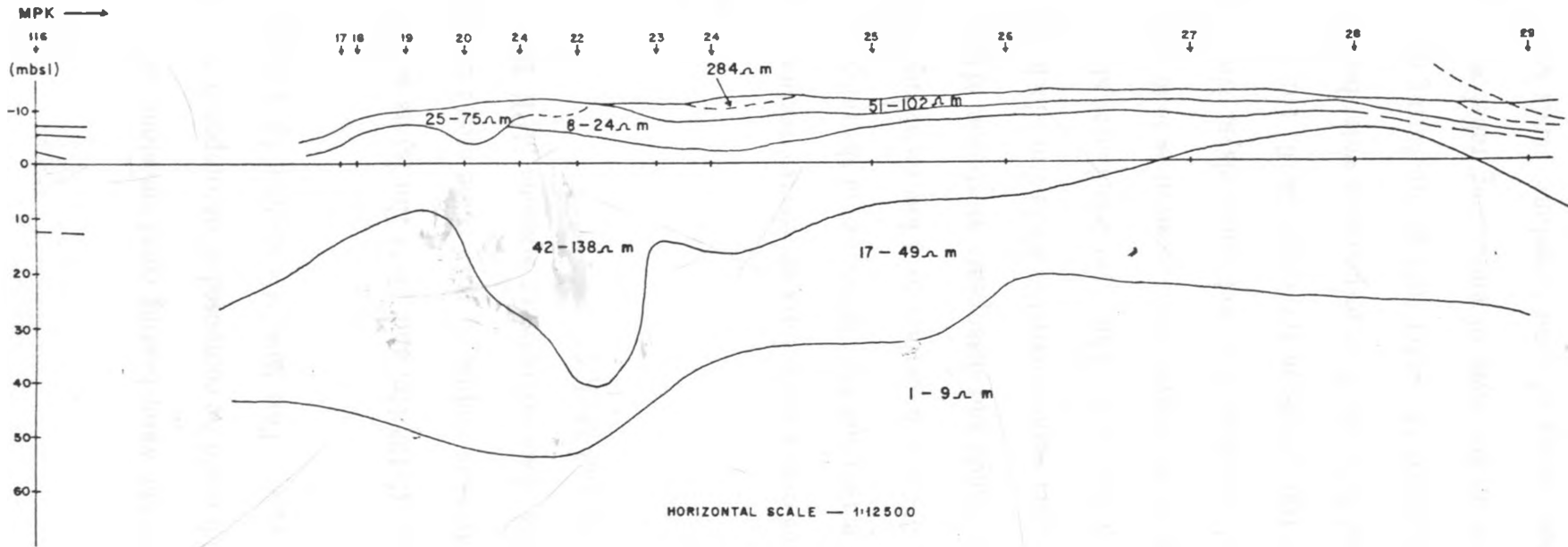
TRAVERSE K – L

Fig. 6.24 Vertical distribution of true resistivity along traverse K-L

161

Ωm layer that corresponds to the water-bearing coral limestone. It is underlain by a thick 17-49 Ωm layer which could be composed of decomposed coral limestones, clayey sands and brackish water. This layer is underlain by a zone of saltwater with resistivity 4 Ωm.

The contact between the 42-138 Ωm and 17-49 Ωm layers and that between the 17-49 Ωm and 4 Ωm layers is undulated with some crests and troughs and sometimes steeply dipping as observed between stations MPK 20 and MPK 22 and between stations MPK 22 and MPK 23.

6.2.3.8 Traverse M-N

Traverse M-N (Fig.6.25) runs over a seven-layer geoelectric section. The topmost layer which consists of sand is thin and has resistivities in the range 83-184 Ωm. It terminates at station MPK 38. It is underlain by a low resistivity 9-32 Ωm layer which corresponds to clayey sands and disappears at station MPK 39. This is followed beneath by a thick layer with resistivities 40-94 Ωm which corresponds to moist sand with decomposed limestone. This layer terminates at around station MPK 40. It is underlain by a thick layer with resistivities 9-30 Ωm. The layer has an undulating relief and corresponds to wet sandy clays. Underlying it is a thick undulating layer with resistivities in the range 55-161 Ωm which outcrops between stations MPK 44 and MPK 46. It corresponds to water-bearing coral with varying resistivities that depend on the water content, fracturing and dissolution. The layer is underlain by a thicker layer of undulating relief with resistivities 27-48 Ωm which is composed mainly of coral limestone, sands and water. It is conformably in contact with the overlying layer. It is followed beneath by a low resistivity layer with less than 10 Ωm that forms an undulating contact with it.
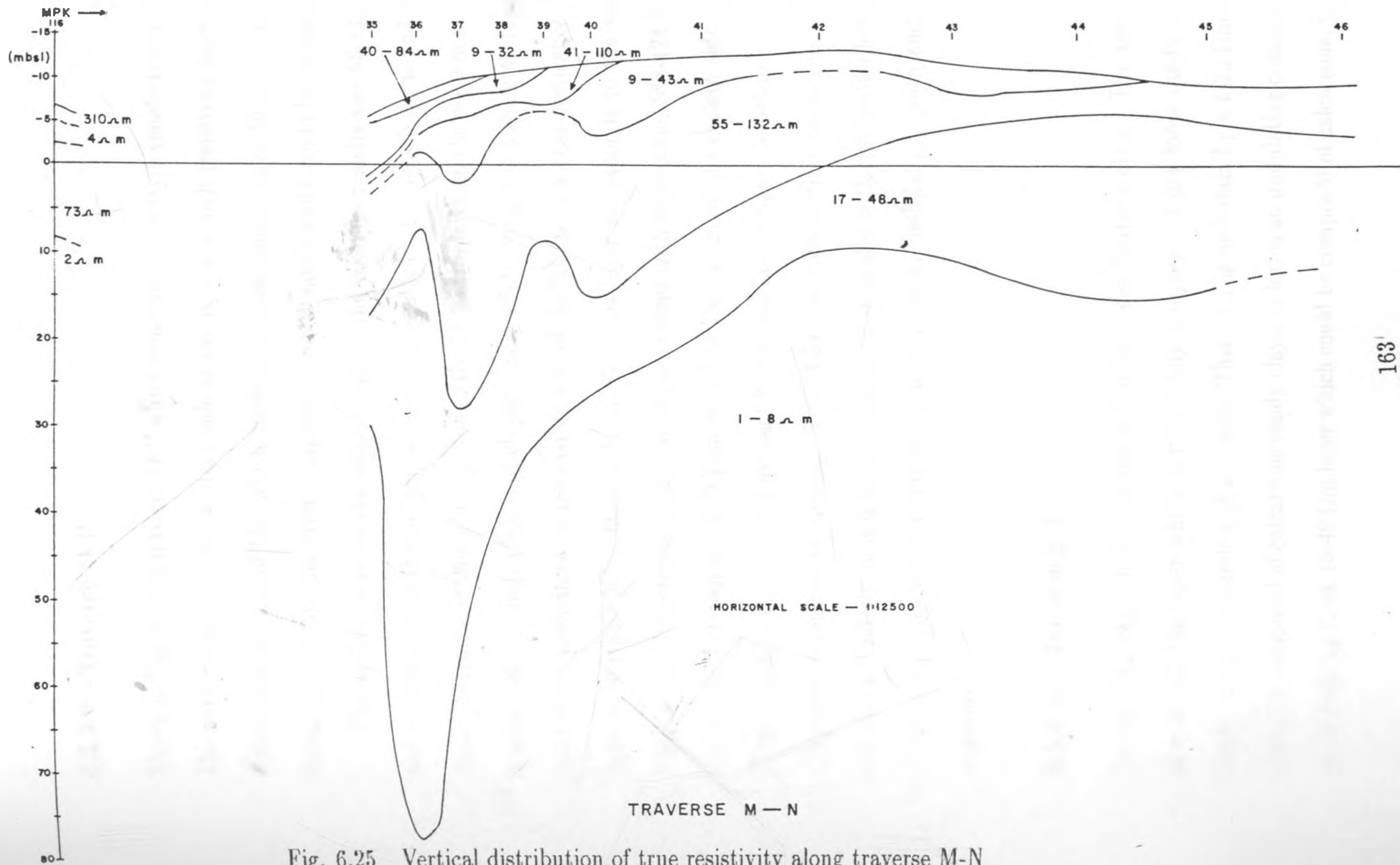
Fig. 6.25 Vertical distribution of true resistivity along traverse M-N

6.2.3.9 Traverse O-P

Shown in Fig. 6.26 is traverse O-P which runs over a five-layer geoelectric section. The surface layer on the western side of the lake is a high resistivity layer with resistivities 5504-6349 Ωm which consists of loose sands. It is underlain unconformably by a 287 Ωm layer composed of moist sands which could be calcareous.

The surface layer on the eastern side of the lake has resistivities 56-139 Ωm and corresponds to the surface layer on the western side. This layer is underlain by a 4-22 Ωm layer that corresponds to the 11-23 Ωm layer on the western side. It corresponds to sandy clays and clayey sands. Underlying it is a thick 45-196 Ωm layer which terminates on the eastern side of the lake with a near-vertical contact between stations MPK 60 and MPK 61. This layer corresponds to the water-bearing coral limestones. A layer of limited extent with resistivities 388-424 Ωm is sandwiched between the 4-22 Ωm and 11-34 Ωm layers on the eastern side. This highly resistive layer could represent buried sand or compact limestone that has undergone extensive weathering. The 11-34 Ωm layer depicts calcareous, clayey wet sands. Underlying it is a layer containing saltwater with resistivities less than 10 Ωm. The geoelectric layers are characterized by undulating, pinch and swell structure.

6.2.3.10 Traverse S-T

Taverse S-T (Fig. 6.27) overlies a four-layer geoelectric section. The top layer is a 35-353 Ωm layer which is most likely composed of dry loose sands, clayey sands, calcareous sands and top soils. This layer is underlain by a 5-23 Ωm layer probably composed of calcareous sandy clays. It forms an undulating contact with an underlying thick 15-49 Ωm layer which could be composed of calcareous, water-

Fig. 6.26   Vertical distribution of true resistivity along traverse O-P

MPK →

(mbsl)

35 – 353 Ω m

5 – 23 Ω m

13 – 49 Ω m

2 – 6 Ω m

HORIZONTAL SCALE – 1 : 10,000
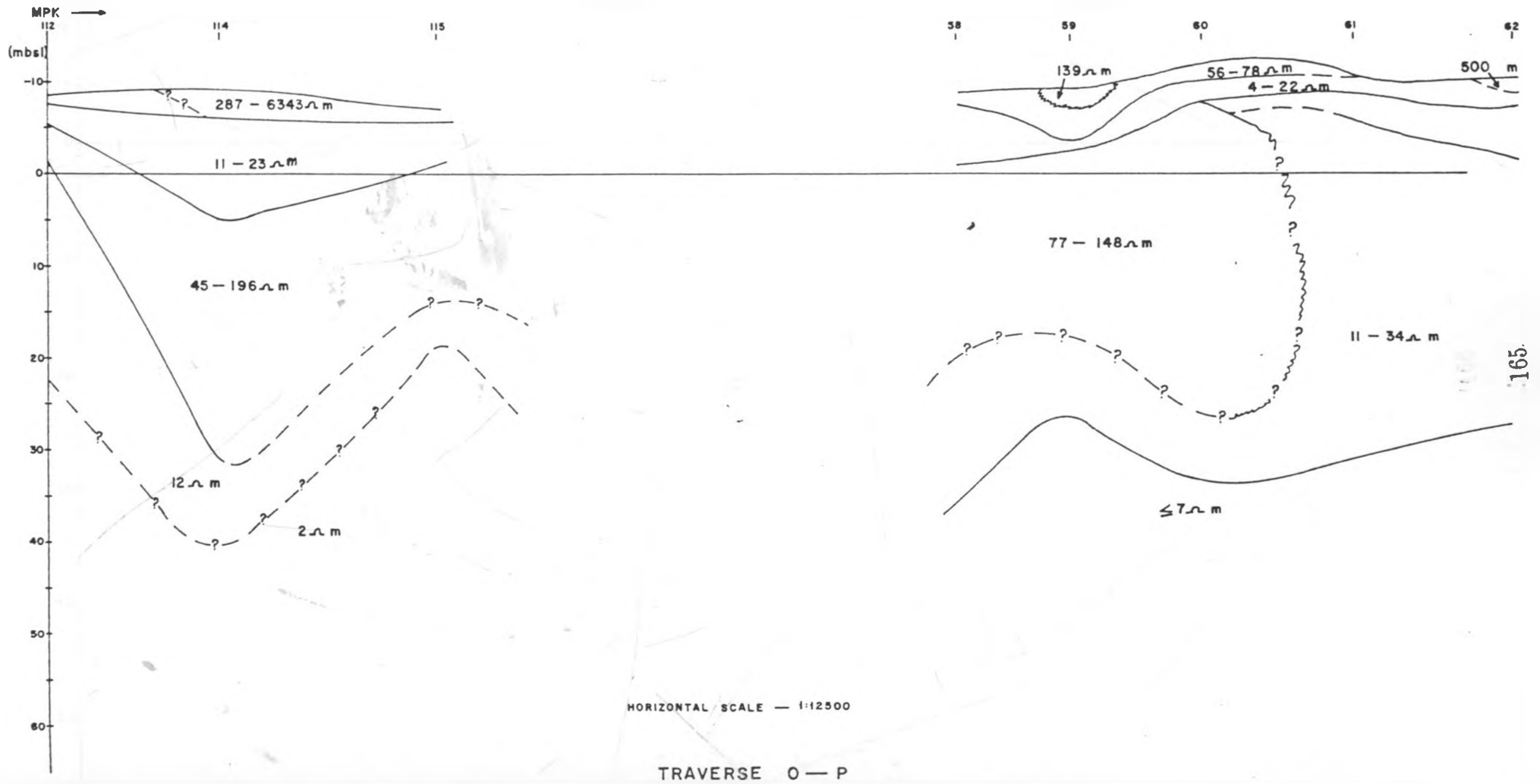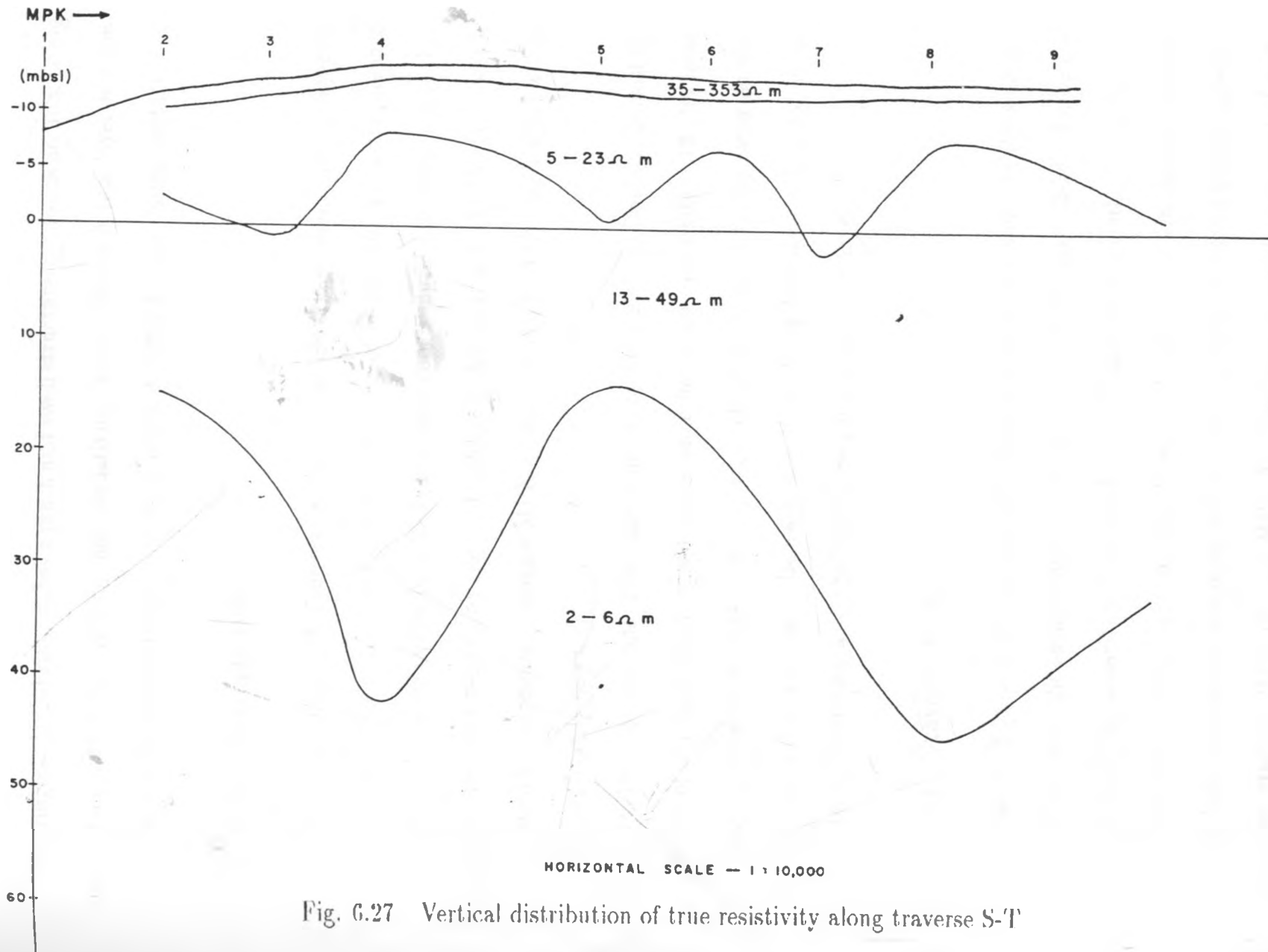
Fig. 6.27 Vertical distribution of true resistivity along traverse S-T

TRAVERSE S — T

166

bearing sands and silts. It has a pinch and swell structure and forms an undulating contact with both overlying and underlying layers. Beneath this layer is a low resistivity 2-5 Ωm saltwater zone with which it forms an undulating contact.

6.2.3.11 Traverse U-V

This traverse (Fig. 6.28) runs over a five-layer geoelectric section. The top layer on the northern side of the lake has a low resistivity of 11 Ωm which depicts presence of clays. This is underlain by a 35-44 Ωm layer consisting of calcareous sands that are either water-bearing or clayey. Underlying this layer is a 180 Ωm layer which apparently disappears at station MPK 3. Beneath is a 9-24 Ωm layer which could consist of sandy clays.

On the southern side of the lake, a highly resistive 99-6300 Ωm layer consisting mostly of dry loose sand to wet sands underlies a low resistivity 4-13 Ωm layer consisting mainly of clays. This layer correlates with the 9-24 Ωm layer on the northern side of the lake. Beneath is a thick 46-88 Ωm layer which forms an undulating boundary with the lowermost 1-6 Ωm saltwater layer.

6.2.3.12 Traverse W-X

Traverse W-X (Fig. 6.29) overlies a five-layer geoelectric section. On the western side of the lake, the surface layer which has a resistivity range 82-287 Ωm corresponds to dry loose sands and top sandy soils. This layer is underlain by a thinner 4-11 Ωm layer which consists mostly of clays and sandy clays. On the eastern side of the lake, the near surface layer with a resistivity range 108-3009 Ωm disappears between stations MPK 106 and MPK 97. The layer is mainly composed of very dry loose sands and wet sandy soils. It is underlain by a low resistivity layer with
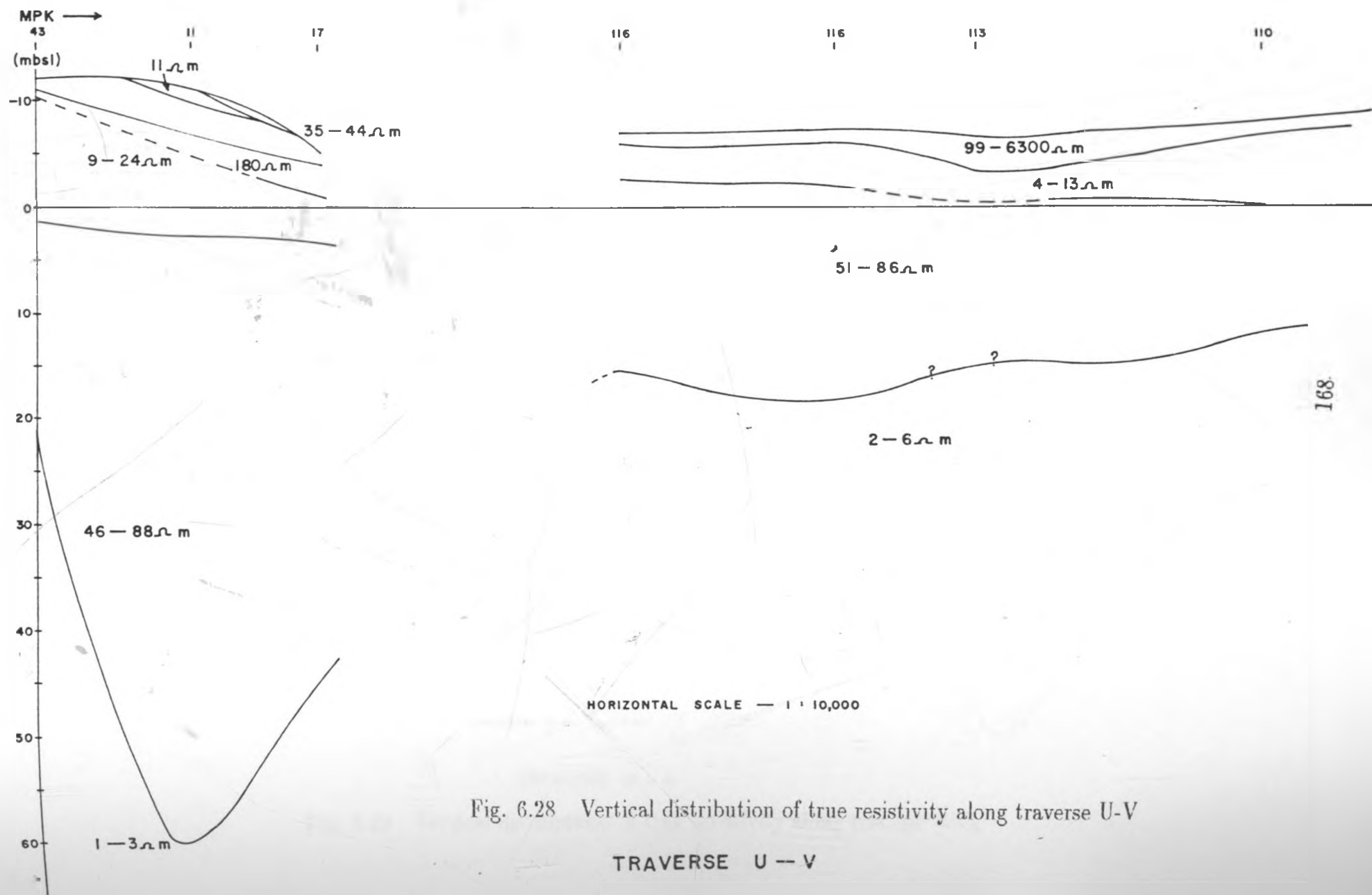
Fig. 6.28   Vertical distribution of true resistivity along traverse U-V

TRAVERSE   U — V
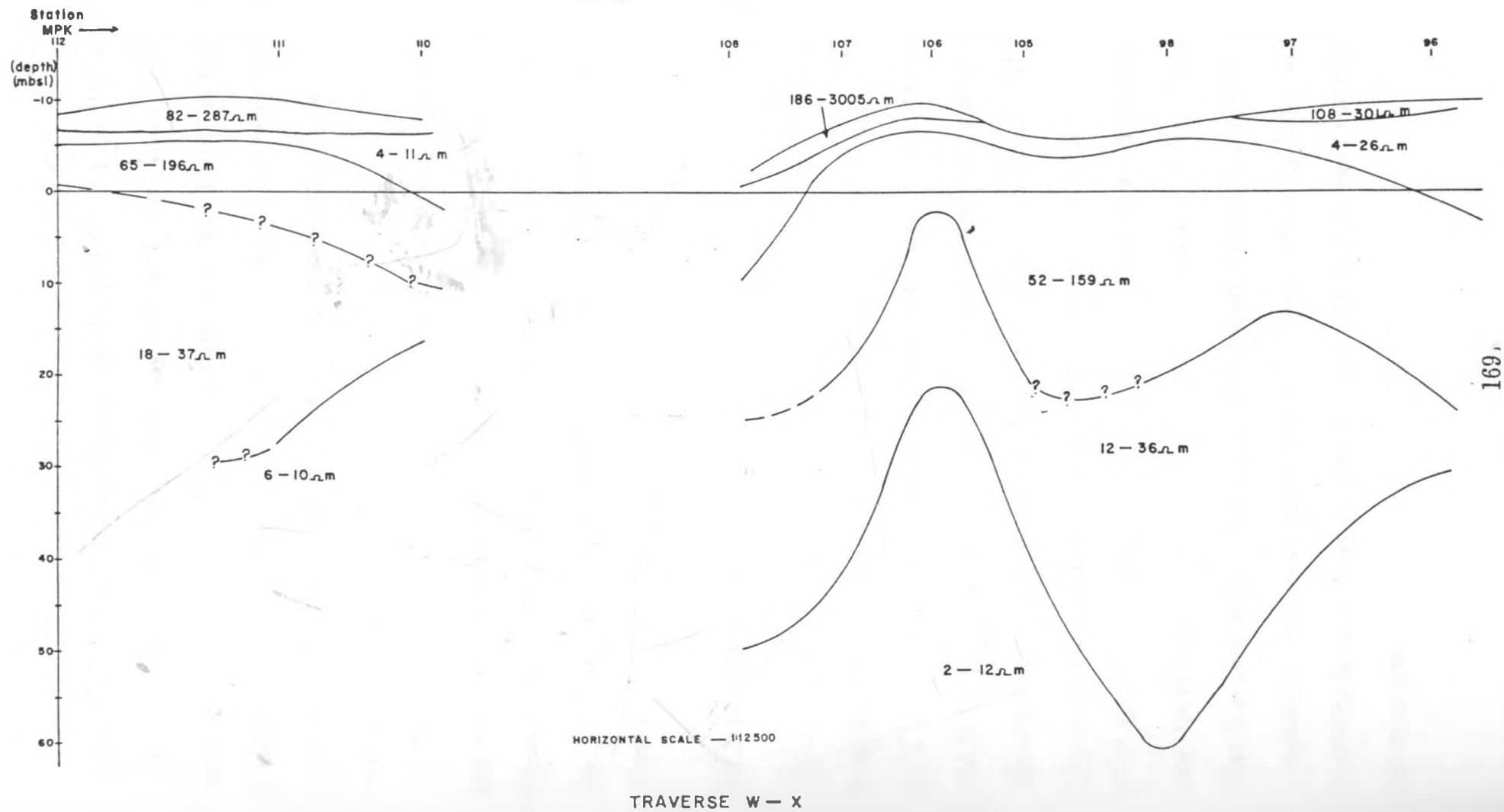
TRAVERSE W — X

Fig. 6.29 Vertical distribution of true resistivity along traverse W-X

resistivities 4-26 Ωm which correlates with the 4-11 Ωm layer on the western side of the lake. Beneath is a thick resistivity layer with resistivities 52-196 Ωm consisting of coral limestone. This is underlain by a thick 12-37 Ωm layer which is possibly composed of clayey silts, sands and calcareous sediments with brackish water zones. Lastly, beneath is a low resistivity saltwater zone with resistivities 2-10 Ωm.

The surface and near surface layers are characterized by undulating relief and show steep rises between stations MPK 108 and MPK 98 and steep declines between stations MPK 106 and MPK 98. The layers with resistivity ranges 52-196 Ωm, 12-37 Ωm and 2-10 Ωm have wavy forms of relief and show pinch and swell structure.

6.2.3.13   Traverse Y-Z

This traverse (Fig. 6.30) runs over a six-layer earth. The surface layer has a small thickness and low resistivities of 2-12 Ωm between stations MPK 81 and MPK 97. It is of limited extent and represents clay between stations MPK 81 and MPK 90. It is underlain by a high resistivity layer with resistivities 60-388 Ωm which apparently disappears between stations MPK 88 and MPK 90. The layer is composed of wet to dry sands. Beneath it is a thick layer with resistivities 17-25 Ωm which is likely to consist of calcareous, clayey water-bearing sands and silts. Underlying it is a thick 72-160 Ωm layer consisting of coral limestone. This layer is in turn underlain by a layer with resistivities 12-33 Ωm which is possibly composed of calcareous sands, silts and clays conformably lying on a very low resistivity layer with resistivities 2-3 Ωm. This bottom layer corresponds to the saltwater zone.

170

VES Station MPK

81   88   90   97   102   103

depth (mbsl)

60 – 388 Ω m

5 – 12 Ω m

13 – 36 Ω m

72 – 160 Ω m

12 – 40 Ω m

2 – 3 Ω m

??

–10

0

10

20

30

40

50

HORIZONTAL SCALE — 1 : 10,000

171'
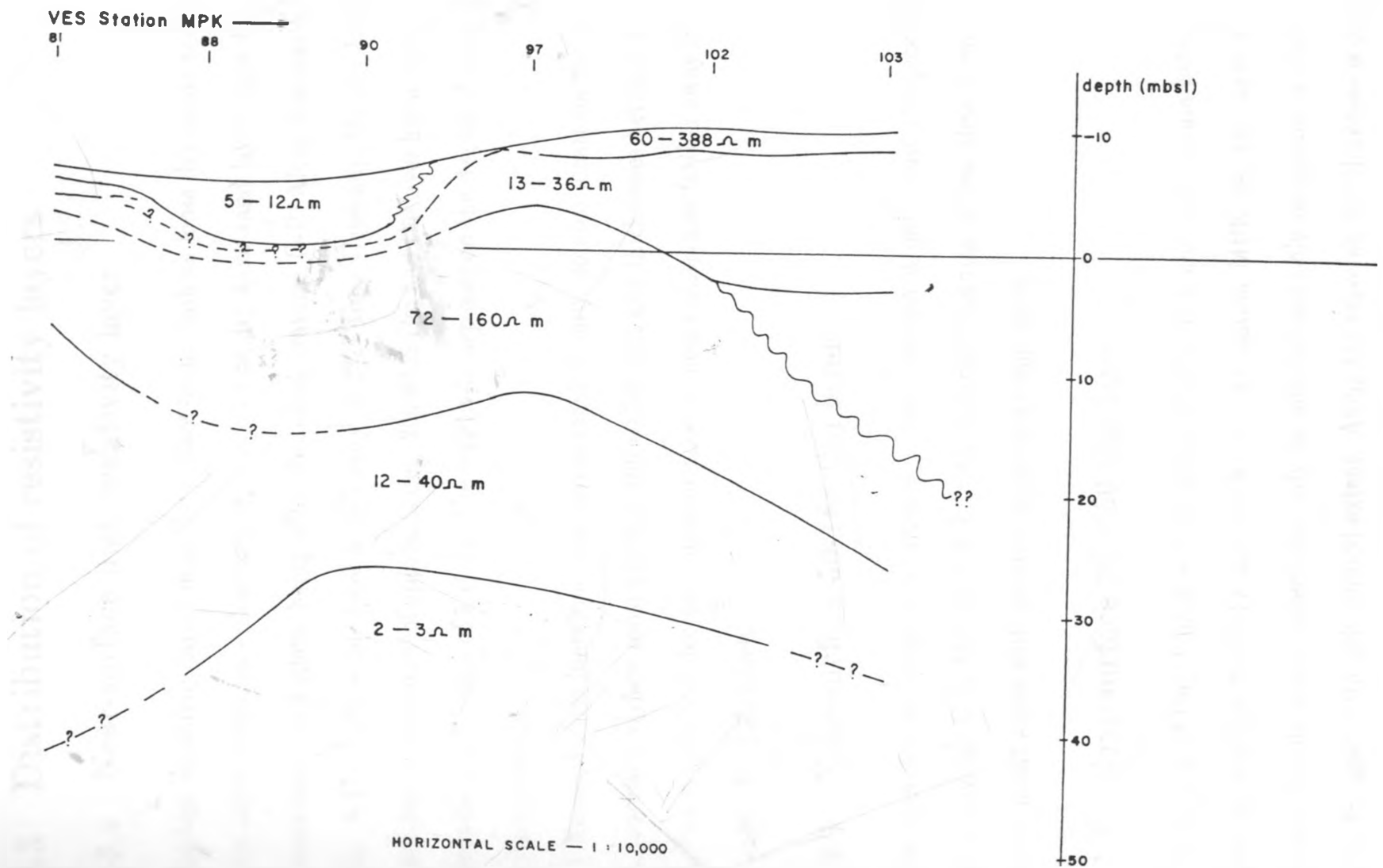
TRAVERSE   Y — Z

Fig. 6.30   Vertical distribution of true resistivity along traverse Y-Z

6.3 Distribution of resistivity layers

6.3.1 Near-surface high resistivity layer

The high resistivity layers near the surface occur both as loose dry sands and in some other instances, calcareous dry sands. The dry loose sand layers have high resistivities, the highest being 6349 Ωm along traverse O-P. Along traverse I-J (Fig. 6.23), loose sands have a resistivity of 2327 Ωm. Generally, the dry loose sands have a resistivity of approximately 200-6349 Ωm and the layer has a variable thickness of a fraction of 1-10 m. The resistivity depends on the degree of wetness and composition.

Exposed coral limestone was encountered at only isolated locations and has characteristic surface resistivities of 100 to 200 Ωm and thicknesses between 1-40 m. This is a distinct decrease in occurrence of these resistivities farther away from the Lake Kenyatta area.

6.3.2 Near-surface 50-188 Ωm layer

This layer has an isolated occurrence in the area and is only most conspicuous along traverse E-F, M-N and Y-Z, with variable thickness of less than 1 m. It depicts moist sands with isolated calcareous compositon.

6.3.3 Near-surface 20-<50 Ωm layer

This layer is of very limited extent along traverse K-L and only occurs between sounding stations MPK 17 and MPK 30. At station MPK 24, the layer also appears, but its lateral extent can only be inferred and only reappears at station MPK 49, again with only limited extent. Along the traverse, the thickness is only less than 3 m. Traverse U-V shows the presence of this layer between sounding

stations MPK 3 and MPK 17 where it has a thickness of approximately 5 m and a south-west dip. The layer thickens towards the north-west and separates into a 4-24 Ωm layer and, locally at station MPK 17, a 180 Ωm layer. It underlies a low resistivity 11 Ωm layer between stations MPK 3 and MPK 17.

6.3.4 Near-surface 4-36 Ωm layer

This layer is most common in the area and underlies the high resistivity surface layer except along traverses K-L, O-P and U-V. Along traverse G-H, on the western shore of Lake Kenyatta, the layer is very thick, approximately 20 m and engulfs a 196 Ωm layer at MPK 112. It underlies the thin high resistivity layer of up to 6349 Ωm and overlies a 45-82 Ωm layer with a thickness of 20-30 m. On the eastern shore of the lake, the 4-36 Ωm layer exhibits only shallow depth and low thickness and underlies a lower resistivity layer with resistivities 132-451 Ωm on the western shore. However, the layer overlies, like on the western shore, a thick layer with rssistivities 43-96 Ωm. Along traverse I-J, the thickness of the layer diminishes to between <5-15 m and underlies a very thick 33-123 Ωm layer. It has an undulating contact with the underlying and overlying geoelectric layers. Traverse K-L shows a similar trend whereby the continuous 4-35 Ωm layer underlies a 331 Ωm layer and a 51-113 Ωm layer. It underlies a low resistivity layer with resistivities 8-24 Ωm. It only appears between MPK 1 and MPK 29. Along traverses M-N, O-P, S-T, W-X and Y-Z, the layer is quite conspicuous like in all the other traverses. However, the layer is repetitive along traverse M-N and sandwiches a 40-94 Ωm layer of limited extent.

Traverse O-P shows a complex layering with a near vertical interface between a 77-148 Ωm layer and a thick 11-34 Ωm layer. On the western side of the lake,

the thickness of the latter layer is small.

6.3.5   3-44 Ωm layer overlying the thick 50-200 Ωm layer

The layers overlying the thick 50-200 Ωm layer exhibit a wide range of resistivity and thickness values, thus depicting a corresponding distribution of deposition material of varying composition. They show a varied disposition. The layers are continuous over most of the area and in particular cases. Traverses C-D, E-F, I-J, M-N, S-T, W-X AND Y-Z show an undulating contact with the 50-200 Ωm layer. The varied resistivity values indicate that the composition of this layer varies from clays to calcareous clays and sandy silts. In particular, low resistivity values were observed at stations MPK 105 and 106 where the values ranged between 3 and 4 Ωm, respectively. This layer is a transition layer representing gradation to the thick 50-200 Ωm layer. An almost similar resistivity layer is observed underlying the 50-200 Ωm layer which suggests that the two layers, one overlying and the other underlying the 50-200 Ωm layer, are essentially a progressive gradation of the 50-200 Ωm layer. This could again be verified from their continuous nature and close association with the latter.

6.3.6   50-200 Ωm layer

This is the thickest layer interpreted in the entire study area and is the most extensive among all the layers. Its importance is attributed to its regional extent, porosity and permeability, all of which govern its storativity and the groundwater flow. It forms the coral limestone whose importance cannot be overemphasized. It mainly overlies a 15-50 Ωm layer in most parts of the area which symbolizes the gradation of the layers into the 50-200 Ωm layer. The upper value of 200 Ωm

may be representative of compact, unweathered coral limestone while the 50 Ωm resistivity depicts the highly fractured, porous and permeable water-bearing coral limestone. It is noteworthy that the thickness of the 50-200 Ωm layer is largest in the area within the proximity of Lake Kenyatta and thins out away from the lake. The layer exhibits undulating relief and in some instants, very steep near-vertical boundaries with adjoining areas. The northwestern part of the study area has the thickest 50-200 Ωm layer which displays a pinch and swell structure.

6.3.7 13-49 Ωm transition layer underlying the 50-200 Ωm layer

It has been noted above that a persistent layer of resistivities 15-50 Ωm occurs above and below the conspicuous 50-200 Ωm layer. The 13-49 Ωm layer forms a very extensive thick bottom layer in most parts of the study area. Its boundary with the 50-200 Ωm layer and the layer with resistivity less than 10 Ωm is not in all cases possible to discern because of its transitional nature as observed along traverses A-B, E-F, O-P and W-X. In most instances, it exhibits an undulating contact with the underlying low resistivity layer. It is not present in all traverses as observed along traverses G-H, I-J and U-V. The apparent absence of this layer in some locations suggests either the abrupt change of the 50-200 Ωm layer to the layer with resitivity less than 10 Ωm or its suppression during interpretation. The latter phenomenon is most likely since there is normally a transition zone between fresh groundwater and saltwater made up of intermediate brackish water. It may therefore be inferred that in those places where the transition layer is not observed from interpreted results, it is too narrow and hence suppressed.

6.3.8 Saltwater layer with resistivity less than 10 Ωm

During the fieldwork, it was possible to determine when the depth to the interface of the thick 50-200 Ω layer and this low resistivity layer has been encountered. This was evident from the behaviour of the sounding curves. This interface has a varying depth between 20 and 50 m below the ground surface. The interface in general is deepest near Lake Kenyatta and shallow away from it. It shows a generally undulating contact with the overlying layer as noted along traverses A-B, C-D, E-F, I-J, M-N, O-P, S-T, U-V and W-X, though in most instances it dips towards the lake in a south-western direction on the eastern side of the lake.

6.4 Distribution of directly measured conductivities, piezometric levels and well hydrographs

6.4.1 Lateral distribution of groundwater conductivity

The electrical conductivities of a large number of shallow hand dug wells have been measured by GASP since 1982. However, the majority of measurements have only been taken since 1985, once a year and in a few cases twice a year. To discern the water quality distribution in space and time over the area, plots of electrical conductivity have been prepared for the period 1985 to 1990 (Appendix II). This enhances a visual appraisal of the water quality deterioration with time and puts in place the saltwater intrusion problem as manifested in the size of the freshwater (1000 μs/cm) body. The electrical conductivity values for the lake water are not available except for two readings taken by GSK (1987, 1990) whereby the electrical conductivity was 100 μs/cm and 800 μs/cm, respectively. Differential conductivity

values have been calculated and contoured (Appendix III) accordingly in order to qualify and quantify the water quality deterioration between successive years since 1985.

At the northern shore of the lake, groundwater is of stable and good quality as illustrated by its salinity (electrical conductivity 400 to 500 μs/cm) which is in general low and only slowly increases during dry spells. During April to June, flooding causes high lake levels, thus causing reversed groundwater flow. This in effect causes the electrical conductivity to drop around the lake due to fresh lake water infiltration into the aquifers and due to recharge by deep percolation of rain water farther inland. During the dry seasons, the electrical conductivity of the lake water increases due to evapotranspiration processes. It has been observed that the aquifer on the south-eastern shore of the lake is recharged directly by the lake water. For this reason, the electrical conductivity of the groundwater on the south-eastern shore increases significantly during the dry periods. Contrary to this, after periods of heavy rainfall and high lake levels, the electrical conductivity attributed to the effects of fresh groundwater recharge into the aquifer from the lake was 100 μs/cm while in 1990, the electrical conductivity observed was approximately 800 μs/cm.

From the electrical plots, it may be observed that the water in the area on the northern shore of the lake changes to lower electrical conductivity values due to recharge from the lake and rainwater percolation into the groundwater storage during the relatively wet years of 1986 and 1987. Thus, the rainfall intensity and distribution has a significant influence on the water quality. Between 1982 and 1988, the electrical conductivity change is merely slight except in the north-west where possible groundwater recharged from farther north and improved the

water quality. However, the changes in electrical conductivity between 1989 and 1990 are only insignificant. It may therefore be legitimately argued that the size of the freshwater body increases considerably, especially between 1985 and 1987. However, the increase is not continuous, but interfered with by isolated sporadic decreases. This intermittent increase and decrease in the size of the freshwater body, as manifested in the electrical resistivity changes, is mainly dependent on the hydrologic factors that interplay in the entire region. A generalized schematic diagram (Fig. 6.31(a-d)) is presented. Fig. 6.31(a) corresponds to high lake levels so that the groundwater aquifer is being recharged by lake surface water. Fig. 6.31(b) corresponds to a diminishing lake level so that the groundwater storage recharges the surface water from the north and north-eastern shores of the lake. Discharge of the lake into groundwater storage occurs in the southern and south-eastern shores. Fig. 6.31(d) corresponds to extremely low lake level such that the groundwater aquifer recharges the lake from all directions.

6.4.2 Lateral distribution of piezometric levels

Piezometric levels for wells were contoured for particular dates, thus giving piezometric maps. From the piezometric contour maps, the groundwater flow pattern can be inferred. Piezometric maps for the dates 1/12/87, 1/8/88, 1/7/89, 1/9/85, 24/3/86 and 4/10/86 have been prepared and are shown in Appendix IV.

The piezometric maps for March and April depict the hydrologic situation before the onset of the long rains, while those for June and July represent the situation shortly after the rains. The maps for October depict the hydrologic situation during the period preceding the short rains. It can be deduced that the inflow into the lake is mainly centred in the north-western shore of the lake. In
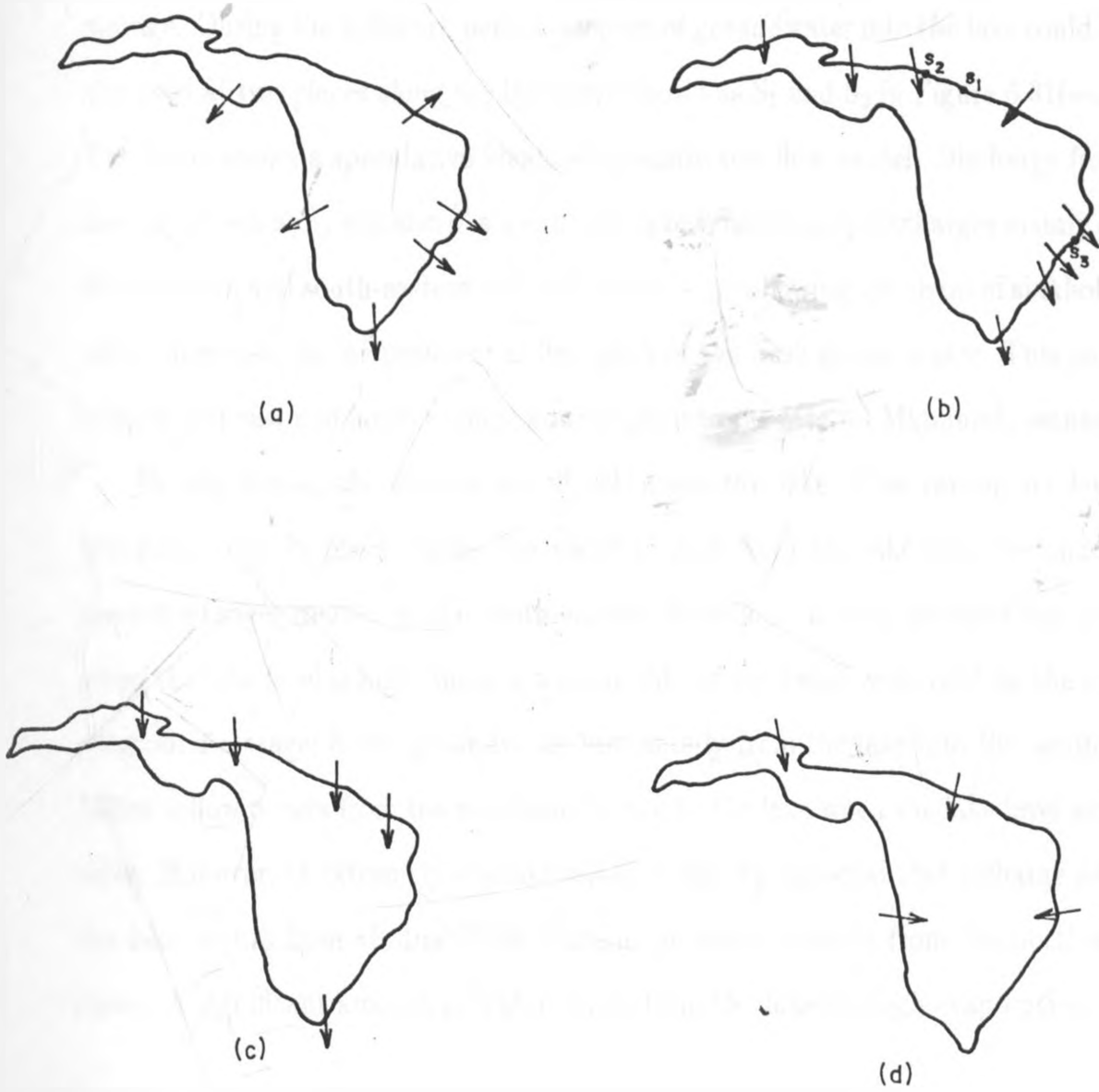
Fig. 6.31 Schematic diagram showing the groundwater flow in the Lake Kenyatta area
at various lake levels

this area, a large number of sinkholes occurs, indicating a subsurface freshwater storage. During the fieldwork period, seepage of groundwater into the lake could be observed at two places along the lakeshore shown as S_1 and S_2 in Figure 6.31(a-d). The figure shows a speculative idealized groundwater flow model. Discharge from the lake shown as S_3 was also observed. The lake subsequently discharges mainly on the southern and south-eastern side, most probably following the chain of sinkholes which demonstrate the preferential flow path of the fresh groundwater. This path turns to the east and farther down, flowing out into the Mto wa Mkunumbi estuary.

During floods, the surface runoff recharges the lake, thus raising its level abruptly. This in effect causes the water to flow from the lake into the underground storage, mainly in the south-eastern direction. It may be observed that when the lake level is high, there is a possibility of not being recharged by the underground storage; hence groundwater flow is only from the lake into the aquifer. Minor inflow occurs from the northern shore into the lake when the lake level subsides. However, at extremely low lake levels, it may be expected that recharge into the lake occurs from all directions, though the main inflow is from the northern shore. A significant amount of water is lost from the lake through evaporation.

6.4.3   Lateral distribution of well hydrographs

The hydrological conditions in the study area are quite variable and differ for consecutive years depending on local conditions. Several evaluated hydrographs (Appendix V) show that the changes in regional groundwater levels are directly related to the intensity and timing of rainfall. During the long rains (May to August), there is a marked rise in groundwater level while the short rains (November to January) cause only a negligible rise in the groundwater levels. The rise of the

lake level is accompanied by a corresponding rise in the groundwater level, even far from the lake. This suggests that the underground storage is charged through the infiltration into the aquifer in the entire recharge area. The rise in groundwater level in 1987 between May and August was approximately 1.5 m as compared to 20 to 30 cm in the years 1988, 1989 and 1990. Thus, during 1987, groundwater level rise was approximately 5 times more than in the rest of subsequent years, though the rainfall total was not five times as high.

This can be explained by the fact that there was an abrupt rise in the lake level due to the runoff from its recharge area, thus enhancing recharge of the aquifer by gravity flow. Also due to high rainfall intensity in May to August 1987 which resulted in flooding, there was a corresponding steady rise in groundwater levels in the region.

The water level and conductivity values of borehole No. 2 very closely resemble those of the lake, thus suggesting a direct hydrological link between the lake and borehole C-7347. This was practically confirmed from the swirl pattern of white dust during the fieldwork. A discharge point of the lake was deduced at sounding station MPK 72. The groundwater levels on the northern shore of the lake are generally higher (from 1988 and 1989 data) than the lake level while those on the south-eastern side of the lake are lower than the lake level. This suggests that there is a general flow of groundwater from the northern coast of the lake and recharge of lake water into the aquifer at the south-eastern coast.

6.5   Depth to the freshwater/saltwater interface

The variation of depth to the interface (Fig. 6.32) indicates its relation to hydrogeology. At the northern and eastern shores of the lake, the freshwater/saltwater
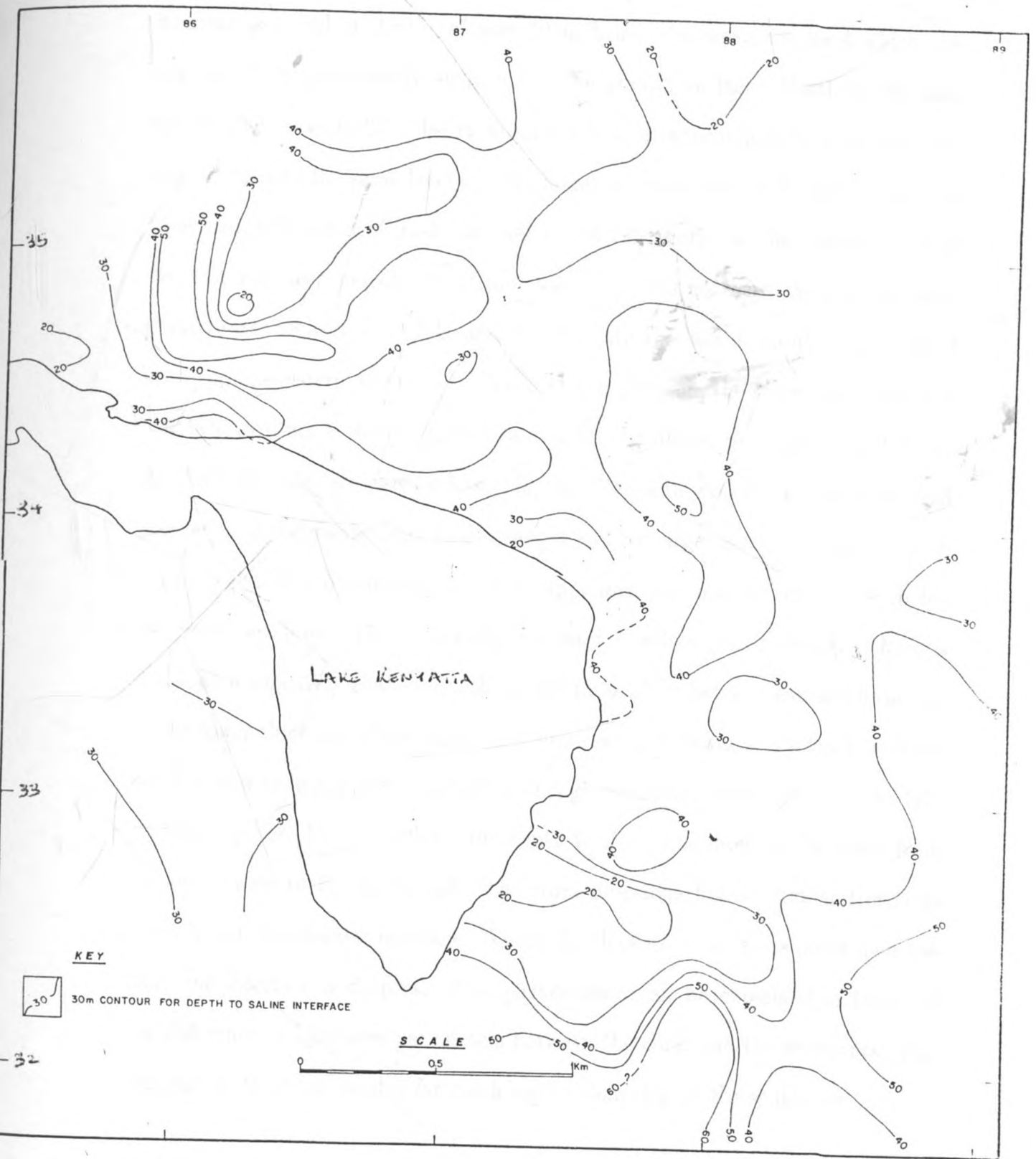
Fig. 6.32   Depth to freshwater/saltwater interface

182

interface is found at depths of over 30 m below the mean sea level which corresponds to approximately 40 m below the ground surface. North of the lake, the interface rises to 20 m below mean sea level at approximately 2 km from the lake. It rises to the same level at a far larger distance east of the lake due to the combined infiltration of fresh lake water into the aquifer at the eastern shore of the lake and deep percolation of rain water. At the northern shore of the lake, groundwater recharges the lake and the flow into the lake is mainly concentrated in the north-western corner of the lake. At this position, the saltwater/freshwater interface exhibits a steep gradient caused by the discharge of groundwater due to which the interface rises to lesser depths. Depending on the groundwater and lake levels, groundwater may be discharged and recharged into and from the lake, respectively. This dynamic system has suppressed the interface to over 30 m below mean sea level. The saltwater/freshwater interface on the western shore is found at a relatively shallow depth of less than 20 m below mean sea level due to the lower thickness of the coral, thus suppressing formation of a thick freshwater lens and reducing the possibilities of high freshwater recharge from the lake into the aquifer. Under the lake, the depth to the saline interface increases from the north-west to the north-east. The coral limestone follows similar trends as the saltwater/freshwater interface. Where the thickest coral layers occur near the lake, the interface is deepest. This phenomenon can be explained in terms of the difference in hydraulic parameters between the coral and the sediments. The transmissivity of the coral is far much higher than that of the sediments.
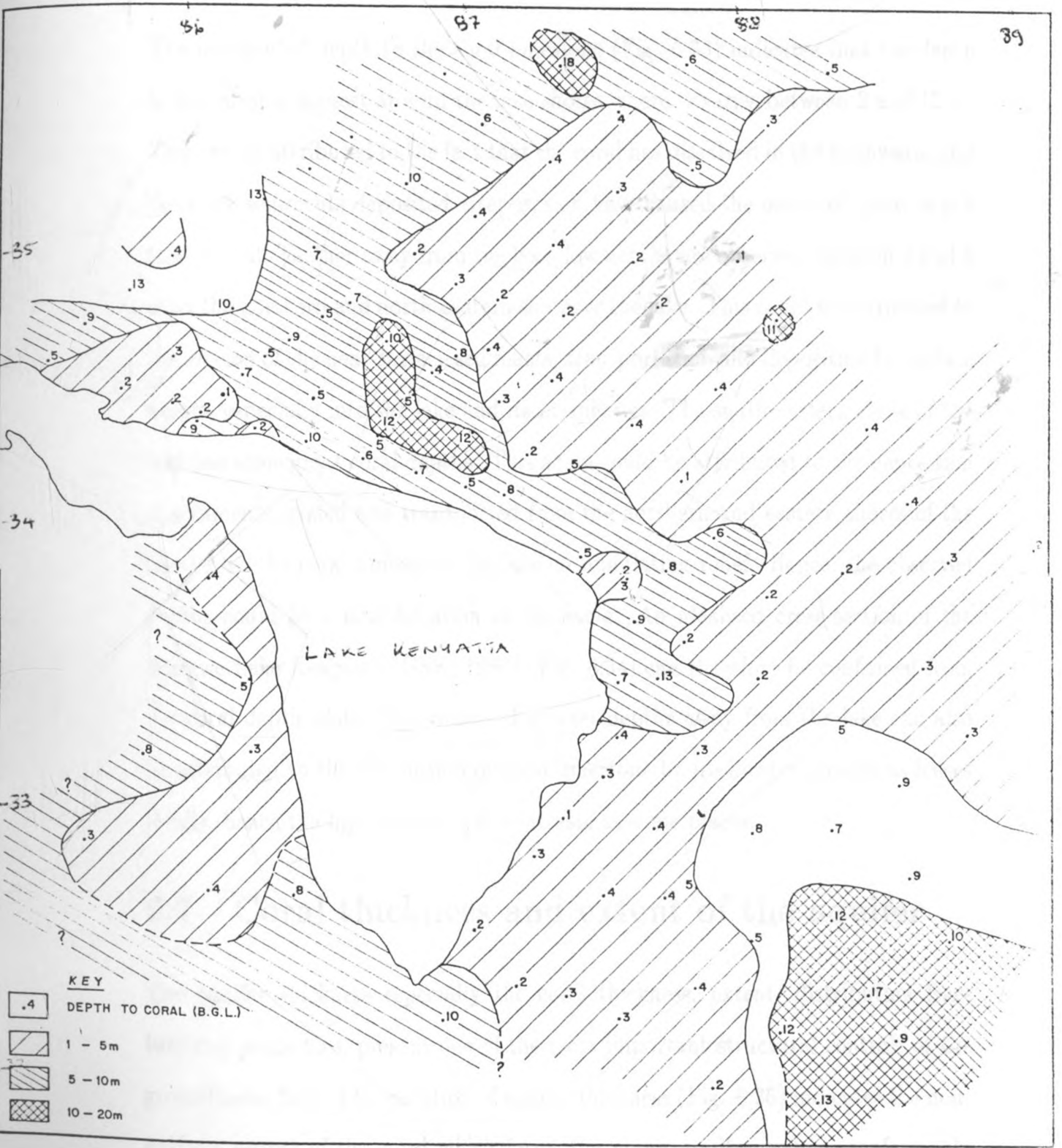
Fig. 6.33   Depth to coral

184

6.6 Depth to the coral

The interpreted depth to the coral limestone (Fig. 6.33) indicates that the depth to the coral is highest around the lake shores where it varies between 2 and 12 m. This can be attributed to the fact that the coral has dissolved in the freshwater and the thick sediments deposited after erosion have caused the observed great depth to the coral. Farther away from the lake, low depths are observed between 2 and 5 m on the northern and north-eastern shores of the lake. This could be attributed to the erosion of the near-surface sediments, transportation and deposition by surface agents, especially into the lake and its peripheries. The south-eastern shore of the lake has some great coral depths. This again could be attributed to the deposition of sediments eroded and transported from the northern and eastern shores of the lake. Also the coral limestone displays an undulating relief. Hence, the observed depths could be a manifestation of the same. An idealised cross-section of the Hongwe-Lake Kenyatta (GSK, 1990) (Fig. 6.34) can therefore be confirmed from the coral depth plots. The observed greater depths away from the lake can also be attributed to the dissolution of coral limestone by freshwater present as lenses locally, hence the high coral depth contrasts at some places.

6.7 Coral thickness and extent of the aquifer

The aquifer thickness especially the coral thickness, extent, distribution fracture and properties, present one of the most important structural controls of the groundwater flow. The variation of aquifer thickness (Fig. 6.35) indicates the non-uniform nature of the coral which forms the major aquifer system, conformably overlying the fresh water-bearing marine sediments. It is an extensive body un-

185

S C A L E

0   1   2   3   4   5 Km.

+30m NNW   SSE

HONGWE
C7349

+20 DOLINE   FOSSIL DUNE

                    C7348   DOLINES   C7345
                                                           C7347   DOLINES

+0   C7346

        REGIONAL GROUNDWATER TABLE   DOLJE LAKE

KSL   L. KENYATTA

                                                  G.W.FLOW ? ?—?—?—?

-10

        CORAL LIMESTONE

-20

-30

                    SALINE INTERFACE   ?

-40m

IDEALIZED CROSS – SECTION HONGWE – LAKE KENYATTA
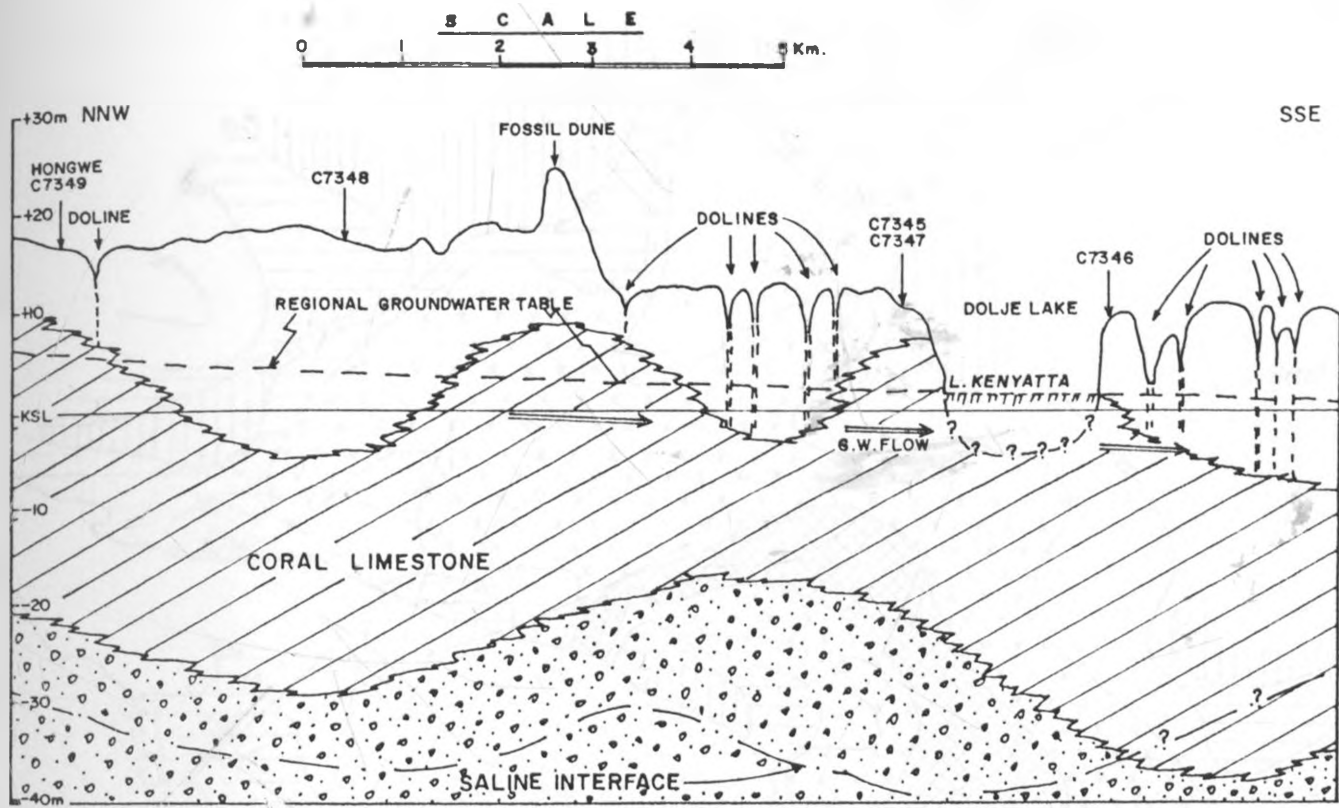
CORAL LIMESTONE   MARINE SEDIMENTS

NB:— Saline interface lies below coral limestone in the marine sands,
     and silty clays.

Fig. 6.34   Idealized cross section Hongwe-Lake Kenyatta

186
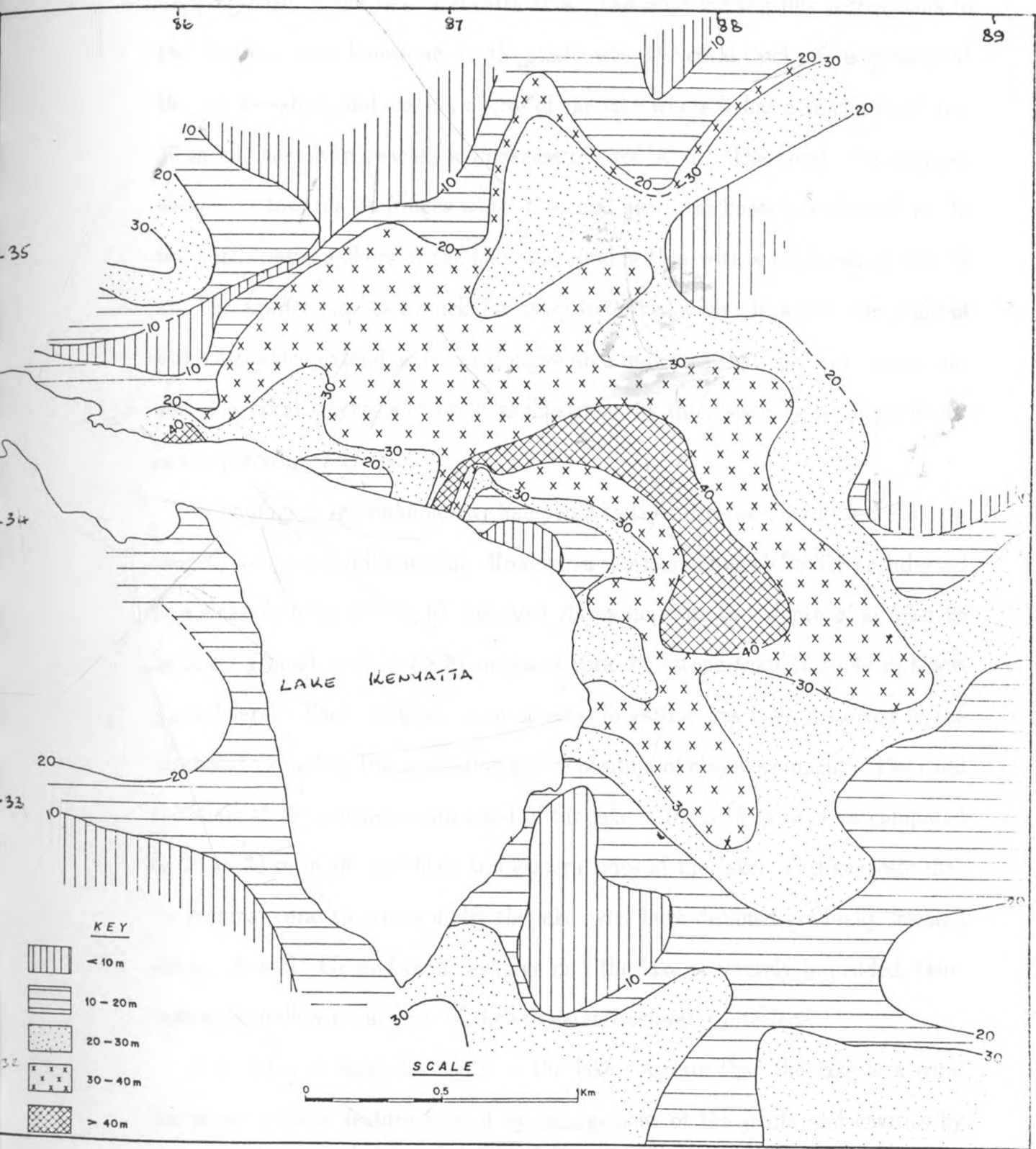
Fig. 6.35   Coral thickness

derlying most of the Lake Kenyatta area. The uppr zig zag line corresponds to the depth to coral limestone. In the study area, the coral thickness is greatest at the north-eastern and eastern shores of the lake where it has a thickness of over 20 m and locally it reaches a thickness of over 30 m. The coral reefs mapped wedge out towards its fringes where the coral has a thickness less than 10 m. In the north-western shore of the lake, the coral is thin with a thickness of 5 to 10 m. The aquifer reaches a thickness of up to 20 m locally. However, the chain of sinkholes which extend as far as Hongwe area indicates that the coral is continuous. The coral pinches and swells as illustrated by the resistivity traverses shown in the preceding sections.

Soundings in the sinkholes are hampered by their dimensions which are insufficient to complete a full sounding. However, a short sounding (VES 37B) conducted in a sinkhole next to VES 37 indicated clayey deposits to a depth of at least 25 m below ground level. VES 37 indicates coral limestone from 16 to 40 m below ground level. Thus, at least 15 m of coral limestone has been dissolved in the sinkhole followed by transportation and deposition of clayey sediments. The coral thickness at the south-western coast of the lake is 10 to 15 m thick as compared to 20 to 30 m in the northern and eastern sides of the lake. This suggests that the original coral thickness under the lake must have declined gradually towards the south-west. Groundwater recharge into the lake is severely impedded, thus, causing a shallow occurrence of the saltwater/freshwater interface.

The chain of sinkholes south of the lake suggests that the lake is a coral limestone solution feature formed by enlargement of the joints and cavities by solution when water flows through the cracks in the limestone. The collapse of these underground cavities creates conical depressions, the sinkholes. When two

or more sinkholes coalesce an uvala is formed and has a diameter of say, 100 to 300 m. Larger depressions (tens of square kilometres) are called poljes which are characterised by steep sides and flat floors upon which small residual hills may remain. Poljes result from lateral extension of uvalas, but structural control by faulting is also assumed in their formation as is the case in the Lake Kenyatta area. The sinkholes and uvalas are easily recognised in the Lake Kenyatta area and the lake itself is a polje lake.

6.8 Geological interpretation

6.8.1 Introduction

From the geoelectric profiles presented in this chapter, the variation and distribution of resistivity in the entire study area can be discerned. Correlation is therefore possible between the interpetated resistivity and thickness of geoelectric layers and the corresponding lithological units in the area. Thus, it is possible to determine a geological model which best corresponds to the geological interpretation. This necessitates correlation with geologic information and borehole logs.

The problem of correlation in the area cannot be overstated, and is due to the fact that the same lithologic unit may exhibit a wide range of resistivity values which in most cases overlap with those of units of different lothologic composition. Therefore, the geological interpretation of lithologic units with only a slight resistivity contrast is only speculative when they occur in the same location. In developing a resistivity calibration scheme, resistivity soundings ("parametric soundings", Flathe, 1967) logs were recovered and interpretated and correlation made between the geological interpretation and the logs. When the vertical lithological boundaries are delineated, for the interpretation the thicknesses are fixed

or more sinkholes coalesce an uvala is formed and has a diameter of say, 100 to 300 m. Larger depressions (tens of square kilometres) are called poljes which are characterised by steep sides and flat floors upon which small residual hills may remain. Poljes result from lateral extension of uvalas, but structural control by faulting is also assumed in their formation as is the case in the Lake Kenyatta area. The sinkholes and uvalas are easily recognised in the Lake Kenyatta area and the lake itself is a polje lake.

6.8 Geological interpretation

6.8.1 Introduction

From the geoelectric profiles presented in this chapter, the variation and distribution of resistivity in the entire study area can be discerned. Correlation is therefore possible between the interpetated resistivity and thickness of geoelectric layers and the corresponding lithological units in the area. Thus, it is possible to determine a geological model which best corresponds to the geological interpretation. This necessitates correlation with geologic information and borehole logs.

The problem of correlation in the area cannot be overstated, and is due to the fact that the same lithologic unit may exhibit a wide range of resistivity values which in most cases overlap with those of units of different lothologic composition. Therefore, the geological interpretation of lithologic units with only a slight resistivity contrast is only speculative when they occur in the same location. In developing a resistivity calibration scheme, resistivity soundings ("parametric soundings", Flathe, 1967) logs were recovered and interpetated and correlation made between the geological interpretation and the logs. When the vertical lithological boundaries are delineated, for the interpretation the thicknesses are fixed

and the resistivities accurately adjusted by the automatic inversion technique. After several interpretations, the ranges of resistivities for a particular lithologic unit in the area can be determined. It may be observed that to achieve an absolute solution is difficult since we may experience a situation whereby thin clay layers are intercalated in the sands and silts. This may lower their resistivities to such an extent that it corresponds to that of brackish water saturated sands. The errors emanating from such situations can be minimized if borehole logs are available. Based on these facts, it is possible to appreciate the problem associated with geological interpretations of the geoelectric sections in the study area. However, based on the available geophysical and geologic data, correlation is made between the two, which is subject to further correction as more information is subsequently obtained from the recommended exploratory drilling and production boreholes.

6.8.2 Geoelectric layers and their correlation with borehole logs

The general resistivity layer distribution in the area as discussed in the earlier sections of this chapter identifies 8 resistivity horizons. In summary, these layers include the high resistivity near-surface layers, the 50-88 Ωm near-surface layer, the 20-<50 Ωm near-surface layer, the 4-36 Ωm near-surface layer, the 3-44 Ωm layer overlying the thick 50-200 Ωm layer, the 13-49 Ωm transition layer underlying the 50-200 Ωm layer, and the very low resisitivity layer. All these layers, in most cases, have heterogeneous resistivity values. However, the most abundant resistivity model is the 5-layer model.

Three boreholes have been drilled in the area. These are C-7345, C-7346 and C-7347 which have been drilled to depths of 37.3 m, 62.3 m and 50 m, respectively. From the borehole logs of borehole no.1 (C-7345) near sounding MPK 20, the

following correlation can be made with the geophysical interpretation:

Table 6.1. Correlation between geophysical interpretation of MPK 20 and borehole no. 1 logs.

Formation	Depth(m)	Resistivity(Ωm)
Clayeysands top soil	0 -0.3	75
Sandy clay with coral	0.3 - 7.2	18
Coral limestones	7.2 - 31	78
Sandy coral limestone	31 - 37	
Medium grained sand	> 37	3

Close agreement exists between interpreted resistivities and thicknesses and the borehole logs. The geophysical interpretation for sounding station MPK 20 was as follows:

Table 6.2. Interpretation results for sounding station MPK 20.

Layer	Depth(m)	Resistivity(Ωm)
1	0.61	75
2	7.45	18
3	43.2	78
4	> 42.2	3

Borehole no. 3 (C-7347) is only 5 metres from borehole 1, therefore the above correlation applies to both boreholes. Results of interpretation of sounding station MPK 74 which is in the neighbourhood of borehole no. 2 (C-7346) are as follows:

Table 6.3. Interpretation results for sounding station MPK 74.

Layer	Depth(m)	Reisistivity(Ωm)
1	1.25	45
2	1.96	13
3	11.64	51
4	41.8	86
5		2

The correlation of the interpreted parameters and the geological logs is as follows:

Table 6.4. Correlation between geophysical interpretation of sounding station MPK 74 and borehole 2 logs.

Formation	Depth(m)	Resistivity(Ωm)
Sand	0.0 - 0.3	45
Sandy clay	0.3 - 2	13
Coral limestone - with clays, sands	2 - 41	86
Sandy clays		2

In this situation, the interpretated parameters, resistivities and thicknesses very closely coincide with the observed geological logs. Both the interpretation and geologic logs suggest that the saltwater saturated formation is mainly sandy clays and medium grained sands.

In borehole No. 1 (Appendix VI), water was struck at a depth of 11 m which indicates that it was in the coral limestone. This is the situation that can be expected at this locality because the overlying formation is sandy clays which have aquitard characteristics. The static water level was 8.5 m below the ground

level. In borehole No. 2 (Appendix VI), water was struck at approximately 13.5 m below the ground level, again within the corals. As in borehole no. 1, the corals are underlying the sandy clays.

Chapter 7

DISCUSSION, CONCLUSION AND RECOMMENDATIONS

7.1 Discussion of results

7.1.1 General

In many vertical electrical soundings, the values measured with large current electrodes spacings are higher than expected. This might be explained by the fact that most resistivity equipment is not powerful enough in circumstances where a contribution is encountered of high contact resistance of the dry dune sands and the very low resistivity of saltwater-saturated layers.

The presence of shallow saltwater lenses in some locations as observed during drilling and well digging (Cowiconsult, 1983) is indicative of the fact that the ground water flow towards the sea is relatively slow and low since a fast and high groundwater flow is capable of washing and dissolving the salts into the sea. It also depicts the fact that the evaporation rates are quite high so that the rate of percolation during dry seasons is low, nothwithstanding the high hydraulic parameters of the sediments in the area. While this is not necessarily wrong, it is noted

ter intrusion during each low in a cycle. The saltwater table will instead seek an equilibrium typical of average water table conditions. The slow movement of the saltwater front may give the misleading impression that the saltwater problem can be managed because the deleterious effects are not observed over a period of years. However, over the years, it will be realized that the saltwater intrusion problem is an irreversable one. Its dependence on the dynamics of the instantaneous groundwater table elevation is merely superficial because the factors that induce recession of the groundwater table are quite different from those that cause saltwater intrusion, e.g., rise in marine sea level. However, in both cases, the outcomes are quite related. It may be necessary to point out that in the development of a model of coastal hydrologic system, especially a complex one as in Lake Kenyatta, potential calibration difficulties will obviously emanate from the response time lag discussed above. It is therefore of paramount importance to confirm that the saltwater/freshwater interface is in stable equilibrium. Thus, predevelopment heads, concentration of the water, electrical conductivity and the piezometric levels are necessary to properly calibrate the model. These are only possible through regularly coordinated well monitoring procedures over an appreciable time spell.

7.1.2 Geophysical results

7.1.2.1 Introduction

The interpretation results of the the vertical electrical soundings (VES) delineate the various boundaries of the geoelectric layers. However, in some instances, it was not possible to get the actual contact between layers at a particular location due to suppression, equivalence and the fact that some very thin layers may be embedded between thick layers. This was countered by extrapolation where a layer is thought

to have been suppressed. Thicknesses of coral and the saltwater/freswater interface were determined due to the large number of soundings. A comprehensive resistivity calibration was done from the interpretation results and the known geologic logs to fit the eight geoelectric layers discussed in chapter 6.

7.1.2.2   Resistivity calibrations

Based on the correlation of the interpretation parameters with the existing geologic logs, an approximate resistivity calibration was made as shown in table 7.1 below. This resistivity calibration forms an approximate scale for the formation resistivities as compared to the hydrogeology. This was established by calibrating the soundings in the proximity of the boreholes and also known electrical conductivity of individual formations. These calibrations are specifically for the area of study and do not in any way reflect the universal parameter values. Indeed the electrical properties of lithologic formations in the area depend on their porosity, water content, the level of saline intrusion and the composition. The presence of intercalated clayey bands reduces the resistivity.

The dry dune sands exhibit the highest resistivities upto over 6,000 Ωm. These values decrease with increased moisture in the sands to 2,000 Ωm and, with greater groundwater storage, values of less than 200 Ωm are observed. Clays are responsible for resistivities less than 50 Ωm, especially where it is intercalated in narrow bands even within the sands. But essentially the clay layers exhibit resistivities <10 Ωm near the surface. Corals exhibit a varying resistivity distribution between 50-200 Ωm where we have an aquifer. Thus, the low values of about 50 Ωm depict highly decomposed coral while the upper value depicts fresh coral-bearing water. However, high values above 200 Ωm are possible as observed by Breusse (1963)

197

Table 7.1 Resistivity calibration for geologic layers in the area

Resistivity (Ωm)	Formation	Groundwater Prospects
<10	Deposits saturated with Saltwater, impermeable clayey deposits, permeable formatives saturated with very brackish water.	Nil
10 - 50	calcareous, cemeted deposts containing freshwater, clayey Saturated deposits highly weathered clayey corals.	Poor to fair.
50 - 200	Decomposed to fresh saturated coral limestone saturated cemented sands	fair to very good
200 - 500	illustrated cemented sands. very hard compact dry coral Gravels	poor
500 - 2000	Dry surficial deposits	nil
>2000	Dry loose dunes sands	nil

whereby values of approximately 400 Ωm were recorded in dry limestones of Morocco. Mwangi (1981) recorded resistivities of 300 Ωm in Msambweni. Intrusion of saltwater may cause apparently low resistivity values in corals and, in some instances, equal to that of saturated sands on calcareous deposits. For this reason, it may be observed that some of the values obtained for the transition zone underlying the 50-200 Ωm coral could actually be coral itself. Low values of resistivities less than 10 Ωm underlying the 50-200 Ωm layer may thus represent saline water-filled or brackish water-filled coral. The other deposits exhibit resistivity values which greatly vary with the composition since they are in no way homogeneous. It

is evident from a comparison between the geoelectric traverses and the resistivity soundings that the coral limestone is not homogeneous, but is composed of hard coral reef with resistivities of 100-200 Ωm and strongly weathered coral of resistivities 50-100 Ωm. Where the latter is located near the main hard coral, it can be argued that it has a detrital origin, whereas at greater distance, sedimentation of calcareous erosion products intermixed with sands and clays took place in a lagoonal environment and has resistivities between 20-50 Ωm.

7.1.2.3 Resistivity model

It has been mentioned in chapter 6 that the best resistivity model for the area is the 5-layer earth model and this corresponds to a geological model comprising, top to bottom, the formations: top clayey sands, clays, sandy calcareous sediments, coral limestone and saltwater layer. However, 4-layer models are also very prominent in the area. Other models occur in terms of larger numbers of layers, e.g., 6-layer and 7-layer models due to an increased number of clayey bands; or a reduced number of layers, e.g., 3-layer and 2-layer cases, where no clayey bands occur prominently. The 5-layer model is exhibited on traverses A-B, C-D, E-F, I-J, K-L, M-N, W-X and Y-Z and the 4-layer model on traverses G-H, O-P, S-T and U-V in both cases ignoring the locally exhibited 2-layer, 3-layer, 6-layer and 7-layer models.

The 5-layer model exhibited in the area shows a high surface resistivity layer overlying a low resistivity layer. The high resistivity layer shows a wide range of values from 40 Ωm to over 2,000 Ωm. On traverse K-L, the values of resistivity, in order, are: 51-113, 8-24, 42-138, 17-42 and 4 Ωm. Traverse E-F has resistivities: >2,000, 28-38, 50-188, 18-45, 2-5 Ωm. The 4-layer model also generally exhibits a near-surface high resistivity layer overlying a low resistivity layer. This in turn

overlies a 50-188 Ωm layer which is underlain by a less than 10 Ωm layer. The major difference between the 5-layer model and the 4-layer model is that there exists another layer with resistivities 11-49 Ωm between the 50-188 Ωm layer in the case of the 5-layer model which in most cases lacks in the 4-layer model.

7.1.2.4 Depth to, and thickness of the coral limestone

The depth to the coral limestone, as observed in chapter 6, varies between 1 m and 23 m. However, it is important to note that the depth to the coral is generally shallower around the lake than further away from the lake. A similar trend is observed for the coral thickness such that the coral thickness is greatest near the lake where it goes above 20 m. This thickness reaches its maximum at the north-eastern and eastern shores of the lake where it locally exceeds 30 m. This trend ensures that the most hydrogeologically suitable area for high groundwater abstraction is only within the proximity of the lake, since natural recharge is fastest and the aquifer thickest. Besides, the saltwater/freshwater interface is deeper near the lake and shallower away from it.

7.1.2.5 Freshwater/saltwater interface

The freshwater/saltwater interface follows the same trends as the coral thickness and depth to the coral; where there are thick coral layers around Lake Kenyatta, the saltwater/freshwater interface is deepest. The interface is deepest at the northern and eastern shores of the lake where it reaches approximately 40 m below the ground surface (30 m below mean sea level). It rises to 20 m below mean sea level at approximately 2 km north of the lake and at a far larger distance east of the lake. In general, the saltwater/freshwater interface rises near the mean sea

level away from the lake. Under ideal static conditions, the shape of the freshwater/saltwater interface can be approximated according to Badon, Ghyben and Herzberg principles which state that: In a freshwater lens on top of saline water, the thickness of the lens above mean sea level will compare to the thickness below mean sea level with a ratio of 1 to 40, assuming a homogeneous formation and density of saline water of 1.025.

Thus, one unit increase (or decrease) in the elevation of the freshwater table results in a 40-unit increase (or decrease) in the depth of freshwater body below the near sea level. Depending on the formation, the depth and drainage of the interface varies considerably. Besides, it also depends on the fresh groundwater storage overlying it. The interference of the interface with fresh groundwater storage is the most common cause of failure in shallow well digging in the Lake Kenyatta settlement scheme.

7.1.2.6 The undulating contact between the coral 50-200 Ωm layer and underlying layers

The present coast was an ancient beach in the Pleistocene. Williams (1962) observed that during the lower Pleistocene, the sea level was very low at 61 m below the mean sea level. Early studies (Caswell, 1953; Thompson, 1956; Williams, 1962) suggest that during the Kamasian pluvial in the Lower Pleistocene, the sea level fell to approximately 60 m below the present level and rose during the Middle Pleistocene to flood the present coastal plain to about 40 m above the present mean sea level. After regression during the Kanjeran Pluvial, a subsequent rise to 10 m above mean sea level can be distinguished in the form of raised beaches in the coastal plains south of the Tana river estuary. The coral reefs were formed

201

during the second interpluvial of Middle Pleistocene.

From the geoelectric layers, it is observed that we have a distinctive undulating layering which may correspond to the actual geological stratification of the coastal sediments in the area. This layering has been explained by Lisitrin (1972) as shown by modern data. He states that the ocean bottom is not smooth and its relief is as dissected and varied as that of land and whose irregular topography greatly influences distribution of the bottom sediments and its qualitative composition. The present coast, having been part of the ancient beach, is subject to the above observation. The possibility of having the steep undulating peaks and troughs as sandridges underlying the coral limestone has also been evaluated. The morphology of the undulating topography of the geoelectric layers on most traverses are near-symmetrical, but assymetry to the east is sometimes seen (Fig. 7.1). Jordan et al. (1964) noted that tidal currents alone are incapable of moving sediments (e.g., in the east-west direction) but need the additional velocity increment by wave action. Since there is a net water transport in the direction of wave propagation, there must also be a net sediment movement in the direction along the bottom of this area. Erosion of these sandridges could produce assymmetrical forms as observed on traverse W-X between stations MPK 98 and MPK 97 where there are gently sloping parts and steep parts of the traverse. The morphology of the relief of the geoelectric layers resembles traverses analysed across the sandridges on Georges Shoal (Fig.7.1). The shoal comprises a shallow submerged sand bank at low waters. The gently sloping parts are tidal overfalls.

Curray (1964) explains the formation of the undulating morphology in terms of transgressions and regressions of the sea level and the direction of relative sea level change. He states that it is attributed to tectonics, geology, climate and
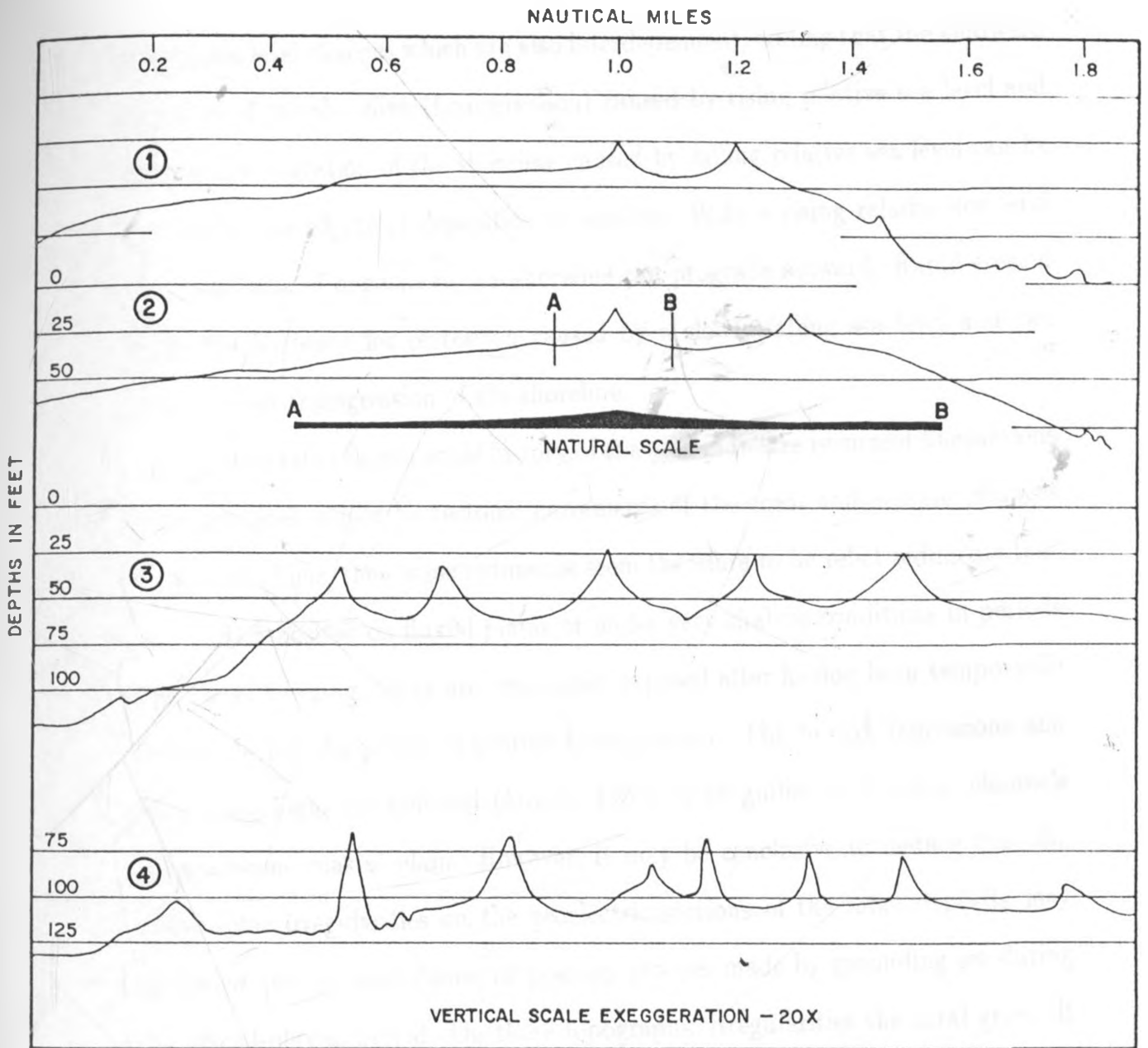
Fig. 7.1   Profiles across the sandridges on Georges shoal constructed from fathograms (After Lisitrin, A. P., 1972)

eustatic sea level changes which are also interdependent, adding that the landward migration of the shoreline (transgression) caused by rising relative sea level and the seaward migration of the shoreline caused by falling relative sea level can be reserved by the effects of deposition or erosion. With a rising relative sea level and a high rate of deposition, the shoreline can prograde seaward. Rapid erosion offsets the tendency for regression caused by a slowly falling sea level and can produce a net transgression of the shoreline.

The integrated depositional history of the area indicates recurrent fluctuations of the sea level caused by tectonic movements of the coast and eustatic changes in sea level. Thus, the coarse sediments seem therefore to be relict sediments that were once deposited on fluvial plains or under very shallow conditions in periods of sea-level lowering. They are once again exposed after having been temporarily covered during the period of marine transgression. The buried depressions and intervening highs are believed (Moore, 1964) to be gullies or drainage channels of Pleistocene coastal plain. However, it may be conclusive to deduce that the topographic irregularities on the geoelectric sections of the relict deposits may be buried ancient sand dunes, or possibly grooves made by grounding ice during the glacial-pluvial period. On these topographic irregularities the coral grew. It is noteworthy that the coral pinches and swells are most likely a combination of erosion, deposition and dissolution by freshwater.

7.1.3 Catchment area

It is not easy to precisely define the catchment area for the groundwater aquifer since it is quite extensive. However, it is true to mention that it comprises the topographic high areas where rain water seeps into the ground through sands,

faults, fractures and weathered material of high porosity and permeability, with high infiltration rate. The catchment area for the aquifer may be quite extensive upto Hongwe where the coral limestone formation extends.

7.1.4 Groundwater flow

The direction of groundwater flow cannot be determined directly from the resistivity data interpretation. From the interpretation of piezometric maps and well hydrographs, it is evident that groundwater recharges the lake from the north and discharges towards south. During heavy rains (high lake lavels), the underground storage is partly recharged by inflow from the lake and directly recharged by deep percolation and no recharge into the lake from underground storage occurs. When the lake levels subside, the groundwater flows from the north shore into the lake and a discharge of lake water into the aquifer occurs at the southern and south-eastern shore of the lake. This groundwater discharge follows the line of shallow valley running from the Mto wa Mkunumbi estuary. This explains the zone of dolines (collapse pits due to solution of limestone) in this valley forming a chain of sinkholes.

At lower lake levels, groundwater discharges into the lake from the north while only little or no lake water discharges into the aquifer from the south and eastern shores of the lake. When the lake levels are extremely low below groundwater level, only recharge of the lake by groundwater from the north occurs and no discharge of the lake water into the aquifer occurs at the southern and eastern lake shores. From the morphology of Lake Kenyatta and that of the low lying shallow valley riddled with sinkholes, it is possible to conclude that Lake Kenyatta was formed as a large continuous zone of dissolved coral and collapsed cavities in the coral

limestone.

7.1.5 Water table elevation

The configuration and movement of the water table is of paramount importance in assessing the total and exploitable water reserves. The shape of the water table will furnish information on the transmissivity of the formation and the natural discharge. Although the water table can be considered continuous in most places, the great variability in permeability of the sediments causes considerable differences in the water quality with brackish water in the less permeable areas. The water table in the vicinity of Lake Kenyatta is controlled by the effects of groundwater recharge from precipitation, groundwater discharge due to pumpage, evaporation from the lake, evapotranspiration, and seaward groundwater gradients.

Seasonal fluctuations in the water levels can be attributted, in part, to changes in precipitation and evapotranspiration. The aquifer responds quickly to recharge while water level recession is relatively slow. The well pumpage has very slight effects on the water table configuration. This may be attributted to the high transmissivity and large storativity of the Lake Kenyatta aquifer. The depth to the phreatic surface is dynamic and is governed by the local hydrologic conditions.

7.1.6 Water balance

From a qualitative water balance analysis, it is evident that the hydrological cycle changes with variations in the lake level. Thus, a careful consideration of abstraction parameters need to be made in designing a well field around the lake. It is important to note that the hydrologic cycle has the main components as rainwater, lakewater and the groundwater. The interplay between these components

limestone.

7.1.5 Water table elevation

The configuration and movement of the water table is of paramount importance in assessing the total and exploitable water reserves. The shape of the water table will furnish information on the transmissivity of the formation and the natural discharge. Although the water table can be considered continuous in most places, the great variability in permeability of the sediments causes considerable differences in the water quality with brackish water in the less permeable areas. The water table in the vicinity of Lake Kenyatta is controlled by the effects of groundwater recharge from precipitation, groundwater discharge due to pumpage, evaporation from the lake, evapotranspiration, and seaward groundwater gradients.

Seasonal fluctuations in the water levels can be attributted, in part, to changes in precipitation and evapotranspiration. The aquifer responds quickly to recharge while water level recession is relatively slow. The well pumpage has very slight effects on the water table configuration. This may be attributted to the high transmissivity and large storativity of the Lake Kenyatta aquifer. The depth to the phreatic surface is dynamic and is governed by the local hydrologic conditions.

7.1.6 Water balance

From a qualitative water balance analysis, it is evident that the hydrological cycle changes with variations in the lake level. Thus, a careful consideration of abstraction parameters need to be made in designing a well field around the lake. It is important to note that the hydrologic cycle has the main components as rainwater, lakewater and the groundwater. The interplay between these components

yields a very complex hydrodynamic equilibrium in the area. No attempt, however, has been made to quantify the interplaying factors and make water balance calculations.

7.1.7 The Lake Kenyatta aquifer

The highly transmissive and permeasive solution cavity-riddled beds of the Lake Kenyatta settlement scheme through the coral limestone comprise the components of the confined arterian Lake Kenyatta aquifer. The aquifer is confined by the overlying low permeability interbedded clays, clayey sands and other sedimentary deposits. It forms the main reservour. The fossil dunes inland are cemented by ferriarete and the voids of the sands are clogged by the calcrete, thus preventing percolation of the water into underground storage. From grain size analysis (Diettrich, 1985), the coefficient of permeability and specific yield are 4×10^{-5} m/s and 3.7×10^{-3}, respectively. For large scale abstraction, the dune sand are not good reservoirs. The mobile dunes along the sea shore are widely covered by vegetation, especially the mangroves which enhance infiltration by retarded runoff. Thus, there is an appreciable amount of underground storage. The groundwater quality is quite good above the level of interface. The coefficient of permeability and the specific yield are respectively 3.6×10^{-4} m/s and 1.7×10^{-2}. Again, these are of little use as high abstraction aquifer.

The lateral extent of the main fresh groundwater aquifer (electrical conductivity of water below 1,500 μS/cm) has been found to be more than 10 km^2 (GSK, 1990) including the freshwater below and around Lake Kenyatta. This aquifer exists mainly in the fossil coral reefs which are very extensive in the region and averages approximately 20 m in thickness. Below the aquifer is the saltwater in-

terface whose depth varies between 20 and 40 m below the ground surface. The karstified coral limestone aquifer system has a very high transmissivity of 1.5×10^4 m^2/day (GSK, 1990). The coefficient of permeability and specific yield of the corals (Diettrich, 1985) are 7.9×10^{-3} m/s and 5.5×10^{-6}, respectively. The fossil coral reef is sedimented by clay or fine sand deposits found in irregular pattern inland and forming karstic sinkholes filled with silty debris. The coral reefs which are not sedimented by clays and silts act as channels draining water from the adjoining formations. Their specific yield is limited by their aerial extent (approximately 100 m). However, their drainage capacity is enhanced by an extremely high permeability and porosity since the corals are highly cavernous and fissured. Where the cavernous coral limestone is in contact with the saltwater/freshwater interface, the water is salty. This is the situation in the Lake Kenyatta settlement scheme where over 80% of the entire area is unsuitable for well sites because of the aquifers tapping the interface. During testpumping of two boreholes drilled in the coral limestone, the drawdown in the aquifers was very small. The dimensions of the aquiferial freshwater body cannot be exactly defined since at its edges there is a transition zone to brackish water.

It is vital that the importance of pumping from the areas of highest permeability is realized, as the smaller the drawdown in a pumped well, the smaller the corresponding upconing of the salt/freshwater interface will be. In the sand dunes forming a morphological ridge along the sea shore and resting on permeable formations, freshwater will form a line-shaped body floating on the salty seawater. The size of such a freshwater body will depend on the dimension of the permeable formations and on the elevation of the freshwater table. The freshwater body (electrical conductivity of water below 1,500 μS/cm) is estimated to have a volume

'of 200×106 m^3. Assumming a porosity of 20%, the total amount of freshwater stored underground is 40×10^6 m^3. Certainly only a meagre percentage of this water can be recovered. Thus, it may be summarized that the Lake Kenyatta area aquifer comprises geologically recent deposits in which groundwater occurs. These deposits include the unconsolidated fossil dunes inland, the fossil coral reefs inland and the mobile dunes along the shores of Indian Ocean. The fossil coral formation is the most important groundwater aquifer.

7.1.8   Groundwater quality

The salinity of the groundwater in the study area reaches upto 4,000 ppm with average salinity being 1,500 ppm (WHO limit 600 ppm, Lake water 150 ppm). This groundwater is unsuitable for agricultural purposes, but may be used blended with rainwater or directly for domestic purposes.

Groundwater at the northern shore of the lake is of stable and good quality in terms of salinity with an electrical conductivity of 400 to 500 μS/cm. The salinity, which is generally low, increases very slowly and only little during dry spells. The viable groundwater quality in the wells at the southern and south-easthern shore of the lake is due to the fact that this aquifer is recharged directly by the lakewater. This borehole water is also known to smell of hydrogen sulphide which is present in non-toxic concetrations, though the smell is unpleasant and offending. To remove the hydrogen present, aeration of the water is necessary.

7.1.9   Upconing of saltwater and the cone of depression

Under natural conditions, saltwater intrusion may take place not only in the case of a uniform change in the water table elevation but also locally where a depression

in the water table has been formed by pumping. This rise in the interface may be crucial in determining the maximum exploitation rate of dune reservoirs. Saltwater incursion will almost normally cause irreparable deleterious effects to the fresh groundwater sources, thus, utmost care must be exercised in the investigation and exploitation of coastal aquifers. Considering the extreme sensitivity of the flow system, three other possible contributions to the intrusion problem in the Lake Kenyatta settlement scheme emerge: (a) a decline in hydraulic heads between the wells and the coast could contribute to the observed intrusion, (b) a rise in mean sea level over time (has not been documented), (c) expansion of shallow saltwater bodies adjacent to the ocean.

From hydrostatic principles, it can be argued that a lowering of the top of the freshwater layer is accompanied by upconing of saltwater as explained from Badon Ghyben and Herzberg principle of hydrostatic equilibrium between freshwater and saltwater bodies. If a well constructed in freshwater under which lies saltwater is pumped, the underlying saltwater begins to drift upward due to the pressure gradient developed in the well. If the pumping proceeds at a steady rate, the saltwater below the well keeps coming up until it reaches the screen after which the well discharges a mixture of fresh and salt water. Alternatively, the upconing of the saltwater reaches a certain equilibrium level at some distance below the well after a certain period of time. In this case, the well continues to produce freshwater since water is being discharged from the freshwater layer only. The flow in the saltwater layer ceases and the saltwater/freshwater interface acts as an impermeable barrier. This type of well is called a skimming well because it is skimming off the freshwater. Development of either the first or the second situation depends on the well and aquifer hydraulic parameters, density of the salt and

fresh water and the discharge. As the upconing of the freshwater occurs at a fixed discharge, we may on the other hand observe that when discharge commences, a cone of depression is formed. With increased discharge rates, the cone of depression taps deeper into the well and also covers a greater area. Eventually the cone of depression may intercept the upconing saltwater interface and in effect introduce saltwater into the well as above.

7.1.10 Construction of the wells in the study area

Due to the complexity of the hydrologic situation in the area, it is necessary to design the well field so that the abstraction of water ensures a long well life and maximum production.

After drilling the borehole to a safe depth from the saltwater/freshwater interface, it should be screened over the aquiferous systems and then geophysically logged to determine location of pockets of saltwater lenses, which can be sealed off by bentonite. The borehole is then gravel packed to enhance maximum lateral flow into the well. The bottom of the borehole should be sealed with bentonite to keep off sporadic saltwater enchroachment and steel surface casings should be used to reinforce the top part of the borehole made up of unconsolidated material. Development of the borehole should then be done so as to improve the yield and hydraulic effeciency. It repairs the disturbance caused to the aquifer during drilling by removing clays and chemical additives from the borehole wells and alters the physical characteristics of the aquifer around the screen and removes fine particles. The development should entail air-lifting followed by water-fetting, which physically agitates the gravel pack and adjacent aquifer material. This is extremely effective in clearing up the wells. Depending on the nature of sediments

encountered, a treatment with Calgon (sodium hexametaphosphate) is necessary, which removes clayey particles in the vicinity of the well. This is followed by testpumping of the borehole for a satisfactory period of time and monitering the water level of the neighbouring wells.

7.1.11 Some other general remarks

It is important to determine the safe yield which can be abstracted from the aquifer without much drawndown. In a proposed well field of six wells in the area, it was decided that a projected pumping rate of 25 m^3/hr (GSK, 1990) during a period of eight hours per day was most ideal to give a minor cone of depression and a corresponding small upconing of the saltwater/freshwater interface. The high transmissivity and storativity of the karstified coral limestone ensures that a very high amount of groundwater can be pumped before any remarkable decline in the groundwater level or the upconing of the saline interface starts affecting the water abstraction. Lateral flow into the wells is so large that the effects of pumping regime on the water table and saline interface is negligible when the well is located in the coral limestones.

7.2 Conclusion

The groundwater situation in the area is a complex one. Generally, the low-lying areas along the coast are unreliable as a source for large scale water supplies since there is little capacity for freshwater storage. The aquifer is confined by the overlying low permeability interbedded clays and limestone. It would be worthwhile to call it Mpeketoni aquiclude and it is the zone that separates the aquifer from the overlying vadose zone made up of sediments.

The cause of saltwater intrusion in the area can be attributed to the following: (a) well sunk too deep beyond the saltwater/frehwater interface, (b) high discharging yields (overpumping), (c) too frequent intervals of discharging, (d) small well diameter, and (e) thin aquifer. The latter is the most common in the area. Thus, geophysical mapping of well sites and their adjoining superficial catchment is a good practice to avoid drilling into the saltwater. Presence of shallow saltwater lenses could have been caused by washing out of large sea salt particles whereby during transport over land, air masses and clouds pick up continental dust and gasses from continental or industrial origins thus charging the composition of rainwater. This phenomenon has been discussed by Appelo (1985) who observed that near the coast, rainwater composition closely resembles diluted seawater with concentration levels lowering as the rain falls further away from the sea.

A hydrodynamic equilibrium exists between the fresh and the salt groundwater. Therefore, it is necessary to develop a model of coastal Lake Kenyatta hydrologic system. The groundwater at the northern shore of the lake is of good and stable quality while the salinity at the south-eastern shore varies and is generally of poorer quality . Evidently, no permanent lake could exist with no substantial groundwater storage beneath it. The fluctuation of annual rainfall and average annual runoff, annual average evaporation are all compensated by an increase or decrease in water stored underground. Besides, there exists a regional groundwater flow system part of which flows into the lake on the northern shore and maintains a corresponding outflow on the southern shore of the lake. This inflow and outflow hydrodynamic equilibrium maintains the salinity of the lake water low. Noteworthy, if no substantial outflow was taking place, the lake would have become a saltwater lake. Only occasionally during heavy flooding does the inflow

towards the aquifer in the northern shore of the lake occur. The water balance is representative of typical tropical terrain with thick soil cover, dense vegetation, thus reducing the surface runoff and has high infiltration capacity.

The presence of an extensive, continuous coral reef around the lake has been established. This coral has its greatest thickness at the northern and the eastern shores. Locally in the sinkhole zone and under the lake, over 10 m of the limestone has dissolved in the freshwater. The coral forms an excellent, extensive aquifer system. Though the aquifer is recharged by deep percolation of rainwater, direct contact with and recharge by the lake could account for the greater depth (30 m below mean sea level) of the saltwater/freshwater interface only found near the lake. The freshwater body extends over at least 10 km^2 (GSK, 1990) north and east of the lake, forming a continuous system. The south-western shore of the lake presents both a smaller coral thickness and shallower saltwater/freshwater interface than the northern and eastern shores. Thus, it cannot enable large scale groundwater abstraction.

The best location of the well field is on the northern and easthern shores of the lake where the coral thickness is maximum and the depth to the interface is high. The resistivity soundings have mapped the freshwater/saltwater interface. The saltwater intrudes into the formations in a 'wedge' form with an undulating interface. The intrusion occurs mainly in the sediments underlying the highly fissured coral limestone. The resistivity between 10 and 20 Ωm of the layer underlying the coral could be due to the presence of brackish water, a transition zone influenced by the saltwater from the sea. The depth to the brackish or saltwater zone varies from 5 m to 40 m below the mean sea level. The coral rests on a low resistivity resistivity substratum.

tion over time and space in the area. The sites of the boreholes should be chosen so that they are at an elevation of above 10 m so that they lie above the highest flood level in the area.

In order to avoid permanent damage of the groundwater storage, modelling and designing of well field and operation should be based on a geophysical survey of the aquifer. Thus, a water quality monitoring program comprising a scientifically designed surveillance system of continuing measurements, observation and evaluation is paramount. This should embody sampling and analysis of groundwater quality, determination of groundwater levels and flow directions, evaluation of water and other pollutants and borehole geophysical techniques. The presence of unconfined aquifers in the area calls for the evaluation of the mobility of the pollutants from the ground surface to the water table and evaluation of attenuation of pollutants within the freshwater saturated zone.

Applications of electromagnetic (EM) profiling technique in conjuction with the resistivity sounding can give more reliable and consistent information on the charges in the subsurface layering and lithology. It is suggested that EM profiling should be done in the area and, supplemented by seismic refraction profiles, the low resistivity layers can be more accurately determined. The EM method is especially ideal to detect the freshwater/saltwater interface since it does not suffer contact resistivity problems.

Exploratory boreholes should be drilled so as to provide the missing information which is necessary in improving the geophysical model, thus improving the interpretations in the area with respect to hydrogeology. The cores may also be used to determine the engineering characteristics of the formations such as porosity and permeability. The water from each aquifer should be sampled geochemically

and bacteriologically to establish its suitability as drinking water.

REFERENCES

Anderson, P. F., Mercer, J. W., White, H. O., and Huyakorn, P. S. Jr., 1988, Numerical modelling of saltwater intrusion at Hallandale, Florida, Groundwater Jour. of Assoc. of Groundwater Scientists and Engineers, 619-630.

Appelo, C. A. J., 1985, Lecture notes for a one week course on hydrochemistry conducted in the Ministry of Water Development. Nairobi, in May, 1985 by WRAP-TNO Institute for Earth Sciences, Free University, The Netherlands.

Barker, R. D., 1981, The offset system of electrical resistivity sounding and its use with a multicore cable, Geophys. Prosp., 29, 128-143.

Barker, R. D., 1981, Application of geophysics in groundwater investigations. Report of the Department of Geological Sciences, University of Birmingham, U. K.

Barker, R. D., Houston, J. C. T., White, C. C., 1988, The Victoria Province Drought Relief Project, 1. Geophysical siting of boreholes. Groundwater Jour. of Assoc. of Groundwater Scientists and Engineers 26, 309-316.

Barongo, J. O., 1989, Application of transient airborne electromagnetic and ground resistivity methods to geological mapping in tropical terrains, Ph.D. Thesis, McGill University.

Barr, R. L., 1979, National Master Water Plan 1 Vol. III. Tana River Preliminary Development Plan, 1-2 - 2-1. Available at TARDA Office, Nairobi.

Bhattacharya, P. K., and Patra, H. P., 1968, Direct current geoelectric sounding. Principles and interpretation, Elsevier, New York, 135p.

Bracewell, R., 1965, The Fourier transform and its application, McGraw Hill, New York.

Breusse, J. J., 1963, Modern geophysical methods for subsurface water exploration, Geophysics 27, 633-657.

Cagniard, L., 1952, La prospection geophysique des eaux sousterrains, UNESCO, 184-190.

Carroll, D., 1962, Rainwater as a chemical agent of geological process, a review. Papers in Marine Geology, United States Geological Survey, Water Supply Paper 1535-G. 18 p.

Carruthers, R. M., 1985, Review of geophysical techniques for groundwater exploration in crystalline basement terrain. Rep. Regional Geophysical Research Group, No. RGRG 85/3, British Geophysical Survey.

Caswell, P. V., 1953, The Geology of the Mombasa-Kwale Area, Report No. 24, Geological Survey of Kenya, Nairobi.

Classen, G. A., 1973, A review of water resources of Lamu District, Technical report, Ministry of Water Development, Nairobi.

Cnudde, J. P., 1976, Interpretation of resistivity soundings in areas with saline groundwater, Compagnie Generale de Geophysique, 1963, Master curves for electrical sounding, 2nd revised edition, Leiden, Eur. Assoc. Expl. Geophys.

Compagnie Generale de Geophysique, 1963, Master Curves for electrical sounding (2nd revised edition), Eur. Ass. of Explor. Geophys., Leiden.

Cowiconsult, 1983, Lake Kenyatta Water Supply Project, Preliminary Design Report, Ministry of Water Development, Nairobi.

Curray, J. R., 1964, Transgressions and regressions; Papers in Marine Geology, 175-203.

Dagan, G., and Bear, J., 1968, Solving the problem of local interface upconing in a coastal aquifer by the method of small perturbations, Jour. Hydr. Research, 6, 15-44.

Dana, J. R., 1890, Corals and Coral Islands, 3rd edition, Dodd, New York.

Davis, P. A., 1979, Interpretation of resistivity sounding data: Computer program for solutions to the forward and inverse problems, 1633 Eustis Street, St. Paul MN 55108.

Davis, R. A., 1937, Coastal sedimentary environments, edited by by R. A. Davis, New York, Springer-Verlag, 1978.

Diettrich, T. E. K., 1985, Rural Water Supply of Lake Kenyatta and Hindi Settlement Schemes, GTZ, Lamu, 12-36.

Diettrich, T. E. K., 1985, 1987, Central Water Supply, Report on pump tests of testwells, GTZ, Lamu.

Ebert, A., 1943, Grundlogen Zur Auswertung geoelectrischer Tietenmessungen, Beitr. Angew, Geophys. 10, 1-17.

Ewbank, 1974, Preliminary feasibility report on the potential development of the Tana River basin, TARDA Office, Nairobi.

Fetter, C. W., 1980, Applied Hydrology, Charles E. Merril Publishing Co., Columbus, Ohio.

Flathe, H., 1955, A practical method of calculating geoelectrical model graphs for horizontally stratified media, Geophys. Prosp., 3, 268-294.

Flathe, H., 1967, Interpretation of geoelectrical resistivity measurements for solving hydrogeological problems, Mining and Groundwater Geophysics/1967, Geological Survey of Canada, Econ. Geol. Report 26, 580-597.

Flathe, H., and Pfeiffer, D., 1964, Outlines on the hydrology of the isle of Madura (Indonesia), Internt. Assoc. Sci. Hydrology, Berkely, 1963, No. 64, 543-560.

Flathe, H. W., 1976, The Smooth Sounding Graph, Hannover.

Gensley, R., and Rouget, F., 1937, Sur L'anisotropie electrique des terrains et la pseudo-anisotropie, World Petroleum Cong., 2d, 723-731.

German Advisory Team, 1980, Coast Settlement Schemes in Kenya, Basic report, Ministry of Lands and Housing, Nairobi.

Ghosh, D. P., 1971a, The application of linear filter theory to the direct interpretation of geoelectrical resistivity sounding measurements, Geophys. Prosp. 19, 192-217.

Ghosh, D. P., 1971b, Inverse filter coefficients for the computation of apparent

resistivity standard curves for a horizontally stratified earth, Geophys. Prosp. 19, 769-775.

Glenn, W. E., and Ward, S. H., 1976, Statistical evaluation of electrical sounding methods, Part 1: Experiment design, Geophysics 41, 1207-1222.

Grant, F. S. and West, G. F., 1965, Interpretation Theory in Applied Geophysics, McGraw-Hill, New York.

Griffiths, D. H., 1976, Application of electrical measurements for the determination of the porosity and permeability in sandstone, Geoexploration 14, 207-213.

Grundy, F., 1953, Lamu Water Supply groundwater investigation. Ministry of Water Development, Nairobi

Groundwater Survey (K) Ltd., 1987, Lake Kenyatta Water Supply Project, Groundwater Investigations Vol. I, II, III, GTZ, Lamu.

Groundwater Survey (K) Ltd., 1990(a), Lake Kenyatta Water Supply Project, Well field design, GTZ. Additional Resistivity Survey.

Groundwater Survey (K) Ltd., 1990(b), Lake Kenyatta Water Supply Project, Well field design, GTZ.

GTZ, Borehole monitoring and rainfall data for 1985 to 199 files, GTZ, Lamu.

Harris, B., Stewart, Jr., and Jordan, G. F., Underwater sand ridges and gorges shoal, Papers in Marine Geology, 102-114.

Hemker, C. J., 1985, Interpretation Package, Schlumbg, Version 2.05, Amsterdam, The Netherlands.

Hetu, R., 1978, Interpretation Report, Airborne Electromagnetic Survey. Barringer INPUT survey of selected areas in Coast and Nyanza Provinces, Republic of Kenya, for the Government of Kenya, Terra Surveys Ltd. (77-18), Geological Survey of Kenya, Nairobi.

Hoerl, A. E., and Kennard, R. W., 1970, Ridge Regression: Biased estimation for non-orthogonal problems, Tectonophysics 12, 55-67.

Homilius, J., and Mundry, E., 1979, Three layer model curves for geoelectrical resistivity measurements - Schlumberger array, Hannover.

Hoversten, G. M., Dey, A., and Morrison, H. F., 1982, Comparison of five least-squares inversion techniques in resistivity sounding, Geophys. Prosp. 30, 688-715.

Hummel, J. N., 1929, Zeit. F. Geoph. 5, 89 and 288.

Inman, J. R., 1975, Resitivity inversion with ridge regression, Geophysics 38, 1088-1108.

Jackson, D. D., 1972, Interpretation of inaccurate, insufficient and inconsistent data, Geophys. J. Roy. Astr. Soc. 28, 97-109.

Johansen, H. K., 1975, An interactive computer/graphic-display-terminal system for interpretation of resistivity soundings, Geophys. Prosp. 23, 449-458.

Jordan, P., 1964, The expanding earth; some consequences of Dirac's gravitation hypothesis. Translated and edited by A. Beer with collaboration of J. B. Hutchings and T. R. Stockly. Pergamon Press, Oxford (1971).

Keller, G. V., and Frischknecht, F. C., 1966, Electrical methods in geophysical prospecting, Pergamon Press, Oxford.

Keller, G. V., 1967, Dipole methods for measuring earth conductivity, Consultants Bureau Enterprises Inc., New York, 35-37.

Koefoed, O., 1968, The application of the kernel function in iterpreting geoelectrical resistivity measurements, Geoexploration Associates, Langenscheidt KG, 1 Berlin 62.

Koefoed, O., 1976, Error propagation and uncertainty in the interpretation of resistivity sounding data, Geophys. Prospect. 4, 31-48.

Koefoed, O., 1979, Geoelectrical Principles, 1 - Resitivity Sounding Measurements, Elsevier, Amsterdam, 103 p.

Kunetz, G., 1966, Principles of Direct Current Resistivity Prospecting, Berlin, Gebruder Borntraeger.

Legget, R. F., 1939, Geology and Engineering. McGraw-Hill, New York.

Levenberg, G., 1944, A method for the solution of certain non-linear problems in least squares, Quart. Applied Math. 2, 164-166.

Lisistrin, A. P., 1972, Sedimentation in the world ocean, Soc. Econ. Palaeont. and Miner. Special Publication No. 17, 31 p.

Maillet, R., 1947, The fundamental equations of electrical prospecting, Geophysics 3, 529-556.

Marquardt, D. W., 1963, An algorithm for least squares estimation of non-linear

parameters, J. Soc. Indust. Applied Math. 11, 431-441.

Mathenge, M. W., 1989, Groundwater occurrence in the Isenya area, MSc thesis, University of Nairobi.

Matheson, F. J., 1963, Geological survey of Lamu-Galole area, Geological Survey of Kenya, Unpublished report, Ministry of Water Development, Nairobi.

Merric, N. P., 1977, A Computer Program for the Inversion of Schlumberger Sounding Curves in the Apparent Resistivity Domain, Hydrogeological Report 1977/5, New South Wales Water Resources Commission, Sydney, Australia.

Mathiez, J. P., Huot, G., 1984, Geophysical prospecting and groundwater exploration, Inter-African Committee for hydrologic studies - Examples of application in West Africa, 1-2.

Ministry of Finance and Planning, 1984, Lamu District Development Plan 1984-1988. Ministry of Finance, Nairobi.

Ministry of Planning and National Development, Rural Planning Department, 1989, Lamu District Development Plan 1989-1993, 1-46. Ministry of Planning and National Development, Nairobi.

Ministry of Water Development (MOWD), 1988, Water resources reconnaissance study in Lamu District, WRAP, TNO-DGV Inst. of Applied Sciences. Ministry of Water Development, Nairobi.

Mooney, H. M., and Wetzel, W. W., 1956, The potentials about a point electrode and apparent resistivity curves for a two-, three-, and four-layer earth,

University of Minesota Press, Minneapolis, 145 p.

Moore, D. G., 1964, Acoustic-Reflection Reconnaissance of continental shelves, Eastern Bering Chukchi Seas, Papers in Marine Geology, 319-349.

Morris, D. B., 1964, The application of resistivity methods to groundwater exploration of alluvial basins in semi-arid areas, Jour. of the Inst. of Water Eng. 18.

Mwangi, M. N., 1981, Resistivity survey for groundwater in the Msambweni area, MSc thesis, University of Nairobi.

Oostrom, A. P., 1988, The geomorphology of south-east Kenya, PhD thesis, Wageningen Agricultural University, Wageningen.

Orellana, E., and Mooney, H. M., 1966, Master tables and curves for vertical electrical sounding over layered structures, Interciencia, Madrid.

Parasnis, D. S., 1979, Principles of applied geophysics,, Chapman and Hall, 3rd edition, London, 275 p.

Patterson, 1957, Lamu Hinterland, Report of the Ministry of Water Development, Nairobi.

Pekeris, C. L., 1940, Direct method of interpretation in resistivity prospecting, Geophysics 31, 31-42.

Petrick, W. R., Pelton, W. H., and Ward, S. H., 1973, Resistivity inversion applied to crustal resistivity sounding data from South Africa, Geophysics 42, 995-1005.

Republic of Kenya, 1980, Ministry of Water Development, Malindi Pipeline Report on Preliminary Hydrological Investigations, 5-31. Ministry of Water Development, Nairobi.

Republic of Kenya, 1981, Athi River Basin Pre-Investiment Study. TARDA Office, Nairobi.

Rijkswaterstaat, The Netherlands, 1975, Standard graphs for resistivity prospecting, Env. Assoc. of Expl. Geophys., The Hague, The Netherlands.

Sandberg, S., 1979, Documentation and analysis of the Schlumberger iterative 1-D inversion program SLUM, Department of Geology and Geophysics, University of Utah, Salt Lake, Utah, U.S.A.

Selby, J., 1969, Lamu Island Water Supply, Hydrological Report, Ministry of Water Development, Nairobi.

Slitchter, L. B., 1933, The interpretation of the resistivity prospecting method for horizontal structures, Physics 4, 307-322.

Stefanescu, S., Slumberger, C., and Schlumberger M., 1930, Sur la distribution electrique pontielle autour d'une prise de terre ponctuelle dans un terrain a couches horizontales homogenes et isotropes, Journal de Physique et du Radium, Series VII 1, 132-140.

Sunde, E. O., 1949, Earth conduction effects in earth systems, Dover Publications, Inc., New York.

Survey of Kenya, 1982, Bouguer gravity anomaly map of Kenya, Scale 1:1,000,000. Survey of Kenya, Nairobi.

Survey of Kenya, 1966, East Africa Mean Annual Rainfall map, Scale 1:2,000,000.

Tana and Athi Rivers Development Authority (TARDA), 1982, The Hydrology of the Tana Basin. TARDA Office, Nairobi

Terra Surveys Ltd., 1982, Interpretation Report: Bouguer Gravity Survey of the Kenya Coastline. Unpublished Report for the Government of Kenya, Geological Survey of Kenya, Nairobi.

Tippetts-Abbett-McCarthy-Stratton (TAMS), 1980, National Master Water Plan, Nairobi, Ministry of Water Development, Nairobi.

Telford, W. M., Geldart, L. P., and Sheriff, R. E., D. A., 1990, Applied Geophysics, Cambridge University Press, London.

Thompson, A. O., 1956, The Geology of the Malindi Area, Geological Survey of Kenya, Report No. 36, 1956.

Todd, D. K., 1980, Groundwater Hydrology, Wiley, New York

Van Dam, J. C., 1976, Possibilities and limitations of resistivity method of geoelectrical prospecting in the solution of geohydrological problems, Geoexploration 14, 179-193.

Van Dongen, P. G., and Kruseman, G. P., 1984, Lamu Water Supply in Lamu. Water Supply Safari Report, Ministry of Water Development, Nairobi.

Vozoff, K., 1958, Numerical resistivity analysis - horizontal layers, Geophysics 28, 536-556.

Water Resources Assessment Project (WRAP), 1988, Report on Reconnaissance

Investigations for Groundwater in Lamu District for 1985, 1986 and 1988. Ministry of Water Development, Nairobi.

Williams, L. A. J., 1962, Geology of the Hadu-Fundi Isa Area, North of Malindi, Nairobi, Geological Survey of Kenya, Report No. 52.

Zohdy, A. A. R., 1965, The auxiliary point method of electrical sounding interpretation and its relation to the Dar Zarrouk parameters, Geophysics 30, 644-660.

Zohdy, A. A. R., Eaton, G. P. and Mabey, D. R., 1974, Techniques of Water Resources Investigations of the United States Geological Survey: Application of Surface Geophysics to Groundwater Investigations, U. S. Government Printing Office, Washington.

Zohdy, A. A. R., 1980, Application of surface geophysics to groundwater investigations, U.S. Geological Survey, Washington.

Appendix I

2-Layer Master Curves and Auxiliary Point Charts

PLATE I
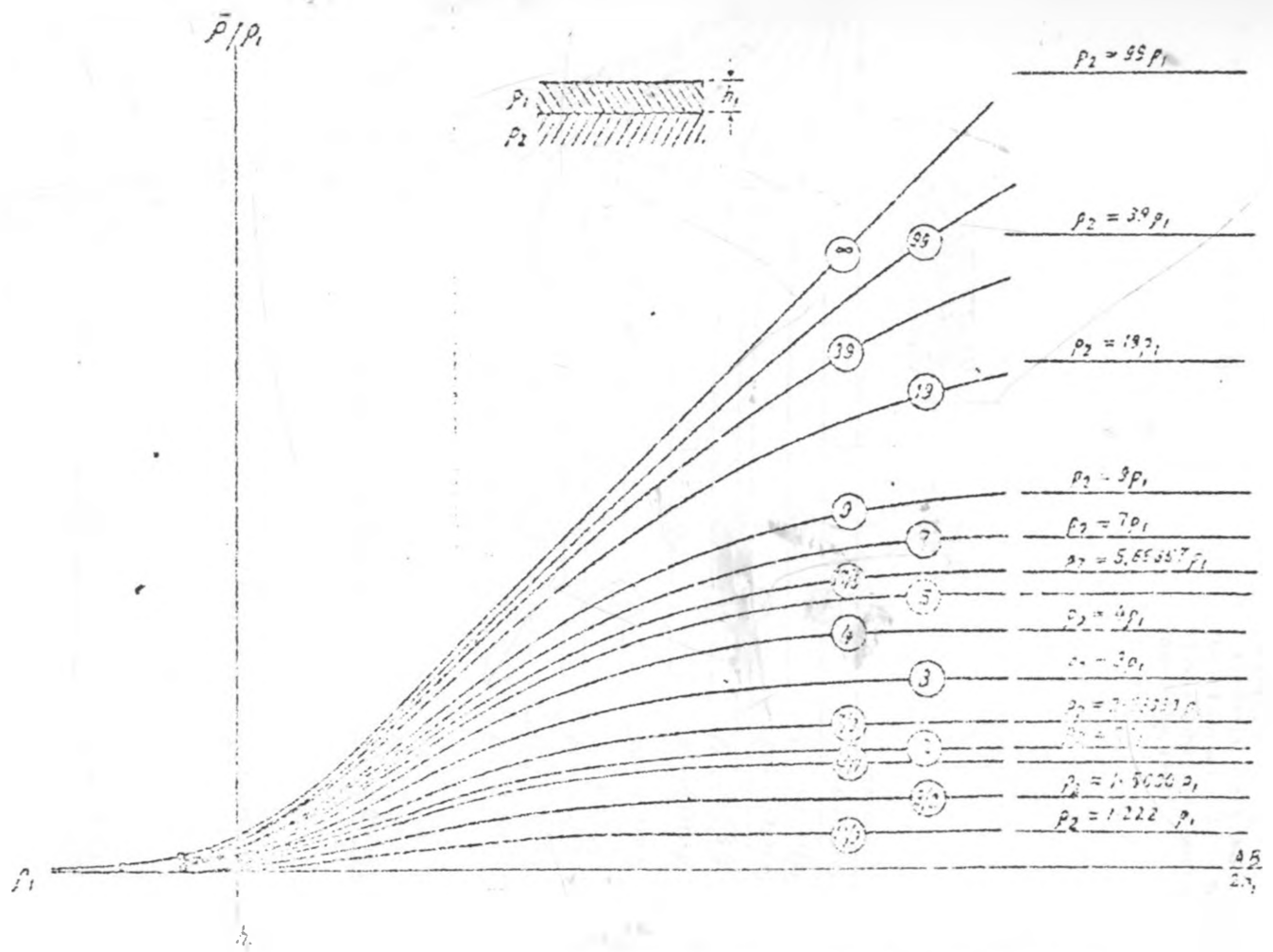
Two-layer master curves, ascending type. ($\rho_2 > \rho_1$). (From ABRAMOVA
(1962).)
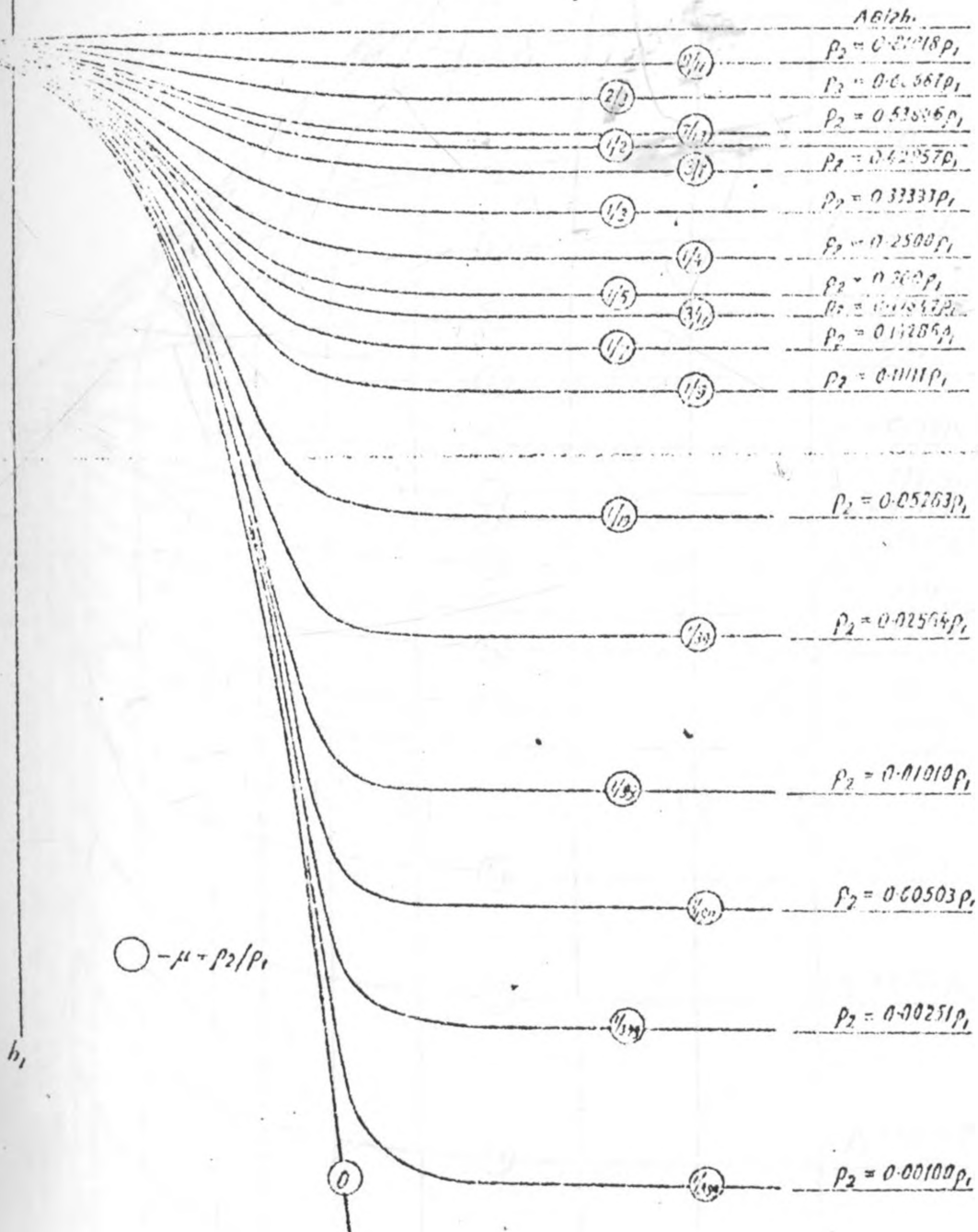
PLATE II

Two-layer master curves, descending type ($\rho_2 < \rho_1$). (From ANONYMOUS, 1963a.)
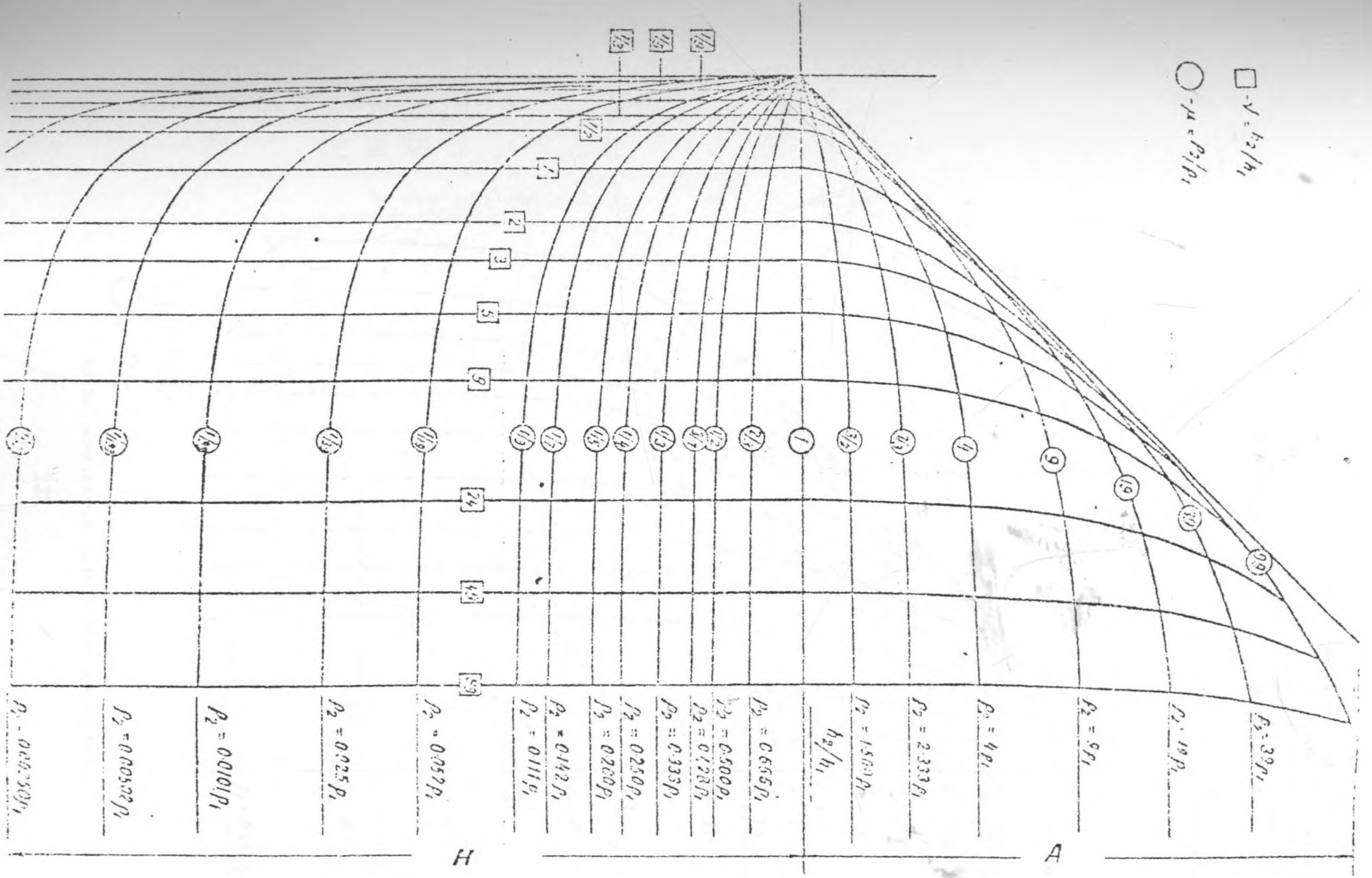
231

□ - $y = k_2/q_1$

○ - $\mu = p_2/p_1$

p_2/q_1

$p_2 = 1.500 p_1$

$p_2 = 2.333 p_1$

$p_2 = 4 p_1$

$p_2 = 9 p_1$

$p_2 = 19 p_1$

$p_2 = 39 p_1$

$p_2 = 0.666 p_1$

$p_2 = 0.500 p_1$

$p_2 = 0.428 p_1$

$p_2 = 0.333 p_1$

$p_2 = 0.250 p_1$

$p_2 = 0.200 p_1$

$p_2 = 0.142 p_1$

$p_2 = 0.111 p_1$

$p_2 = 0.052 p_1$

$p_2 = 0.025 p_1$

$p_2 = 0.0101 p_1$

$p_2 = 0.00502 p_1$

$p_2 = 0.00250 p_1$

H

A

PLATE IV

Auxiliary point charts, E and O. (from Bhattacharya, 1968)
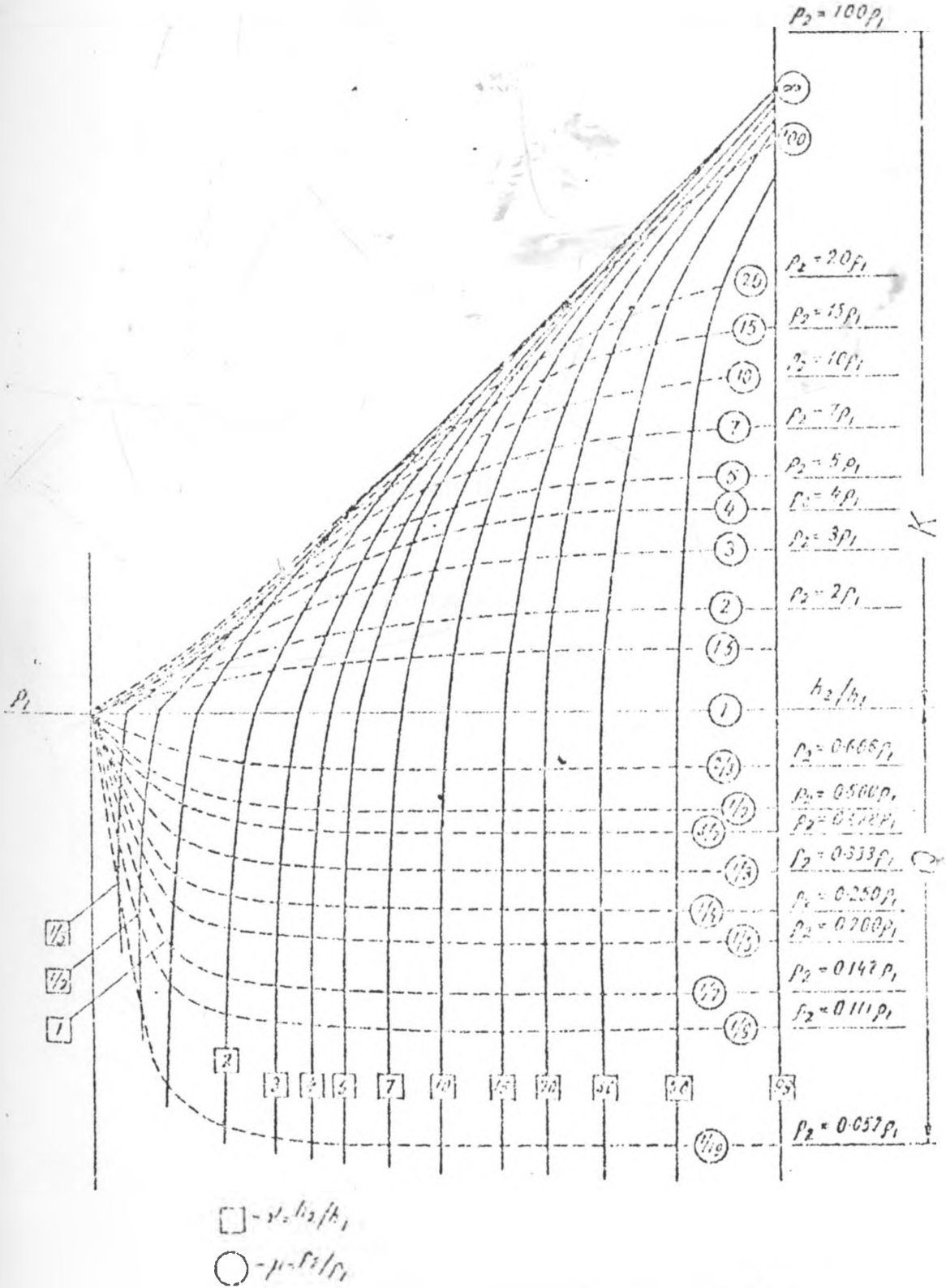
233

Appendix II

Well Hydrographs

N side of Lake

LKSS Hydrographs 1990

234
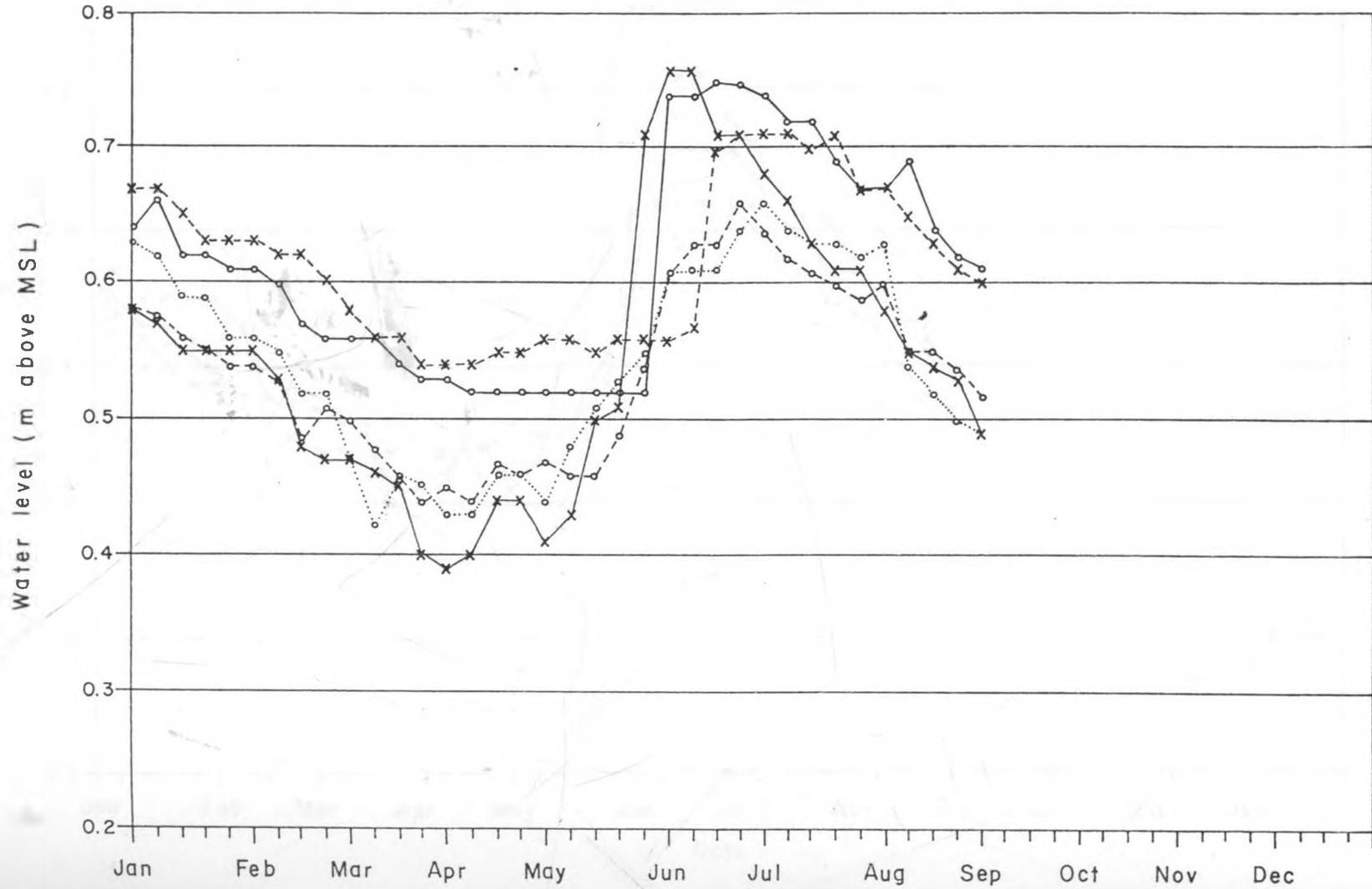
SE side of Lake
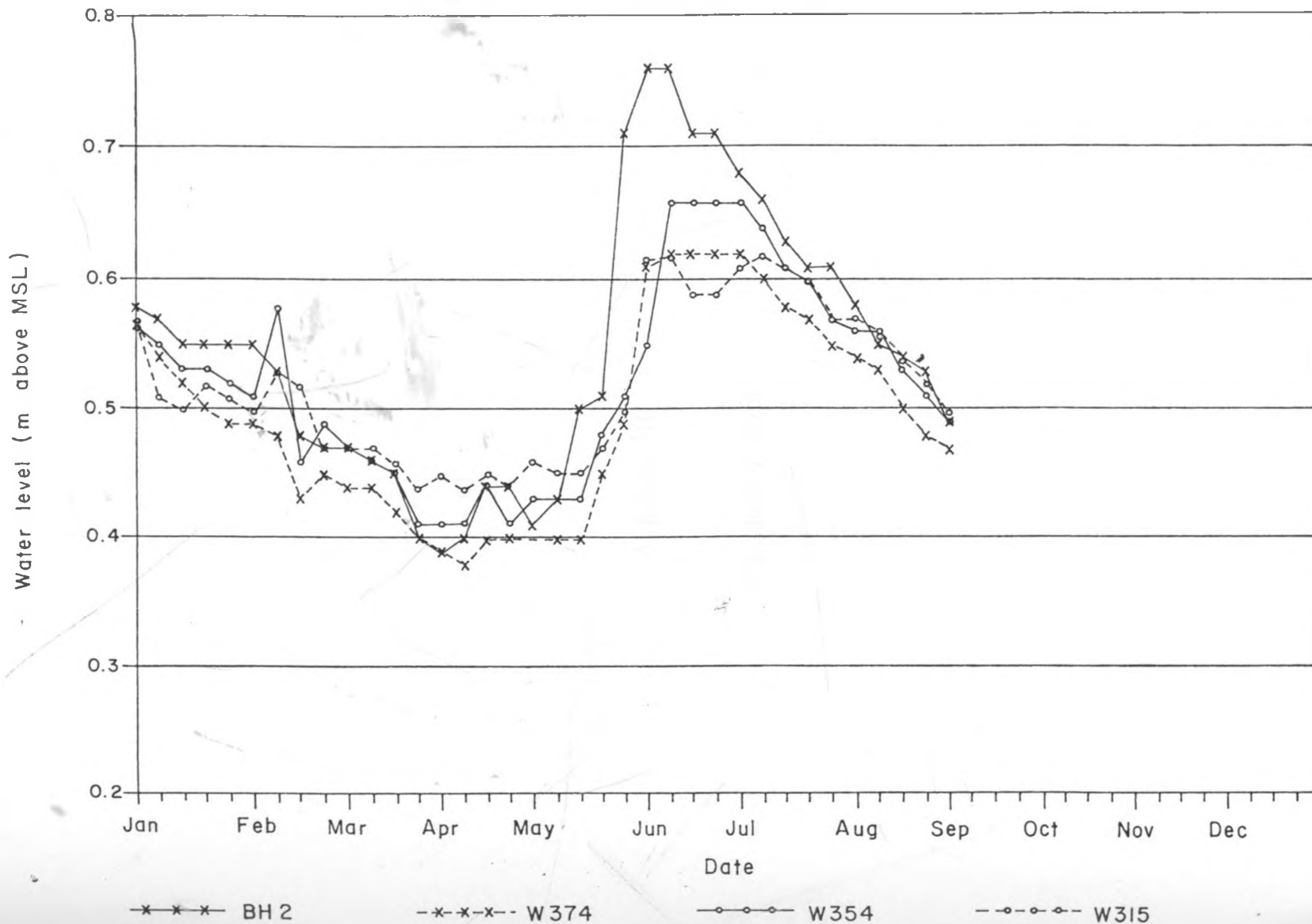
LKSS Hydrographs Wells 1990

Appendix III

Piezometric Maps
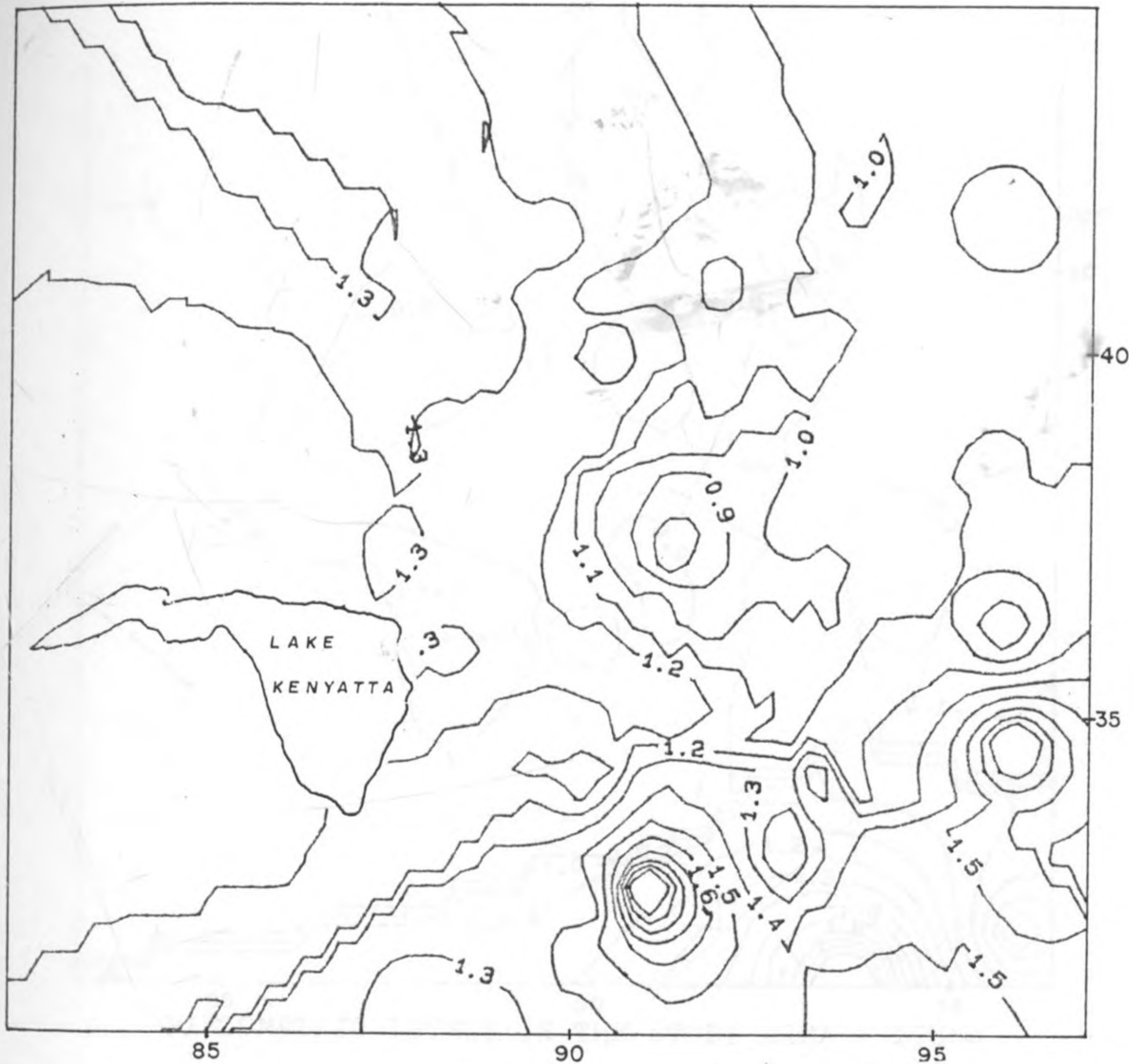
PIEZOMETRIC LEVELS IN THE STUDY AREA - 1985
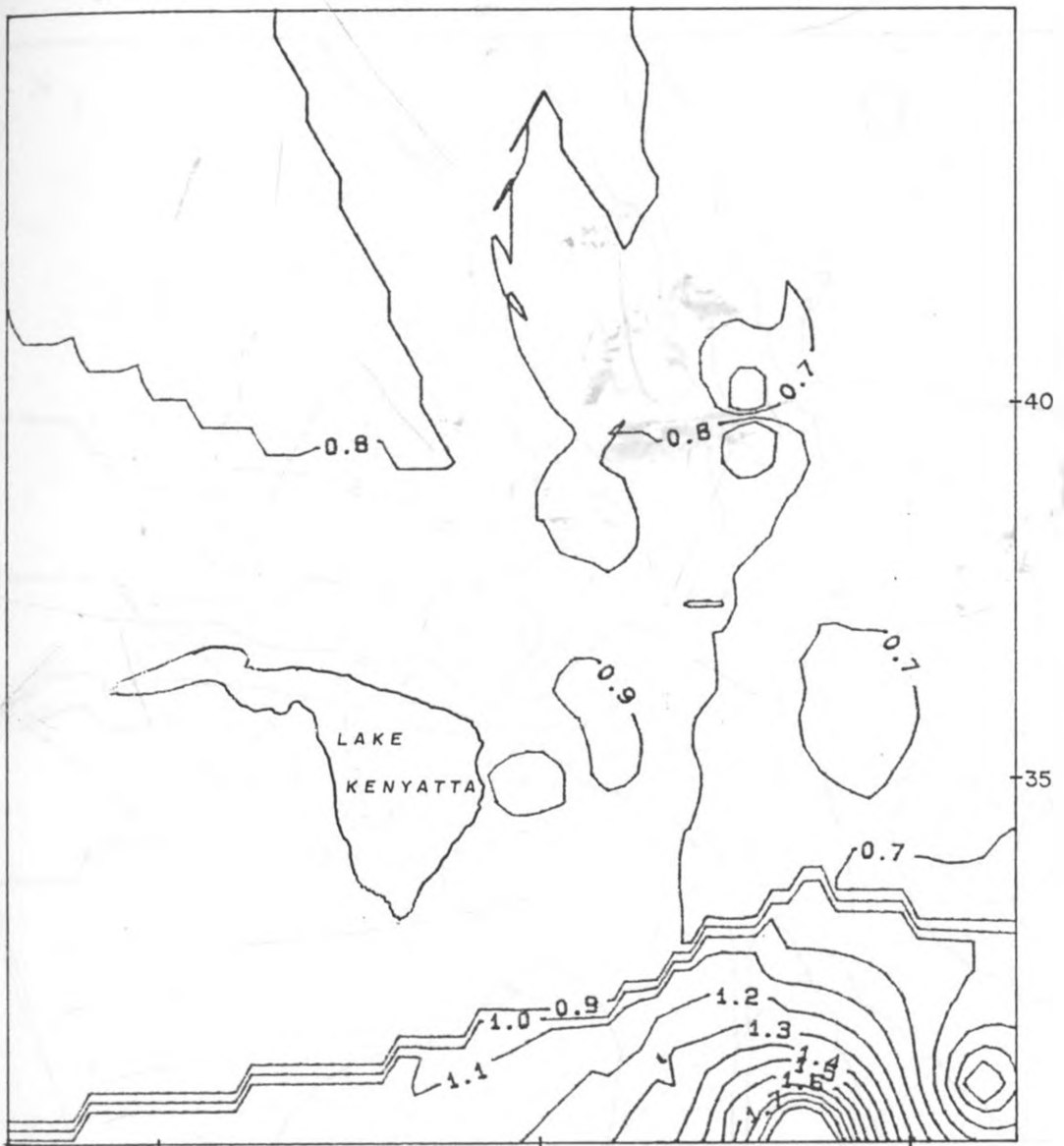
SCALE

0   5 KM

236

PIEZOMETRIC LEVELS IN THE STUDY AREA - 1986a
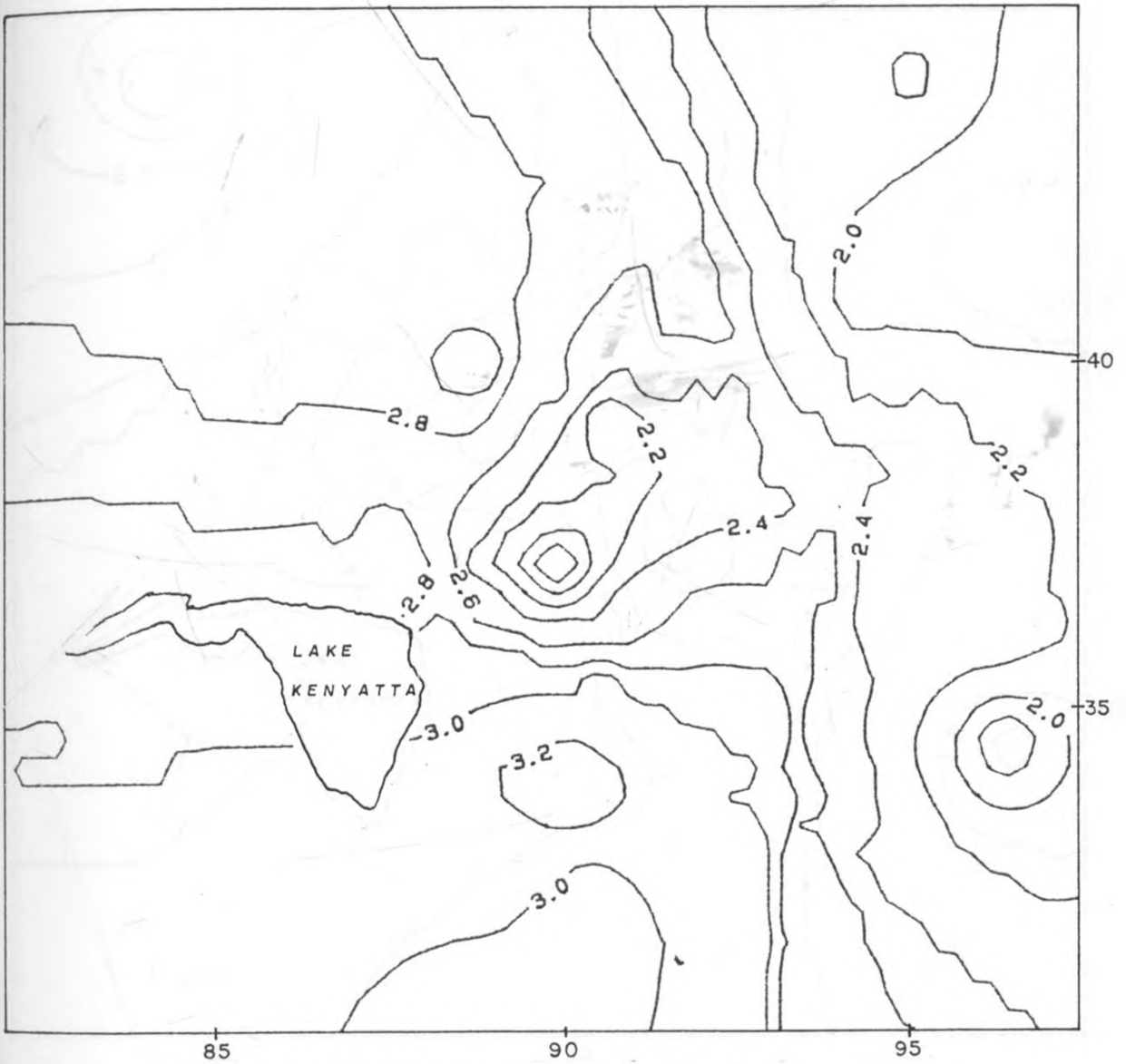
SCALE

0   5 KM

PIEZOMETRIC LEVELS IN THE STUDY AREA - 1986b

0   5 KM

PIEZOMETRIC LEVELS IN THE STUDY AREA - 1987

SCALE

0   5 KM

PIEZOMETRIC LEVELS IN THE STUDY AREA – 1988

SCALE

0   5 KM

PIEZOMETRIC LEVELS IN THE STUDY AREA - 1989

SCALE

0   5 KM

PIEZOMETRIC LEVELS IN THE STUDY AREA - 1990

SCALE

0   5 KM
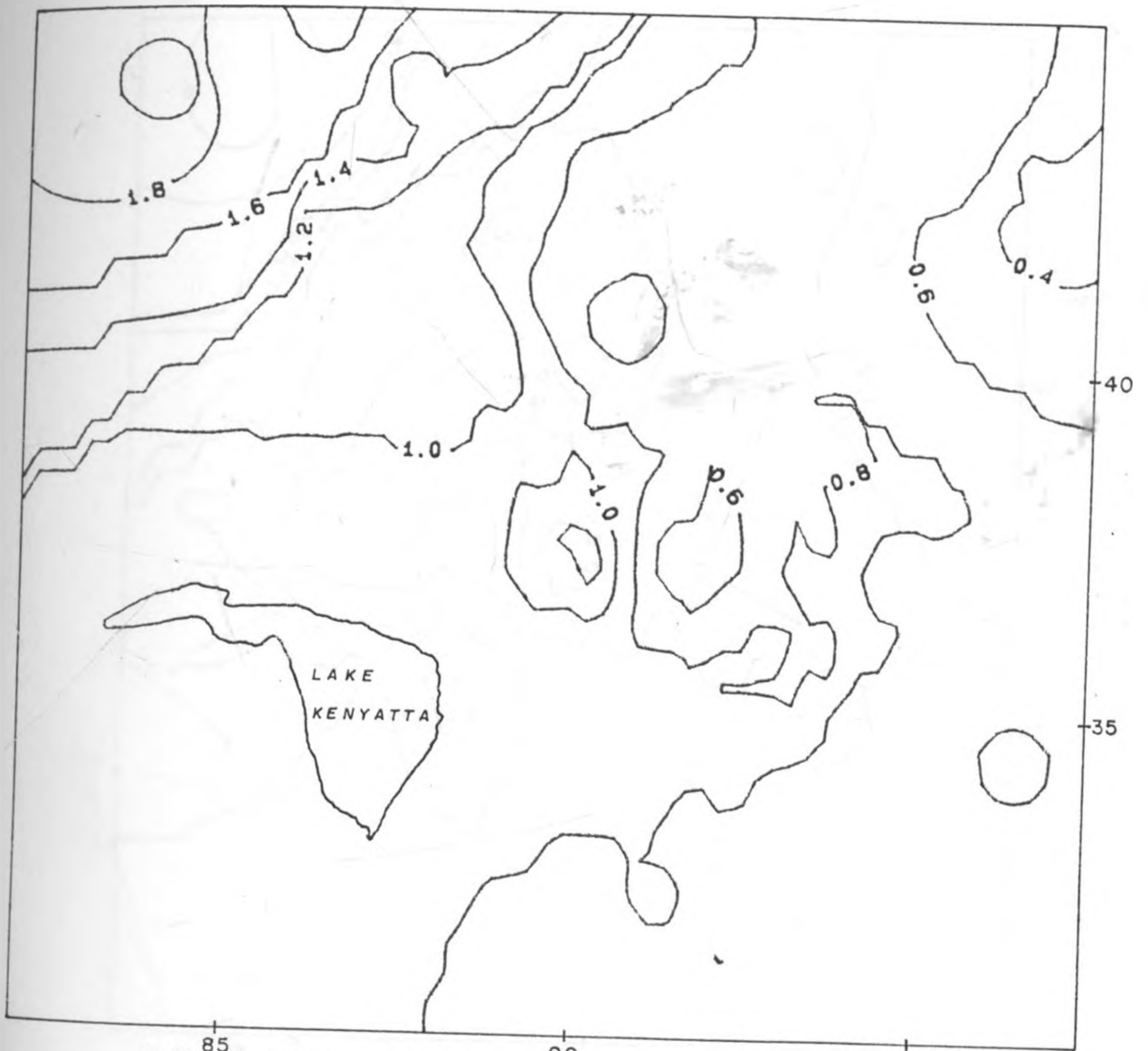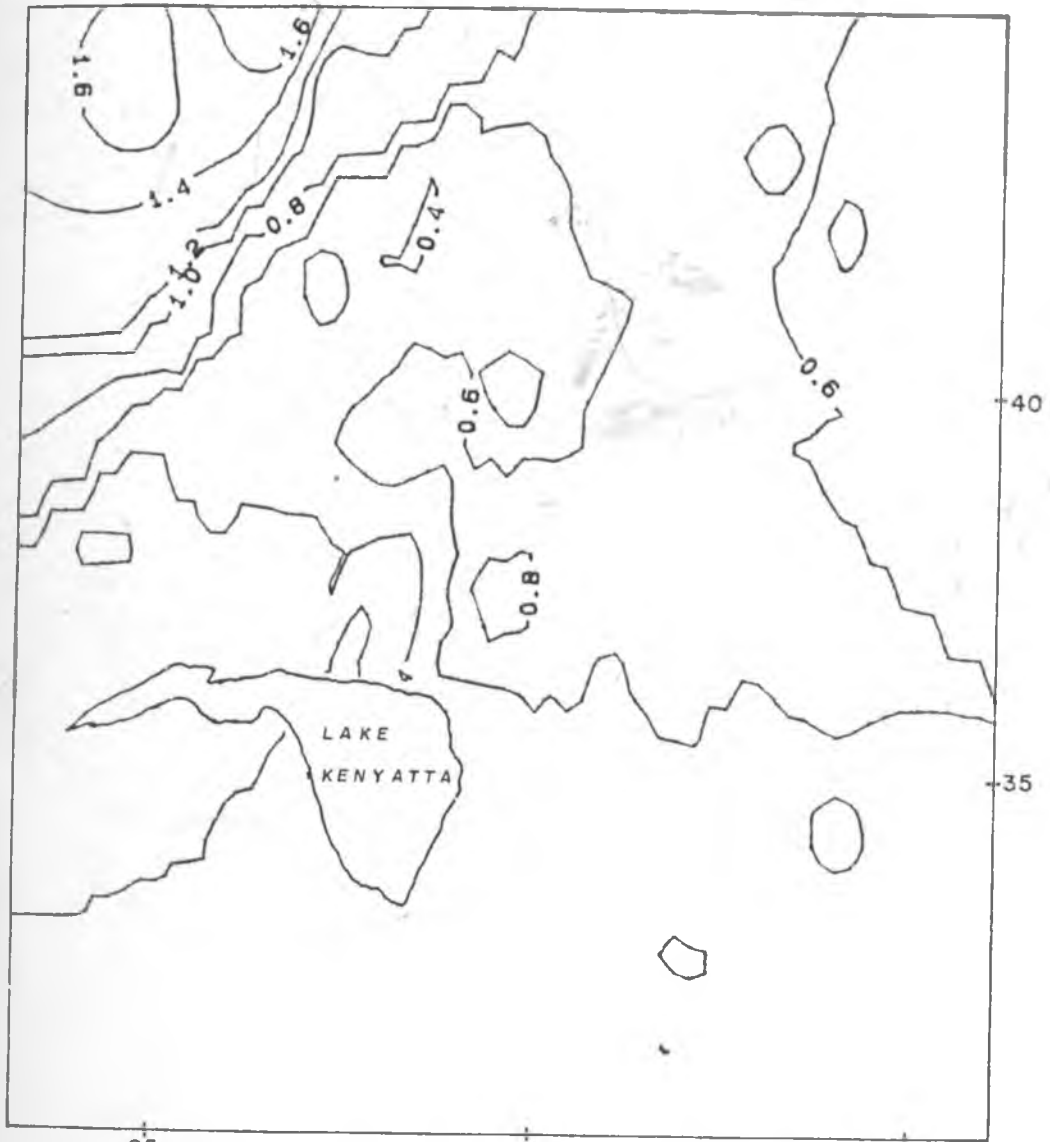
Appendix IV

Electrical Conductivity Maps for 1985 to 1990
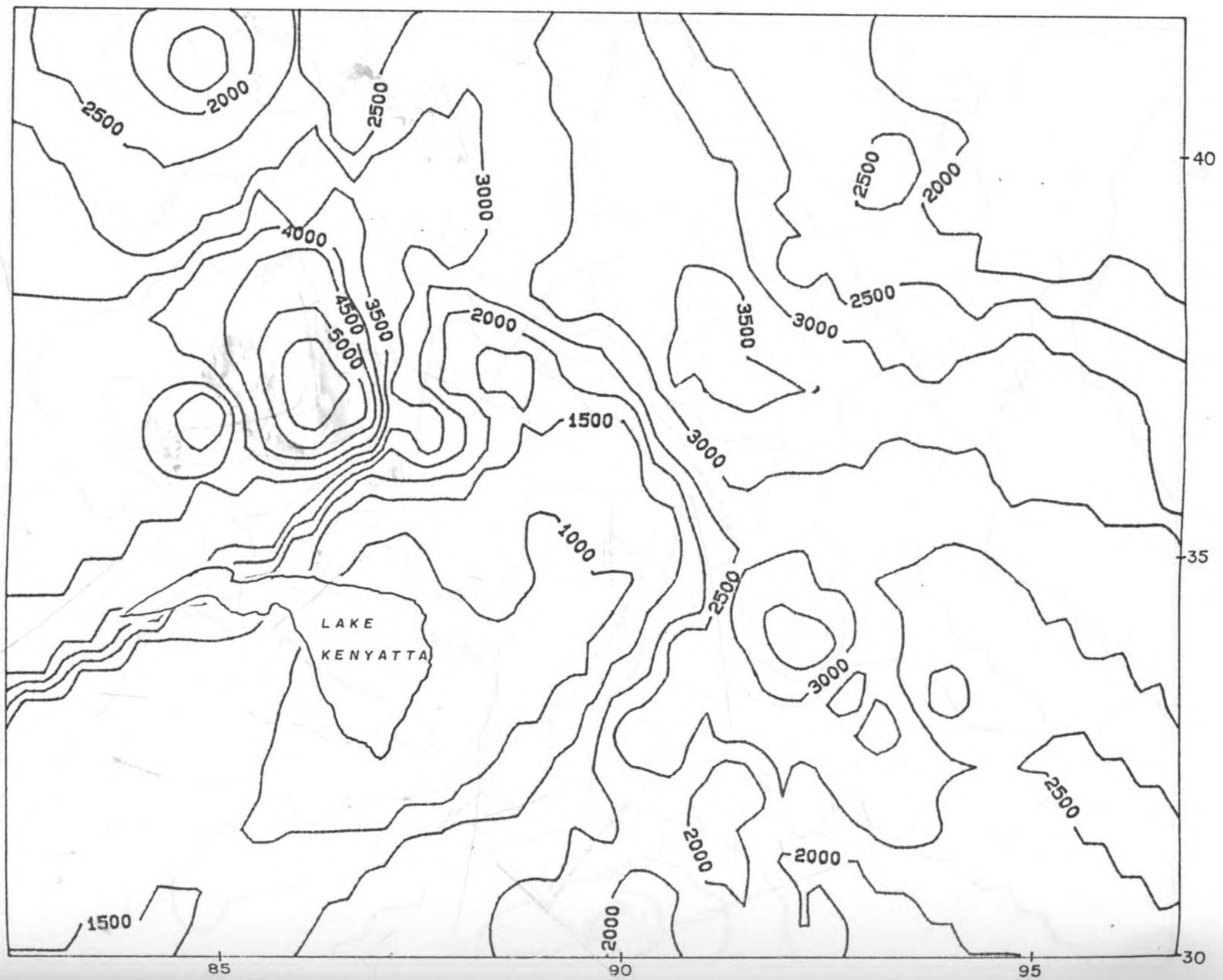
ELECTRICAL CONDUCTIVITY IN THE STUDY AREA - 1985

SCALE

0   5 KM

ELECTRICAL CONDUCTIVITY IN THE STUDY AREA - 1987

SCALE

244

ELECTRICAL CONDUCTIVITY IN THE STUDY AREA - 1988

SCALE

0   5 KM

245'
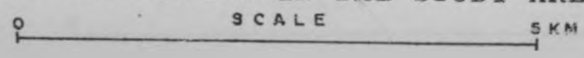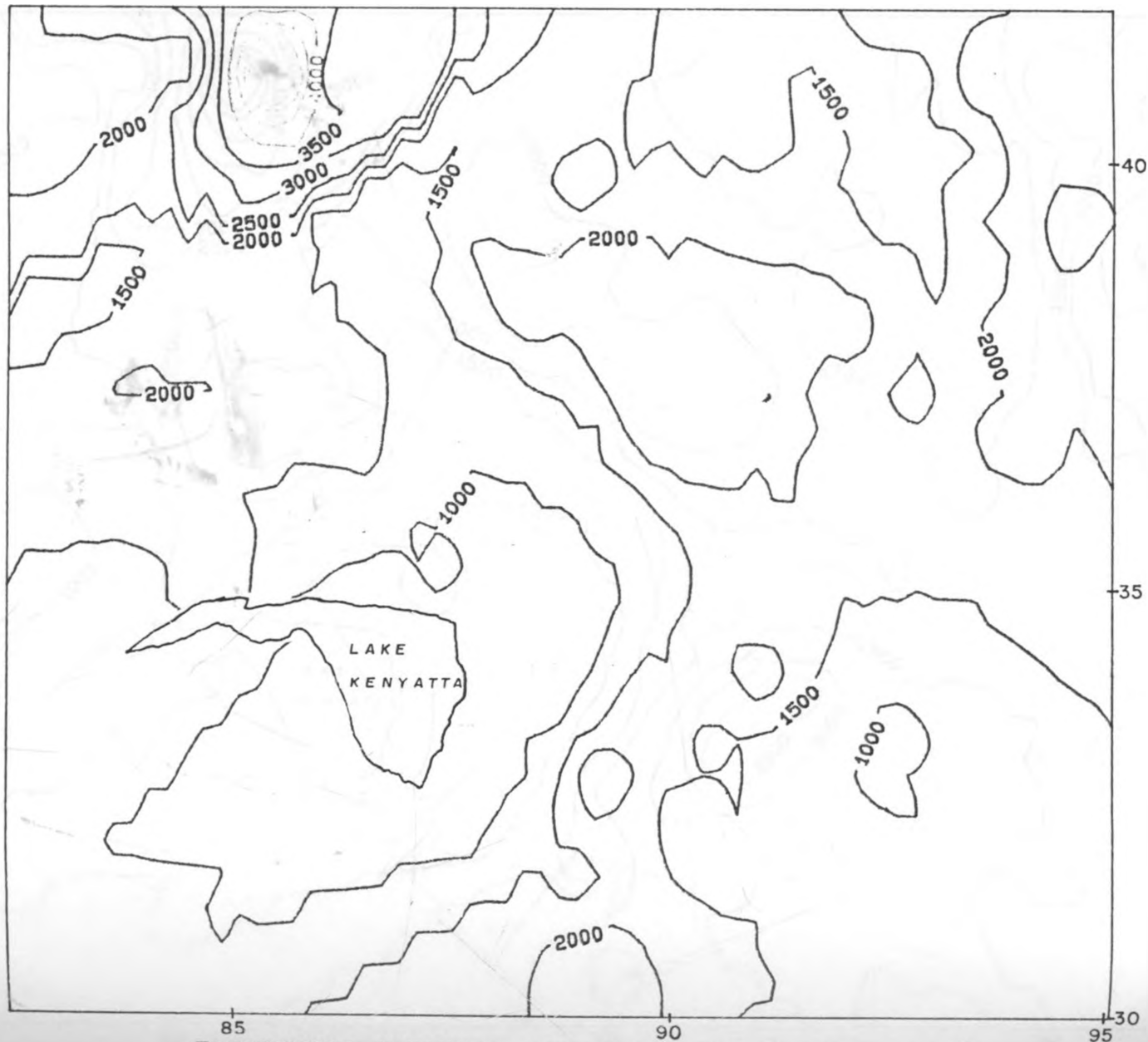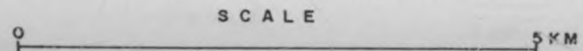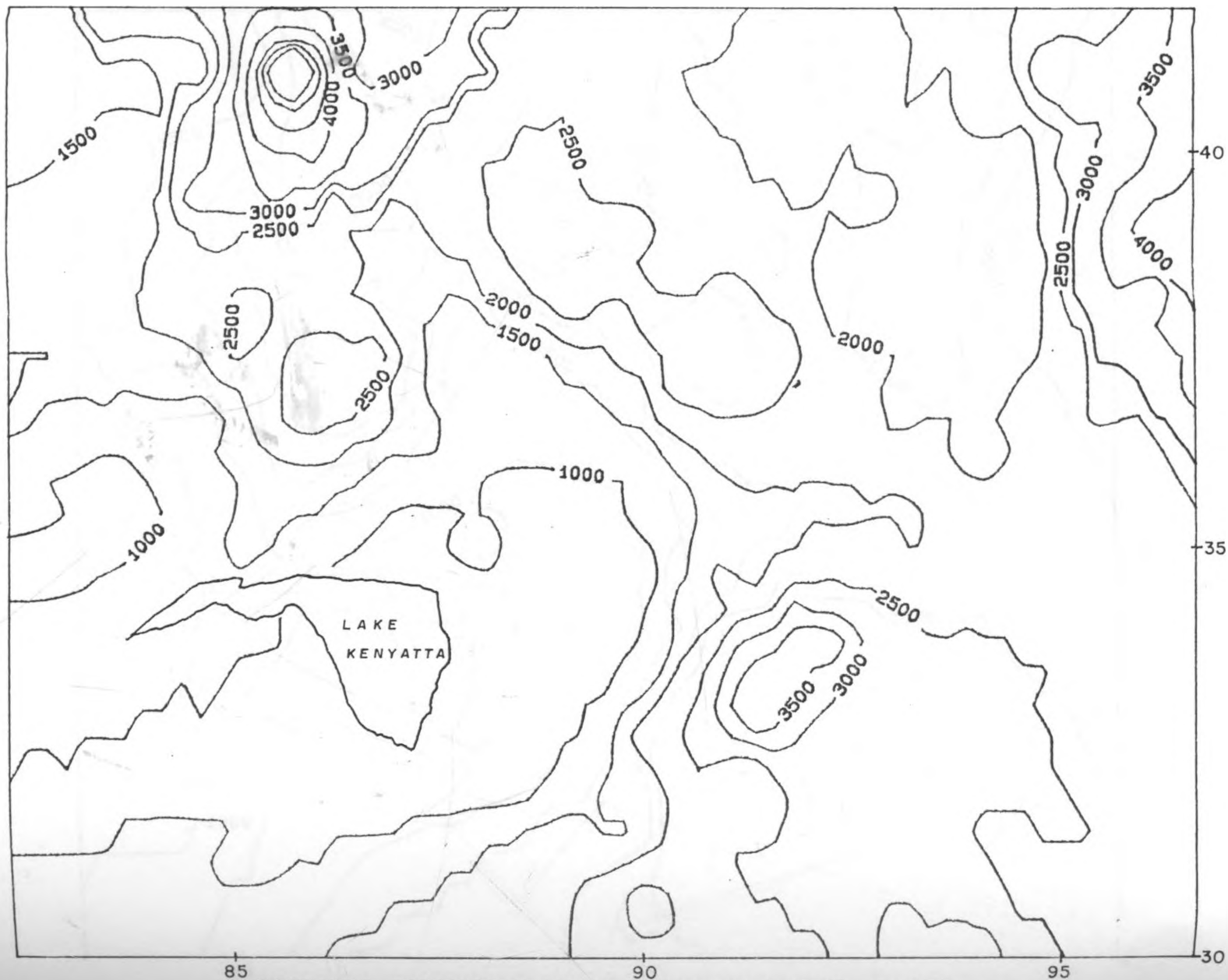
ELECTRICAL CONDUCTIVITY IN THE STUDY AREA - 1989
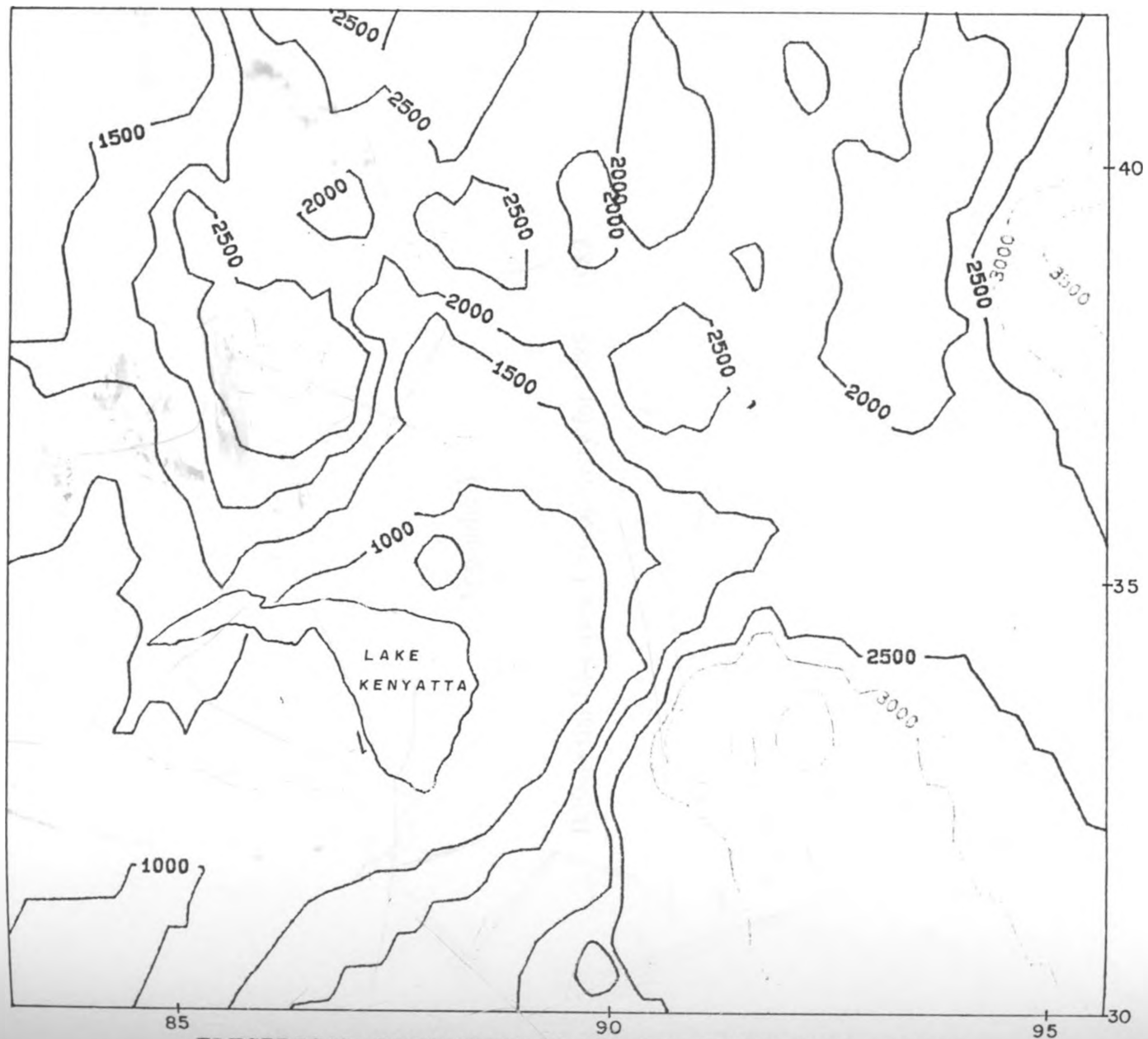
SCALE

0   5 KM

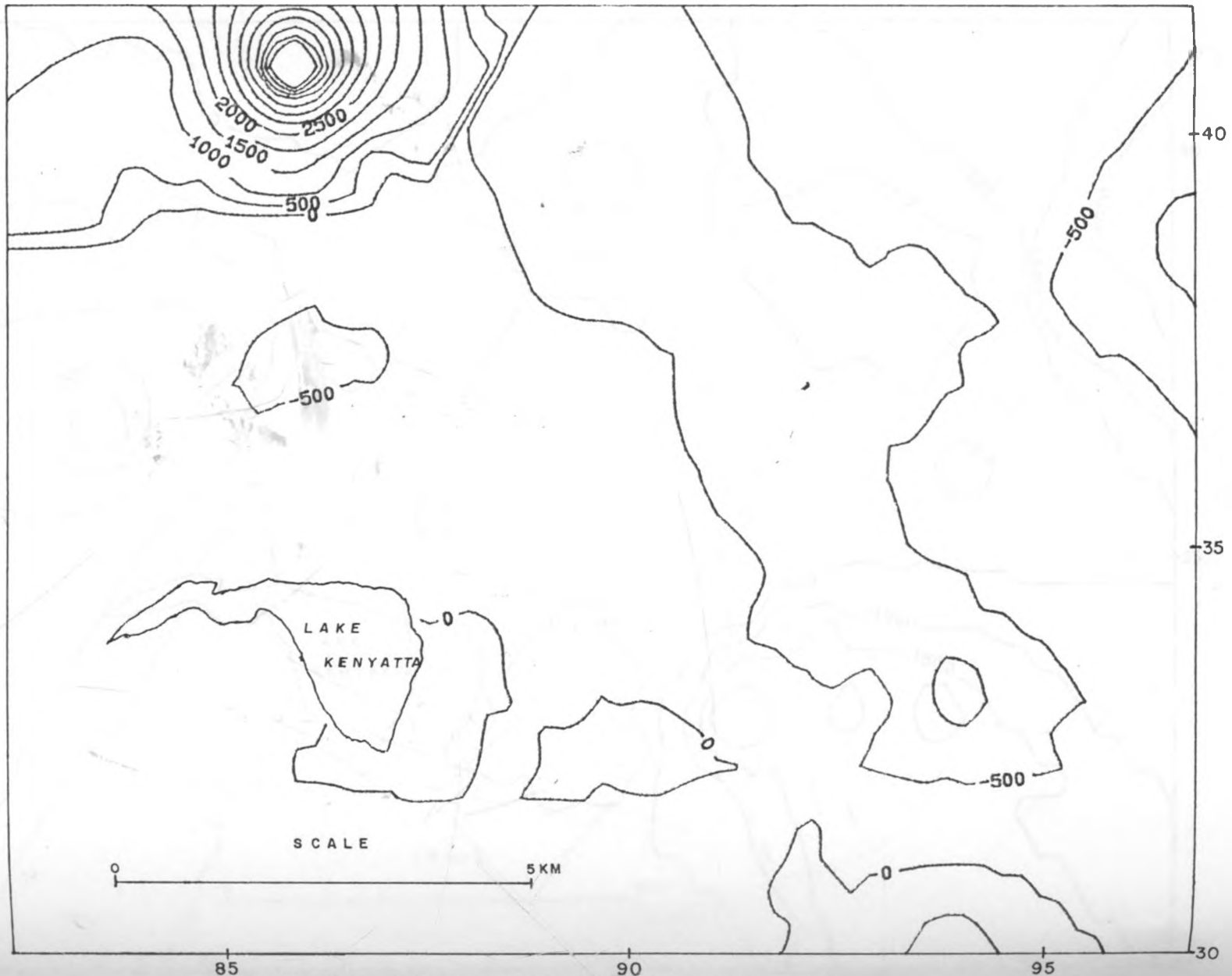ELECTRICAL CONDUCTIVITY IN THE STUDY AREA - 1990

SCALE

0   5 KM

Appendix V

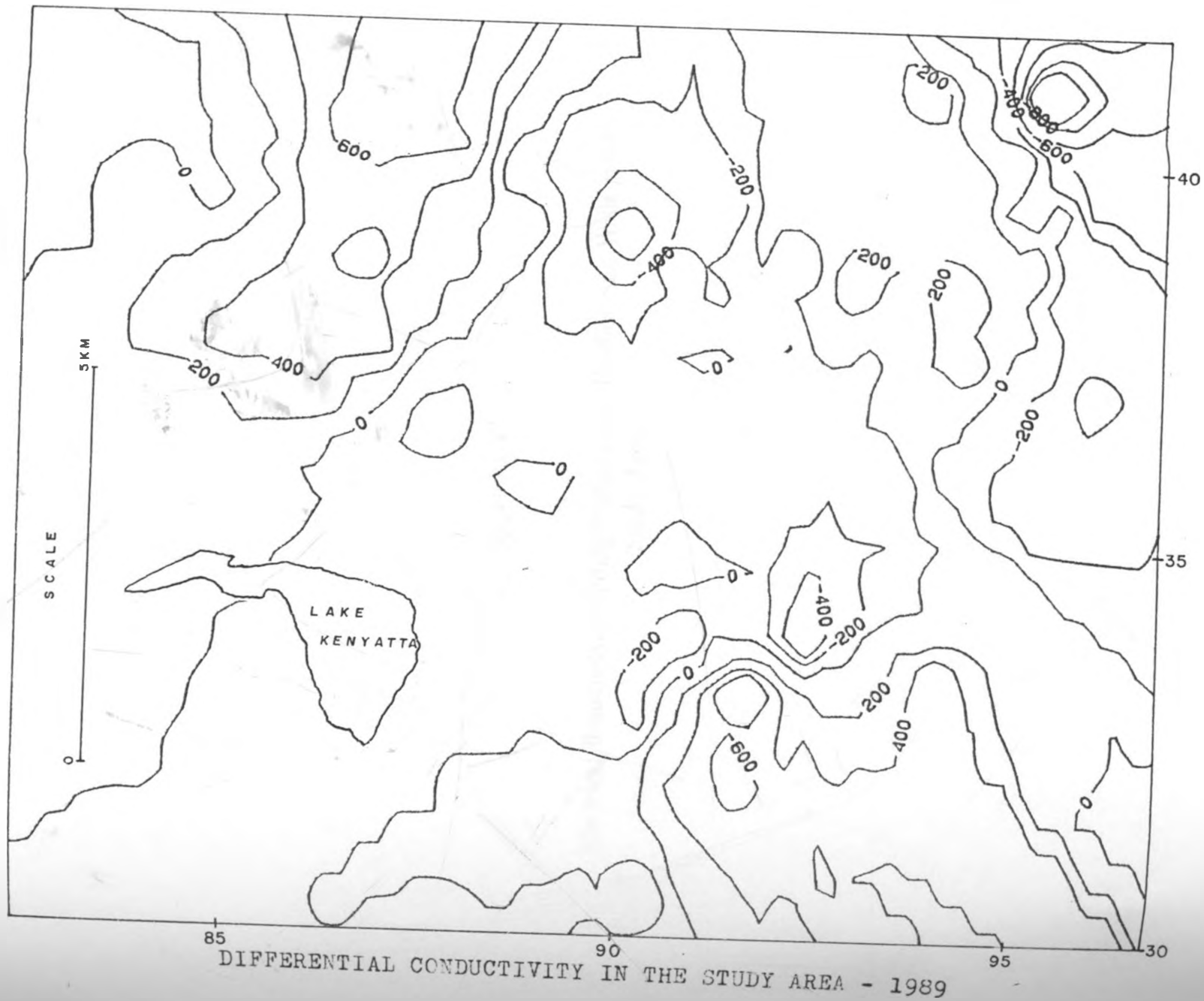## Differential Electrical Conductivity for 1985 to 1989
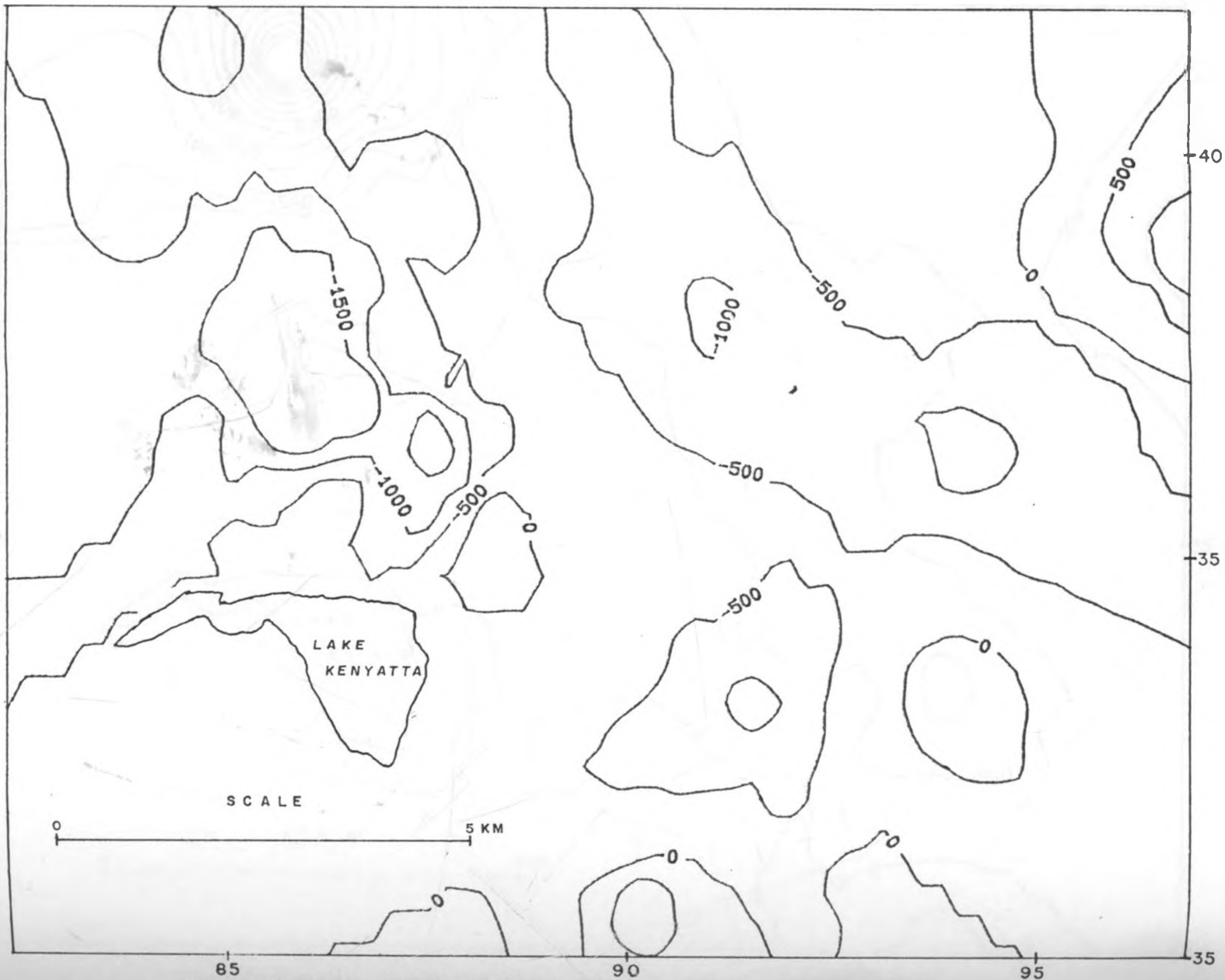
DIFFERENTIAL CONDUCTIVITY IN THE STUDY AREA - 1985

DIFFERENTIAL CONDUCTIVITY IN THE STUDY AREA - 1987

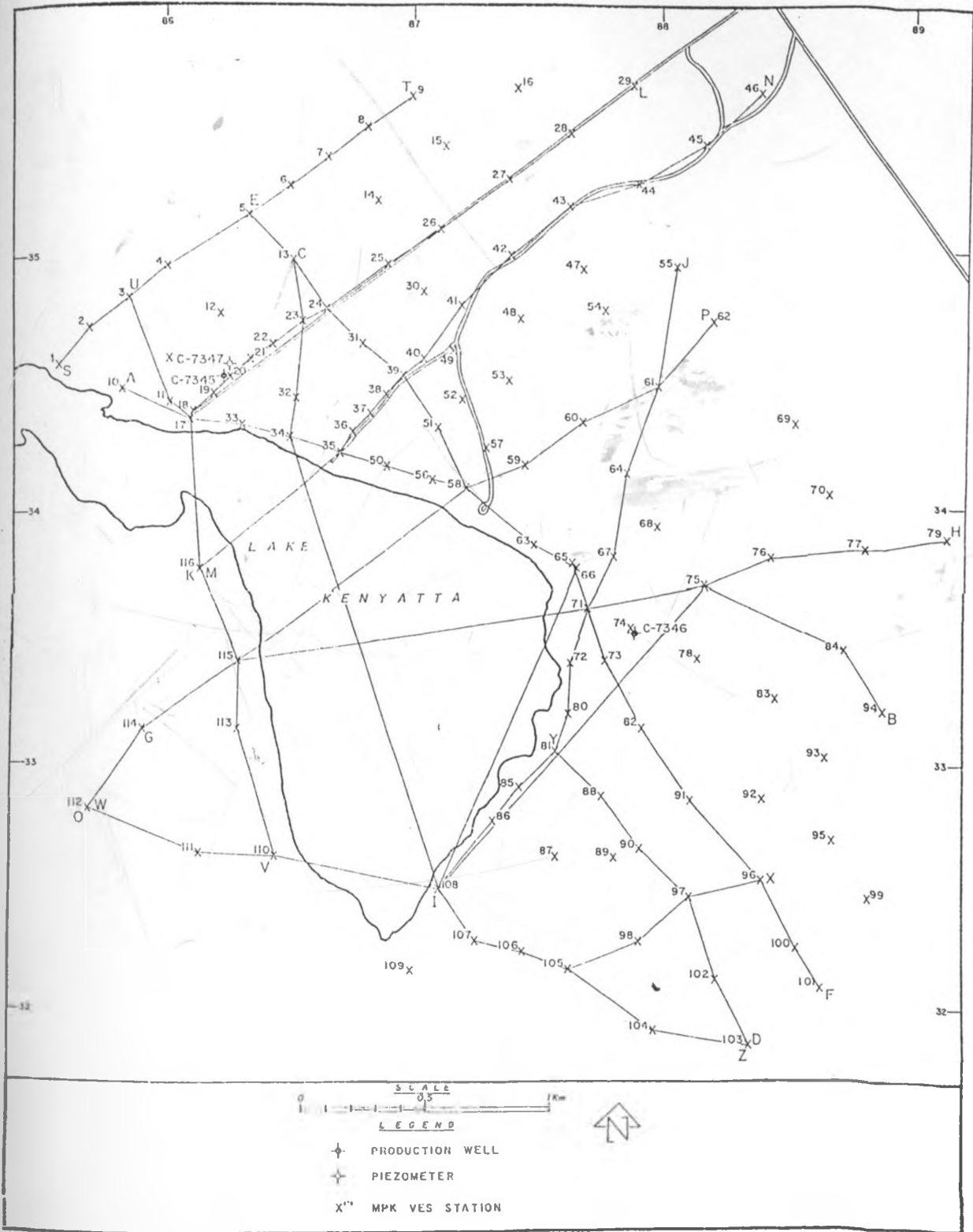DIFFERENTIAL CONDUCTIVITY IN THE STUDY AREA - 1988

DIFFERENTIAL CONDUCTIVITY IN THE STUDY AREA - 1989

Appendix VI

Electrical Resistivity Sounding Stations and Profiles, and Wells in the
Study Area

ELECTRICAL RESISTIVITY SCUNDING STATICNS
AND PROFILES IN THE STUDY AREA

WELLS IN THE SCULY AREA

253